Universidade do Minho
Escola de Engenharia

Ricardo Emanuel Silva Carvalho

Amorphous polysaccharide-drug formulations for intramacrophagic treatment of infectious diseases

March 2022

Amorphous polysaccharide-drug formulations for intramacrophagic treatment of infectious diseases
Ricardo Emanuel Silva Carvalho
UMinho | 2022

Universidade do Minho
Escola de Engenharia

Ricardo Emanuel Silva Carvalho

Amorphous polysaccharide-drug formulations for intramacrophagic treatment of infectious diseases

Dissertation for PhD degree in
Biomedical Engineering

Work carried out under the supervision of:
Francisco Miguel Portela da Gama, PhD
Jorge Manuel Rolo Pedrosa, PhD

March 2022

ACKNOWLEDGEMENTS

The preparation of this thesis would not be possible without the support of several people, to which I am and always will be deeply thankful. They contributed to my growth not only as a person but also as a scientist through the share of some knowledge (which I expect to have accurately transposed to this work). I would like to start by expressing my gratitude to my supervisor, Professor Miguel Gama, for giving me the opportunity to join his research group as a researcher, and later as a PhD student. He always supported my work and progress but most importantly believed in my work and in my capacity to overcome all the difficulties during this journey, even when my levels of confidence were low. To Professor Jorge Pedrosa for accepting to be my co-supervisor and allowing me to do some work at ICVS, which was kindly supported by Alexandra Fraga. To professor Pier Parpot for all the availability to help and for allowing me to use the HPLC. To the Centre of Biological Engineering (CEB) and all its technical staff for the excellent support. To all the people from LTEB lab at CEB, who made my life richer, both professionally and personally. For their friendship and for always sparing time to help when I needed. In particular to Daniela Martins that backed me up since the beginning of this journey. We shared the good, the bad and the worst moments together, frustrations and achievements. A special word of appreciation and gratitude goes to Professor Ana Tomás for accepting me in the Molecular Parasitology group at i3S and for always providing me with everything I needed to perform an important part of my work. To everyone that constitutes the group and accompanied me through this project, especially to Teresa Leão for always being around helping me to organize and perform the *in vivo* studies. To my friend Pedro Oliveira, for all the "red pill" talks that helped me to relativize and overcome daily problems and for all the workouts in the gym that contributed to free my mind from the work and worries. My truly and deeply-felt thanks to my parents that gave me unconditional love, education and support and for making me the person I am today. To my sister, Maria Carvalho, for all the love and understanding, for always being by my side in everything. Finally, I would like to thank the Portuguese Foundation for Science and Technology (FCT) for the PhD grant (SFRH/BD/118880/2016) and all the funding entities that supported the work.

FCT under the scope of the strategic funding of UIDB/04469/2020; BioTecNorte operations (NORTE-01-0145-FEDER-000004 and NORTE-01-0145-FEDER-000012) funded by the European Regional Development Fund under the scope of Norte2020 - Programa Operacional Regional do Norte; i3S Scientific Platform BioSciences Screening, member of the PPBI (PPBI-POCI-01-0145-FEDER-022122).

STATEMENT OF INTEGRITY

I hereby declare having conducted this academic work with integrity. I confirm that I have not used plagiarism or any form of undue use of information or falsification of results along the process leading to its elaboration. I further declare that I have fully acknowledged the Code of Ethical Conduct of the University of Minho.

RESUMO

FORMULAÇÕES AMORFAS DE POLISSACARÍDEO-FÁRMACO PARA O TRATAMENTO INTRA-MACROFÁGICO DE DOENÇAS INFECIOSAS

O tratamento da leishmaniose é normalmente baseado em formulações de anfotericina B (AmB), que apresentam sérias limitações. Apesar dos progressos realizados nesta área, continua a ser necessário desenvolver alternativas menos dispendiosas e menos tóxicas. Esta tese tem como objetivo desenvolver um processo simples e de baixo custo para produzir nanocomplexos de AmB-polissacarídeo solúveis em água, com atividade anti-leishmaniose e reduzida toxicidade. Foram produzidas formulações não covalentes de dextrino (Dex-AmB) e de ácido hialurónico (HA-AmB) (genericamente designados de nanocomplexos) e covalentes (designados de complexos covalentes), neste caso pelo método de aminação redutiva (HA-AmBi). Foram testadas diversas soluções para a secagem das formulações, por liofilização (FD) e pulverização (*spray-drying*, SD). Todas as formulações testadas permitiram melhorar a solubilidade da AmB, possivelmente devido à amorfização do fármaco. O teor de AmB nos nanocomplexos é comparável ao obtido para o conjugado covalente, o que valoriza o processo operacionalmente mais simples da conjugação não química. Contrariamente às formulações com dextrino (Dex), as obtidas com ácido hialurónico (HA) apresentam uma estabilidade coloidal elevada, devido ao seu potencial zeta (-30mV). Estudos de atividade *in vitro* mostraram que as formulações apresentam boa atividade anti-leishmaniose (IC_{50}: 0.017 e 0.023 μM para Dex-AmB FD e Dex-AmB SD, respetivamente; 0.026 e 0.030 μM para HA-AmB FD e HA-AmB SD, respetivamente; 0.023 μM para HA-AmBi), associada a uma redução significativa na toxicidade do fármaco. Este efeito foi mais acentuado no nanocomplexo HA-AmB, obtido usando SD. Foi testado o desempenho *in vivo* das formulações HA-AmB SD e HA-AmBi, tendo-se observado uma redução da toxicidade em ratinhos após administração intravenosa. As formulações promoveram uma supressão similar da carga de parasitas no baço e no fígado. Embora os nanocomplexos sejam menos eficazes na redução da infeção no fígado, comparativamente ao AmBisome®, os resultados demonstram que usando um método muito simples e direto é possível obter uma formulação promissora para o tratamento de leishmaniose visceral.

Palavras-chave: Anfotericina B, atividade anti-leishmaniose, leishmaniose, polissacarídeos, toxicidade.

ABSTRACT

AMORPHOUS POLYSACCHARIDE-DRUG FORMULATIONS FOR INTRAMACROPHAGIC TREATMENT OF INFECTIOUS DISEASES

The treatment of leishmaniasis is usually based on amphotericin B (AmB) and its formulations, which have serious limitations. Despite the progress made in this area, there is still a need to develop less expensive and less toxic alternatives. This thesis aims to develop a simple and low-cost process to produce water-soluble AmB-polysaccharide nanocomplexes with anti-leishmaniasis activity and reduced toxicity. Non-covalent formulations of dextrin (Dex-AmB) and hyaluronic acid (HA-AmB) (generically called nanocomplexes) and covalent formulations (called covalent complexes) were produced, in this case by the reductive amination method (HA-AmBi). Several solutions were tested for drying the formulations, namely using lyophilization (FD) and spraying (spray-drying, SD). All tested formulations improved the AmB solubility, possibly due to drug amorphization. The AmB content in the nanocomplexes is comparable to that obtained for the covalent conjugate, which favors the operationally simpler process of non-chemical conjugation. Unlike formulations with dextrin (Dex), those obtained with hyaluronic acid (HA) have a high colloidal stability, due to the higher zeta-potential (–30mV). *In vitro* activity studies showed that the formulations have good anti-leishmanial activity (IC_{50}: 0.017 and 0.023 μM for Dex-AmB FD and Dex-AmB SD, respectively; 0.026 and 0.030 μM for HA-AmB FD and HA-AmB SD, respectively; 0.023 μM for HA-AmBi), associated with a significant reduction in drug toxicity. This effect was more pronounced in the HA-AmB nanocomplex obtained using SD. The *in vivo* performance of the HA-AmB SD and HA-AmBi formulations was tested and a reduction in toxicity was observed in mice, after intravenous administration. Both formulations promoted a similar suppression of parasite load in the spleen and liver. Although nanocomplexes are less effective in reducing liver infection compared to AmBisome®, the results demonstrate that using a very simple and straightforward method it is possible to obtain a promising formulation for the treatment of visceral leishmaniasis.

Keywords: Amphotericin B, anti-leishmanial activity, leishmaniasis, polysaccharides, toxicity.

LIST OF CONTENTS

LIST OF FIGURES

Chapter 2

Chapter 3

Chapter 4

Chapter 5

LIST OF TABLES

Chapter 2

Chapter 3

Chapter 4

Chapter 5

LIST OF ABBREVIATIONS AND ACRONYMS

A

ACPs - Antigen-presenting cells;

ADO - Adenosine;

AE - Association efficiency;

AG - Arabinogalactan;

AmB - Amphotericin B;

ANOVA - Analysis of variance;

AP-1 - Activator protein 1;

B

BMMΦ - Bone marrow-derived macrophages;

C

CC_{50} -Cytotoxicity concentration 50%;

CCR - Chemokine receptor;

CD - Cluster differentiation;

CL - Cutaneous leishmaniasis;

CO_2- Carbon dioxide;

CR - Complement receptor;

CRP - C-reactive protein;

Cryo-SEM - Scanning Electron Cryomicroscopy;

D

D_2O - Deuterium oxide;

DAPI - 4',6-diamidino-2-phenylindole;

DCL - Diffuse cutaneous leishmaniasis;

DCs - Dendritic cells;

DEG - diethylene glycol;

Dex - Dextrin;

Dex FD - Dextrin freeze-dried;

Dex SD - Dextrin spray-dried;

Dex-AmB FD - Dextrin-Amphotericin B freeze-dried;

Dex-AmB SD - Dextrin-Amphotericin B spray-dried;

dH_2O - Distilled water;

DLS - Dynamic Light Scattering;

DMEM - Dulbecco's Modified Eagle Medium;

DMSA - Dimercaptosuccinic acid;

DMSO - Dimethylsulfoxide;

DNA - Deoxyribonucleic acid

DSC - Differential Scanning Calorimetry;

DsCL - Disseminated cutaneous leishmaniasis;

E

ESI - ElectroSpray Ionization source;

F

FBS - Fetal bovine serum;

f-CNTs - Functionalized multi-walled carbon nanotubes;

FD - Freeze-dryer

FDA - Food and Drug Administration;

FTIR - Fourier-Transform Infrared Spectroscopy;

G

Gp63 - 63-kDa surface metalloproteinase;

GRAS - Generally regarded as safe;

H

H&E - Hematoxylin and eosin;

HA - Hyaluronic acid;

HA FD - Hyaluronic acid freeze-dried;

HA SD - Hyaluronic acid spray-dried;

HA-AmB FD - Hyaluronic acid-Amphotericin B freeze-dried;

HA-AmBi - Hyaluronic acid-Amphotericin B imine conjugate;

HA-AmB SD - Hyaluronic acid-Amphotericin B spray-dried;

HBMEC - Human brain microvascular endothelial cell line;

HCS CellMask™ Deep Red stain - High-content screening CellMask™ Deep Red stain

HEK293T - Human embryonic kidney cell line;

HIV/AIDS - Immunodeficiency virus/acquired immunodeficiency syndrome;

HPLC - High-Performance Liquide Chromatography;

HPγCD - Hydroxypropyl-γ-cyclodextrin;

I

i.p. - Intraperitoneal;

i.v. - Intravenous;

IC_{50} - Half maximal inhibitory concentration;

iFBS - Inactive fetal bovine serum;

IFN-β - Interferon beta;

IFN-γ - Interferon gamma;

IL - Interleukin;

iNOS - Inducible nitric oxide synthase;

IO_4^- - Periodate ion;

J

JAK/STAT - Janus kinases-signal transducer and activator of transcription proteins pathway;

K

KHP - Potassium hydrogenphthalate;

KIO_4-Potassium periodate;

L

LAMPs - Lysosome-associated membrane glycoproteins;

LCCM - L929-cell conditioned medium;

LPG - Lipophosphoglycans;

LR - Leishmaniasis recidivans;

M

m/z - Mass-to-charge ratio;

MAPK - Mitogen-activated protein kinase;

MBL - Mannan binding lectin;

MCL - Mucocutaneous leishmaniasis;

M-CSF - macrophage colony-stimulating factor;

MERS - Middle east respiratory syndrome;

MHC - Major histocompatibility complex;

MOI - multiplicity of infection;

MR - Mannose receptor;

MS - Mass Spectrometer;

MTD - Maximum tolerated dose;

mTOR - Mechanistic target of rapamycin pathway;

MW - Molecular weight;

MWCO - Molecular weight cut-off;

N

NADPH oxidase - Nicotinamide adenine dinucleotide phosphate oxidase;

NaOH - Sodium hydroxide;

NF-κB - Nuclear factor kappa-light-chain-enhancer of activated B cells;

NK cells - Natural killer cells;

NMR - Nuclear magnetic resonance;

NO - Nitric oxide;

NTA - Nanoparticle Tracking Analysis;

NTDs - Neglected Tropical Diseases;

O

O/W - Oil in water;

OxHA - Oxidized hyaluronic acid;

P

p - p-value;

PBS - Phosphate-buffered saline;

PCL - Poly(ε-caprolactone;

PDA - Photodiode Array Detector;

PDC - Polymer-drug conjugates;

PDI - Polydispersity index;

PEG - Poly (ethylene glycol);

PES - Polyethersulfone;

PGA - Polyglutamic acid;

PKC - Protein kinase C;

PKDL - Post kala-azar leishmaniasis.

PLGA - Poly (D, L-lactide-*co*-glycolide);

PS - Phosphatidylserine;

PSG - Promastigote secretory gel;

XRD - Powder X-Ray Diffraction;

R

RBCs - Red blood cells;

RNS - Reactive nitrogen species;

ROS - Reactive oxygen species;

RPMI - Roswell Park Memorial Institute 1640;

S

s.c. - Subcutaneous;

SARS - Severe acute respiratory syndrome;

SD - Spray-dryer;

SD - Standard deviation;

SEM - Scanning Electron Microscope;

SI - Selectivity index;

SLNs - Solid lipid nanoparticles;

SR - Scavenger receptor;

T

TB - Tuberculosis;

TFs - Transfersomes;

TGF-β - Transforming growth factor beta;

Th1 - T helper 1 cells;

Th2 - T helper 2 cells;

TLR - Toll-like receptor;

TNF-α - Tumor necrosis factor alpha;

U

UV-vis - Ultraviolet-visible;

V

VL - Visceral leishmaniasis;

W

WHO - World Health Organization;

"There are painters who transform the sun to a yellow spot, but there are others who with the help of their art and their intelligence, transform a yellow spot into the sun."

Pablo Picasso

CHAPTER 1 – MOTIVATION AND OUTLINE

This chapter introduces an overview of the work developed in this thesis. The motivation and outline of the research work produced is also described, as well as the main scientific outputs.

1.1. Context and Motivation

More than a century after the discovery of leishmaniasis and its causative agent, *Leishmania spp.*, this disease continuous to represent a major public health concern throughout the world, especially in developing countries [1], were high infection and morbidity rates are observed [2, 3]. Despite the knowledge developed over the years on this form of disorder, that involves a complex vector-host, host-pathogen and pathogen-vector interactions, it still remains uncontrollable [4, 5]. To date, there is no effective vaccine available and, therefore, the current treatment strategies rely on the use of chemotherapeutic drugs [6]. Amphotericin B (AmB) and its formulations (Fungizone®, AmBisome®, among others) are the most used ones for leishmaniasis treatment. Although presenting high efficacy, they are somehow inadequate due to toxicity, high cost and/or parasite drug resistance [7-9]. Thus, it is very important to improve the AmB formulations for an effective control of this neglected and fatal disease, namely by reducing its toxicity, while preserving its therapeutic efficacy, at lower costs.

Different naturally occurring polymers, such as polysaccharides, have been widely used as drug carriers in nanomedicine [10]. In fact, water-soluble polysaccharide-drug formulations has attracted considerable attention in recent years since these conjugates, and in particular AmB-polysaccharide conjugates, may enable drug targeting while reducing drug toxicity [7, 11-14]. Many of those formulations are synthesized by a complex process involving reductive amination [15]. Nevertheless, the quest for better therapeutic options for human leishmaniasis still continues, always taking in mind that this life-saving strategy needs to be accessible to developing and third-world countries.

Thus, this PhD work addresses the question: **Is it possible to create non-covalent polysaccharide-AmB self-assembly formulations that improves the drug solubility while reducing its toxicity and maintaining/improving the efficacy against leishmaniasis?**

Towards this end, amorphous dispersions/self-assembly formulations were developed with a suitable polysaccharide non-covalently bound to AmB, taking as reference a similar formulation based on covalent polysaccharide conjugate and commercial formulations. For that, a very simple process was employed using the ability of two polysaccharides (Dextrin – Dex and Hyaluronic acid – HA) to interact with AmB and a production process which relies solely on drying methods (freeze drying and nano spray drying were tested). Covalent conjugates were obtained by reductive amination since this technique has been widely reported in the literature. Dex and HA were used because of their high-water solubility, biocompatibility, biodegradability, non-immunogenicity and availability in medical grade. In addition, the use of HA may provide an active and selective targeting to cells that overexpress CD44, such as *Leishmania*-infected macrophages. A combination of characterization techniques and *in vitro* and *in vivo*

biological activity assays described along this thesis were carried out mainly at the Centre of Biological Engineering (CEB) and Centre of Chemistry of the University of Minho (Braga, Portugal) and at i3s - institute for research and innovation in health of the University of Porto (Porto, Portugal). A collaboration with the Food Processing group of International Iberian Nanotechnology Laboratory (Braga, Portugal) was also made with the sole purpose of using the nano spray dryer for the development of some nanocomplexes.

1.2. Thesis outline

This document is divided in 6 chapters. The current chapter (**Chapter 1**) consists in the description of the motivation, research focus and the thesis outline. The scientific outputs are also outlined.

Chapter 2 comprehends an up-to date review of the main subjects covered in this work, namely i) infectious diseases: Neglected Tropical Diseases (NTDs); ii) *Leishmania* spp. and leishmaniasis and iii) Management and treatment, including nanostructured delivery systems for leishmaniasis treatment: AmB-based formulations. **Chapters 3 to 5** contain the main experimental results obtained. **Chapter 3** describes the methodology used for the production of non-covalent Dextrin-Amphotericin B nanocomplexes, comparing the use of freeze- (FD) and spray-dryer (SD) in the process. A newly developed high-performance liquid chromatography coupled to diode array and mass spectrometry detectors (HPLC-PDA-MS) quantification method is also described. Different *in vitro* assays using cell lines, primary cultures of macrophages and *Leishmania* parasites were also employed to prove the safety and efficacy of the nanocomplexes. In the **chapter 4**, the use of hyaluronic acid to produce new amorphous HA-AmB nanocomplexes (HA-AmB FD and HA-AmB SD) was described, which ensures both an active and selective targeting by taking advantage of the ability of this polysaccharide to bind the CD44 receptor (highly expressed in infected macrophages). Both formulations were extensively characterized and their *in vitro* safety as well as efficacy were evaluated using relevant models (cell lines, dog's blood, *Leishmania* parasites and *Leishmania*-infected and non-infected macrophages). The *in vivo* nanocomplexes activity was achieved in this chapter. The formulations toxicity and their anti-leishmanial efficacy were assessed against *Leishmania*-infected mice, using as reference the commercial formulation AmBisome®. **Chapter 5** addresses the use of reductive amination methodology to link covalently AmB to oxidized hyaluronic acid. *In vitro* and *in vivo* safety and efficacy were evaluated as in the previous chapters. Finally, on **chapter 6** the major breakthroughs of this thesis are briefly discussed and suggestions for future work in this field are given.

1.3. Scientific outputs

The elaboration and execution of the experimental work during this PhD thesis originated the following publications in international scientific journals, as well as the participation in several scientific meeting with oral and poster communications.

PUBLICATIONS IN PEER REVIEWED JOURNALS

- **Silva-Carvalho, R.**, Fidalgo, J., Melo, K. R., Queiroz, M. F., Leal. S., Rocha, H. A., Cruz, T., Parpot, P., Tomás, A. M., Gama, F. M. "Development of dextrin-amphotericin B formulations for the treatment of Leishmaniasis." International Journal of Biological Macromolecules, 2020, 153: 276-288. DOI: 10.1016/j.ijbiomac.2020.03.019.
- **Silva-Carvalho, R.**, Leão, T., Bourbon, A. I., Gonçalves, C., Pastrana, L. M., Parpot, P., Amorim, I., Tomás, A. M., Gama, F. M. "Hyaluronic acid-amphotericin B nanocomplexes: a promising anti-leishmanial drug delivery system." Biomaterials Science, 2022, In Press. DOI: 10.1039/D1BM01769A.
- **Silva-Carvalho, R.**, Leão, T., Gama, F. M., Tomás, A. M. "Covalent conjugation of amphotericin B to hyaluronic acid: an injectable water-soluble conjugate with reduced toxicity and anti-leishmanial potential." Biomacromolecules, 2022, 23:1169-1182. DOI: 10.1021/acs.biomac.1c01451

ORAL COMMUNICATIONS IN SCIENTIFIC MEETINGS

- **Silva-Carvalho, R.**, Gonçalves, C., Bourbon, A. I., Pastrana, L. M., Parpot, P., Tomás, A., Gama, M. Hyaluronic Acid-Amphotericin B Nanocomplexes: a Promising Anti-leishmanial Targeted Drug Delivery System. XIII Spanish-Portuguese Conference on Controlled Drug Delivery. Santiago de Compostela (Spain), 22nd – 24th January 2020.
- **Silva-Carvalho, R.**, Fidalgo, J., Leal, S., Gonçalves, C., Bourbon, A. I., Cruz, T., Pastrana, L. M., Parpot, P., Tomás, A., Gama, M. Dextrin-Amphotericin B nanocomplexes: New water-soluble formulations for Leishmaniasis treatment. 13th International Meeting of the Portuguese Carbohydrate Group (GLUPOR 13), Porto (Portugal), 3rd – 5th September 2019.

POSTER COMMUNICATIONS IN SCIENTIFIC MEETINGS

- **Silva-Carvalho, R.**, Gonçalves, C., Bourbon, A. I., Pastrana, L. M., Parpot, P., Tomás, A., Gama, M. Hyaluronic Acid-Amphotericin B Nanocomplexes: a Promising Anti-leishmanial Targeted Drug

Delivery System. 2019 MRS Fall Meeting and Exhibition – Soft Material and Biomaterials symposium (Multiscale Materials Engineering Within Biological Systems), Boston (United States of America), 1st – 6th December 2019.

- Fidalgo, J., **Silva-Carvalho, R.**, Leal. S., Cruz, T., Tomás, A. M., Parpot, P., Gama, M. Development of a water-soluble Dextrin-Amphotericin B conjugate for the treatment of Leishmaniasis. 13th International Chemical and Biological Engineering Conference (ChemPor 2018), Aveiro (Portugal), 2nd – 4th October 2018.

1.4. References

1. Vale-Costa, S., et al., *Iron overload favors the elimination of Leishmania infantum from mouse tissues through interaction with reactive oxygen and nitrogen species.* PLoS Negl Trop Dis, 2013. **7**(2): p. e2061.
2. Alvar, J., et al., *Leishmaniasis worldwide and global estimates of its incidence.* PLoS One, 2012. **7**(5): p. e35671.
3. Torres-Guerrero, E., et al., *Leishmaniasis: a review.* F1000Res, 2017. **6**: p. 750.
4. Kaye, P. and P. Scott, *Leishmaniasis: complexity at the host-pathogen interface.* Nat Rev Microbiol, 2011. **9**(8): p. 604-15.
5. Olivier, M., *Culprit within a culprit.* Nature, 2011. **471**: p. 173.
6. Zulfiqar, B., T.B. Shelper, and V.M. Avery, *Leishmaniasis drug discovery: recent progress and challenges in assay development.* Drug Discov Today, 2017. **22**(10): p. 1516-1531.
7. Ehrenfreund-Kleinman, T., et al., *Synthesis and characterization of novel water soluble amphotericin B–arabinogalactan conjugates.* Biomaterials, 2002. **23**(5): p. 1327-1335.
8. Baginski, M., J. Czub, and K. Sternal, *Interaction of amphotericin B and its selected derivatives with membranes: molecular modeling studies.* Chem Rec, 2006. **6**(6): p. 320-32.
9. Bruni, N., et al., *Nanostructured delivery systems with improved leishmanicidal activity: a critical review.* International journal of nanomedicine, 2017. **12**: p. 5289-5311.
10. Duncan, R. and M.J. Vicent, *Polymer therapeutics-prospects for 21st century: The end of the beginning.* Advanced Drug Delivery Reviews, 2013. **65**(1): p. 60-70.
11. Golenser, J., et al., *Efficacious treatment of experimental leishmaniasis with amphotericin B-arabinogalactan water-soluble derivatives.* Antimicrobial agents and chemotherapy, 1999. **43**(9): p. 2209-2214.
12. Sokolsky-Papkov, M., A.J. Domb, and J. Golenser, *Impact of Aldehyde Content on Amphotericin B–Dextran Imine Conjugate Toxicity.* Biomacromolecules, 2006. **7**(5): p. 1529-1535.
13. Nishi, K.K., et al., *Amphotericin B-Gum Arabic Conjugates: Synthesis, Toxicity, Bioavailability, and Activities Against Leishmania and Fungi.* Pharmaceutical Research, 2007. **24**(5): p. 971-980.
14. Kothandaraman, G.P., et al., *Anti-fungal and anti-leishmanial activities of pectin-amphotericin B conjugates.* Journal of Drug Delivery Science and Technology, 2017. **39**: p. 1-7.
15. Volmer, A.A., A.M. Szpilman, and E.M. Carreira, *Synthesis and biological evaluation of amphotericin B derivatives.* Nat Prod Rep, 2010. **27**(9): p. 1329-49.

CHAPTER 2 – LITERATURE REVIEW

This chapter presents an overview on the Neglected Tropical Disease Leishmaniasis, still a public health problem causing high infections and morbidity rates. A brief description on the history and epidemiology of this disease as well as on the *Leishmania* parasites life cycle, host-parasite interaction and clinical manifestations are addressed. Leishmaniasis control and elimination remains troublesome and this chapter seeks to give an overview on the current treatments and as well as on new strategies, with special emphasis to polysaccharides-based nanostructured delivery systems, to produce alternative approaches to improve the efficacy of the anti-*Leishmania* drug AmB.

2.1. Infectious diseases: Neglected Tropical Diseases (NTDs)

Over the history, infectious diseases have been responsible for the largest global burden of death and disability. With the development of safe, effective and affordable vaccines and increased availability of antibiotics, a reduction of infectious diseases was possible in high-income countries by the middle of 20th century [1]. Nevertheless, despite the enormous advance in medical sciences, infectious diseases remained a significant threat throughout the world in the 21st century [2]. In fact, the potential of infectious diseases to cause deaths still is very present not only in low-income countries but also in high-income ones, with particular concern for human immunodeficiency virus/acquired immunodeficiency syndrome (HIV/AIDS), tuberculosis (TB), malaria, avian flu, middle east respiratory syndrome (MERS), severe acute respiratory syndrome (SARS), among others [2, 3]. Actually, and after the extensive experience acquired by global public health with the novel coronavirus SARS-CoV in 2003 and with avian influenza virus (H7N9) in 2015, the world and the public health was challenged, in the end of 2019, by the appearance of the new ongoing pandemic disease Covid-19, caused by SARS-CoV-2 virus. Globalization (interdependent trade, travelling, migration and international economic markets) [2, 4] as well as increased contact between humans and animals (leading to zoonotic diseases) [5], all contributed significantly to this effect of spreading infectious agents (that can range from viruses to complex protozoan and multicellular organisms [1]) and promoting the emergence and reemergence of old and new infectious diseases. Nevertheless, while the health care systems are struggling to fight novel diseases and pathogens, “older” diseases are still a threat with high global impact – noteworthy the Neglected Tropical Diseases (NTDs) [6]. The lack of global priority and attention towards this group of diseases occurs since they only have a major and devastating impact in low-incoming countries (decreasing survival rates and preventing opportunities for economic growth and development) [2, 4], being minimal for developed countries.

Currently, NTDs affect more than 1 billion of the poorest and most marginalized people in the world [2, 7], living with inadequate nutrition and without potable water, without proper sanitation and in remote and rural areas, informal settlements or conflict zones and in the vicinity of animals and infective disease vectors [8]. Furthermore, the limited access to necessary public health and healthcare system makes it impossible to treat many of these diseases, that with a very low-cost intervention are normally preventable or treatable [9]. The World Health Organization (WHO) identifies at least 20 NTDs (Figure 2.1) [8].

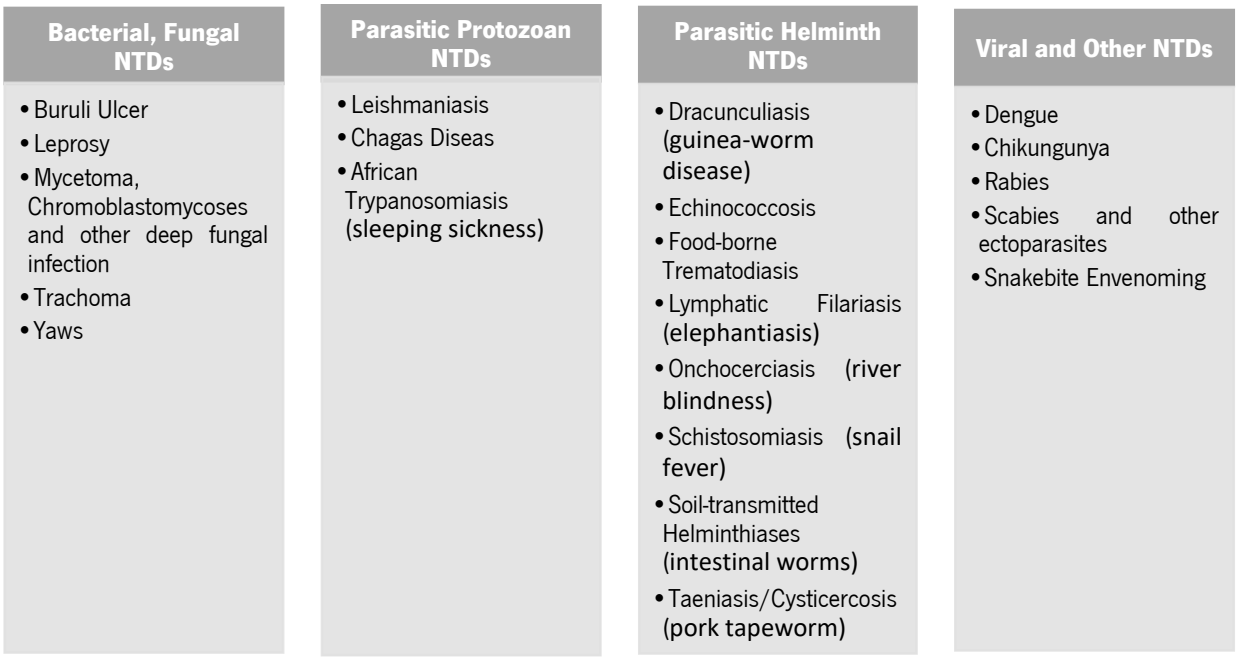

Figure 2.1 - List of Neglected Tropical Diseases according to World Health Organization (WHO) and its categorization according to the causative pathogen. Adapted from Hotez, P. J. (2020) [10].

A few key interventions could help preventing or treating a number of the above referred diseases, such as:

- preventive chemotherapy by mass drug administration [11] or increased human immunity through vaccination programs [1];
- innovative and intensified disease management: development of active surveillance to reduce human exposure to pathogens or vectors; educational campaigns to increase the population's knowledge about the transmissibility of a disease and how to avoid it [1, 4, 12];
- early diagnosis and treatment by surgery to eliminate or control the disease by removing any continued source of infection [1, 4, 12];
- vectors control, aiming to limit the transmission of pathogens by reducing or eliminating human contact with the vector using ecologically friendly methods (e.g.: safe insecticides, insecticide-treated nets, insecticide-treated dog collars, among others, use of personal protective equipment, environment management through vegetation removal, improve sanitation and removal of suitable aquatic habitats to disrupt breeding sites, biological control though introduction of competitor species to a vector, genetic manipulated mosquitoes or bacterial infection vectors) [4, 13].

Nowadays, vector control continuous to be crucial to prevent vector-borne NTDs like leishmaniasis, which persists as a significant public health threat, provoking high levels of morbidity [13], and is potentiated

by hunger, poverty and international conflicts that leads to human migration from rural to urban areas and cross-border movements of refugee populations, poor sanitation in suburban areas, deforestation, HIV/AIDS, among others [14, 15]. Nevertheless, despite being responsible for the ninth largest disease burden among other individual infectious diseases [16], only surpassed by malaria amongst protozoan parasitic diseases, leishmaniasis continues to be largely ignored.

2.2. *Leishmania* spp. and leishmaniasis

2.2.1. History and taxonomy

Leishmaniasis has a long history, with some primitive reports of *Leishmania*-like species presence in fossil ambers of extinct sandflies. Initial evidence of the disease trace back to the ancient human history (2,500 to 1,500 B.C.) and the first accounts of the infection to medieval times (first century A.D.). The discovery of the causative agent of this disease occurred only in modern times [17, 18]. In fact, at the beginning of the 20th century (1903), protozoan parasites in the spleen aspirates from patients in India were identified as the responsible agent of leishmaniasis by two independent reports from William Boog Leishman and Charles Donovan. These parasites were then named, in 1903, as *Leishmania* by Ronald Ross. Meanwhile, in 1908, dogs were considered an important reservoir host for visceral leishmaniasis due to the observations of Charles Jules Henry Nicolle and his colleague Charles Comte. Finally, in 1921, sandflies were proven, by Edmond Sergent and Étienne Sergent, to be the vectors responsible for transmission of *Leishmania* parasites [18].

Up to date, of the more than 30 species of *Leishmania* genus that have been described, at least 20 are pathogenic for humans [19] and belong to the *Trypanosomatidae* family in the *Kinetoplastidae* order. Concerning the pathogens that cause leishmaniasis in humans, they are further classified in two subgenera: *Leishmania*, present in both the Old and the New Worlds, and *Viannia*, restricted to the New World [20, 21]. Table 2.1 present some of the main *Leishmania* species that are pathogenic to humans.

Table 2.1 - Clinical manifestations and distribution of the main *Leishmania* species pathogenic to humans. Adapted from Burza et al. (2018) [22], Torres-Guerrero et al. (2017) [23], Kaye et al. (2011) [24] and Dassoni et al. (2017) [25].

Species[a]	Clinical manifestation	Geographical Distribution
Old World leishmaniasis		
L. (L.) donovani	VL, PKDL	India, Bangladesh, Ethiopia, Sudan and South Sudan
L. (L.) infantum	VL, CL	China, southern Europe, Brazil, and South America for VL and CL; Central America for CL
L. (L.) major	CL	Iran, Saudi Arabia, north Africa, the Middle East, central Asia, and west Africa
L. (L.) tropica	CL, LR, VL (rare)	Eastern Mediterranean, the Middle East, and northeastern and southern Africa
L. (L.) aethiopica	CL, DCL, DsCL, LR	Ethiopia and Kenya
New World leishmaniasis		
L. (L.) amazonensis	CL, DCL, DsCL, LR, MCL, VL (rare)	South America
L. (L.) chagasi	VL, CL (rare)	Latin America
L. (L.) mexicana	CL, DCL, DsCL	Central and South America (Mexico, Colombia, the Caribbean Sea region, and Ecuador)
L. (L.) pifanoi	CL	South America (Venezuela)
L. (V.) braziliensis	CL, MCL, LR	South America
L. (V.) guyanensis	CL, DsCL, MCL, LR	South America (north of the Amazon River, the Guianas, Venezuela, and Peru)
L. (V.) panamensis	CL, LR	South America (Panama, Costa Rica, Colombia, Ecuador, and Honduras)
L. (V.) peruviana	CL	Central and South America

VL, visceral leishmaniasis; CL, cutaneous leishmaniasis; MCL, mucocutaneous leishmaniasis; DCL, diffuse cutaneous leishmaniasis; DsCL, disseminated cutaneous leishmaniasis; LR, leishmaniasis recidivans; PKDL, post kala-azar leishmaniasis.

[a] Both subgenera *Leishmania Leishmania* L. (L.) and *Leishmania Viannia* L. (V.) are indicated;

2.2.2. Epidemiology/Global incidence

According to WHO, leishmaniasis is a disease with a significant public health impact and a worldwide distribution, being classified as one of the most neglected tropical diseases. Leishmaniasis is endemic in 98 countries (see examples in Table 2.1), covering 5 continents [26] (mainly affecting the Americas, sub-Saharan Africa, East Africa, Mediterranean, Middle East to Central Asia and South Asia) (Figure 2.2). Over 350 million people are living at risk of being infected and develop one of the many forms of the disease [23].

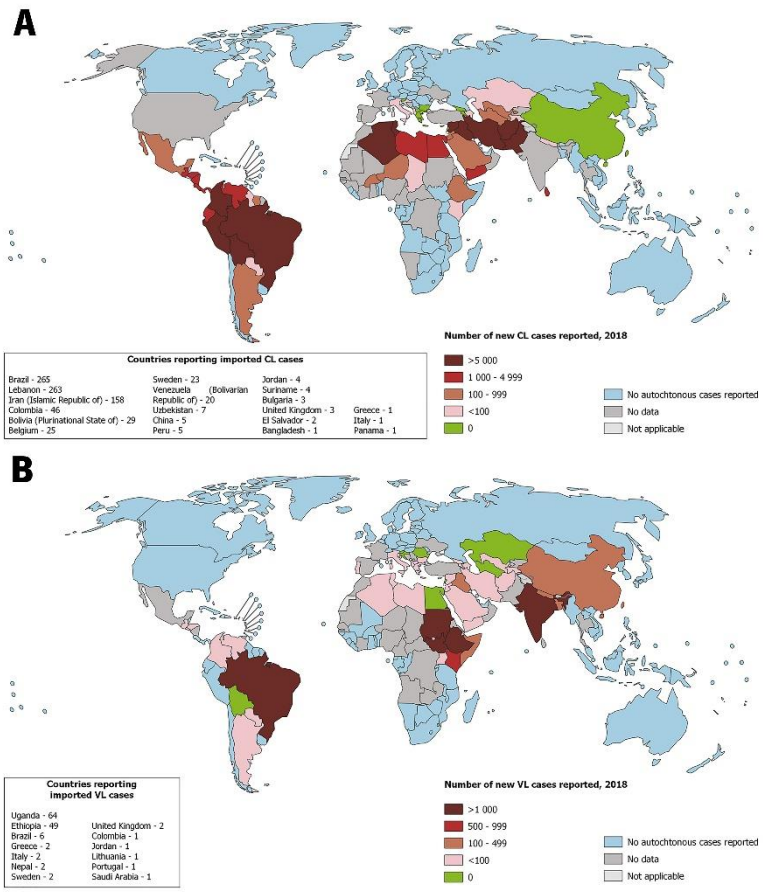

Figure 2.2 – Endemicity/geographical distribution of **(A)** cutaneous leishmaniasis and **(B)** visceral leishmaniasis reported by WHO in 2018. Adapted from WHO (https://www.who.int/leishmaniasis/burden/en/).

Global authorities estimate that there are 12 - 15 million people currently infected worldwide and every year this disease affects around 2 million new people causing 70,000 deaths [21, 23]. However, due to scarcity of the data obtained from numerous regions all over the world, there is no doubt that the number of the reported cases are even bigger [27].

The main clinical varieties of leishmaniasis in human are the Cutaneous (CL), Mucocutaneous (MCL), Visceral (VL) and Post kala-azar dermal (PKDL). Table 2.1 shows the parasite species that normally causes those manifestations. Globally, the annual incidence of CL is estimated to be 0.7 to 1.2 million new cases per year [22]. Despite being widely distributed for more than 70 countries, 90 % of the CL cases occurs in Afghanistan, Saudi Arabia, Syria, Pakistan, Iran, Algeria, Peru, and Brazil [26]. In most endemic areas, less than 5 % of the CL infections led to MCL, which is more restricted to South America [28].

Regarding VL, WHO estimates that there is an incidence of approximately 0.2 to 0.4 million cases every year [21] which is fatal if not treated, causing 20,000 to 40,000 estimated deaths each year. More than 90 % of these cases occur in India, Bangladesh, Sudan, South Sudan, Brazil and Ethiopia

[26]. Humans are the main reservoir of *L. donovani* transmission for VL in East Africa and the Indian subcontinent while domestic dogs are the main reservoir of *L. infantum* for VL in the Mediterranean Basin, the Middle East, Central Asia, China and South America [22, 28]. PKDL, considered a VL complication that arises after treatment, is frequent in Sudan and in Indian subcontinent, with a maximum reported rate after VL of 60 % and 10-20 %, respectively [29]. The increasing incidence of VL has been also associated to immunosuppressive conditions such as HIV/AIDS. Cases of HIV/*Leishmania* co-infection were firstly reported from south-western Europe, mainly from Spain, Italy, France and Portugal [30]. Nowadays, almost 35 countries have reported co-infections, with 5 to 6 % of total cases of VL and HIV co-infection occurring in the Mediterranean areas whereas in Ethiopia up to 30 % of VL patients are also infected with HIV [31, 32].

2.2.3. Clinical manifestations

Leishmaniasis is associated to a plethora of clinical manifestation that are dependent on the above shown heterogeneity between the *Leishmania* species and their virulence and tropism (viscerotropism and/or dermotropism) as well as vector characteristics (specific vectors that support the growth of only one species of *Leishmania* or permissive vectors that support the growth of more than one species) and the coordinated action of complex immunological response of the host, that differs depending on the infecting species [33]. The host immune response and, consequently, the establishment, outcome and severity of the disease, can further be influenced by the parasite load and persistence, number, localization and duration of lesions, age, host genetic background, nutritional status, pregnancy, co-morbidities, co-infection, immunosuppression, drug metabolism and irregular treatment [34].

CL, that is caused by most of *Leishmania* species that are pathogenic to humans, is not life-threatening and comprises cutaneous lesions that, depending on the species involved, are more or less difficult to heal [35]. This disfiguring and stigmatizing disease starts with the development of erythematous papules at the sandfly's biting site, due to parasite replication in the dermis, which usually transform to nodules that ulcerate slowly over time becoming crusted ulcerated lesions (Figure 2.3 A) [22]. These ulcers (with a few millimeters to centimeters in diameter), although sometimes itchy, are painful and self-heal; yet patients often remain with a permanent damage [22, 36]. A more extreme and chronic forms of CL can also occur, namely diffuse cutaneous leishmaniasis (DCL), disseminated cutaneous leishmaniasis (DsCL), and leishmaniasis recidivans (LR). DCL is characterized by the dissemination

to different skin areas of non-ulcerating, painless papules and nodules and these conditions are associated to a dermis highly infiltrated with parasites and lack of immunological response [19, 22].

Figure 2.3 – Clinical signs of leishmaniasis: **(A)** Cutaneous leishmaniasis; **(B)** Mucocutaneous leishmaniasis; **(C)** Visceral leishmaniasis; **(D)** Post kala-azar dermal leishmaniasis. Reproduced from WHO (https://www.who.int/leishmaniasis/disease/clinical_forms_leishmaniases/en/).

DsCL is associated to the presence of a large (ten or more) number of different types of lesions (normally small papule that appear simultaneously or secondarily to one or several ulcerated lesions) at several parts of the body, being mucosal involvement frequent [22, 37]. In turn, LR likely represent a reactivation of an initial infection and is associated to new lesions around the old scars, due to the persistence of parasites in that tissue, that might expand and are highly infiltrated with lymphocytes [22, 25]. MCL is a disfiguring and mutilating naso-oropharyngeal form of leishmaniasis that is characterized by progressive ulcerations in mucosal tissues, mainly affecting the nasal septum, soft and hard palate, pharynx, tonsils, gums, and/or lip, and is caused by a strong and destructive immunological response [22, 38]. Mucosa and associated cartilage are progressively eroded leading to a disfigurement and deformity of the face (Figure 2.3 B) that result in social discrimination and, in extreme cases, causing death [23, 39]. Usually, MCL cases arise from inefficacious or inexistent CL treatments, since the amastigotes can disseminate from the skin to the naso-oropharyngeal mucosa through the blood and lymphatic system, with the exception of immunocompromised individuals, who have more predisposition to develop this form of leishmaniasis [22, 39].

VL, also known as kala-azar, is a febrile infectious illness considered the most acute clinical form of the disease and the most frequently fatal form if left untreated [22]. Following inoculation into the skin, parasites (commonly *L. donovani* and *L. infantum)* disseminate through the lymphatic and vascular systems and multiplies in monocytes and macrophages of the reticuloendothelial system, affecting visceral organs such as the liver, spleen, bone marrow or the lymph nodes [40]. High and intermediate fever, substantial weight loss, anaemia, and prostration of the abdomen (Figure 2.3 C) due to swelling of the liver (hepatomegaly) and spleen (splenomegaly) are the main symptoms of this disease [23] that can occur within weeks to years after infection [22]. Further, with the bone marrow cell infection as well as of macrophages and other phagocytic mononuclear cells, patients develop pancytopenia (reduced production of three types of blood cells: red blood cells, white cells, and platelets) and dysfunctional T cells start to accumulate, leading to inability to generate cell-mediated immune responses [22, 41].

VL become more common and more severe in HIV infection, presenting clinical syndromes more complicated to interpret, since both diseases share a common immune pathway. In fact, in co-infection conditions, parasites replication increases potentiating the progression of both diseases [22, 42]. Sometimes therapeutic cure of VL leads to clinical complications in the form of a dermal leishmaniasis that is referred to as PKDL (Figure 2.3 D). It was reported that this complication develops in as many as 60 % of VL patients, which are then considered as human reservoirs for anthroponotic VL due to the presence of parasites in the skin [42]. This manifestation, that could appear weeks to years after cure of VL, is characterized by hypopigmented macules, papulo-erythematous eruption, dispersed papules, nodules and plaques which can gradually spread from the face to other part of the body [22, 39].

2.2.4. Parasite morphology and life cycle

Leishmania parasites have a digenetic life cycle involving both an insect vector stage and a mammalian host stage exhibiting a diversity of morphologies that allow their adaptability to each stage [43]. Therefore, two main morphological forms are normally distinguished (Figure 2.4): slender and elongated promastigote (5-15 µm) with a long motile flagellum (the extracellular form found in the sandfly) and rounded or fusiform non-motile amastigote (5 µm in maximum diameter) with a short flagellum that scarcely emerges from the flagellar pocket (the intracellular mammalian form found in the phagocytic mononuclear cells) [19]. Despite the heterogeneity and functional complexity of the *Leishmania* species, the cellular architecture of the two main forms above referred are identical, conserved and very precisely defined through the life cycle; parasite cells contain flagellum, nucleus,

kinetoplast (mitochondrial DNA) situated at the base of the flagellum, the Golgi and a flagellar pocket (a cell membrane invagination in the base of the flagellum important in these parasites as it is the only site of endocytosis and exocytosis) [43, 44].

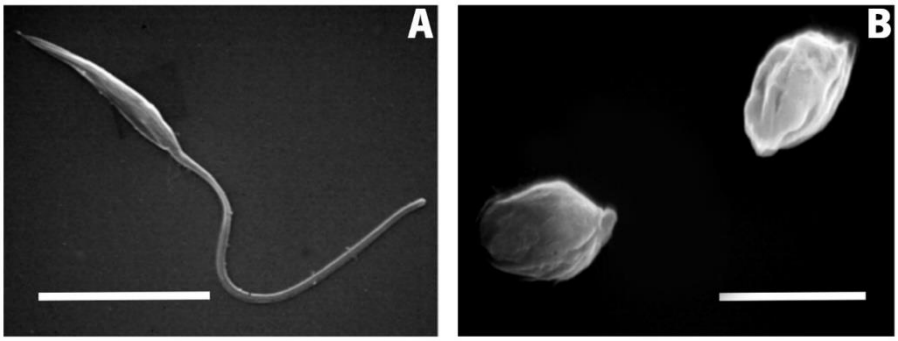

Figure 2.4 – Scanning Electron Microchip images of the two major morphological forms of *Leishmania* parasites: **(A)** promastigote; **(B)** amastigote. Adapted from Sarkar et al. (2018) [45].

This vector-borne disease is transmitted to mammalian hosts by the bite of a female phlebotomine sandfly, a diptera insect within the family of *Psychodidae* and subfamily of *Phlebotominae*. Approximately 1000 species of sandflies have been described but the transmission of leishmaniasis is attributed to about 70 species that belong to the genera *Phlebotomus* (present in the Old World – Europe, Asia and Africa) and *Lutzomyia* (present in the New World - America) [28, 33]. Phlebotomine sandflies are only active at dusk when the temperature drops and humidity rises and, to lay eggs, females need a blood meal that could be obtained from different mammalian reservoirs. Domestic dogs are the principal reservoir of zoonotic leishmaniasis, humans with untreated VL and PKDL are considered reservoirs for anthroponotic leishmaniasis [28]. Figure 2.5 summarizes the *Leishmania* parasites life cycle.

When female sandfly take a blood meal from an infected reservoir, it ingest blood containing free amastigotes or amastigote-infected macrophages by inserting their barbed mouthparts into the skin, lacerating dermal capillaries to form a pool of blood [46]. Those parasites became covered in the peritrophic matrix in the posterior midgut of the sandfly and suffer a decrease in temperature and increase in pH, promoting the amastigote transformation to the early promastigote stage – procyclic promastigote, a weakly motile and replicative form of the parasite [43, 46]. Considering the subgenus of the parasite, further transformations occur in the midgut and foregut (*Leishmania*) or in the hindgut and midgut (*viannia*) [43, 47].

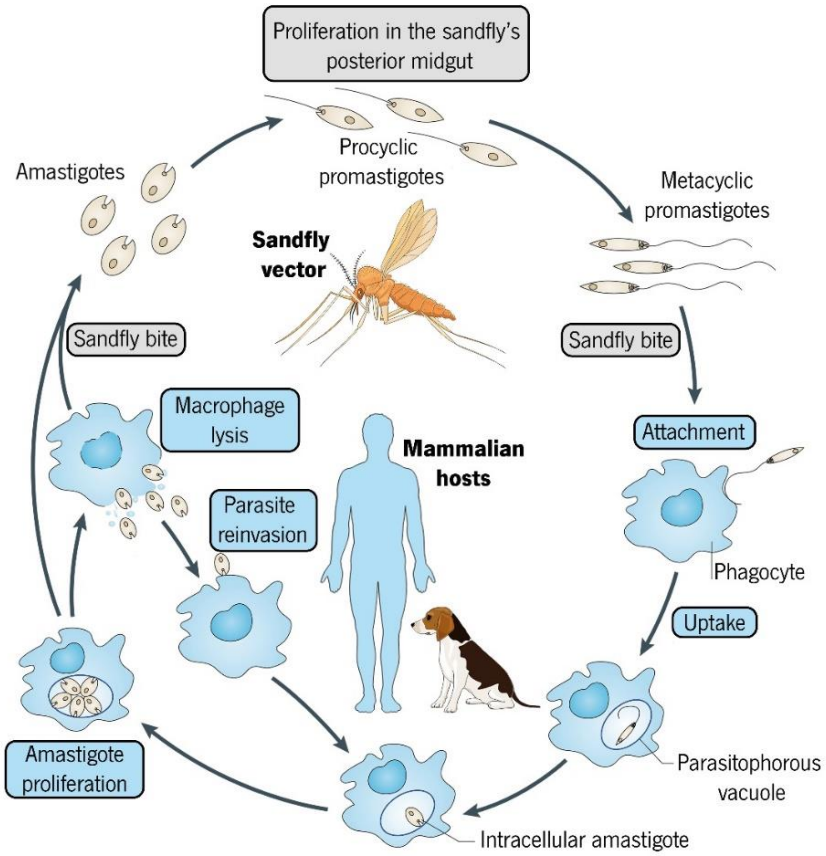

Figure 2.5 – *Leishmania* parasite life cycle. Depending on its host, the parasite can assume two main forms: promastigote, found in the sandfly vector, and amastigote, found in the mammalian host. Adapted from Kaye et al. (2011) [24].

Briefly, procyclic promastigotes gives rise to a highly motile nectomonad form whose function is to escape the confinement of the peritrophic matrix and move towards the midgut (stomodeal valve) where it becomes the shorter leptomonad promastigote, that resumes replication and produce the promastigote secretory gel (PSG) [46, 48]. Finally, some leptomonads differentiate into non-motile haptomonad promastigote, that become anchored to the chitin surface at the stomodeal valve, and metacyclic promastigotes, the non-dividing and highly infective form [43, 47, 48]. A successful transmission to the mammalian reservoir happens when a *Leishmania*-infected sandfly bites for another blood meal, creating a blood pool where the metacyclic promastigotes are regurgitated [28]. The damage caused in the dermis triggers an immune response that results in the phagocytosis of the parasites by immune cells such as neutrophils and macrophages [43, 49]. Once inside macrophages and due to microenvironment changes (temperature and low pH), promastigotes differentiate into aflagellate amastigotes that are more prone to survive to the harsh environment of the phagolysosome [28, 43, 49]. Therefore, amastigotes are able to proliferate promoting

macrophages lysis and their release, enabling the infection of more macrophages and the perpetuation of the infection [28].

2.2.5. Host cells-parasite interactions

Similarly to other pathogens, after host infection the parasite invade different phagocytes for the establishment of a persistent infection, such as dendritic cells, neutrophils and macrophages, being the last ones the definitive host cells for parasite replication and long-term survival [49]. Macrophages are phagocytic cells of the innate immune system that play a central role in the host's response to infections, promoting the destruction of pathogens and triggering the defensive functions of the host's immune response [50]. However, *Leishmania* parasites have several strategies to avoid macrophage functions and to persevere within this hostile environment. During a blood meal, metacyclic promastigotes as well as sandfly saliva (composed of proteins that induce vasodilation, prevent blood clotting and potentiate parasite multiplication), are deposited into the bite wound in the dermis [51, 52]. Immediately after this process and before phagocytosis, promastigotes must evade cell lysis mediated through the complement activation. For that, parasites are covered by a dense glycocalyx composed mainly by lipophosphoglycans (LPG) and 63-kDa surface metalloproteinase (gp63, also known leishmanolysin) [53]. In the case of LPG, which is longer in the metacyclic comparatively to procyclic promastigotes, it prevents the attachment of the complement membrane attack complex C5b-C9 and pore formation in the parasite surface. The surface glycoprotein gp63 inhibits complement activity by binding to C3b and converting it into iC3b, an inactive form of C3 [49, 53, 54]. Further, *Leishmania* parasites can use the complement factor iC3b to promote a "silent entry" into macrophages via complement receptor 3 (CR3) and CR1, respectively. The uptake through the later represents a predominant and important mechanism, since it promotes the failure of interleukin 12 (IL-12) production by infected macrophages, which in turn is important to stimulate T cells [49, 54]. LPG is also important for a direct or indirect attachment and internalization of the parasites by macrophages since it can interact with mannose-fucose receptor [55] or with C-reactive protein (CRP), triggering phagocytosis by the CRP receptor [56].

An indirect approach of delivering metacyclic promastigotes to macrophages through apoptotic cells was also suggested by Laskay and colleagues [57]. In this strategy, parasites take advantage of neutrophil, the primary cells of the innate immune system to be recruited to the inoculation site, by using them as "Trojan horse" [24, 58]. In fact, non-apoptotic and apoptotic parasites (mortality occurs naturally within the gut of infected sandflies and generates apoptotic-like parasites that display phosphatidylserine (PS) at their surface [49]) are phagocytosed in an opsonin-independent manner,

hampering thus cell activation and consequently increasing the non-apoptotic parasite survival. Moreover, the uptake of apoptotic parasites also allows to potentiate the silencing effect and to increase the survival of the viable parasites inside neutrophils through the inhibition of nitric oxide (NO) production [49, 54, 59]. Infected neutrophils, which present an extend life span that coincides with infiltration of the macrophages to the infected site [60], become apoptotic approximately two days after infection. These cells exhibit a PS signaling and are subsequently ingested by macrophages through receptor-mediated pathways. This process fails to trigger macrophage defense responses allowing an efficient entry of the parasites to the macrophages [24, 57]. Once inside, promastigotes are confined to a phagosome, also known as parasitophorous vacuole, that eventually will fuse with late endosomes/lysosomes forming the phagolysosomes. Promastigotes are highly vulnerable to the acidic pH and hydrolytic environment in that compartment. Therefore, to retard the contact with those conditions until complete differentiation to the more resistant amastigote form (process that is triggered by the increase in temperature, a decrease in pH, iron uptake and generation of reactive oxygen species [61]), promastigotes delay the phagosome fusion with endosomes and lysosomes by disrupting the phagosomal lipid microdomains, a process mediated by the LPG [62]. After differentiation, amastigotes replicate inside of macrophages until they undertake apoptosis. The parasite cargo is then released in a process mediated by parasitophorous extrusions, where the presence of lysosome-associated membrane glycoproteins (LAMPs) stimulates an anti-inflammatory response (e.g. expression of IL-10) by vicinal macrophages, allowing amastigotes internalization and the infection propagation [63]. Additionally, it was described that *in vivo* amastigotes released from disrupted macrophages that have a strong downregulation or even absence of surface glycoconjugates (LPG or gp63), use opsonization with IgG's to interact with FCγ receptors and enter in the macrophages without triggering their activation [64].

The survival of parasites inside of macrophages is vital for replication and propagation of infection and dependent on their ability to successfully disrupt several host cells functions, mainly microbicidal functions, cytokine production and antigen presentation and effector cell activation [54].

2.2.5.1. Inhibition of microbicidal functions

One of the major tactics employed by M1 macrophages to eliminate pathogens consists in the generation of two distinct molecules: reactive oxygen species (ROS), by the phagocyte NADPH oxidase system, and NO, by the inducible nitric oxide synthase (iNOS) [65]. Evidently, some *Leishmania* parasite molecules play a crucial role interfering with the above referred microbicidal molecules. For instance, LPG and/or gp63 are able to inhibit both oxidative burst and NO

production in a mechanism involving the inhibition of protein kinase C (PKC) [66, 67]. This leads to an impairment of NADPH oxidase activation, due to a defective phosphorylation of one of the cytoplasmic subunits (p47), and prevents its assembly at the phagosome by a disrupting lipid microdomains. Apart from the impairment of vacuole acidification, this also affects the phagosome fusogenicity towards endosome and lysosomes [49, 68]. Recently, a gp63-mediated activation of protein tyrosine phosphatases (PTPs) was described, more specifically of SHP1, that is involved in the inhibition of JAK/STAT pathway responsible for the regulation of iNOS and hence of nitric oxide production [67, 69]. Besides that, parasites can secrete or induce macrophages to produce arginase, which competes with iNOS for arginine leading to a decrease in NO production [70] (effect that is also potentiated by a Th2 response, characterized by IL-4 and IL-13 production [71]), or can impair cellular and mitochondrial ROS via the induction of mitochondrial uncoupling protein 2 [72].

2.2.5.2. Cytokine production

Resistance to infection by *Leishmania* parasites is mediated by interferon gamma (IFN-γ), mainly secreted by T helper 1 cells (Th1) and natural killer (NK) cells, in response to IL-12 that is predominantly secreted by active macrophages and dendritic cells (DCs) [52]. IFN-γ is very important since it stimulates iNOS activity in macrophages, enhancing the release of NO, and the expression of pro-inflammatory cytokines (tumor necrosis factor alpha (TNF-α), IL-1 and IL-6) while blocking the production of the anti-inflammatory cytokine IL-10 [73]. Besides IFN-γ, the inflammatory cytokines IL-1, TNF, IFN-α and IFN-β are also involved in the increased production of NO [74]. Nevertheless, in *Leishmania* susceptible macrophages, the parasite is known to modulate the secretion of specific immune factors in order to prevent the activation of an effective and specific immune response. Despite not fully understood, *Leishmania* parasites phagocytosis through CR3 [75] and Fcγ receptor [76] can impair IL-12 production, creating conditions for the establishment and propagation of the infection. Also, uptake of parasites expressing the apoptotic marker PS at surface or through the binding of opsonized parasite to the macrophage FCγ receptor leads to the production of the anti-inflammatory cytokines IL-10 and transforming growth factor beta (TGF-β), favoring parasite multiplication [77, 78]. *Leishmania*-infected neutrophils secrete also large amounts of TGF-β and IL-10, associated to a Th2 susceptible response [49], and suffer a down-regulation of TNF-α, responsible to induced an oxidative burst in these cells [79]. Briefly, IL-10 play an important role in decreasing the production of reactive nitrogen intermediates and pro-inflammatory cytokines (IL-12, IL-1, IL-6 and TNF-α) by macrophages and the production of

IFN-γ by Th1 and NK cells [73, 80] whereas TGF-β suppress the expression of iNOS by macrophages, due to the shift of arginine pool to arginase 1 for the production of polyamines (essential for parasite growth) [81] and impairs IFN-γ-induced macrophage activation [82]. The biosynthesis of polyamines used for parasite proliferation is associated to the M2 macrophages that are activated through a Th2 response characterized by IL-4 and IL-13 production [83].

2.2.5.3. Antigen presentation and effector's cell activation

Development of an effective immune reaction against *Leishmania* requires antigen presentation to T lymphocytes by specialized antigen presenting cells (APC), such as macrophages and DCs [65]. In fact, the adaptative immune response is initiated after presentation of endogenous small peptides, obtained through phagocytosis of parasite debris or intracellular parasite degradation, to cytotoxic CD8+ T cells or CD4+ T helper cells through major histocompatibility complex (MHC) class I or class II molecules, respectively [84]. In leishmaniasis, complete parasite removal is achieved by an efficient MHC II-mediated antigen presentation while, in some cases, a protective role against this disease is achieved by an MHC I-mediated antigen presentation [85, 86]. Interestingly, *Leishmania* can inhibit antigen cross-presentation in an MHC I context through cleavage of the vesicle-associated membrane protein 8. Disruption of this protein, mediated by gp63, prevents NADPH oxidase assembly on phagosomes, which promotes an alteration in their pH and proteolytic activity, thus inhibiting the presentation of *Leishmania* antigens on MHC I and T cell activation [87]. Parasites can also disrupt membrane lipid microdomains in order to inhibit antigen cross-presentation. The decrease in membrane cholesterol in infected macrophages may lead to altered conformation of MHC II molecules, contributing to a faster dissociation of the peptide and a defective antigen presentation to CD4+ T helper cells [88, 89]. In addition, MHC II molecules can be internalized by amastigotes and degraded by cysteine proteases in lysosome-like organelles known as megasomes [90]. Antigen presentation is also dependent of adhesion molecules that help the contact between APCs and T cells. *Leishmania* can interfere with APCs cluster differentiation 40 (CD40) presentation or signaling, affecting its interaction with CD40 ligand (CD40L) primarily expressed in activated T cells. This event avoids Th1 immune response and increases the susceptible towards a *Leishmania* infection [91]. Regarding *Leishmania*-infected DCs, parasites are able to modulate host cell maturation, motility and migration (by promoting a defective expression of the chemokine receptor CCR7) [92]. Furthermore, *Leishmania* is able to abolish full DC differentiation, causing a delay in the immune response, by promoting a downregulation of MHC class I/II expression and the host molecule CD80, CD86 and CD1a, that

are involved in the presentation of microorganism lipids and glycol [93, 94]. Also, *L. amazonensis* infection can stimulate the production of adenosine (ADO) due to the increase expression of CD39 and CD73 in DCs. This molecule activates A_{2B} receptor that impairs the activation of infected DCs, especially by inhibiting CD40 expression and IL-12 production, and decrease their ability to stimulate T cells proliferation [95].

By interfering and modulating the host cell signaling pathways (e.g. intracellular calcium signaling and PKC, JAK/STAT pathway, MAPK cascades, mTOR pathway [67, 96]), in ways which are still yet to be completely understood, and some important transcription factors (e.g. AP-1 and NF-κB [96]), *Leishmania spp.* becomes remarkably adapted to evade or subvert the immune responses into their own advantage. Figure 2.6 resumes in a very simplified way some of the above described complex capabilities of the parasites to overcome the immune system. With that, the treatment approaches used to overcome the various forms of leishmaniasis are not very effective and subsequent fail to achieve a cure since the parasites are able to survive and thrive in the referred hostile environments which, in most of the cases, potentiate their capability of developing resistance against the available treatment options.

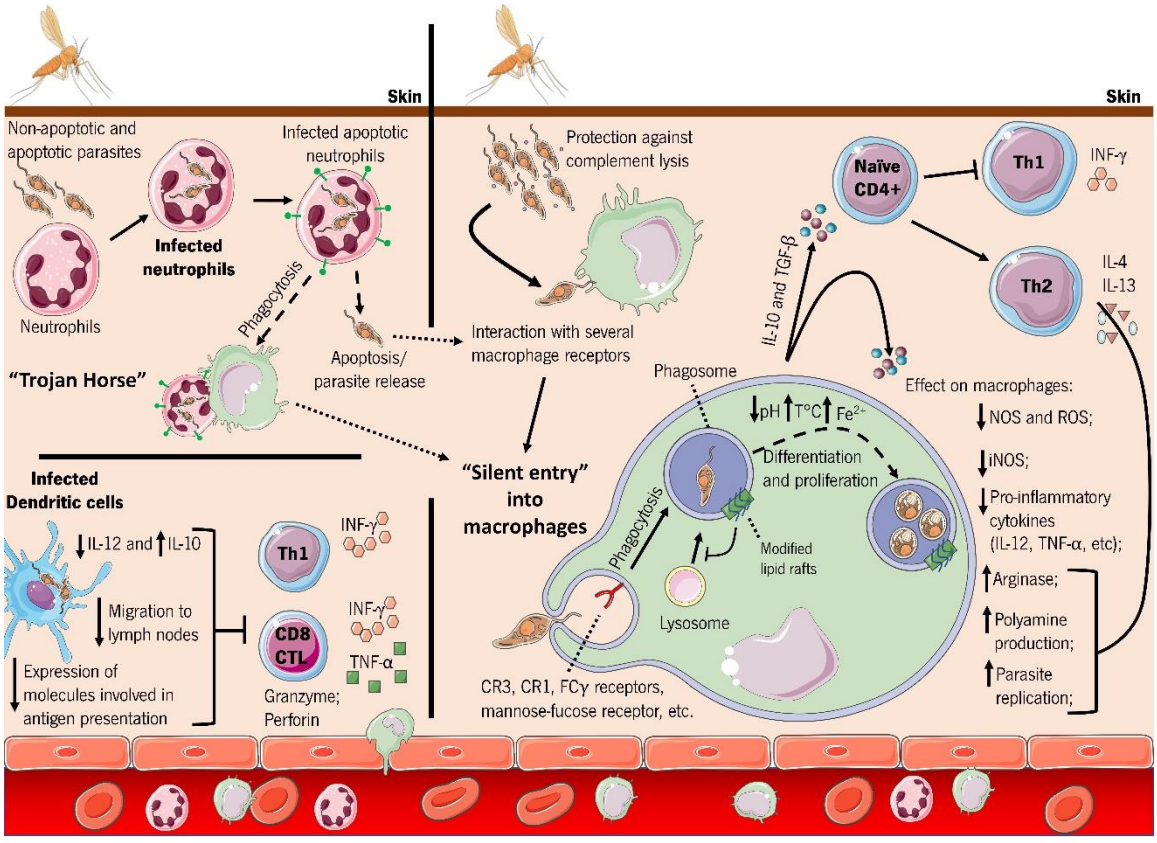

Figure 2.6 - Representation of a simple view of the *Leishmania* parasites interaction with the host immune system for survival. Neutrophils are rapidly recruited to the site of infection where they internalize parasites by phagocytosis and become responsible for dendritic cells (DCs) and macrophages recruitment to the site of the infection. Although some *Leishmania* are killed by neutrophils, some survive within neutrophils until they undergo apoptosis, being released. Those parasites as well as the ones that can avoid the complement lysis (through the presence of LPG and gp63) can interact with several macrophage receptors triggering phagocytosis. This "silent entry" into macrophages potentiates promastigote survival into the phagosome by delaying the phagosome fusion with lysosomes; inhibiting both oxidative burst and NO production; promoting the release of IL-10 and TGF-β (which supports a T helper 2 (Th2) response associated with IL- 4 and IL-13 production while promoting an inefficient activation of Th1; upregulating arginase activity and the production polyamines, favoring intracellular parasite proliferation. The decrease in pH and increase in temperature and ferrous iron uptake trigger promastigote-to-amastigote differentiation and acidification of the parasitophorous vacuole (where amastigotes will use some nutrients to replicate). Also, uptake of apoptotic infected neutrophils by macrophages (referred as "Trojan horse") potentiates the silencing effect by promoting an anti-inflammatory macrophage state and intracellular parasite replication. DCs that take up parasites or apoptotic infected neutrophils show a decreased capability to generate a CD4+ Th1 (associated to an INF-γ production) and CD8+ T cells response (associated to an INF-γ, TNF-α, perforin and granzyme production) since the infection hampers the migration of those cells to the lymph nodes, increases the production of IL-10 instead of IL-12 and defects the antigen presentation. This figure was created using the Servier Medical Art image portfolio (smart.servier.com).

2.3. Management and Treatment

2.3.1. Current treatments for leishmaniasis

The geographic distribution of leishmaniasis shows that this disease is more prevalent in low-income population of sub-developed regions. The access to ready diagnosis and affordable treatment in these regions is very limited due to economical restrictions, making the control of this disease troublesome despite the great efforts made by WHO and other organizations to reduce prices and increase availability of leishmaniasis medicines [97]. Considering the extensive and well-established knowledge that has been gathered on the understanding of *Leishmania*–host interactions, *Leishmania* pathogenesis and protective immunity [65] (summarized on section 2.2.5) and knowing that healing and recovery from infection develops immunity that protects individuals from re-infection [98], vaccinations appears to be the best cost-effective and safe option for leishmaniasis control. During the years, extensive efforts have been made to search for an effective *Leishmania* vaccine that should ensure a long-lasting immunity to the host due to a well-balanced T cell immune response [99]. So far, there are mainly five different vaccine groups: i) live, ii) first-, iii) second- and iv) third generation and v) vector-derived vaccines [100]. Briefly, contrarily to the live vaccines that are based on the use of live, attenuated and/or drug-sensitive parasites obtained through maintenance of the *in vitro*

cultures for long periods of time or through chemical, radiation or genetic manipulation, first-generation vaccines are made of dead parasites or fractions of them, which elicit an immune response while no pathology is expected, even in immune-compromised individuals. Second-generation vaccines are based on defined antigens (membrane and soluble proteins, peptides and polyproteins) that could be native from parasites or produced through DNA recombinant technology. Third-generation vaccines, also called DNA vaccines, are based on the use of recombinant viral or bacterial vectors. Finally, vector-derived vaccines are based in the use of recombinant or DNA coding for sandfly derived proteins. Many candidates of vaccines were tested in clinic context, being vector-derived vaccines the only exception, but despite the good protective response in some animals or strong possibility of human immunogenicity and safety [100], they were not effective enough and still there is no vaccine for any human leishmaniasis. In turn, chemotherapy is difficult to administer, expensive and becomes ineffective due to the emergence of drug resistance. Yet, this is nowadays the primary method to fight this disease [39]. To date, the current treatments available for the treatment of leishmaniasis mainly includes pentavalent antimonials (SB(V)) (sodium stibogluconate and meglumine antimoniate), amphotericin B (AmB) (in deoxycholate form and lipid formulations), miltefosine, paromomycin and pentamidine [21] (Figure 2.7). These recommended drugs, which are decades old, should be selected based on the patient characteristics (immune status, pharmacokinetics, pharmacogenetics, drug metabolism, adherence to treatment), geographical area, and *Leishmania* species [101-103]. Combined therapy of the referred above drugs is currently considered as an useful approach to control this disease since it allows to increase treatment efficacy, to reduce the treatment duration promoting an increase in the patient compliance and a reduction in the therapy costs, to prevent drug resistance development and to reduce toxicity [104]. Another important factor in the combined therapy is the fact that the used drugs must be of synergistic and additive effect, one with short half-life having strong and immediate effect and the other displaying a retarded action and longer half-life, to ensure that all the parasite burden is removed [105]. For instance, there are some successful combinations of drugs that promote high cure rates, such as sequential treatment with miltefosine and liposomal AmB (AmBisome®) (single dose), that were highly effective against VL in India [106], and sodium stibogluconate and paromomycin, as standard treatment in East Africa [107]. Also, a Phase III study

conducted in India showed that several treatment regimens using combinations of AmBisome®, miltefosine and paromomycin were highly efficacious and safe [108].

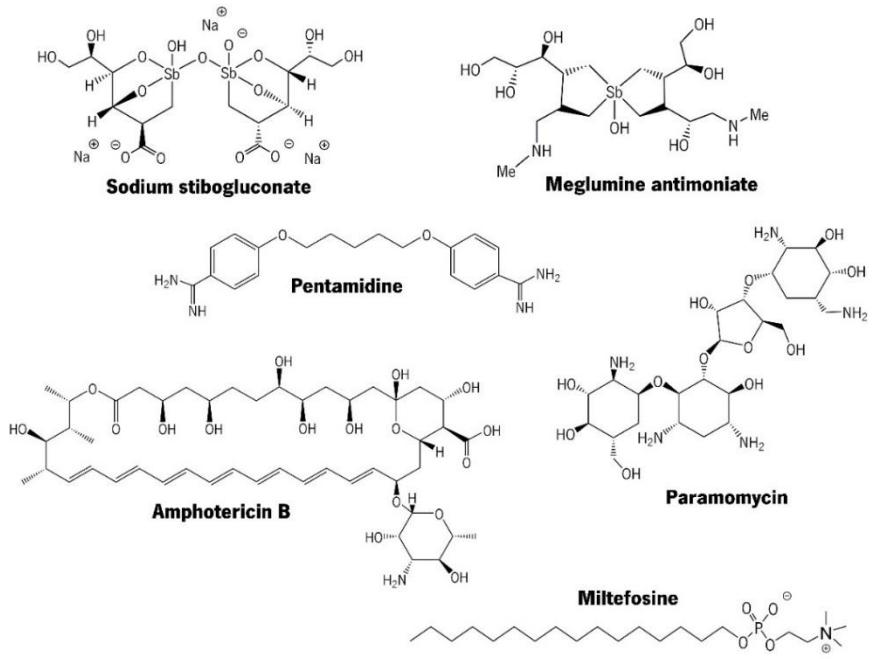

Figure 2.7 – Structure of the drugs most commonly used against leishmaniasis.

2.3.1.1. Pentavalent antimonials

The first-choice drugs recommended by WHO belong to the pentavalent antimonial family (Sb(V)) and have been introduced over 70 years ago. Antimonials are currently available commercially as two organoantimony complexes represented by sodium stibogluconate (Pentostam®) and meglumine antimoniate (Glucantime®) and have been used as key agents in VL (administered through intramuscular or intravenous route) and CL (administered through intralesional route) therapy around the globe [21]. The exact mechanism of action of pentavalent antimonials is still not well understood, despite the long standing clinical use, being associated to i) the biological reduction of the prodrug Sb(V) to the trivalent antimonials (Sb(III)), which is more toxic and can kill the parasite [104]; ii) to the modulation of few macrophage gene expression and some of their encoding proteins [109]; iii) to the inhibition of the activity of the glycolytic and oxidative pathways of the fatty acids [104]; iv) or to the selective action against the topoisomerase of the parasites [110]. However, the utility of this drug has been limited due to severe side effects, such as vomiting, nausea, abdominal pain, arthralgia, myalgia, acute pancreatitis, hepatitis and cardiac arrhythmias and development of resistance [28]. To overcome the treatment failure, pentamidine, paromomycin and amphotericin B, are used as second-line drugs and miltefosine as third-line treatment.

2.3.1.2. Pentamidine

Pentamidine (available as the isethionate salt for human use - Pentacarinat®) is an aromatic diamidine used as second-line treatment for pentavalent antimony-resistant VL in India. Nevertheless, its efficacy declined progressively (cure rates of 70 %) suggesting the emergence of drug resistances [28]. This drug promotes parasite death by modifying the morphology of the kinetoplast, which interferes with the synthesis of *Leishmania* DNA, and by promoting mitochondrial membrane fragmentation [102]. Although pentamidine can be used for all forms of leishmaniasis, its problematic administration by intramuscular or, preferably, intravenous route, low efficacy and toxicity (diabetes mellitus, severe hypoglycemia, myocarditis and renal toxicity) limited its application [21, 102].

2.3.1.3. Paramomycin

Paromomycin (formerly known as aminosidine) is a wide spectrum antibiotic belonging to the aminoglycoside group with a good anti-leishmanial activity, introduced in 2006 [40]. It was demonstrated, in a phase III clinical trial in India, that paromomycin efficacy is not inferior to AmB in the treatment of VL [111]. This drug is the cheapest anti-*Leishmania* compound available today with good efficacy and short duration of administration, it is given intramuscularly, being ototoxicity, elevation of liver enzymes and pain at the injection site the most common adverse effects [112]. Paromomycin is believed to exerts its effects by inferring with ribosomes, inhibiting protein synthesis, and with the mitochondrial membrane, disrupting its potential and promoting a respiratory dysfunction [102, 103].

2.3.1.4. Miltefosine

Miltefosine (Impavido®), a phosphorylcholine ester of hexadecanol (aliphatic long-chain alcohol) initially introduced as anticancer drug, was approved in 2002 as the first (and only, still today), marketed oral drug for the treatment of VL [113]. This drug was highly effective (in both adults and children) and well tolerated, with some side effects - mild to moderate vomiting in 40 % and diarrhea in 20 % of patients and more adverse effects, including toxicity to the gastrointestinal, hepatic, and renal systems in up to 1.5 % of patients. It is also teratogenic, which restricts its use in pregnant women [28, 113]. Despite its efficacy there are some disadvantages that affects the use of miltefosine: the long duration of the treatment (28 days), which lead to a decrease in patient compliance; the long drug half-life (around 150 h), which contributes to the emergence of parasite resistance (associated to a decreased accumulation in the cell due to an increased drug efflux [114]). The mechanism of action is not well understood but involves an apoptosis-like process and

disturbance of lipid-dependent cell signaling pathways, inhibiting phospholipid and sterol biosynthesis [102, 113].

2.3.1.5. Amphotericin B

Amphotericin B (AmB), a polyene macrolite antibiotic firstly isolated from the filamentous bacteria *Streptomyces nodusus*, not only possesses broad antifungal activity but also the most effective anti-leishmanial activity. Currently, AmB is used as first-line treatment in some areas of India, where antimonial resistance has high incidence, and is recommended for VL and MCL leishmaniasis, especially with human HIV co-infection [105, 115, 116]. The mechanism of action is still not fully investigated but it is hypothesized that AmB promotes cell death by interacting with cell membrane sterols - ergosterol and cholesterol - promoting the formation of ionic transmembrane channels. These channels disturb membrane permeability leading to potassium ions and other small molecules/cell components leakage [117]. Notwithstanding the advantages, this therapy is limited since AmB is difficult to solubilize and causes pain after intravenous administration, promote side effects (nausea, fever and chills) and is toxic, mainly to the kidneys (nephrotoxicity), central nervous system and liver (hepatotoxicity) [117, 118].

Deoxycholate-solubilized AmB (Fungizone®), the first parenteral AmB formulation developed, present excellent cure rates (nearly 97 %) after a slow intravenous administration of 0.75-1 mg/kg for 15 to 20 infusions daily or in alternate days. Nevertheless, the administration requires close medical supervision due to high toxicity, namely nephrotoxicity and renal disfunction [28, 118]. To improve the therapeutic efficacy and reduce the toxicity, even at high doses, several marketed lipid-based formulations which differ in lipid composition, shape, size, stability, pharmacokinetics and toxicity [119], were developed. These are: i) liposomal AmB (AmBisome®), spherical liposomes with a mean diameter below 100 nm, composed mainly with AmB, hydrogenated soy phosphatidylcholine, cholesterol and distearoyl phosphatidylglycerol; ii) AmB lipid complex (Abelcet®), ribbon-like structures with sizes between 1-11 μm, composed with AmB and phospholipid (dimyristoyl phosphatidylcholine and dimyristoyl phosphatidylglycerol mixture), and iii) AmB colloidal dispersion (Amphocil® or Amphotec®), thin discoid-like structures with size around 100 nm, composed with AmB and cholesteryl sulfate [120, 121]. All of these formulations were found to be effective, providing a better therapeutic index for the drug [116]. Ambisome® exhibits a shorter circulating half-life and is the best tolerated formulation, despite the reported hypersensitivity reactions [122, 123]. It can be administered at high doses with reduced toxicity to mammalian cells, despite the high accumulation in the liver and spleen. This is possible since the

interaction between AmB and the host cell membrane is decreased due to the presence of cholesterol in the formulation [102]. Ambisome® was approved by Food and Drug Administration (FDA) as an anti-*Leishmania* drug and the disease remission with this formulation goes over 90 %. In fact, in Europe, clinical trials demonstrated 90–98 % efficacy in immunocompetent patients using total dose of 18–21 mg/kg [124], while in India a single dose of 10 mg/kg promote a cure rate of > 95 % [125]. Notwithstanding the fact that Ambisome® remains the most efficient formulation, issues like the instability of liposomes, the need for continuous intravenous injection for successful treatments, treatment duration and high costs come as a downside, limiting its use across the world, especially by the low-income populations of developing countries [115].

2.3.2. Nanostructured delivery systems for leishmaniasis treatment: AmB-based formulations

Drug discovery and development is an expensive process that requires an average of 10-20 years [126]. The development of drugs for parasitic diseases in not attractive for the large multinational pharmaceutical companies, as these diseases are considered to affect only people who cannot afford new pharmaceuticals [10].

Drug delivery system have been the cornerstones to reduce the toxicity of drugs, and to improve the therapeutic efficacy, by increasing the solubility of some anti-*Leishmania* drugs that are poorly water-soluble [127]. In 1906, Paul Ehrlich postulated the concept of “magic bullets” - association of a drug with a carrier in order to reach only the affected area, avoiding side effects [128]. In fact, over the last two decades, nanotechnology has been explored to improve the conventional free-antibiotic delivery for more sustained and targeted drug delivery systems [129], avoiding the need of frequent administrations. New strategies to target *Leishmania*-infected macrophages and delivery AmB are being given a great attention [121, 127, 130-132]. A great challenge to efficiently treat leishmaniasis lies in the fact that the parasites reside in the macrophages [49], which constitutes a protective shield. Nanomedicines can take advantage of the ability of these phagocytic cells to efficiently internalize colloidal particles with size in the range of 50–500 nm [133], releasing their cargo inside the cells [134] and killing the parasites with minimal side effects. This way several advantages are achieved: improved compliance due to lower drug toxicity, enhanced treatment efficacy, controlled release within the therapeutic window and only to target cells, increased drug stability and solubility and modulation of drug pharmacokinetics. These systems should ideally be biodegradable or easily excreted [134]. Different types of drug carriers have been synthesized and used in the controlled delivery of AmB for leishmaniasis treatment, more specifically liposomes, lipid-based delivery systems (including

examples of nanodiscs, Transfersomes, lipid–polymer hybrid micelles, nanoemsulsions (with an example of a self-emulsifying drug delivery systems (SEDDS)) and solid lipid nanoparticles (SLNs)), carbon nanotubes and polymeric nanoparticles (with synthetic and natural matrices), that will be more prominently reviewed in this work [121, 127, 130, 135]. Table 2.2 resumes the important *in vivo* findings of the reviewed AmB delivery systems.

2.3.2.1. Liposomes

Liposomes are small spherical vesicles (mean diameter of 80 to 100 nm) created from cholesterol and phospholipids. Liposomes have been widely studied for leishmaniasis since, as other nanoformulations, they can be formulated in such a way that macrophages targeting is optimized, namely through control of size, charge and surface decoration. Liposomes are able to encapsulate both hydrophilic and hydrophobic drugs (such as AmB, Figure 2.8), enhancing their therapeutic index [135, 136].

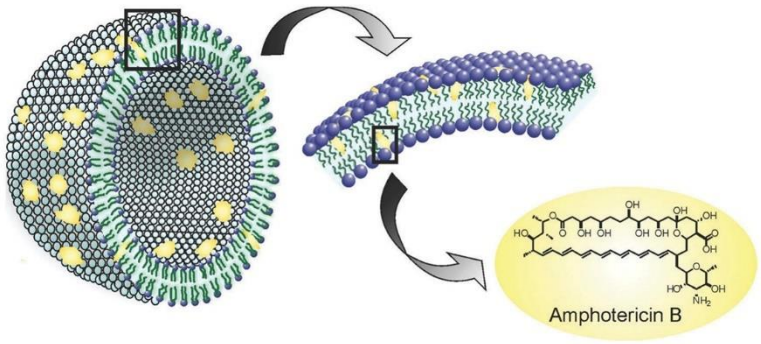

Figure 2.8 – Representation of liposomal formulation of AmB that is composed by a phospholipid bilayer (with a polar head group and non-polar tail) and cholesterol (that acts as a stabilizer). Reproduced from Gutiérrez et al. (2016) [134].

The best example of liposome is AmBisome® (above described), an FDA approved product for the treatment of VL [135]. Different *in vivo* studies showed the capacity of liposome to improve the therapeutic index of AmB. For instance, Berman et al. [137] showed that AmB encapsulated within liposomes at 4 mg/kg per day (administered only three times over 1 week) was able to eliminate more than 98 % of parasites from monkeys. Gangneux et al. [138] showed that administration of AmBisome® in a dosage of 5 or 50 mg/kg of body weight to *L. infantum*-infected BALB/c mice, completely eradicated the parasites from the tissues. Despite the great efficacy, the production cost of AmBisome® is high. The cost reduction could be achieved by identifying alternatives to cholesterol for the formulation of liposomes. Iman et al. [139] showed that a stigmasterol-based liposome containing AmB displayed an *in vitro* anti-leishmanial activity comparable to AmBisome®

with lower hemolytic activity [139, 140]. Furthermore, likely AmBisome®, this new formulation was able to significantly reduce the *in vivo* parasite load in the BALB/c mice spleen at 5 mg/kg multiple intravenous doses [140]. Another liposomal formulation without cholesterol, where AmB is intercalated with ergosterol and phosphatidyl choline (KALSOME™10), was developed. This formulation was shown to be more effective than AmBisome® in promoting the clearance of *L. donovani* parasites through an apoptotic-like cell death after endocytosis by the infected macrophages [141]. Furthermore, treatment of *L. donovani*-infected mice with a double intravenous administration of KALSOME™10 at 7.5 mg/kg resulted in almost complete parasite clearance from both liver and spleen after one month without any sign of nephrotoxicity and hepatotoxicity [142]. Apart from the beneficial properties of the liposomal formulation itself, the risk of side effects promoted by AmB leakage, due to liposomes unstable nature, can be further reduced by promoting surface modification that will increase the specificity of action. For instance, it was demonstrated that AmB-loaded liposomes surface decorated with 4-sulphated acetyl galactosamine [143], tetrapeptide tuftsin [144] or p-aminophenyl-α-D-mannoside [145] displayed an increased *in vivo* specific uptake by macrophages, being the drug more rapidly localized in the liver and spleen, owing to effective macrophage targeting.

2.3.2.2. Lipid-based delivery systems

Lipid-based systems are of great interest for drug delivery as they have capacity to encapsulate poorly-water soluble drugs, are biocompatible and biodegradable, and can be administered through different routes [127].

Nanodiscs, phospholipid bilayer whose periphery is circumscribed by amphipathic apolipoprotein molecules, are a strategy for the generation of AmB-enriched particles. Nelson et al. [146] showed that a AmB-loaded disc-like lipidic carrier (composed of dimyristoyl phosphatidylcholine, dimyristoyl phosphatidylglycerol and lipoproteins) reduced the toxicity of the drug and, after six administrations at 5 mg/kg (delivered at 1 to 10 day intervals over the course of 3 to 5 weeks) was able of clearing the cutaneous *L. major* infection in BALB/c mice.

Transfersomes (TFs) are ultradeformable vesicles made of lipids (phosphatidylcholine lipoid S100), an edge activator (sodium deoxycholate) and a small amount of ethanol. TFs with encapsulated AmB showed *in vivo* efficacy in a cutaneous mice model. Similarly to the antimonials Glucantime (50 mg/kg, once daily), the intralesionally administered formulation (at 0.5 mg/mL, 20 mg of formulation/day) for 10 consecutive days promoted a parasitic load reduction of more than 98 % after 56 days pos-infection [147].

Lipid-polymer hybrid nanoparticles (or micelles), which exhibit complementary characteristics of both polymeric nanoparticles and liposomes, are developed to overcome problems that normally arise for some lipid-based systems, such as disintegration upon parenteral administration and cargo release before reaching the target. Asthana et al. [148] developed an AmB formulation of cationic stearylamine lipid–polymer (poly (D, L-lactide-co-glycolide) (PLGA)) hybrid nanoparticles (AmB-LPNPs) that displayed *in vivo* high macrophage uptake and anti-leishmanial activity against *L. donovani*-infected hamsters (around 89 % parasite inhibition). Furthermore, AmB-LPNPs treatment suppressed Th2 response (reduction in levels of IL-10, IL-4 and TGF-β gene expression) and induced a Th1 response, by upregulating the levels of IL-12, TNF-α and IFN-γ production, and the iNOS pathway.

Nanoemulsions are attractive colloidal particulate carriers for AmB. These stable lipidic systems able to reduce drug-related toxicity, in addition to being inexpensive, submicron in size and easy to manufacture [135, 149]. Caldeira et al. [149] prepared a nanoemulsion containing cholesterol and loaded with AmB and stearylamine that significantly reduced drug toxicity against macrophages comparatively to free-AmB and presented *in vitro* anti-leishmanial efficacy. Another nanoemulsion containing an oil phase composed of medium-chain triglycerides, Tween 80®, cholesterol, butylhydroxytoluene (an antioxidant), and an aqueous phase composed of glycerol and purified water was developed for AmB loading. Administration of this formulation for 5 consecutive days (at same 2 mg/kg) to *L. chagasi*-infected BALB/c mice promoted a significant reduction in liver and spleen parasite burden comparatively to the free-AmB at 1 mg/Kg (safe dose to be used in the animals), without any signs of acute toxicity [150]. In another study, a self-emulsifying drug delivery systems (SEDDS) composed of monoglycerides, diglycerides and vitamin E-TPGS was developed for oral administration. The formulation showed to reduce AmB *in vivo* toxicity, since higher steady state concentrations could be achieved in the tissues after multiple doses, while by promoting a 99 % inhibition of *L. donovani* burden in BALB/c mice (oral administration of 10 mg/kg twice a day for 5 days) [151, 152].

SLNs are nanospheres with less than 1000 nm that consist of a solid lipid matrix stabilized by surfactants. The lipids used are solid at room temperature and most of them have low toxicity. These systems present good biocompatibility, lower cytotoxicity, good production scalability and the possibility to incorporate both hydrophilic and lipophilic drugs. Chitosan-coated SLNs carrying AmB presented a more efficient *in vitro* anti-leishmanial activity against *L. donovani*-infected J774A.1 macrophages, than commercial AmB formulations. Furthermore, cytotoxic evaluation in

J774A.1 cells and acute toxicity study in mice, after intravenous administration at a dose equivalent to 5 mg/kg body weight of AmB, evidenced a good safety profile, since no specific toxicity and degeneration or necrosis was observed [153]. Gupta et al. [154] developed an AmB-loaded tristearin-based SLNs modified with a macrophage-specific ligand *O*-palmytoyl mannan that showed improved *in vitro* anti-leishmanial efficacy against *L. donovani*-infected macrophages comparatively to the non-modified formulation. Furthermore, a higher accumulation of the coated formulation in the macrophage-rich organs (liver and spleen) of rats was observed, and an *in vivo* assay with *L. donovani*-infected hamsters evidenced a better anti-leishmanial activity.

2.3.2.3. Carbon nanotubes

Although still poorly explored, carbon nanotubes, cylindrical hollow molecules consisting of a hexagonal arrangement of carbon atoms, can also be used as AmB carrier for leishmaniasis treatment since their tubular shape offers a high surface area and enables adsorption or conjugation of the drugs [135, 155]. Prajapati et al. [156] functionalized multi-walled carbon nanotube (f-CNTs) with AmB to yield AmB-f-CNTs and showed that the *in vitro* anti-leishmanial efficacy of this formulation against intracellular *L. donovani* amastigotes was significantly higher (almost 14-fold) than that of free-AmB. Furthermore, no toxicity to kidney and liver in BALB/c mice was observed and intraperitoneal administration of AmB-f-CNTs in *L. donovani*-infected hamsters, at 5 mg/kg body weight per day for 5 days, led to a higher percentage suppression of parasites in the spleen (89.8 %) than with AmB (68.9 %). In another study, the same formulation was also orally administered at 15 mg/kg body weight for a 5-day course in *L. donovani*-infected hamsters and promote a 99 % inhibition of parasite growth in the spleen tissue [157]. Despite the potential demonstrated, carbon nanotubes have not been approved for use in humans and may bring issues related to lack of *in vivo* biodegradation [157].

2.3.2.4. Polymeric nanoparticles

Polymeric nanoparticles have been widely used in nanomedicine for the treatment of infectious diseases such as leishmaniasis [118]. Their nanometric size enables cellular uptake upon parenteral administration, increasing the delivery of the therapeutic agents to the host cells/infected tissues. Drug may be loaded in different ways, such as by adsorption, encapsulation, dissolution, entrapment or covalent conjugation. Also, they present low toxicity, are biocompatible and biodegradable, stable, avoid drug leakage into the blood and allow a controlled drug release [118, 135]. Up to now, AmB polymeric-based delivery systems for leishmaniasis treatment have been mostly made of biodegradable polymers [135, 158] including synthetic polymers (e.g. poly

(D, L-lactide-*co*-glycolide) (PLGA) [159-167], poly(ε-caprolactone (PCL) [168]), poly (amino acids) (e.g. polyglutamic acid (PGA) [169]), natural protein (e.g. albumin [170, 171]) and polysaccharides (e.g. chitosan [172-175], alginate [175], arabinogalactan [176-178], dextran [179], pectin [180], gum arabic [181]).

Several research groups have shown the good biodistribution, higher therapeutic efficacy and more importantly, reduced toxicity of the PLGA-based AmB formulations. Costa Lima et al. [159] demonstrated in a *L. infantum*-infected BALB/c mice model that AmB-loaded PLGA nanospheres show a preferential accumulation in the liver and spleen, promoting a burden reduction by approximately 95.9 % and 99 % in the spleen and liver, respectively, after one intravenous administration at 1 mg/kg of AmB, effect that was comparable with that obtained using AmBisome®. Kumar et al. [160] developed AmB-encapsulated PLGA-PEG nanoparticles and proved that administration of 5 mg/kg (for 7 days) of this system to *L. donovani*-infected hamsters promoted a higher amastigote inhibition in the splenic tissue comparatively to free-AmB (93.02 % versus 74.42 %, approximately). With regard to the active targeting approach, surface modified PLGA nanoparticles have been designed to further improve AmB-targeting to macrophages [161-164]. AmB-loaded mannose-grafted PLGA nanoparticles (with a PEG spacer) showed to be effective in decreasing the *in* vitro *L. donovani* burden in infected macrophages, since a more efficient uptake was observed in comparison to free-AmB or to the formulation without the PEG spacer [161]. More recently, Gosh et al. [162] proved that AmB-loaded mannose-modified PLGA nanoparticles are efficacious in the treatment of VL, as intraperitoneal injections for 5 consecutive days (at 1 mg/kg/day) promoted a suppression of the amastigote burden in the spleen of the *L. donovani*-infected BALB/c mice (approximately 98 %). Surface modification of AmB-loaded PLGA nanoparticles with the polysaccharide chitosan [163] or with the glycoprotein lactoferrin [164], also illustrated effective *in vitro* anti-*Leishmania* activity and reduced tissue toxicity due to selective macrophage internalization. In the case of the lactoferrin-modified formulation, a preferential accumulation in liver and spleen and a significant reduction (± 88.6 % compared with AmBisome® (± 68.8 %) and Fungizone® (± 55.6 %)) of the splenic parasite burden of *L. donovani*-infected hamsters after intraperitoneal administration (1 mg/kg/day AmB for 5 consecutive days) was observed. Recent studies also proposed the intralesional administration of AmB- or deoxycholate AmB-loaded PLGA formulations for CL treatment. Their *in vivo* efficacy in *L. amazonensis*-infected BALB/c mice, after a single-dose treatment, was demonstrated [165-167]. Despite the reported anti-leishmanial efficacy, PLGA-based formulations containing AmB present some limitations such

as low drug content, influenced by drug–polymer interaction and drug miscibility in the polymer, slow rate of solvent removal (allowing more time for drug molecules to spread into the aqueous phase and precipitate, resulting in a lower drug entrapment efficiency) [161] and need of organic solvents [127]. The systemic administration of this type of formulations has not been approved for clinical use up to now [182].

Polysaccharides, which are easily obtained from natural sources, arise as ideal candidates for the development of AmB carriers for leishmaniasis treatment. These natural polymers possess a plethora of attractive features that offer a great deal of advantages, including high biocompatibility, lack of toxicity, biodegradability, high water solubility and high abundance associated to relative low cost [183, 184]. More importantly, the use of polysaccharides increases drug solubility and stability, reduces drug toxicity and allows prolonged circulation lifetime and activity [184]. Interestingly, it has also been described that polysaccharides can be recognized by some macrophage receptors (e.g. Toll-like receptor (TLR), scavenger receptor (SR), complement receptor type 3 (CR3), mannose receptor (MR) and mannan binding lectin (MBL) [185]) promoting phagocytosis enhancement, production of ROS, reactive nitrogen species (RNS) and different cytokines. These immunomodulatory effects could be beneficial for leishmaniasis treatment as demonstrated elsewhere for sulphated heterorhamnan, iota-/nu-carrageenans, arabinogalactan and galactomannan polysaccharides [186-188]. Therefore, the development of AmB-polysaccharide formulations might provide a promising approach to improve leishmaniasis treatment, as it increases the safety and activity of the drug while enhancing host cell immunological responses. Ribeiro et al. [172] developed a nanoparticle system for AmB encapsulation, using the positively charged chitosan and the negatively charge chondroitin sulphate. This system allowed to decrease the drug hemolytic activity and toxicity against macrophages (10-fold lower than that of pure AmB) and promoted a reduction of the parasite burden in *L. amazonensis*-infected macrophages (90 %). Asthana et al. [189] developed a stable nanoemulsion template-based chitosan nanocapsules containing AmB, that showed lower *in vitro* toxicity comparatively Fungizone® and AmBisome®. These nanocapsules promoted an *in vivo* parasite reduction of around 86 % in *L. donovani*-infected hamsters, protection that was associated with Th2 to Th1 switching. Mehrizi et al. [173] also showed that AmB-loaded chitosan nanoparticles at 10 mg/kg could considerably inhibit the parasite by 80 % in *L. major*-infected BALB/c mice, without any side effects and toxicity. Chitosan was also chemically modified with oleic acid and mixed with α-cyclodextrin, yielding non-spherical self-assembly structures in water. This system

exhibited intrinsic anti-leishmanial activity and exerted an additive effect when associated with deoxycholate AmB, promoting a healing process in *L. major*-infected BALB/c mice after intralesional injection [174]. Gupta et al. [175] showed that AmB-loaded into sodium alginate-glycol chitosan stearate nanoparticles present an *in vivo* distribution towards *Leishmania* infected organs - spleen and liver - while lesser towards kidney (which explains the reduced toxicity). These formulations promote a parasite inhibition around 70 % after intraperitoneally administered to *L. donovani*-infected hamsters (1 mg/kg dose for 5 consecutive days).

In addition to the above mentioned strategies, another possibility that has been largely used recently, to increase water solubility of AmB, consists in the drug conjugation into the polysaccharide chain network [190]. To achieve AmB-polysaccharide conjugation, mild periodate oxidation (also known as glycol cleavage oxidation), which is a simple and effective method for introduction reactive groups in polysaccharide backbones [191], has been extensively used [176, 178-181]. In this type of catalysis-free reaction, periodate ions attacks vicinal diols in the monosaccharide units of polysaccharides that undergo a carbon–carbon bond cleavage to give two aldehyde groups [191]. Those groups along the polysaccharide backbone serve as reactive chemical anchors for further reaction with drugs possessing amino groups, such as AmB. Golenser et al. [176] have investigated the increase of AmB solubility through its conjugation to arabinogalactan (AG) and its anti-leishmanial activity. The conjugation of AmB to AG was achieved through reductive amination in three steps (Figure 2.9): i) oxidation of AG to obtain di-aldehydes using potassium periodate (KIO_4); ii) conjugation of AmB to oxidized AG *via* Schiff base (imine bond formation); iii) reduction of imine bond to amine bond. It was shown that reduced (rAmB-AG) and unreduced (uAmB-AG) conjugates were effective in decreasing the *in vitro* parasite burden in *L. infantum*-infected macrophages (ED_{50} of 0.035 and 0.027 μg/mL). These formulations presented reduced toxicity in BALB/c mice (maximum tolerated dose (MTD) of 40 and 45 mg/kg for uAmB-AG and rAmB-AG, respectively) [115]. Subcutaneous administration of conjugates prepared in a pilot scale [184], delayed the appearance of lesions two days after BALB/c mice infection with *L. major*, comparatively to the control [176]. The better therapeutic efficacy of the AmB-AG conjugates, comparatively to the commercial formulation Fungizone®, could be explained by the increased production of TNF-α by treated cells and its lower inhibitory effect on lymphocyte stimulation [178].

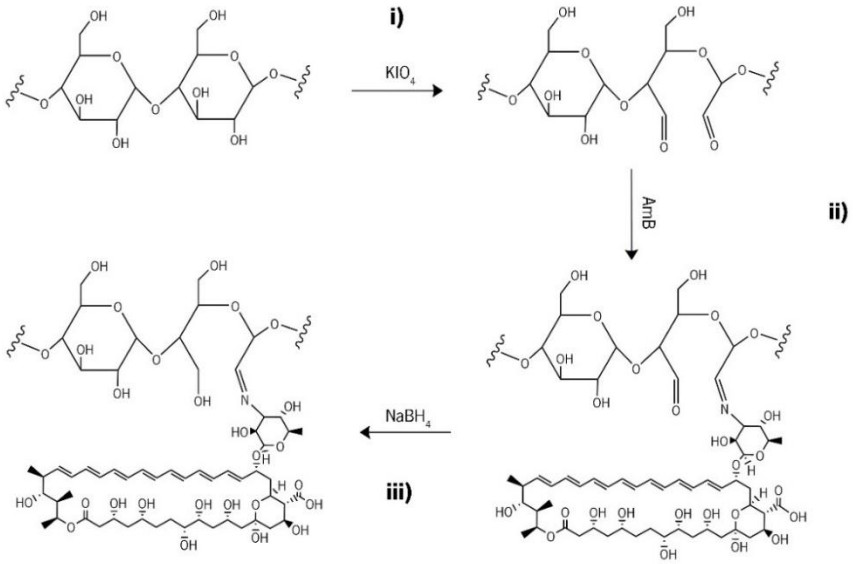

Figure 2.9 – Schematic representation of AmB-AG conjugation *via* **i)** periodate oxidation; **ii)** imine bond formation; **iii)** reductive amination with sodium borohydride ($NaBH_4$) (amine bond formation). Adapted from Volmer et al. (2010) [190].

This type of conjugation was also performed using other polysaccharides. Sokolsky-Papkov et al. [179] conjugated AmB to oxidized dextran through imine bond and, in order to reduce the toxicity of the conjugate against the RAW 264.7 cell line (IC_{50} of 3 μmol/mL aldehydes), modified the remaining aldehyde groups with ethanolamine. The *in vitro* toxicity against macrophages was significantly reduced and, comparatively to free AmB, the conjugate was at least 15 time less hemolytic. Additionally to the lower toxicity, this conjugate was also more effective against *L. major* than the sodium borohydride-reduced conjugate (amine bond) [179]. Other studies proved that pectin-AmB [180] and gum arabic [181] conjugates displayed negligible hemolysis and a good *in vitro* anti-leishmanial activity against promastigotes and amastigotes of *L. donovani* strains. The IC_{50} values for the amine conjugate were slightly superior to the ones obtained for the imine conjugates (probably due the higher stability of the amine linkages that are less prone to hydrolysis) [180, 181]. Regarding the AmB-gum arabic conjugates, mice survived to a dosage of 20 mg/kg of both imine and amine conjugates after intravenous administration, and showed no lesions on kidney, brain, heart or liver. Despite the high molecular weight of the polysaccharide, AmB was still bioavailable since the highest concentration of the drug was found in the rabbits spleen after a single injection at 5 mg/kg [181].

As described above, the literature indicates a notable increase in the AmB-polymer formulations with potential to play a key role in a major shift in treating leishmaniasis. For the majority of the examples using polysaccharides, some chemical modifications are performed. Beyond that type of

formulations, the development of AmB solid dispersions with polysaccharides, that have the capacity to retaining the drug in an amorphous form in the polymeric matrix [192], should be further explored as a simple, economically and feasible approach to obtain water-soluble AmB formulations with activity against leishmaniasis.

Table 2.2 – Examples of AmB delivery system for *in vivo* leishmaniasis treatment.

Formulation	Targeting	Route	Efficacy (*in vivo*)
AmBisome®	-	i.v.	Reduction of hepatosplenic *L. donovani* parasites in monkeys after 3 administrations of 4 mg/kg over one week [137];
			Reduction of *L. infantum* parasites in mice at a dose of 5 or 50 mg/kg. [138].
Stigmasterol-based liposomes	-	i.v.	Reduction of *L. major* parasites in mice from liver and spleen after multiple doses of 5 mg/kg, but less effectively from footpad [140].
Ergosterol-based liposomes	-	i.v.	Suppression of *L. donovani* burden from both liver and spleen of mice after a triple dose of 7.5 mg/kg associated with an immune response shifting from Th2 to Th1 type [142].
4-SO_4GalNAc-modified liposomes	4-sulphated acetyl galactosamine	i.v.	Accumulation of AmB in liver and spleen of rats treated with 1 mg/kg of the formulation, that remained higher in comparison to mannose-based liposomes [143].
Mannosylated liposomes	Mannose (p-aminophenyl-α-D-mannoside)	i.p.	High accumulation of mannosylated liposomes in the liver and spleen of hamsters (single administration at 0.8 mg/kg) and reduction of *L. donovani* parasite burden by 79 % in hamster [145].
Disc-like lipid carrier (apolipoprotein-stabilized phospholipid bilayer)	-	i.p.	Complete clearance of *L. major* parasites from mice after administration of 5 mg/kg (delivered at 1 to 10 day intervals over the course of 3 to 5 weeks) with cure of the footpad lesion [146].
Stearylamine lipid–polymer hybrid nanoparticles	Stearylamine	i.v.; i.p.	High drug allocation in macrophages present in the liver and spleen of rats (dose of 1 mg/kg) and reduction of *L. donovani* parasite burden by 89 % in hamsters after a dose of 1 mg/kg for 5 consecutive days [148].
AmB-TFs	-	Intralesional	Reduction of *L. amazonensis* burden from mice skin by 98 % after administration of 0.5 mg/mL (20 mg of formulation/day) for 10 consecutive days [147].
AmB-loaded NE	-	i.v.	Reduction of *L. chagasi* burden by > 99 % from mice liver and spleen after administration of 2 mg/mL for 5 consecutive days [150].
Lipid-based self-emulsion (monoglycerides, diglycerides and vitamin E-TPGS)	-	Oral	Reduction of *L. donovani* parasite burden by 99 % in mice after a dose of 10 mg/kg twice a day for 5 days and 95 % after 20 mg/kg, once daily for 5 days [152].
Tristearin-based SLNs	Mannan (*O*-palmitoyl mannan)	i.v.; Intracardiac	High accumulation in the liver and spleen of rats (dose of 1 mg/kg) and reduction of splenic *L. donovani* parasite burden by 72 % in hamsters after a dose of 0.5 mg/kg given at day 31 and 33 post infection [154].

AmB-functionalized Carbon nanotubes	-	i.p.	Reduction of renal toxicity in mice (doses of 5 mg/kg, 10 mg/kg and 20 mg/kg) and inhibition of splenic *L. donovani* parasite burden by 89 % in hamsters after a dose of 5 mg/kg per day for 5 days [156];
		Oral	Reduction of splenic *L. donovani* parasite burden by 99 % in hamsters after a dose of 15 mg/kg for 5 days [157].
PLGA nanoparticles	-	i.v.	Accumulation in the liver and spleen of mice (dose of 1 mg/kg) and reduction of *L. infantum* parasite burden in the spleen and liver of mice by 2-$\log_{10}$ with a single dose or 3-daily doses at 1 mg/kg [159].
		Intralesional	Reduction of the lesion area at the base of the *L. major*-infected mice tail after a single dose at 1 mg/kg [166].
PLGA-PEG nanoparticles	-	i.v.	Reduction of splenic *L. donovani* parasite burden by 93% in hamsters after a dose of 5 mg/kg for 7 days [160].
Mannose-modified PLGA nanoparticles	Mannose	i.p.	Formulation displayed 98 % inhibition of splenic *L. donovani* parasite burden in mice at a dose of 1 mg/kg/day given for 5 days [162].
Lactoferrin-appended PLGA nanoreservoirs	Lactoferrin	i.v.; i.p.	Accumulation in the liver and spleen of rats (dose of 1 mg/kg) and reduction of *L. donovani* parasite burden in the spleen of hamsters by 88 % with a dose of 1 mg/kg/day given for 5 days [164].
D-AmB-coated PLGA-DMSA nanoparticles	-	i.p.	Higher reduction of the *L. amazonensis* number in the mice paw after treatment with 6 mg/kg on the 1st, 4th and 7th days and 2 mg/kg on the 10th day, comparatively to the D-AmB (2 mg/kg/day for 10 days) [165].
D-AmB-loaded PLGA nanoparticles	-	Intralesional	A single injection at 0.2 mg/kg in *L. amazonensis*-infected mice (10 days post infection) delayed lesion growth for at least 80 days, being the lesions 37 % smaller and the parasite burdens in the ear and lymph nodes 85 % and 78 % smaller, comparatively to PBS controls and after 120 days of infection. In established 30-day lesions, the same treatment promoted a reduction of the lesion sizes (69 %) and a reduction of parasite burdens in the ear (97 %) and lymph nodes (87 %) [167].
AmB-PGA non-covalent complexes	-	i.v.	Reduction of *L. donovani* parasite burden by 84 and 94 % after a dose of 1.25 or 2.50 mg/kg (formulation with 51 % of AmB-load), respectively, administered in mice for 3 alternate days over a 5-day period [169].
Chitosan nanoparticles	-	i.p.	Inhibition of *L. major* parasite burden by 80 % in mice after 10 mg/kg for 21 days, every other day, with complete footpad wound healing [173].
Nanoemulsion Template-Based Chitosan Nanocapsules (O/W emulsion)	Chitosan (immune-enhancing effects)	i.p.	Inhibition of *L. donovani* parasite burden by 83 % in hamsters at a dose of 1 mg/kg for 5 consecutive days, effect that was a result of effective macrophage uptake and was associated with Th2 to Th1 switching [189].
Chitosan platelets + D-AmB	-	Intralesional	Promotion of an additive effect when associated with D-AmB, leading to a healing process in *L. major*-infected mice with a decrease in inflammatory granuloma and a reduction of the parasitic load [174].
Sodium alginate-glycol chitosan	-	i.v. i.p.	Accumulation in the liver and spleen of rats (dose of 1 mg/kg) and reduction of *L. donovani* parasite

stearate nanoparticles			burden in hamsters by 70 % with a dose of 1 mg/kg/day for 5 consecutive days [175].
AmB-AG conjugates	-	s.c.	Formulation displayed capacity in delaying the appearance of lesions in *L. major*-infected mice tails after treatment with 12 mg/kg, administered six times on alternate days [176].
AmB-Gum arabic conjugates	-	i.v.	Reduction of both imine and amine conjugates toxicity at 20 mg/kg towards mice kidney, brain, heart or liver and accumulation in the rabbits spleen after a single injection at 5 mg/kg [181].

AG – arabinogalactan; AmB - Amphotericin B; D-AmB - deoxycholate amphotericin b; DMSA - dimercaptosuccinic acid; i.p. – intraperitoneal; i.v. – intravenous; s.c. -subcutaneous; NE – nanoemulsion; O/W - oil in water; PEG - poly (ethylene glycol); PGA - poly(α-glutamic acid); PLGA – poly (D, L-lactide-co-glycolide); SLNs – solid lipid nanoparticles; TFs - transfersomes

2.4. References

1. Saker, L., et al., *Globalization and infectious diseases : a review of the linkages / Lance Saker ... [et al.]*. 2004, World Health Organization: Geneva.
2. Tulchinsky, T.H. and E.A. Varavikova, *Chapter 4 - Communicable Diseases*, in *The New Public Health (Third Edition)*, T.H. Tulchinsky and E.A. Varavikova, Editors. 2014, Academic Press: San Diego. p. 149-236.
3. Bloom, D.E. and D. Cadarette, *Infectious Disease Threats in the Twenty-First Century: Strengthening the Global Response.* Frontiers in immunology, 2019. **10**: p. 549-549.
4. Mackey, T.K., et al., *Emerging and reemerging neglected tropical diseases: a review of key characteristics, risk factors, and the policy and innovation environment.* Clinical microbiology reviews, 2014. **27**(4): p. 949-979.
5. Heymann, D.L. and M. Dixon, *Infections at the animal/human interface: shifting the paradigm from emergency response to prevention at source.* Curr Top Microbiol Immunol, 2013. **366**: p. 207-15.
6. Butler, C.D., *Infectious disease emergence and global change: thinking systemically in a shrinking world.* Infectious Diseases of Poverty, 2012. **1**(1): p. 5.
7. Fenwick, A., *The global burden of neglected tropical diseases.* Public Health, 2012. **126**(3): p. 233-236.
8. Engels, D. and X.-N. Zhou, *Neglected tropical diseases: an effective global response to local poverty-related disease priorities.* Infectious Diseases of Poverty, 2020. **9**(1): p. 10.
9. Liese, B., M. Rosenberg, and A. Schratz, *Programmes, partnerships, and governance for elimination and control of neglected tropical diseases.* Lancet, 2010. **375**(9708): p. 67-76.
10. Hotez, P.J., et al., *World neglected tropical diseases day.* PLOS Neglected Tropical Diseases, 2020. **14**(1): p. e0007999.
11. Chami, G.F. and D.A.P. Bundy, *More medicines alone cannot ensure the treatment of neglected tropical diseases.* The Lancet Infectious Diseases, 2019. **19**(9): p. e330-e336.
12. Hotez, P.J., et al., *Control of neglected tropical diseases.* N Engl J Med, 2007. **357**(10): p. 1018-27.
13. Wilson, A.L., et al., *The importance of vector control for the control and elimination of vector-borne diseases.* PLoS neglected tropical diseases, 2020. **14**(1): p. e0007831-e0007831.
14. Hotez, P.J., et al., *Combating tropical infectious diseases: report of the Disease Control Priorities in Developing Countries Project.* Clin Infect Dis, 2004. **38**(6): p. 871-8.

15. Hotez, P.J., *The rise of leishmaniasis in the twenty-first century.* Transactions of The Royal Society of Tropical Medicine and Hygiene, 2018. **112**(9): p. 421-422.
16. Alvar, J., et al., *Leishmaniasis worldwide and global estimates of its incidence.* PloS one, 2012. **7**(5): p. e35671-e35671.
17. Akhoundi, M., et al., *A Historical Overview of the Classification, Evolution, and Dispersion of Leishmania Parasites and Sandflies.* PLoS Negl Trop Dis, 2016. **10**(3): p. e0004349.
18. Steverding, D., *The history of leishmaniasis.* Parasit Vectors, 2017. **10**(1): p. 82.
19. Ashford, R.W., *The leishmaniases as emerging and reemerging zoonoses.* Int J Parasitol, 2000. **30**(12-13): p. 1269-81.
20. Ramirez, J.D., et al., *Taxonomy, diversity, temporal and geographical distribution of Cutaneous Leishmaniasis in Colombia: A retrospective study.* Sci Rep, 2016. **6**: p. 28266.
21. *WHO Expert Committee on the Control of the Leishmaniases & World Health Organization. Control of the leishmaniases: report of a meeting of the WHO Expert Commitee on the Control of Leishmaniases, Geneva, 22-26 March 2010*. World Health Organization: Geneva.
22. Burza, S., S.L. Croft, and M. Boelaert, *Leishmaniasis.* Lancet, 2018. **392**(10151): p. 951-970.
23. Torres-Guerrero, E., et al., *Leishmaniasis: a review.* F1000Res, 2017. **6**: p. 750.
24. Kaye, P. and P. Scott, *Leishmaniasis: complexity at the host-pathogen interface.* Nat Rev Microbiol, 2011. **9**(8): p. 604-15.
25. Dassoni, F., et al., *Leishmaniasis recidivans in Ethiopia: cutaneous and mucocutaneous features.* J Infect Dev Ctries, 2017. **11**(1): p. 106-110.
26. Alvar, J., et al., *Leishmaniasis worldwide and global estimates of its incidence.* PLoS One, 2012. **7**(5): p. e35671.
27. Desjeux, P., *Leishmaniasis: current situation and new perspectives.* Comp Immunol Microbiol Infect Dis, 2004. **27**(5): p. 305-18.
28. Boelaert, M. and S. Sundar, *47 - Leishmaniasis*, in *Manson's Tropical Infectious Diseases (Twenty-third Edition)*, J. Farrar, et al., Editors. 2014, W.B. Saunders: London. p. 631-651.e4.
29. WHO, *The Post-Kala-azar Dermal Leishmaniasis (PKDL) Atlas: A Manual for Health Workers.* 2012.
30. Alvar, J., et al., *Leishmania and human immunodeficiency virus coinfection: the first 10 years.* Clinical microbiology reviews, 1997. **10**(2): p. 298-319.
31. Diro, E., et al., *Visceral Leishmaniasis and HIV coinfection in East Africa.* PLoS Negl Trop Dis, 2014. **8**(6): p. e2869.
32. Monge-Maillo, B., et al., *Visceral leishmaniasis and HIV coinfection in the Mediterranean region.* PLoS Negl Trop Dis, 2014. **8**(8): p. e3021.
33. Saporito, L., et al., *Visceral leishmaniasis: host–parasite interactions and clinical presentation in the immunocompetent and in the immunocompromised host.* International Journal of Infectious Diseases, 2013. **17**(8): p. e572-e576.
34. Conceição-Silva, F., J. Leite-Silva, and F.N. Morgado, *The Binomial Parasite-Host Immunity in the Healing Process and in Reactivation of Human Tegumentary Leishmaniasis.* Frontiers in microbiology, 2018. **9**: p. 1308-1308.
35. David, C.V. and N. Craft, *Cutaneous and mucocutaneous leishmaniasis.* Dermatol Ther, 2009. **22**(6): p. 491-502.
36. Zulfiqar, B., T.B. Shelper, and V.M. Avery, *Leishmaniasis drug discovery: recent progress and challenges in assay development.* Drug Discovery Today, 2017. **22**(10): p. 1516-1531.
37. Couppie, P., et al., *Disseminated cutaneous leishmaniasis due to Leishmania guyanensis: case of a patient with 425 lesions.* Am J Trop Med Hyg, 2004. **71**(5): p. 558-60.
38. Murray, H.W., et al., *Advances in leishmaniasis.* The Lancet, 2005. **366**(9496): p. 1561-1577.

39. Zulfiqar, B., T.B. Shelper, and V.M. Avery, *Leishmaniasis drug discovery: recent progress and challenges in assay development.* Drug Discov Today, 2017. **22**(10): p. 1516-1531.
40. Chappuis, F., et al., *Visceral leishmaniasis: what are the needs for diagnosis, treatment and control?* Nat Rev Microbiol, 2007. **5**(11): p. 873-82.
41. Ready, P.D., *Epidemiology of visceral leishmaniasis.* Clinical epidemiology, 2014. **6**: p. 147-154.
42. Zijlstra, E.E., *PKDL and other dermal lesions in HIV co-infected patients with Leishmaniasis: review of clinical presentation in relation to immune responses.* PLoS neglected tropical diseases, 2014. **8**(11): p. e3258-e3258.
43. Sunter, J. and K. Gull, *Shape, form, function and Leishmania pathogenicity: from textbook descriptions to biological understanding.* Open Biol, 2017. **7**(9).
44. Wheeler, R.J., J.D. Sunter, and K. Gull, *Flagellar pocket restructuring through the Leishmania life cycle involves a discrete flagellum attachment zone.* Journal of Cell Science, 2016. **129**(4): p. 854.
45. Sarkar, A., et al., *Quantification of Intracellular Growth Inside Macrophages is a Fast and Reliable Method for Assessing the Virulence of Leishmania Parasites.* J Vis Exp, 2018(133).
46. Bates, P.A., *Transmission of Leishmania metacyclic promastigotes by phlebotomine sand flies.* Int J Parasitol, 2007. **37**(10): p. 1097-106.
47. Kamhawi, S., *Phlebotomine sand flies and Leishmania parasites: friends or foes?* Trends in Parasitology, 2006. **22**(9): p. 439-445.
48. Bates, P.A., *Revising Leishmania's life cycle.* Nat Microbiol, 2018. **3**(5): p. 529-530.
49. Séguin, O. and A. Descoteaux, *Leishmania, the phagosome, and host responses: The journey of a parasite.* Cellular Immunology, 2016. **309**: p. 1-6.
50. Hirayama, D., T. Iida, and H. Nakase, *The Phagocytic Function of Macrophage-Enforcing Innate Immunity and Tissue Homeostasis.* International journal of molecular sciences, 2017. **19**(1): p. 92.
51. and, D.S. and S. Kamhawi, *Molecular Aspects of Parasite-Vector and Vector-Host Interactions in Leishmaniasis.* Annual Review of Microbiology, 2001. **55**(1): p. 453-483.
52. Iborra, S., et al., *Vaccine candidates against Leishmania under current research.* Expert Rev Vaccines, 2018. **17**(4): p. 323-334.
53. Franco, L.H., S.M. Beverley, and D.S. Zamboni, *Innate immune activation and subversion of Mammalian functions by Leishmania lipophosphoglycan.* J Parasitol Res, 2012. **2012**: p. 165126.
54. Silvestre, R., et al., *Recognition of Leishmania Parasites by Innate Immunity.* Immunology, Endocrine & Metabolic Agents - Medicinal Chemistry, 2009. **9**: p. 106-127.
55. Wilson, M.E. and R.D. Pearson, *Evidence that Leishmania donovani utilizes a mannose receptor on human mononuclear phagocytes to establish intracellular parasitism.* The Journal of Immunology, 1986. **136**(12): p. 4681.
56. Culley, F.J., et al., *C-reactive protein binds to a novel ligand on Leishmania donovani and increases uptake into human macrophages.* J Immunol, 1996. **156**(12): p. 4691-6.
57. Laskay, T., G. van Zandbergen, and W. Solbach, *Neutrophil granulocytes–Trojan horses for Leishmania major and other intracellular microbes?* Trends Microbiol, 2003. **11**(5): p. 210-4.
58. Nylen, S. and S. Gautam, *Immunological perspectives of leishmaniasis.* J Glob Infect Dis, 2010. **2**(2): p. 135-46.
59. Laufs, H., et al., *Intracellular survival of Leishmania major in neutrophil granulocytes after uptake in the absence of heat-labile serum factors.* Infection and immunity, 2002. **70**(2): p. 826-835.
60. van Zandbergen, G., et al., *Cutting Edge: Neutrophil Granulocyte Serves as a Vector for Leishmania Entry into Macrophages.* The Journal of Immunology, 2004. **173**(11): p. 6521.

61. Mittra, B. and N.W. Andrews, *IRONy OF FATE: role of iron-mediated ROS in Leishmania differentiation.* Trends in parasitology, 2013. **29**(10): p. 489-496.
62. Desjardins, M. and A. Descoteaux, *Inhibition of phagolysosomal biogenesis by the Leishmania lipophosphoglycan.* The Journal of experimental medicine, 1997. **185**(12): p. 2061-2068.
63. Real, F., et al., *Cell-to-cell transfer of Leishmania amazonensis amastigotes is mediated by immunomodulatory LAMP-rich parasitophorous extrusions.* Cellular microbiology, 2014. **16**(10): p. 1549-1564.
64. Miles, S.A., et al., *A role for IgG immune complexes during infection with the intracellular pathogen Leishmania.* The Journal of experimental medicine, 2005. **201**(5): p. 747-754.
65. Podinovskaia, M. and A. Descoteaux, *Leishmania and the macrophage: a multifaceted interaction.* Future Microbiol, 2015. **10**(1): p. 111-29.
66. Descoteaux, A. and S.J. Turco, *Glycoconjugates in Leishmania infectivity.* Biochimica et Biophysica Acta (BBA) - Molecular Basis of Disease, 1999. **1455**(2): p. 341-352.
67. Gregory, D.J. and M. Olivier, *Subversion of host cell signalling by the protozoan parasite Leishmania.* Parasitology, 2005. **130 Suppl**: p. S27-35.
68. Lodge, R. and A. Descoteaux, *Phagocytosis of Leishmania donovani amastigotes is Rac1 dependent and occurs in the absence of NADPH oxidase activation.* European Journal of Immunology, 2006. **36**(10): p. 2735-2744.
69. Isnard, A., M.T. Shio, and M. Olivier, *Impact of Leishmania metalloprotease GP63 on macrophage signaling.* Frontiers in cellular and infection microbiology, 2012. **2**: p. 72-72.
70. Gaur, U., et al., *An Effect of Parasite-Encoded Arginase on the Outcome of Murine Cutaneous Leishmaniasis.* The Journal of Immunology, 2007. **179**(12): p. 8446.
71. Liu, D. and J. Uzonna, *The early interaction of Leishmania with macrophages and dendritic cells and its influence on the host immune response.* Frontiers in Cellular and Infection Microbiology, 2012. **2**(83).
72. Basu Ball, W., et al., *Leishmania donovani activates uncoupling protein 2 transcription to suppress mitochondrial oxidative burst through differential modulation of SREBP2, Sp1 and USF1 transcription factors.* The International Journal of Biochemistry & Cell Biology, 2014. **48**: p. 66-76.
73. Dayakar, A., et al., *Cytokines: Key Determinants of Resistance or Disease Progression in Visceral Leishmaniasis: Opportunities for Novel Diagnostics and Immunotherapy.* Front Immunol, 2019. **10**: p. 670.
74. Bronte, V. and P. Zanovello, *Regulation of immune responses by L-arginine metabolism.* Nat Rev Immunol, 2005. **5**(8): p. 641-54.
75. Ricardo-Carter, C., et al., *Leishmania major inhibits IL-12 in macrophages by signalling through CR3 (CD11b/CD18) and down-regulation of ETS-mediated transcription.* Parasite immunology, 2013. **35**(12): p. 409-420.
76. Sutterwala, F.S., et al., *Selective suppression of interleukin-12 induction after macrophage receptor ligation.* The Journal of experimental medicine, 1997. **185**(11): p. 1977-1985.
77. Sutterwala, F.S., et al., *Reversal of proinflammatory responses by ligating the macrophage Fcgamma receptor type I.* The Journal of experimental medicine, 1998. **188**(1): p. 217-222.
78. de Freitas Balanco, J.M., et al., *Apoptotic mimicry by an obligate intracellular parasite downregulates macrophage microbicidal activity.* Curr Biol, 2001. **11**(23): p. 1870-3.
79. Salei, N., et al., *Enhanced survival of Leishmania major in neutrophil granulocytes in the presence of apoptotic cells.* PloS one, 2017. **12**(2): p. e0171850-e0171850.
80. Cunningham, A.C., *Parasitic Adaptive Mechanisms in Infection by Leishmania.* Experimental and Molecular Pathology, 2002. **72**(2): p. 132-141.

81. Iniesta, V., L.C. Gómez-Nieto, and I. Corraliza, *The Inhibition of Arginase by Nω-Hydroxy-l-Arginine Controls the Growth of Leishmania Inside Macrophages.* Journal of Experimental Medicine, 2001. **193**(6): p. 777-784.
82. Wilson, M.E., et al., *The Importance of TGF-β in Murine Visceral Leishmaniasis.* The Journal of Immunology, 1998. **161**(11): p. 6148-6155.
83. Raes, G., et al., *Alternatively activated macrophages in protozoan infections.* Current Opinion in Immunology, 2007. **19**(4): p. 454-459.
84. Rock, K.L., E. Reits, and J. Neefjes, *Present Yourself! By MHC Class I and MHC Class II Molecules.* Trends Immunol, 2016. **37**(11): p. 724-737.
85. Locksley, R.M., et al., *Helper T cells without CD4: control of leishmaniasis in CD4-deficient mice.* Science, 1993. **261**(5127): p. 1448-51.
86. Uzonna, J.E., K.L. Joyce, and P. Scott, *Low dose Leishmania major promotes a transient T helper cell type 2 response that is down-regulated by interferon gamma-producing CD8+ T cells.* J Exp Med, 2004. **199**(11): p. 1559-66.
87. Matheoud, D., et al., *Leishmania Evades Host Immunity by Inhibiting Antigen Cross-Presentation through Direct Cleavage of the SNARE VAMP8.* Cell Host & Microbe, 2013. **14**(1): p. 15-25.
88. Roy, K., et al., *Cholesterol Corrects Altered Conformation of MHC-II Protein in Leishmania donovani Infected Macrophages: Implication in Therapy.* PLoS Negl Trop Dis, 2016. **10**(5): p. e0004710.
89. Chakraborty, D., et al., *Leishmania donovani affects antigen presentation of macrophage by disrupting lipid rafts.* J Immunol, 2005. **175**(5): p. 3214-24.
90. De Souza Leao, S., et al., *Intracellular Leishmania amazonensis amastigotes internalize and degrade MHC class II molecules of their host cells.* J Cell Sci, 1995. **108 (Pt 10)**: p. 3219-31.
91. Campbell, K.A., et al., *CD40 ligand is required for protective cell-mediated immunity to Leishmania major.* Immunity, 1996. **4**(3): p. 283-9.
92. Ato, M., et al., *Defective CCR7 expression on dendritic cells contributes to the development of visceral leishmaniasis.* Nat Immunol, 2002. **3**(12): p. 1185-91.
93. Favali, C., et al., *Leishmania amazonensis infection impairs differentiation and function of human dendritic cells.* J Leukoc Biol, 2007. **82**(6): p. 1401-6.
94. Xin, L., K. Li, and L. Soong, *Down-regulation of dendritic cell signaling pathways by Leishmania amazonensis amastigotes.* Mol Immunol, 2008. **45**(12): p. 3371-82.
95. Figueiredo, A.B., et al., *Leishmania amazonensis impairs DC function by inhibiting CD40 expression via A2B adenosine receptor activation.* European Journal of Immunology, 2012. **42**(5): p. 1203-1215.
96. Gupta, G., S. Oghumu, and A.R. Satoskar, *Mechanisms of immune evasion in leishmaniasis.* Advances in applied microbiology, 2013. **82**: p. 155-184.
97. den Boer, M., et al., *Leishmaniasis impact and treatment access.* Clinical Microbiology and Infection, 2011. **17**(10): p. 1471-1477.
98. Porrozzi, R., et al., *Cross-immunity experiments between different species or strains of Leishmania in rhesus macaques (Macaca mulatta).* Am J Trop Med Hyg, 2004. **71**(3): p. 297-305.
99. Gillespie, P.M., et al., *Status of vaccine research and development of vaccines for leishmaniasis.* Vaccine, 2016. **34**(26): p. 2992-2995.
100. Cecílio, P., F. Oliveira, and A.C.d. Silva, *Vaccines for Human Leishmaniasis: Where Do We Stand and What Is Still Missing? In Leishmaniases as Re-emerging Diseases.* InTech, 2018.
101. Fernández, O.L., et al., *Miltefosine and Antimonial Drug Susceptibility of Leishmania Viannia Species and Populations in Regions of High Transmission in Colombia.* PLOS Neglected Tropical Diseases, 2014. **8**(5): p. e2871.

102. Lindoso, J.A.L., et al., *Review of the current treatments for leishmaniases.* Research and reports in tropical medicine, 2012. **3**: p. 69-77.
103. Kapil, S., P.K. Singh, and O. Silakari, *An update on small molecule strategies targeting leishmaniasis.* Eur J Med Chem, 2018. **157**: p. 339-367.
104. Ghorbani, M. and R. Farhoudi, *Leishmaniasis in humans: drug or vaccine therapy?* Drug Des Devel Ther, 2018. **12**: p. 25-40.
105. Singh, O.P., et al., *Current challenges in treatment options for visceral leishmaniasis in India: a public health perspective.* Infectious diseases of poverty, 2016. **5**: p. 19-19.
106. Sundar, S., et al., *New Treatment Approach in Indian Visceral Leishmaniasis: Single-Dose Liposomal Amphotericin B Followed by Short-Course Oral Miltefosine.* Clinical Infectious Diseases, 2008. **47**(8): p. 1000-1006.
107. Musa, A., et al., *Sodium Stibogluconate (SSG) & Paromomycin Combination Compared to SSG for Visceral Leishmaniasis in East Africa: A Randomised Controlled Trial.* PLOS Neglected Tropical Diseases, 2012. **6**(6): p. e1674.
108. Sundar, S., et al., *Comparison of short-course multidrug treatment with standard therapy for visceral leishmaniasis in India: an open-label, non-inferiority, randomised controlled trial.* The Lancet, 2011. **377**(9764): p. 477-486.
109. El Fadili, K., et al., *Modulation of gene expression in human macrophages treated with the anti-leishmania pentavalent antimonial drug sodium stibogluconate.* Antimicrob Agents Chemother, 2008. **52**(2): p. 526-33.
110. Walker, J. and N.G. Saravia, *Inhibition of Leishmania donovani promastigote DNA topoisomerase I and human monocyte DNA topoisomerases I and II by antimonial drugs and classical antitopoisomerase agents.* J Parasitol, 2004. **90**(5): p. 1155-62.
111. Sundar, S., et al., *Injectable paromomycin for Visceral leishmaniasis in India.* N Engl J Med, 2007. **356**(25): p. 2571-81.
112. Wiwanitkit, V., *Interest in paromomycin for the treatment of visceral leishmaniasis (kala-azar).* Therapeutics and clinical risk management, 2012. **8**: p. 323-328.
113. Dorlo, T.P.C., et al., *Miltefosine: a review of its pharmacology and therapeutic efficacy in the treatment of leishmaniasis.* Journal of Antimicrobial Chemotherapy, 2012. **67**(11): p. 2576-2597.
114. Perez-Victoria, F.J., et al., *Mechanisms of experimental resistance of Leishmania to miltefosine: Implications for clinical use.* Drug Resist Updat, 2006. **9**(1-2): p. 26-39.
115. Ehrenfreund-Kleinman, T., et al., *Synthesis and characterization of novel water soluble amphotericin B–arabinogalactan conjugates.* Biomaterials, 2002. **23**(5): p. 1327-1335.
116. Minodier, P., et al., *Liposomal amphotericin B in the treatment of visceral leishmaniasis in immunocompetent patients.* Fundam Clin Pharmacol, 2003. **17**(2): p. 183-8.
117. Baginski, M., J. Czub, and K. Sternal, *Interaction of amphotericin B and its selected derivatives with membranes: molecular modeling studies.* Chem Rec, 2006. **6**(6): p. 320-32.
118. Bruni, N., et al., *Nanostructured delivery systems with improved leishmanicidal activity: a critical review.* International journal of nanomedicine, 2017. **12**: p. 5289-5311.
119. Adler-Moore, J.P. and R.T. Proffitt, *Amphotericin B lipid preparations: what are the differences?* Clin Microbiol Infect, 2008. **14 Suppl 4**: p. 25-36.
120. Dupont, B., *Overview of the lipid formulations of amphotericin B.* Journal of Antimicrobial Chemotherapy, 2002. **49**(suppl_1): p. 31-36.
121. Lemke, A., A.F. Kiderlen, and O. Kayser, *Amphotericin B.* Appl Microbiol Biotechnol, 2005. **68**(2): p. 151-62.
122. Nath, P., et al., *Immediate hypersensitivity reaction following liposomal amphotericin-B (AmBisome) infusion.* Tropical doctor, 2014. **44**(4): p. 241-242.

123. Mukhtar, M., et al., *First report on Ambisome-associated allergic reaction in two Sudanese leishmaniasis patients.* The American journal of tropical medicine and hygiene, 2011. **85**(4): p. 644-645.
124. Saravolatz, L.D., et al., *Liposomal Amphotericin B for the Treatment of Visceral Leishmaniasis.* Clinical Infectious Diseases, 2006. **43**(7): p. 917-924.
125. Sundar, S., et al., *Single-dose liposomal amphotericin B for visceral leishmaniasis in India.* N Engl J Med, 2010. **362**(6): p. 504-12.
126. Hughes, J.P., et al., *Principles of early drug discovery.* Br J Pharmacol, 2011. **162**(6): p. 1239-49.
127. de Souza, A., et al., *Promising nanotherapy in treating leishmaniasis.* Int J Pharm, 2018. **547**(1-2): p. 421-431.
128. Gaspar, M.M., et al., *Developments on drug delivery systems for the treatment of mycobacterial infections.* Curr Top Med Chem, 2008. **8**(7): p. 579-91.
129. Griffiths, G., et al., *Nanobead-based interventions for the treatment and prevention of tuberculosis.* Nat Rev Microbiol, 2010. **8**(11): p. 827-34.
130. Cuddihy, G., et al., *The Development of Oral Amphotericin B to Treat Systemic Fungal and Parasitic Infections: Has the Myth Been Finally Realized?* Pharmaceutics, 2019. **11**(3): p. 99.
131. Mohamed-Ahmed, A.H., S. Brocchini, and S.L. Croft, *Recent advances in development of amphotericin B formulations for the treatment of visceral leishmaniasis.* Curr Opin Infect Dis, 2012. **25**(6): p. 695-702.
132. Chavez-Fumagalli, M.A., et al., *New delivery systems for amphotericin B applied to the improvement of leishmaniasis treatment.* Rev Soc Bras Med Trop, 2015. **48**(3): p. 235-42.
133. Siefert, A.L., et al., *Immunomodulatory nanoparticles ameliorate disease in the Leishmania (Viannia) panamensis mouse model.* Biomaterials, 2016. **108**: p. 168-176.
134. Gutierrez, V., et al., *New approaches from nanomedicine for treating leishmaniasis.* Chem Soc Rev, 2016. **45**(1): p. 152-68.
135. Saleem, K., et al., *Applications of Nanomaterials in Leishmaniasis: A Focus on Recent Advances and Challenges.* Nanomaterials (Basel), 2019. **9**(12).
136. Date, A.A., M.D. Joshi, and V.B. Patravale, *Parasitic diseases: Liposomes and polymeric nanoparticles versus lipid nanoparticles.* Adv Drug Deliv Rev, 2007. **59**(6): p. 505-21.
137. Berman, J.D., et al., *Antileishmanial activity of liposome-encapsulated amphotericin B in hamsters and monkeys.* Antimicrob Agents Chemother, 1986. **30**(6): p. 847-51.
138. Gangneux, J.P., et al., *Therapy of visceral leishmaniasis due to Leishmania infantum: experimental assessment of efficacy of AmBisome.* Antimicrobial agents and chemotherapy, 1996. **40**(5): p. 1214-1218.
139. Iman, M., et al., *Characterization of the colloidal properties, in vitro antifungal activity, antileishmanial activity and toxicity in mice of a distigmasterylhemisuccinoyl-glycero-phosphocholine liposome-intercalated amphotericin B.* International Journal of Pharmaceutics, 2011. **408**(1): p. 163-172.
140. Iman, M., et al., *Biodistribution and In Vivo Antileishmanial Activity of 1,2-Distigmasterylhemisuccinoyl-sn-Glycero-3-Phosphocholine Liposome-Intercalated Amphotericin B.* Antimicrobial Agents and Chemotherapy, 2017. **61**(9): p. e02525-16.
141. Shadab, M., et al., *Apoptosis-like cell death in Leishmania donovani treated with KalsomeTM10, a new liposomal amphotericin B.* PLOS ONE, 2017. **12**(2): p. e0171306.
142. Asad, M., et al., *Therapeutic and immunomodulatory activities of short-course treatment of murine visceral leishmaniasis with KALSOME™10, a new liposomal amphotericin B.* BMC Infectious Diseases, 2015. **15**(1): p. 188.

143. Singodia, D., et al., *Investigations into an alternate approach to target mannose receptors on macrophages using 4-sulfated N-acetyl galactosamine more efficiently in comparison with mannose-decorated liposomes: an application in drug delivery.* Nanomedicine: Nanotechnology, Biology and Medicine, 2012. **8**(4): p. 468-477.
144. Agrawal, A.K., et al., *Superior chemotherapeutic efficacy of amphotericin B in tuftsin-bearing liposomes against Leishmania donovani infection in hamsters.* J Drug Target, 2002. **10**(1): p. 41-5.
145. Rathore, A., et al., *Mannosylated liposomes bearing Amphotericin B for effective management of visceral Leishmaniasis.* Journal of Liposome Research, 2011. **21**(4): p. 333-340.
146. Nelson, K.G., et al., *Nanodisk-associated amphotericin B clears Leishmania major cutaneous infection in susceptible BALB/c mice.* Antimicrobial agents and chemotherapy, 2006. **50**(4): p. 1238-1244.
147. Fernández-García, R., et al., *Ultradeformable Lipid Vesicles Localize Amphotericin B in the Dermis for the Treatment of Infectious Skin Diseases.* ACS Infectious Diseases, 2020. **6**(10): p. 2647-2660.
148. Asthana, S., et al., *Th-1 biased immunomodulation and synergistic antileishmanial activity of stable cationic lipid-polymer hybrid nanoparticle: biodistribution and toxicity assessment of encapsulated amphotericin B.* Eur J Pharm Biopharm, 2015. **89**: p. 62-73.
149. Caldeira, L.R., et al., *Nanoemulsions loaded with amphotericin B: A new approach for the treatment of leishmaniasis.* European Journal of Pharmaceutical Sciences, 2015. **70**: p. 125-131.
150. Santos, D., et al., *A new nanoemulsion formulation improves antileishmanial activity and reduces toxicity of amphotericin B.* J Drug Target, 2018. **26**(4): p. 357-364.
151. Ibrahim, F., et al., *Pharmacokinetics and tissue distribution of amphotericin B following oral administration of three lipid-based formulations to rats.* Drug Development and Industrial Pharmacy, 2013. **39**(9): p. 1277-1283.
152. Wasan, E.K., et al., *A novel tropically stable oral amphotericin B formulation (iCo-010) exhibits efficacy against visceral Leishmaniasis in a murine model.* PLoS neglected tropical diseases, 2010. **4**(12): p. e913-e913.
153. Jain, V., et al., *Chitosan-Assisted Immunotherapy for Intervention of Experimental Leishmaniasis via Amphotericin B-Loaded Solid Lipid Nanoparticles.* Applied Biochemistry and Biotechnology, 2014. **174**(4): p. 1309-1330.
154. Swati, G., D. Anuradha, and P.V. Suresh, *Development and Characterization of Amphotericin B Loaded Solid Lipid Nanoparticles Against Experimental Visceral Leishmaniasis.* Pharmaceutical Nanotechnology, 2013. **1**(1): p. 54-67.
155. Herlem, G., et al., *Chapter 16 - Carbon Nanotubes: Synthesis, Characterization, and Applications in Drug-Delivery Systems*, in *Nanocarriers for Drug Delivery*, S.S. Mohapatra, et al., Editors. 2019, Elsevier. p. 469-529.
156. Prajapati, V.K., et al., *Targeted killing of Leishmania donovani in vivo and in vitro with amphotericin B attached to functionalized carbon nanotubes.* The Journal of antimicrobial chemotherapy, 2011. **66**(4): p. 874-879.
157. Prajapati, V.K., et al., *An oral formulation of amphotericin B attached to functionalized carbon nanotubes is an effective treatment for experimental visceral leishmaniasis.* The Journal of infectious diseases, 2012. **205**(2): p. 333-336.
158. Banik, B.L., P. Fattahi, and J.L. Brown, *Polymeric nanoparticles: the future of nanomedicine.* WIREs Nanomedicine and Nanobiotechnology, 2016. **8**(2): p. 271-299.

159. Costa Lima, S.A., et al., *Crucial CD8+ T-lymphocyte cytotoxic role in amphotericin B nanospheres efficacy against experimental visceral leishmaniasis.* Nanomedicine: Nanotechnology, Biology and Medicine, 2014. **10**(5): p. e1021-e1030.
160. Kumar, R., et al., *Study the effects of PLGA-PEG encapsulated Amphotericin B nanoparticle drug delivery system against Leishmania donovani.* Drug Delivery, 2015. **22**(3): p. 383-388.
161. Nahar, M. and N.K. Jain, *Preparation, Characterization and Evaluation of Targeting Potential of Amphotericin B-Loaded Engineered PLGA Nanoparticles.* Pharmaceutical Research, 2009. **26**(12): p. 2588.
162. Ghosh, S., et al., *Amphotericin B-loaded mannose modified poly(d,l-lactide-co-glycolide) polymeric nanoparticles for the treatment of visceral leishmaniasis: in vitro and in vivo approaches.* RSC Advances, 2017. **7**(47): p. 29575-29590.
163. Singh, P.K., et al., *Macrophage-targeted chitosan anchored PLGA nanoparticles bearing doxorubicin and amphotericin B against visceral leishmaniasis.* RSC Advances, 2016. **6**(75): p. 71705-71718.
164. Asthana, S., et al., *Targeted chemotherapy of visceral leishmaniasis by lactoferrin-appended amphotericin B-loaded nanoreservoir: in vitro and in vivo studies.* Nanomedicine (Lond), 2015. **10**(7): p. 1093-109.
165. de Carvalho, R.F., et al., *Leishmanicidal activity of amphotericin B encapsulated in PLGA–DMSA nanoparticles to treat cutaneous leishmaniasis in C57BL/6 mice.* Experimental Parasitology, 2013. **135**(2): p. 217-222.
166. Abu Ammar, A., et al., *Amphotericin B-loaded nanoparticles for local treatment of cutaneous leishmaniasis.* Drug Deliv Transl Res, 2019. **9**(1): p. 76-84.
167. Sousa-Batista, A.J., et al., *Novel and safe single-dose treatment of cutaneous leishmaniasis with implantable amphotericin B-loaded microparticles.* International Journal for Parasitology: Drugs and Drug Resistance, 2019. **11**: p. 148-155.
168. Espuelas, M.S., et al., *In Vitro Antileishmanial Activity of Amphotericin B Loaded in Poly(ε-Caprolactone) Nanospheres.* Journal of Drug Targeting, 2002. **10**(8): p. 593-599.
169. Mohamed-Ahmed, A.H.A., et al., *Antileishmanial activity, uptake, and biodistribution of an amphotericin B and poly(α-Glutamic Acid) complex.* Antimicrobial agents and chemotherapy, 2013. **57**(10): p. 4608-4614.
170. Sánchez-Brunete, J.A., et al., *Treatment of experimental visceral leishmaniasis with amphotericin B in stable albumin microspheres.* Antimicrobial agents and chemotherapy, 2004. **48**(9): p. 3246-3252.
171. Casa, D.M., et al., *Bovine serum albumin nanoparticles containing amphotericin B were effective in treating murine cutaneous leishmaniasis and reduced the drug toxicity.* Experimental Parasitology, 2018. **192**: p. 12-18.
172. Ribeiro, T.G., et al., *Novel targeting using nanoparticles: an approach to the development of an effective anti-leishmanial drug-delivery system.* International journal of nanomedicine, 2014. **9**: p. 877-890.
173. Mehrizi, T.Z., et al., *Novel nano-sized chitosan amphotericin B formulation with considerable improvement against Leishmania major.* Nanomedicine (Lond), 2018. **13**(24): p. 3129-3147.
174. Malli, S., et al., *Combination of amphotericin B and chitosan platelets for the treatment of experimental cutaneous leishmaniasis: Histological and immunohistochemical examinations.* Journal of Drug Delivery Science and Technology, 2019. **50**: p. 34-41.
175. Gupta, P.K., et al., *Self Assembled Ionically Sodium Alginate Cross-Linked Amphotericin B Encapsulated Glycol Chitosan Stearate Nanoparticles: Applicability in Better Chemotherapy and Non-Toxic Delivery in Visceral Leishmaniasis.* Pharmaceutical Research, 2015. **32**(5): p. 1727-1740.

176. Golenser, J., et al., *Efficacious treatment of experimental leishmaniasis with amphotericin B-arabinogalactan water-soluble derivatives.* Antimicrobial agents and chemotherapy, 1999. **43**(9): p. 2209-2214.
177. Ehrenfreund-Kleinman, T., J. Golenser, and A.J. Domb, *Conjugation of amino-containing drugs to polysaccharides by tosylation: amphotericin B-arabinogalactan conjugates.* Biomaterials, 2004. **25**(15): p. 3049-57.
178. Ehrenfreund-Kleinman, T., et al., *The effect of amphotericin b derivatives on Leishmania and immune functions.* J Parasitol, 2005. **91**(1): p. 158-63.
179. Sokolsky-Papkov, M., A.J. Domb, and J. Golenser, *Impact of Aldehyde Content on Amphotericin B–Dextran Imine Conjugate Toxicity.* Biomacromolecules, 2006. **7**(5): p. 1529-1535.
180. Kothandaraman, G.P., et al., *Anti-fungal and anti-leishmanial activities of pectin-amphotericin B conjugates.* Journal of Drug Delivery Science and Technology, 2017. **39**: p. 1-7.
181. Nishi, K.K., et al., *Amphotericin B-Gum Arabic Conjugates: Synthesis, Toxicity, Bioavailability, and Activities Against Leishmania and Fungi.* Pharmaceutical Research, 2007. **24**(5): p. 971-980.
182. Palma, E., et al., *Antileishmanial Activity of Amphotericin B-loaded-PLGA Nanoparticles: An Overview.* Materials (Basel, Switzerland), 2018. **11**(7): p. 1167.
183. Desbrieres, J., et al., *10 - Chemically Modified Polysaccharides With Applications in Nanomedicine*, in *Biomass as Renewable Raw Material to Obtain Bioproducts of High-Tech Value*, V. Popa and I. Volf, Editors. 2018, Elsevier. p. 351-399.
184. Ickowicz, D.E., et al., *Activity, reduced toxicity, and scale-up synthesis of amphotericin B-conjugated polysaccharide.* Biomacromolecules, 2014. **15**(6): p. 2079-89.
185. Leung, M.Y.K., et al., *Polysaccharide biological response modifiers.* Immunology Letters, 2006. **105**(2): p. 101-114.
186. Kangussu-Marcolino, M.M., et al., *Acid heteropolysaccharides with potent antileishmanial effects.* International Journal of Biological Macromolecules, 2015. **81**: p. 165-170.
187. Adriazola, I.O., et al., *Macrophage activation and leishmanicidal activity by galactomannan and its oxovanadium (IV/V) complex in vitro.* Journal of Inorganic Biochemistry, 2014. **132**: p. 45-51.
188. Amaral, A.E.d., et al., *Leishmanicidal activity of polysaccharides and their oxovanadium(IV/V) complexes.* European Journal of Medicinal Chemistry, 2015. **90**: p. 732-741.
189. Asthana, S., et al., *Immunoadjuvant Chemotherapy of Visceral Leishmaniasis in Hamsters Using Amphotericin B-Encapsulated Nanoemulsion Template-Based Chitosan Nanocapsules.* Antimicrobial Agents and Chemotherapy, 2013. **57**(4): p. 1714.
190. Volmer, A.A., A.M. Szpilman, and E.M. Carreira, *Synthesis and biological evaluation of amphotericin B derivatives.* Nat Prod Rep, 2010. **27**(9): p. 1329-49.
191. Pereira, I., et al., *Effects of gamma irradiation and periodate oxidation on the structure of dextrin assessed by mass spectrometry.* European Polymer Journal, 2018. **103**: p. 158-169.
192. Mehenni, L., et al., *Preparation and Characterization of Spherical Amorphous Solid Dispersion with Amphotericin B.* Pharmaceutics, 2018. **10**(4).

CHAPTER 3 - DEVELOPMENT OF DEXTRIN-AMPHOTERICIN B FORMULATIONS FOR THE TREATMENT OF LEISHMANIASIS

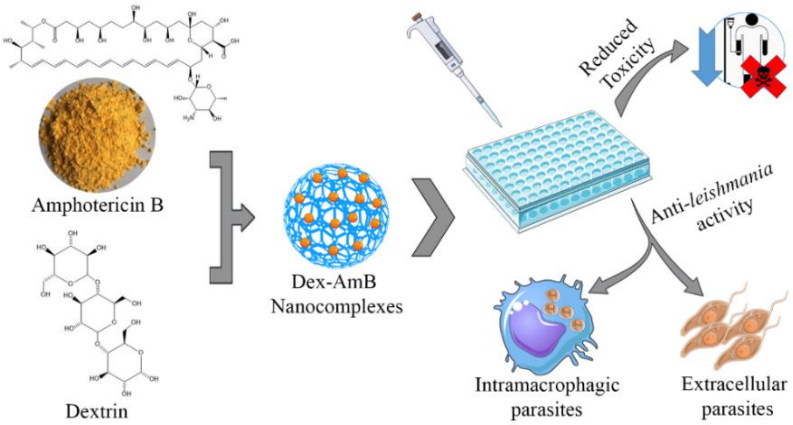

The most effective medicines available for the treatment of leishmaniasis, a life-threatening disease, exhibits serious toxicological issues. To achieve better therapeutic efficiency while decreasing toxicity associated with amphotericin B (AmB), water-soluble dextrin-AmB (Dex-AmB) formulations were developed. Self-assembled nanocomplexes were formed by dissolving Dex and AmB in alkaline borate buffer, followed by dialysis and either freeze-drying (FD) or nano spray-drying (SD), yielding water dispersible particles with a diameter of 214 nm and 348 nm, respectively. The very simple production process allowed the formation of amorphous inclusion complexes containing 14 % of AmB in the form of monomers and water-soluble aggregates. Nanocomplexes were effective against parasites in axenic culture (IC_{50} of 0.056 and 0.096 μM for *L. amazonensis* and 0.030 and 0.044 μM for *L. infantum*, respectively for Dex-AmB FD and Dex-AmB SD) and in decreasing the intramacrophagic infection with *L. infantum* (IC_{50} of 0.017 and 0.023 μM, respectively for Dex-AmB FD and Dex-AmB SD). Also, the formulations were able to significantly reduce the cytotoxicity of AmB. Overall, this study demonstrates the suitability of dextrin as an AmB carrier and the facile and inexpensive development of a delivery system for the treatment of leishmaniasis.

Adapted from Silva-Carvalho, R. et al. (2020). International journal of Biological Macromolecules, 153, 276-288.

3.1. Introduction

Leishmaniasis has been classified as one of the most neglected tropical morbidity and mortality causing diseases [1]. In fact, about 12-15 million people are currently infected and 350 million people in 89 countries mainly in tropical and subtropical areas live at risk of developing one of the many forms of the disease [1-3]. Protozoan parasites of the genus *Leishmania*, which are responsible for this life-threatening disease [4], can maintain their life cycle through transmission between two forms: the extracellular motile promastigote that multiplies in the gut of *Phlebotomus* and/or *Lutzomyia* sandflies [4, 5], and the intracellular non-motile amastigote which replicates inside macrophages of mammalian hosts [6]. These parasites can cause a plethora of pathological manifestations such as cutaneous, mucocutaneous or diffuse cutaneous leishmaniasis, characterized by localized symptoms in the skin or mucosal surfaces. Other *Leishmania* species that are more aggressive, target internal organs causing visceral leishmaniasis (associated to approximately 70,000 deaths per year) [2, 6].

Despite the well-established knowledge and the recent advance in our understanding of leishmaniasis biology, some aspects of this disease remain enigmatic and the current control or treatment strategies are rather inadequate [6, 7]. This is due both to limited availability of effective parenteral drug formulations and constant appearance of resistant parasites. Besides, as there are currently no effective vaccines to prevent human leishmaniasis, the cure relies on chemotherapy, using drugs of high toxicity, low efficacy and difficult to administer due to low solubility [2, 8]. Amphotericin B (AmB) interacts with cell membrane sterols promoting cell death [9-11]. This drug is recommended as a second-line treatment for visceral and mucocutaneous leishmaniasis, but it presents toxicity and side effects mainly related to the kidneys, central nervous system and liver [8]. Strategies to overcome these shortcomings, such as combination therapy, modification of AmB or drug delivery systems have been the cornerstones to improve the therapeutic efficacy and reduce the toxicity. Some marketed AmB-based products are available (e.g., Fungizone® and Ambisome®) which, despite higher efficiency, still raise concerns regarding toxicity and high production costs [8, 12]. Therefore, it is of urgent need the development of alternative effective strategies to facilitate use of AmB for leishmaniasis treatment.

Different polymers have been widely used as drug carriers [13]. In fact, polysaccharides (e.g., arabinogalactan [8, 14, 15], dextran [16, 17], gum arabic [18], sodium alginate [19], pectin [20], galactomannan [21]) and synthetic polymers (e.g. polymannose [22] and polyglucose [23]) bearing high water-solubility, low toxicity, a high degree of biodegradability and biocompatibility [15], have attracted considerable attention in recent years for producing water-soluble polymer-drug formulations. Besides drug targeting, the use polysaccharides enhances drug solubility and stability, allowing prolonged

circulation lifetime and activity and reduction of drug toxicity [8]. Nevertheless, most of the polysaccharide-based AmB formulations reported in literature are prepared by reductive amination where polysaccharides are oxidized to render di-aldehyde derivatives reactive with AmB via Schiff base (imine bond) or via amine bond (reduction) [14]. In this work, we hypothesize that dextrin, a class of low molecular weight carbohydrates, may be used for development of an AmB drug delivery system as it is biocompatible, non-immunogenic and degradable *in vivo* by amylases [24]. Further, we demonstrate that time consuming and complex steps involving a pre-oxidation of the polysaccharides are not required to obtain a polysaccharide-AmB formulation. We show that by simply mixing and processing new water-soluble dextrin-amphotericin B (Dex and AmB) in a freeze-drier or spray-dyer, Dex-AmB nanocomplexes with a promising role in the treatment of leishmaniasis can be produced.

3.2. Materials and Methods

3.2.1. Reagents

Amphotericin B (AmB, molecular weight of 924.08 g/mol) powder from Streptomyces sp., resazurin Sodium salt, 4',6-diamidino-2-phenylindole (DAPI), triton X-100, paraformaldehyde, Schneider's Insect medium, sodium tetraborate decahydrate, potassium bromide, phenol red and hemin were purchased from Sigma-Aldrich (Missouri, USA). Dextrin Tackidex® (medical grade dextrin from potato starch) with a degree of polymerization (DP) of 16 glucose residues and a branching degree of 9 % was a gift from Roquette (Lestrem, France). Dulbecco's Modified Eagle Medium (DMEM), fetal bovine serum (FBS) and penicillin-streptomycin were obtained from Merck Millipore (Massachusetts, USA). Roswell Park Memorial Institute (RPMI) 1640 Glutamax supplemented medium and L-glutamine (GlutaMAX™-I) was purchased from Gibco (Massachusetts, USA). Dimethylsulfoxide (DMSO ATCC® 4-X™) solution for cell culture was acquired from American Type Culture Collection (ATCC, Virginia, USA). Dialysis tubing with a molecular weight cut-off of 1000 Da was obtained from Orange Scientific (Braine-l'Alleud, Belgium). High-content screening (HCS) CellMask™ Deep Red stain was acquired from Invitrogen (California, USA). Acetonitrile and Formic acid were purchased from Fisher Scientific (New Hampshire, USA).

3.2.2. Dextrin-Amphotericin B production

Before the procedure, 1.5 g of dextrin (apparent molecular weight of 4.5 kDa [24]) was diluted in distilled water (dH_2O) at a concentration of 10 mg/mL, dialyzed using a dialysis membrane with a molecular weight cut-off 1000 Da against dH_2O for 72 h and then freeze-dried. Freeze-dried dextrin (Dex) was mixed with amphotericin B (AmB) in a mass ratio of 4:1 and dissolved in 32 mL of 0.1 M

borate buffer (pH 11), resulting in a final concentration of 2.5 mg/mL of AmB in the solution. The mixture, protected from light, was gently stirred at 4 °C for 48 h and then dialyzed at 4 °C against dH_2O using a membrane with a molecular weight cut-off 1000 Da. During this process, the pH was kept at ± 6. Afterward, the solution was freeze-dried (Coolsafe 100-9 Pro, Labogene, Allerød, Denmark) to obtain a yellow-orange material (Dex-AmB FD) or processed in a Nano Spray Dryer B-90 HP (Büchi Labortechnik AG, Flawil, Switzerland), yielding a yellow-orange powder (Dex-AmB SD). Briefly, in the latter case the solution was fed into the instrument by a peristaltic pump and sprayed using a piezoelectric nebulizer, operated at a vibrational frequency of 120 kHz, with mean micron-sized pores of 2-25 µm. The feeding rate was set to 40 %, where the gas flow rate was adjusted at 10 L/min. The inlet temperature was 120 °C. The obtained powder was separated, collected from the drying chamber and stored at 4 °C in a recipient containing silica gel. Dex without AmB was also processed by freeze-drying (Dex FD) or nano spray-drying (Dex SD), to be tested as control.

3.2.3. Dex-AmB Characterization

3.2.3.1. Nanoparticle Tracking Analysis (NTA)

Size of the nanocomplexes was measured by the laser-scattering technique Nanoparticle Tracking Analysis (NTA) using a NanoSight NS 500 (Malvern Instruments Ltd., Worcestershire, UK) equipped with a sample chamber and a 640 nm laser. The produced material was dissolved at 1 mg/mL in dH2O. The solutions (0.3 mL) were introduced in the sample chamber and analyzed for 60 s, using manual shutter and gain adjustments. Measurements were performed in triplicate at room temperature and the NTA 2.3 Build 0017 software (Malvern) was used to collect the data.

3.2.3.2. Zeta potential

The zeta potential of Dex-AmB nanocomplexes was estimated by Dynamic Light Scattering (DLS) using a Zetasizer NanoZS, (Malvern Instruments Ltd., Worcestershire, UK). Three measurements of each solutions were performed and the zeta potential values were determined using Henry's equation [25].

3.2.4. Morphology Analysis

3.2.4.1. Scanning Electron Cryomicroscopy (Cryo-SEM)

Dex-AmB nanocomplexes were dispersed in dH_2O at a concentration of 2 mg/mL and rapidly cooled plunging it into sub-cooled nitrogen. The samples were transferred under vacuum to the cryo stage (Gatan, Alto 2500, UK) and then fractured and sublimated for 120 s at -90 °C to remove the superficial ice layer and allow the exposure of the nanocomplexes. Then, the samples were

sputter-coated with gold and palladium for 45 s and transferred to the observation chamber of an electron microscope (SEM/EDS: JEOL JSM 6301F/Oxford Inca Energy 350 from the Laboratory for Scanning Electron Microscopy and X-Ray Microanalysis at Materials Centre of the University of Porto (CEMUP)). The observation was performed at -150 °C and 15 kV.

3.2.4.2. Scanning Electron Microscopy (SEM)

The powder material produced in the nano spray dryer was observed using a scanning electron microscopy (SEM; FEI Quanta 650 FEG Environmental, Field Electron and Ion Company, Oregon, USA). Samples were fixed using a double-sided electrically conductive carbon adhesive tape (PELCO Tabs™, California, USA) on an aluminum pin stub and then sputter coated with a 20 Å gold layer. Images were obtained at an excitation voltage of 5 kV.

3.2.5. HPLC-PDA-MS Analysis

The HPLC system Finnigan LXQ from ThermoElectron Corporation (Thermo Fisher Scientific, Massachusetts, USA) equipped with a Surveyor Autosampler (Thermo fisher Scientific, Massachusetts, USA) was used to quantify the AmB content in the produced materials. The analytical column used was a Kinetex® C18 100 Å 100 x 4.6 mm (2.6 µm particle size) from Phenomenex (California, USA) and the analysis was performed using an ion trap Mass Spectrometer (MS) equipped with an ElectroSpray Ionization (ESI) source (Thermo Fisher Scientific, Massachusetts, USA) and a 2998 photodiode array (PDA) wavelength detector (Waters Corporation, Massachusetts, USA). The MS analysis was operated using Selected Ion Monitoring (SIM) Mode with scan ranges from 923 to 925 m/z, and the instrument was operated in positive ionization mode. The UV detection wavelengths were defined to 387 and 408 nm. The mobile phase was composed by two filtered and degassed solvents: (A) ultrapure water with 0.1 % (v/v) formic acid and (B) acetonitrile with 0.1 % (v/v) formic acid. The solvent gradient started with 80 % A and 20 % B, reaching 10 % A and 90 % B at 15 min and 80 % A and 20 % B at 25 min, condition that was maintained until the end of the analysis. The run time was 30 min, with a flow rate of 0.3 mL/min and the analysis was performed at a 25 °C with a sample injection volume of 25 µL. Moreover, the source dependent parameters such as Sheath Gas flow rate, Auxiliar Gas flow rate, Sweep Gas flow rate, Tube Lens, Capillar Voltage, Capillar Temperature and Spray Voltage were optimized to 50, 10, 10, 115 V, 29 V, 250 °C and 5000 V, respectively. All spectral data was acquired and analyzed using Xcalibur Chromatography Software (Thermo Fisher Scientific, Massachusetts, USA).

The stock standard solution of AmB (150 µg/mL) and Dex-AmB nanocomplexes (3 mg/mL) were prepared by dissolving 6 and 9 mg of each material in 40 and 3 mL of acetonitrile:ultrapure

water:formic acid (39.22:58.33:2.45 % (v/v)) respectively, under mild stirring and protected from light during 2 h at room temperature. Subsequently, the calibration curves were obtained using seven standard solutions for the MS analysis - 2, 5, 10, 20 60, 80 and 120 µg/mL - and five standard solutions for the UV analysis - 0.5, 1, 2, 10 and 20 µg/mL - and were prepared from the stock standard solution using acetronitrile:ultrapure water (39.22:60.78 % (v/v)). Similarly, for the Dex-AmB nanocomplexes, solutions of 25, 50 and 100 µg/mL were prepared using the above-mentioned solvent. Prior to injection, standards and samples were filtered through a 0.22 µm pore size Nylon filter (Tecnocroma, Caldas da Rainha, Portugal). A linear regression was used to determine slopes, intercepts and correlation coefficients. The percentage of drug association efficiency (AE%) as well as the drug content (% w/w) in the produced nanocomplexes were determined using the following equations 1 and 2, respectively:

$$AE\ (\%) = \frac{m_{AmB}}{m_{AmB\_initial}} \times 100 \quad (1)$$

$$AmB\ Content\ (\%) = \frac{m_{AmB}}{m_{Dex-AmB}} \times 100 \quad (2)$$

Where $m_{AmB\_initial}$ is the initial mass of AmB used in the process, m_{AmB} is the AmB mass in the final formulation that was obtained via HPLC-MS and HPLC-PDA analysis and $m_{Dex-AmB}$ is the final mass of the produced material.

3.2.6. Fourier-transform infrared spectroscopy (FTIR)

FTIR spectroscopic studies of free-AmB, Dex FD, Dex SD, Dex-AmB FD and Dex-AmB SD were carried out employing an ABB Bomem FTLA2000-104 spectrophotometer (Québec, Canada). About 2 mg of the different samples was mixed with 200 mg of dry potassium bromide to obtain a solid pellet. Samples were examined at transmission mode and 64 scans were co-added for each spectrum over a wavenumber range of 4000-700 cm^{-1}.

3.2.7. Differential scanning calorimetry (DSC)

DSC thermograms of AmB, Dex FD, Dex SD, Dex-AmB FD and Dex-AmB SD were obtained by using a DSC 600 Perkin-Elmer (Massachusetts, USA). An empty aluminum pan was used to calibrate the apparatus. A known amount of samples equivalent to 0.7 mg of AmB were weighed and hermetically sealed in standard aluminum pans. Samples were scanned from 25-235 °C at a ramp speed of 10 °C/min under nitrogen purge with a flow rate of 20 mL/min. All samples were analyzed in triplicate.

3.2.8. Powder X-ray diffraction (XRD)

XRD patterns of the dried samples (AmB, Dex FD, Dex SD, Dex-AmB FD and Dex-AmB SD) were recorded using a PANalytical X'Pert Pro X-ray diffractometer equipped with X'Celerator detector and secondary monochromator (Malvern Panalytical, United Kingdom). For the analysis, the samples were placed in a Bragg-Brentano geometry and scanned from 7° to 50° 2θ angular range using a Cu Kα radiation (40 kV operating voltage; 30 mA current).

3.2.9. Spectrophotometric analysis of Dex-AmB nanocomplexes

AmB and Dex-AmB nanocomplexes were analyzed by UV-vis spectroscopy in the range of 300-450 nm using a UV-visible spectrophotometer (JASCO V-560 series, Jasco Inc., Maryland, USA) operated at a band width of 5 nm, data pitch of 1 nm and scanning speed of 400 nm/min. The nanocomplexes were dissolved in dH_2O at the final AmB concentration of 144 μM (1 $mg_{nanocomplex}$/mL) and then, to avoid spectrum saturation, samples were diluted to 10 μM using dH_2O. A stock solution of AmB at 1082 μM (1 mg/mL) was prepared using 0.1 M borate buffer pH 11. Then, as performed for the nanocomplexes, this solution was diluted to 10 μM using dH_2O. A volume of 200 μL of the solutions was used for the measurements in a quartz cuvette. The ratio of the absorbance of peak I (315-350) to the peak IV (408-410) was used to monitor the aggregation state of AmB.

3.2.10. *In vitro* assays

3.2.10.1. Culture of *Leishmania* parasites

Leishmania infantum promastigotes (MHOM/MA/67/ITMAP-263) were cultured in RPMI 1640 Glutamax supplemented with 10 % (v/v) iFBS, 50 U/mL penicillin, 50 μg/mL streptomycin and 20 mM HEPES pH 7.4 (complete RPMI medium). *Leishmania amazonensis* promastigotes (MHOM/BR/LTB0016) were cultured in Schneider's Insect medium supplemented with 10 % (v/v) heat inactivated FBS (iFBS), 100 U/mL penicillin, 100 μg/mL streptomycin, 5 mM HEPES pH 7.4 and 5 μg/mL phenol red (complete Schneider's insect medium). Both parasite strains were cultured at 25 °C. Infectivity was secured as previously described by Gomes-Alves, et al. [26].

Axenic amastigotes of *L. infantum* were obtained as described in the literature [27]. Axenic *L. infantum* amastigotes were derived from the above referred strain by maintaining the culture at 37 °C with 5 % CO_2 in MAA/20 medium (medium for axenically grown amastigotes) supplemented with 20 % (v/v) iFBS, 2 mM L- Glutamine and 0.023 mM hemin. Purity, assessed by microscopy on the basis of morphology (round and immobile organisms, about 2-3 μm and without visible flagella), was around 95 %.

3.2.10.2. Effect of Dex-AmB against axenic parasite cultures

L. infantum (3 days culture) and *L. amazonensis* (5 days culture) axenic promastigotes, at a late exponential phase of growth, were seeded in 96-well plates using complete RPMI medium or complete Schneider's Insect medium, respectively, at a density of 3 x 10^5 cells/well. Then, increasing concentrations of free-AmB, Dex FD and SD and Dex-AmB FD and SD (0.0029, 0.0059, 0.0117, 0.0234, 0.0469, 0.0938, 0.1875, 0.375 and 0.75 μM), previously sterilized by ethylene oxide for 15 h at 53 ± 1 °C, were added to the wells and the plates were incubated for 24 h at 26 °C. Parasite viability was assessed by resazurin assay. Briefly, 20 μL of a 2.5 mM resazurin solution freshly prepared in phosphate buffer saline pH 7.4 and filtered using sterile 0.22 μm pore filters was added to each well and then the plates were incubated for 24 h at 26 °C. Fluorescence intensity was measured (λex 560/λem 590) in a SpectraMAX GeminiXS microplate reader (Molecular Devices LLC, California, USA). The results were expressed as the mean percentage ± SD of viable parasites relatively to control condition (considered as 100 % viability). The half maximal inhibitory concentration (IC_{50}) was calculated by nonlinear regression analysis using the GraphPad Prism software. The assay was performed in triplicate at least three times.

3.2.10.3. Cell lines and cell culture

Mouse fibroblast L929 cell line was purchased from American Type Culture Collection (ATCC, Virginia, USA), Human brain microvascular endothelial cell line (HBMEC) was kindly provided by Dr. Rui M. Reis (ICVS/3B's-PT Government Associate Laboratory, Braga, Portugal and Barretos Cancer Hospital, São Paulo, Brazil) and Human embryonic kidney (HEK293T) cell line was kindly provided by Dr. Tiago dos Santos (i3S - Instituto de Investigação e Inovação em Saúde, Universidade do Porto, Portugal; INEB - Instituto de Engenharia Biomédica, Universidade do Porto, Portugal). Both cell lines were maintained in Dulbecco's modified essential medium (DMEM) supplemented with 10 % (v/v) iFBS and 1 % (v/v) Penicillin (10000 U/mL)-Streptomycin (10000 μg/mL) (complete DMEM medium) at 37 °C and 5 % CO_2.

3.2.10.4. Bone Marrow-derived Macrophages (BMMΦ) differentiation

Mouse bone marrow cells were differentiated *in vitro* according to previous reported methods with some modifications [28]. C57BL/6 mice were anesthetized using a CO_2 chamber and euthanized by cervical dislocation. Femurs and tibias were removed and cleaned in aseptic conditions. Bones were disconnected by the articulations and then flushed using complete DMEM medium. The obtained cell suspension of bone marrow cells was centrifuged (300 x g, 10 min) and the pellet re-

suspended in 15 mL of complete DMEM medium supplemented with 20 % (v/v) L929-cell conditioned medium (LCCM) as source of macrophage colony-stimulating factor (M-CSF). Bone marrow was cultured overnight at 37 °C in a 5 % CO_2 atmosphere. The non-adherent cells were collected with warm complete DMEM medium supplemented with 20 % (v/v) LCCM, plated in a 96-well plate and incubated once again at 37 °C in a 5 % CO_2 atmosphere. On the 4th and 7th days the half of the medium was renewed and on the 10th day cells became fully differentiated into macrophages.

3.2.10.5. Cell viability assay

The cytotoxic effect of the nanocomplexes was assessed in BMMΦ primary cells and in HEK293T, L929 and HBMEC cell lines using a standard resazurin assay, as described elsewhere [1]. Briefly, a monolayer of BMMΦ (at a density of 3 x 10^4 cells/well), HEK293T and L929 (at a density of 1 x 10^4 cells/well) and HBMEC (at a density of 5 x 10^3 cells/well) were incubated for 24 h (37 °C in a 5 % CO_2 atmosphere) with increasing concentrations of free-AmB, Dex FD or SD and Dex-AmB FD or SD (0.78, 1.17, 1.76, 2.63, 3.95, 5.93, 8.89, 13.33 and 20 μM), previously sterilized by ethylene oxide for 15 h at 53 °C ± 1 °C. After the incubation period, 10 % (v/v) of a 2.5 mM resazurin solution was added to each well and the cells were incubated at 37 °C in a 5 % CO_2 atmosphere for another 4 h. Fluorescence was measured (λex 560/λem 590) in a SpectraMAX GeminiXS microplate reader (Molecular Devices LLC, California, USA). Results were expressed as the mean percentage ± SD of viable cells relatively to control condition (considered as 100 % viability). The concentration of a drug that kills half the BMMΦ cells (CC_{50}) was calculated by nonlinear regression analysis using the GraphPad Prism software. The assay was performed in triplicate at least three times.

3.2.10.6. Hemolysis assay

Blood was obtained from a healthy dog after owners' agreement and collected to an EDTA tube. Whole blood was centrifuged (10 min at 1200 x g, 4 °C) and the supernatant and buffy coat were discarded. Red blood cells (RBCs) were resuspended in isotonic PBS pH 7.4. The purified RBCs were counted using a Neubauer chamber and diluted to a concentration of 1 x 10^8 cells/mL. Afterwards, 450 μL of RBCs were placed in a 48-well plate containing 50 μL of AmB, Dex FD or SD, Dex-AmB FD or SD (final concentrations of 32, 16, 8, 4, 2 and 1 μM) and the plates were incubated for 30 min at 37 °C under agitation (120 rpm). After incubation, solutions were collected to eppendorfs and centrifuged (10 min at 1200 x g, 4 °C). The supernatants were collected for

analysis of the extent of hemolysis by reading the absorption of the hemoglobin at 540 nm. Results were expressed as a percentage of hemolysis with respect to the amount of hemoglobin released in the presence of 1 % of triton X-100, which was taken as measure of complete (100 %) lysis (Equation 3).

$$Hemolysis\ (\%) = \frac{Abss - Absb}{Abst - Absb} \quad (3)$$

Abss is the absorbance of the sample, Absb is the average absorbance of the negative control, and Abst is the average absorbance of the lysed samples. The assay was performed in triplicate at least three times.

3.2.10.7. Anti-leishmanial activity of the Dex-AmB nanocomplexes against intramacrophagic amastigotes

BMMΦ were seeded in 96-well plates, at a cell density of 2 x 10^5 cells/mL. Subsequently, BMMΦ were infected with *L. infantum* amastigotes at a multiplicity of infection (MOI) of 10 for 6 h. After the infection period, non-internalized parasites were removed with complete DMEM medium and infected cells were incubated for an additional 24 h. Increasing concentrations of free-AmB, Dex FD or SD, Dex-AmB FD or SD (0.0039, 0.0078, 0.0156, 0.03125, 0.0625, 0.125, 0.25, 0.5, 1 µM) were added to the respective wells. After 24 h of incubation, cell monolayers were fixed with 4 % (w/v) paraformaldehyde, permeabilized with 0.1 % (v/v) Triton X-100 for 30 min at room temperature and then stained with 4',6-diamidino-2-phenylindole (DAPI) and with high-content screening (HCS) CellMask™ Deep Red stain, which labels parasite DNA and macrophages nucleus and cytoplasm, respectively. The number of infected cells in each condition was determined in an IN Cell Analyzer 2000 microscope (GE Healthcare, Illinois, USA) as described by Gomes-Alves, A. G. et al. [26]. Anti-leishmanial activity results were expressed as the mean percentage ± SD of infected cells relatively to the control. The IC_{50} concentration was calculated by nonlinear regression analysis using the GraphPad Prism software. The assay was performed in triplicate at least three times.

3.2.11. Statistics

Statistical analysis was performed using GraphPad Prism 5 (GraphPad Software, San Diego, CA, USA). Results were expressed as mean ± SD. Two-way ANOVA followed by Bonferroni's multiple comparison post-test was performed wherever appropriate. Significance was considered as $p < 0.05$.

3.3. Results and Discussion

3.3.1. Production and characterization of Dex-AmB nanocomplexes

The prepared nanocomplexes were firstly characterized in terms of size, zeta potential and morphology. Dex-AmB FD and Dex-AmB SD presented a mean diameter of 214 ± 17 and 348 ± 36 nm, respectively (Table 3.1). Size of nanomedicines is important as it influences biodistribution and clearance. Small particles (< 5-10 nm) tend to have a reduced circulation time since they are rapidly cleared from circulation through extravasation or renal clearance [29], while particles from 100-200 nm have been associated with increased phagocytosis by *Leishmania*-infected macrophages [30]. Additionally, some studies refer that nanoparticles larger than 200 nm are effective in targeting infected macrophages [31]. Table 3.1 shows that the produced material is polydisperse, presenting a wide size distribution. The size of the nanocomplexes may be considered safe both for intralesional or intravenous injection, since capillary blockage and embolism is only promoted by particles with size > 5 μm [32]; it has been reported that Fungizone®, which consist of particles with a mean size of 3310 nm [33], can be applied without any harmful effects [34].

Table 3.1 - Average size, distribution and zeta potential of the Dex-AmB nanocomplexes dissolved in dH_2O. Results are expressed as mean ± SD.

Nanocomplex	Size (nm)	Size distribution			ζ potential
		D10	D50	D90	(mV)
Dex-AmB FD	214 ± 17	113 ± 9	194 ± 14	343 ± 41	-13.67 ± 1.72
Dex-AmB SD	348 ± 36	155 ± 25	317 ± 39	577 ± 51	-1.90 ± 0.21

The morphology of Dex-AmB FD and Dex-AMB SD was examined by Cryo-SEM (Figure 3.1 A and B) and SEM (Figure 3.1 C and D) (SEM analysis was only possible to perform with Dex-AmB SD powder). As shown in Figure 3.1 A and B, when in aqueous solution Dex-AmB FD and Dex-AMB SD nanocomplexes have a spherical morphology, bearing a size consistent with the previously referred size distribution analysis. This result proves also that the rehydrated nanocomplexes are colloidally stable, as no aggregates are observed. Moreover, Dex-AmB SD powder analyzed by SEM (Figure 3.1 C and D) showed mostly spherical particles, with some concavities (possible due to collapse upon drying), smooth and non-porous surface. Similar results were obtained in another study where cyclodextrin-AmB spherical amorphous solid microparticles were prepared by spray drying [35]. The

zeta potential of the Dex-AmB FD and Dex-AmB SD nanocomplexes was found to be –13.67 ± 1.72 and – 1.90 ± 0.21 mV, respectively (Table 3.1) whereas Dex, non-charged glucose oligomers, has a zeta potential of –8.34 ± 2.71 mV. Generally, when particles have a high surface charge (>|30 mV|), they repel each other, which favors stability. In the current case, although the particles observed by Cryo-SEM do not exhibit signs of aggregation, the low zeta potential may compromise the long-term colloidal stability in aqueous suspension. However, the dry formulation is easy to disperse in water and to prepare just before use, thus the long-term stability in aqueous suspension is not a pivotal feature.

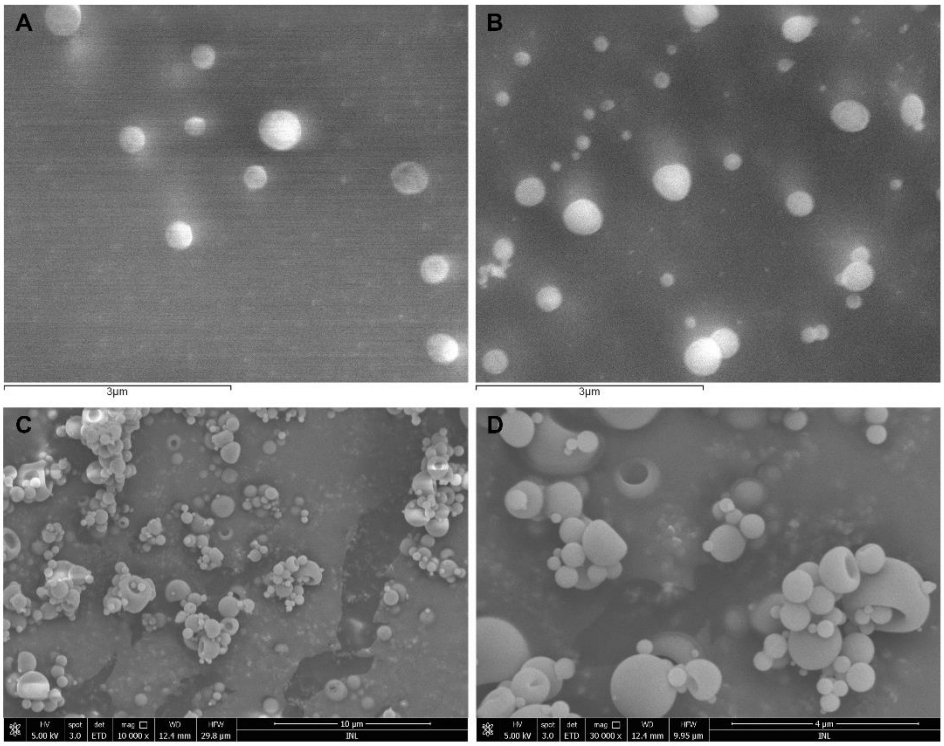

Figure 3.1 - Representative Cryo-SEM microphotographs of **(A)** Dex-AmB FD and **(B)** Dex-AmB SD nanocomplexes in dH_2O (magnification of 20000x. Scale bars = 3 µm) and representative SEM microphotographs of Dex-AmB SD nanocomplex obtained at a magnification of **(C)** 10 000x (scale bar = 10 µm) and **(D)** 30 0000x (scale bar = 4 µm).

The interaction of AmB with the polysaccharide was confirmed using different techniques, including FTIR, DSC, XRD. Figure 3.2 displays the FTIR spectra, in the range of 700-4000 cm^{-1}, for AmB, Dex FD, Dex-AmB FD, Dex SD and Dex-AmB SD. Polysaccharide processing by freeze- or spray-dryer did not cause any chemical alterations since all characteristic peaks of the dextrin are observed. More specifically, a strong and prominent absorption band at about 3386.7 cm^{-1} is observed which can be assigned to -OH stretching vibrations. The stretching of C-H group vibrations and the -OH bending vibration is observed at 2927.7 and 1639.3 cm^{-1}, respectively and the absorption bands at 1157.2 and 1026.0 cm^{-1} can be assigned to the stretching vibrations of C-O and C-C, and the bending mode

of C-H and stretching vibration of C-O-C [36, 37]. Regarding the spectra of AmB crystals, it is possible to notice the absorption bands at 1558.3 and 1689.5 cm^{-1} which corresponds to the C=C stretching vibration from polyene and C=O stretching vibration from the carbonyl ester group, respectively [38, 39].

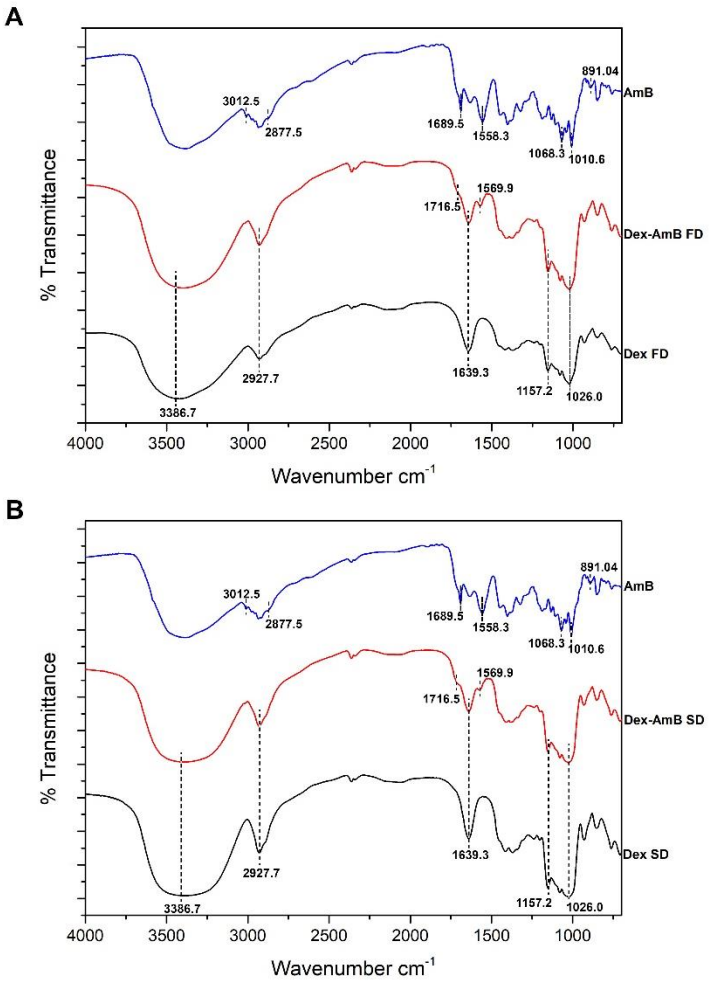

Figure 3.2 - FTIR spectra of **(A)** Dex and Dex-AmB processed by freeze-dryer and **(B)** Dex and Dex-AmB processed by spray-dryer, where is visible characteristic functional groups of AmB after nanocomplexes production.

In addition, the peaks corresponding to C-H stretching (3012.5 cm^{-1}), CH_2 and CH_3 symmetric stretching vibrations (2877.5 cm^{-1}), C-C-H (chromophore) bending as well as CH bending (trans-polyene) (1010.6 cm^{-1}), C=O asymmetric stretching vibrations (1068.4 cm^{-1}) and C-H bending and CH_3 rocking vibrations due to the C=O asymmetric stretching vibrations (891.04 cm^{-1}) are recognized [40, 41]. FTIR spectra of Dex-AmB FD (Figure 3.2 A) and Dex-AmB SD (Figure 3.2 B) nanocomplexes are almost identical to their counterparts, but they also present characteristic peaks of the AmB. More specifically, both spectra feature the peaks corresponding to C=O and C=C stretching vibration, that suffer a slight shift from 1689.5 and 1558.3 cm^{-1} to 1716.5 and 1569.9 cm^{-1}, respectively, probably

due to the interaction with the polysaccharide. Similar results, where characteristic peaks of AmB were still visible in the FTIR analysis, were reported in the literature after drug conjugation to bovine serum albumin (BSA) [38] or encapsulation in glutaraldehyde cross-linked BSA microparticles [42], formation of AmB nano-assemblies with Aloe vera leaf extract [43] and conjugation of AmB to oxidized sodium alginate [19] or oxidized polymannose [22].

Thermal studies are useful to ascertain the compatibility, stability and physical state of drugs conjugated to polymers or encapsulated in nanoparticles [36]. Figure 3.3 A and B shows the thermal behavior of AmB, Dex FD, Dex-AmB FD, Dex SD and Dex-AmB SD in the range 25-235 °C. As described in the literature, AmB was characterized by a double endothermic peak [39, 44], here determined at 165.9 and 199.5 °C whereas Dex FD (Figure 3.3 A) and Dex SD (Figure 3.3 B) only showed a broad endothermic peak (152.4 °C and 162.2 °C, respectively).

The almost complete disappearance of the AmB endothermic peak was observed in the Dex-AmB FD (Figure 3.3 A) and Dex-AmB SD (Figure 3.3 B) nanocomplexes. Kim et al. [39] also showed that the incorporation of AmB in the cavities of the hydroxypropyl-γ-cyclodextrin (HPγCD) promoted formation of an amorphous inclusion complex, as concluded from the lack of the AmB endothermic peak. Similar results were observed for conjugates of curcumin in dextrin [36] and of AmB in pegylated poly(D, L-lactide-co-glycolide) (PLGA) copolymer nanoparticles [45]. These results were further confirmed by XRD (Figure 3.3 C and D). Free-AmB in pure state presents a crystalline lattice characterized by sharp peaks at diffraction angles of 2θ = 14.06, 17.26, 18.4, and 21.7, as reported elsewhere [39]. In the presence of the polysaccharide, after freeze (Figure 3.3 C) or spray dying (Figure 3.3 D), amorphization of the AmB is observed as characterized by the loss of the drug characteristic peaks, being only visible a large diffraction peak as in the processed free-polysaccharide. Similar results were reported in the literature where amorphous AmB nanoparticles were successfully prepared through liquid antisolvent precipitation followed by freeze-drying [46] and where AmB was encapsulated in polymeric micelle of PLGA grafted-dextran copolymer [47] or incorporated in the cavities of HPγCD [39]. Thus, we conclude that an amorphous inclusion complex between the AmB and the dextrin chain networks was formed.

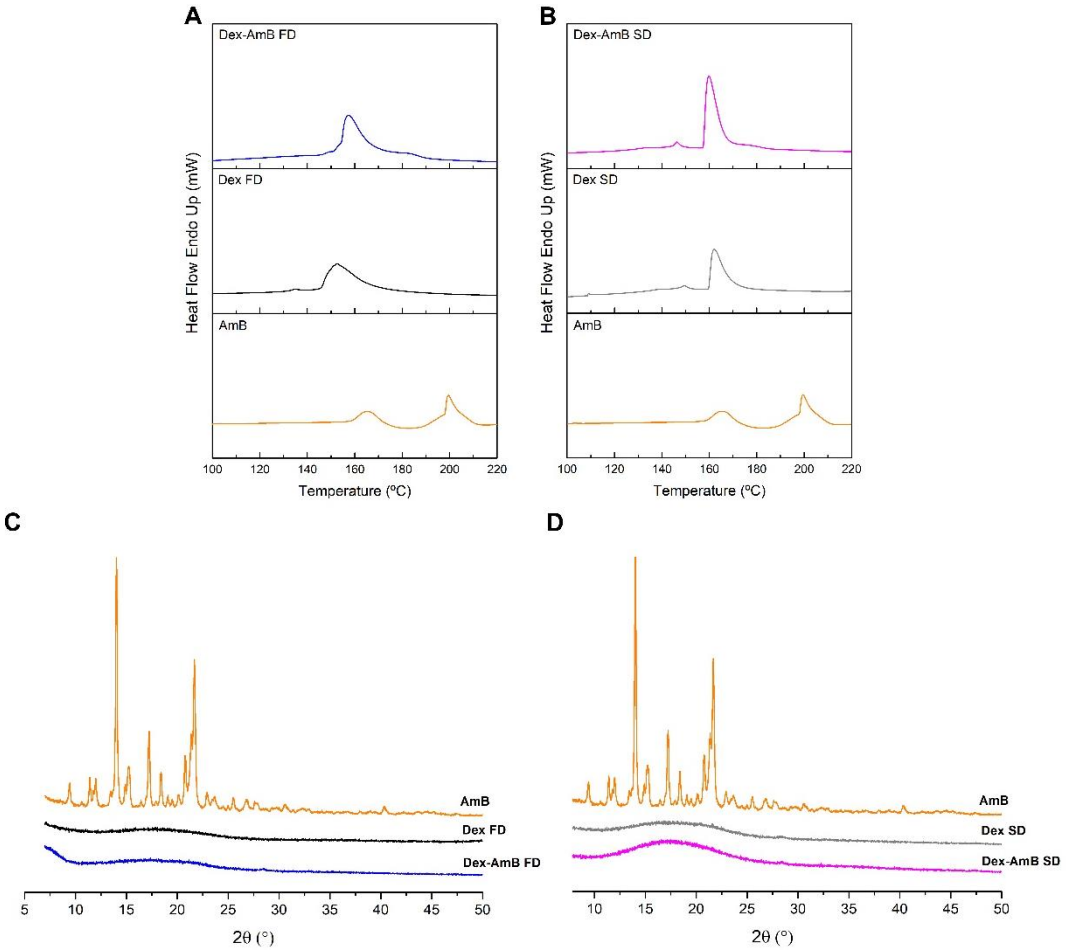

Figure 3.3 - DSC curves **(A** and **B)** and X-ray powder diffraction **(C** and **D)** of free-AmB and **(A, C)** Dex, Dex-AmB nanocomplex processed by freeze-dryer and **(B, D)** Dex, Dex-AmB nanocomplex processed by spray-dryer.

3.3.2. Spectroscopic analysis of Dex-AmB nanocomplexes

UV-vis spectroscopy was used to investigate the aggregation state of the AmB in its free form or in the nanocomplexes, after dispersion in dH_2O. It is known that the AmB aggregation state is a key factor with direct impact on its cytotoxicity and activity [48, 49]. In solution, AmB may exists in three forms: i) monomers, which is the soluble form, that normally associates with ergosterol in fungal and protozoan cell membranes; ii) oligomers (small soluble water aggregates; e.g. Fungizone®), which can form pores in cholesterol-containing membranes, leading to toxicity towards host cells [50]; and iii) poly-aggregates [18, 43], which is associated to lower *in vitro* and *in vivo* toxicity [51, 52]. The UV-vis spectrum of AmB is very sensitive to aggregation and characterized by four well-separated bands when in a monomeric state [53, 54]. Moreover, the spectral modifications induced by the extent of AmB aggregation can be represented by the ratio of the first to the fourth peaks, being a value of < 1 characteristic of the monomeric form [38] and a value of > 2 to a super-aggregated form [43]. Our results, showing four well-defined peaks at approximately 349 (I), 369 (II), 387 (III) and 408 nm (IV),

indicates that free-AmB exists in monomeric form when firstly dissolved in 0.1 M borate buffer pH 11 and then diluted in dH_2O (Figure 3.4 - A). Furthermore, the peak I/IV (A349/A408) ratio for the AmB dispersed in the aqueous solution was 0.4, confirming its presence in monomeric form. This value is similar to the one obtained in a study where AmB was dissolved in 50 % methanol [54]. The dissolution of the Dex-AmB FD nanocomplex (Figure 3.4 - B) in dH_2O promoted a hypsochromic shift of the peak I to lower wavelength (335 nm), meaning that the AmB in the nanocomplex acquired a water-soluble aggregated form. In the case of the Dex-AmB SD nanocomplex (Figure 3.4 - C), even though the hypsochromic shift of the peak I is not prominent, we concluded that the AmB in this material is also present in a water-soluble aggregated form, since the UV-vis spectra of both nanocomplexes are very similar. As referred above, AmB is highly toxic in its aggregated state, promoting cytotoxicity [50]. For instance, the highly toxic formulation Fungizone® dissolved in 5 % dextrose has a value of 2.9 [55]. For Dex-AmB FD (A335/A409) and Dex-AmB SD (A348/A409) nanocomplexes the degree of AmB aggregation appears not to be significant since the ratio values were 1.13 and 1.11, respectively. Furthermore, the higher the aggregation ratio, the lower the amount of monomeric AmB present [53]. Therefore, our results enable us to assume the presence of monomeric AmB in the nanocomplex, which may attenuate the toxicity of the formulation.

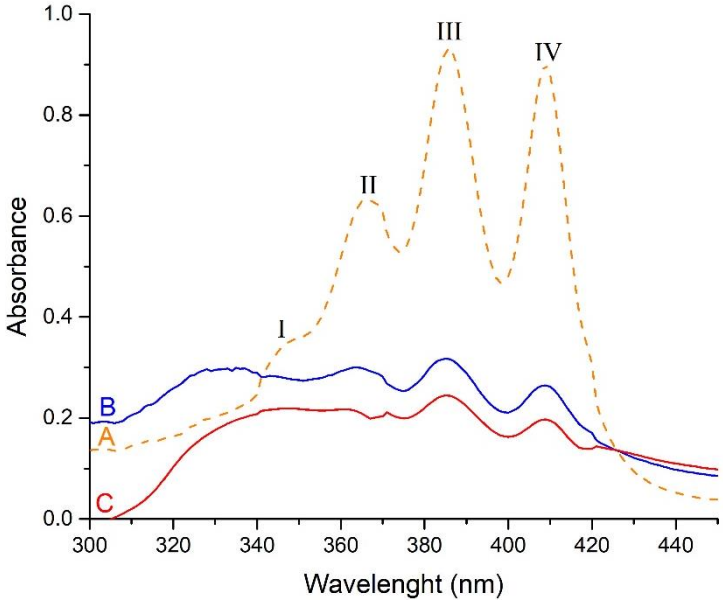

Figure 3.4 - Study of AmB aggregation state by UV-vis spectroscopy. Changes in the characteristic absorption peaks of AmB (at a final concentration of 10 μM) in **(A)** its free form (dissolved in 0.1 M borate buffer pH 11 and diluted in dH_2O), **(B)** Dex-AmB FD nanocomplex and **(C)** Dex-AmB SD nanocomplex (both dissolved and diluted in dH_2O).

3.3.3. AmB quantification by HPLC-PDA-MS

The nanocomplexes were analyzed by HPLC using double detection (PDA and MS). The overall yield values (%) are listed in Table 3.2. For Dex-AmB FD, the overall yield (86.8 %) is within the values reported for other polysaccharide-AmB formulations (approximately 60 – 90 %) [8, 18-21]. Considering the Dex-AmB SD nanocomplex, a lower yield was achieved (51.5 %), as commonly reported in the development of spray dried pharmaceuticals at the small scale used, regardless the improvements achieved in the development of a nano spray dryer (final product yields increased theoretically to ± 90 %) [56].

While using spectrophotometry to assess the concentration of AmB, as it is widely used in the literature [8, 14, 20, 57], we noticed some lack of reproducibility and consistency, probably due to differences on the aggregation state. Therefore, an HPLC method was developed using a Kinetex® C18 column. For the analyzed mass range of 923-925 m/z and wavelength of 387 and 408 nm, linear regression in the range of concentrations used (2 – 120 µg/mL and 0.5 – 20 µg/mL, respectively), with R^2 between 0.9983 - 0.9991 was obtained. The AmB content (% w/w) and association efficiency (%) in the produced nanocomplexes were estimated using both detection methods (Table 3.2). The AmB content results obtained are quite similar regardless of whether they are estimated using the UV or the MS detection method or of the type of processing method used in the nanocomplexes production. As expected, comparatively to the freeze-dried material, the association efficiency determined for the spray-dried material is slightly inferior, since the obtained yields are also lower.

In the literature reporting other polysaccharides- or synthetic polysaccharide-based AmB formulations, AmB contents of 34.4, 36.6 and 32.9 % were described for a dextran-AmB conjugate (amine), dextran-AmB (imine) and dextran-AmB-ethanolamine (imine), respectively [17], 23 % and 26 % for a arabinogalactan-AmB conjugates [8], 20 % for a galactomannan-AmB conjugate [21], 19.5 % for AmB-polymmanose conjugates [22] and 18 % for polyglucose-AmB conjugates [23]. Similarly to our work, Mehenni et al. [35] produced in a spray dryer a poly-γ-cyclodextrin-based AmB microspheres with a drug content of 13.7 %. Even in works reporting AmB encapsulation in nanoparticles, the drug content and/or association efficiency are in some cases slightly superior or comparable to our results [34, 47, 53, 54, 57, 58].

In this study, a Dex/AmB mass ratio of 4:1 was tested. However, since the nanocomplex production process is extremely simple, without any type of encapsulation or chemical modification being performed, increasing the drug content could be easily achieved by changing the polysaccharide/drug mass ratio used at the beginning of the process. Furthermore, the use of the spectrophotometric

methods for drug content determination, a technique widely used in many of the above referred works, should be performed with caution as AmB UV-vis spectra is very sensitive to modifications (as discussed in the section 3.3.2). This spectral instability might influence the determined absorbance values decreasing the reproducibility and consistency of the method and accuracy of the drug content determination.

Table 3.2 - Overall yield (%), AmB association efficiency (%) and drug content (% w/w) of Dex-AmB FD and Dex-AmB SD nanocomplexes obtained through HPLC, using MS detector (at 923-925 m/z) and UV detector (at 387 and 408 nm). *(n = 3).

Nanocomplex	Overall Yield (%)	Drug content (%) *			AmB association efficiency (%) *		
		MS (923-925 m/z)	UV (387 nm)	UV (408 nm)	MS (923-925 m/z)	UV (387 nm)	UV (408 nm)
Dex-AmB FD	86.8	14.68 ± 2.16	15.85 ± 0.61	14.85 ± 0.54	60 ± 8.83	64 ± 2.38	59 ± 2.17
Dex-AmB SD	51.5	14.38 ± 2.79	16.22 ± 0.83	15.35 ± 0.61	33 ± 5.24	34 ± 1.73	32 ± 1.27

3.3.4. *In vitro* cytotoxicity assays

Before testing the Dex-AmB formulations as a potential leishmanicidal therapy approach, the associated intrinsic toxicity was assessed. Thus, the cytotoxic effect of the free-AmB and of the different formulations were assessed using a variety of cells. For this purpose, a primary culture of BMMΦ and a kidney-derived HEK293T cell line (because AmB is associated with nephrotoxicity [59]) were employed. Moreover, L929 (fibroblasts) and HBMEC (endothelial) cell lines were also used since the produced material is intended to be applied either directly to a cutaneous lesion or intravenously.

As seen in Figure 3.5 A and C, free-AmB was cytotoxic, in a dose-dependent way, towards BMMΦ cells, reducing the cell viability to levels under the 70 % threshold (usually regarded as denoting cytotoxic potential [60]) at concentrations between 1.76 and 2.63 μM (CC_{50} of 2.060 ± 0.186 μM). Regarding the HEK293T cells (Figure 3.5 B and D), free-AmB also promoted a dose-dependent reduction of the cell viability at concentrations between 8.89 and 13.33 μM. These results showing toxicity of AmB against the two types of cells described above are in agreement with the literature. Toxic effects of AmB against J774.2 or Raw 264.7 macrophage cell lines at concentrations above 10 μg/mL [53, 61], peritoneal macrophages at 23.1 μM [62] or 7.6 μM [63] and THP1 and BMMΦ cells at 19.8 and 21.8 μg/mL, respectively [64] were described in the literature. Gurudevan et al. [38]

showed that AmB at 15.6 µg/mL was highly cytotoxic against HEK293T cell line, promoting more than 80 % of cell death. In other studies, it was described that 7.8 µg/mL [22] or 10 µg/mL [19, 23] of AmB promoted 50 % or 90 % of HEK293T cells death, respectively. Considering the variability in the doses of free-AmB that causes cytotoxicity, it is not surprising that our results differ somewhat from those reported.

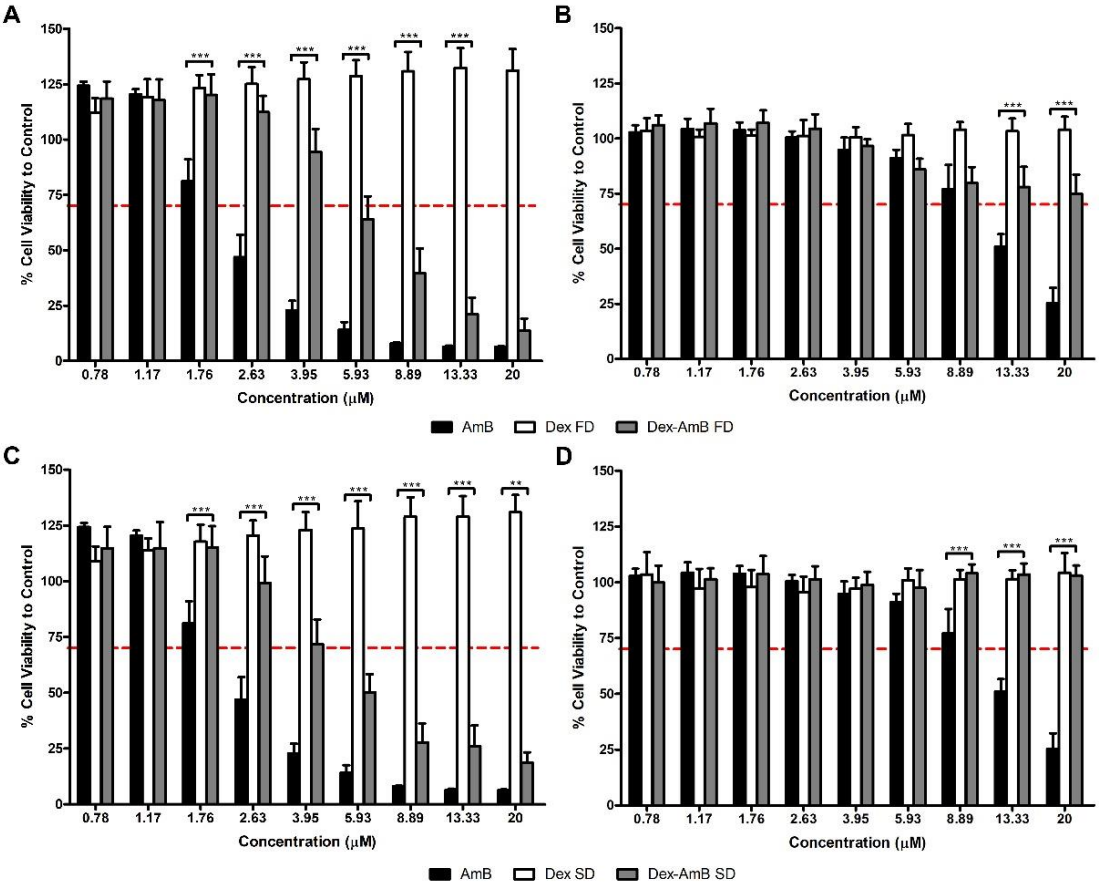

Figure 3.5 - Viability of (**A** and **C**) BMMΦ and (**B** and **D**) HEK293T cells after treatment with Dex-AmB nanocomplexes. Cell viability was evaluated by resazurin assay after treatment with different doses of Dex-AmB FD (**A** and **B**) and Dex-AmB SD (**C** and **D**) for 24 h. Data is expressed as percentage relative to the control and presented as mean ± SD of three independent experiments. Dex-AmB FD and Dex-AmB SD treatment conditions were compared with the AmB treatment condition using Bonferroni's multiple comparison post-test (*p < 0.05, **p < 0.01 and *** p < 0.001).

On the other hand, at the same concentrations, both Dex-AmB nanocomplexes were significantly less toxic against BMMΦ comparatively to the free drug. A reduction in cell viability to levels under the 70 % threshold was only visible at concentrations between 3.95 and 5.93 µM (Figure 3.5 A and C) (CC_{50} of 5.77 ± 1.27 and 6.26 ± 1.96 µM for Dex-AmB FD and Dex-AmB SD, respectively). Figure 2.5 B and D shows that none of the Dex-AmB nanocomplexes promoted a reduction in HEK293T cell viability to levels under the 70 % threshold even at the highest dose tested. The reduction of AmB toxicity after

inclusion or conjugation to polysaccharides or encapsulation into polymeric nanoparticles was also reported in the literature [19, 23, 38, 39, 53]. As expected, Dex was safe at all the tested concentrations (Figure 3.5), since it is generally recognized as safe (GRAS) and previously developed dextrin-based formulations did not show cytotoxicity against BMMΦ cells [65, 66]. Furthermore, the viability values above 100 % seen for the Dex may be explained by the cell growth stimulant character of dextrin [67]. The AmB inclusion in the polysaccharide chain networks also allowed to attenuate the toxicity of the drug against L929 and HBMEC cell lines (Figure 3.6). The presented data appears to indicate that the Dex-AmB FD or Dex-AmB SD nanocomplexes are safe and reduce the toxicity of AmB. Furthermore, we speculate that *in vivo* the toxicity reduction may be even more significant as the nanocomplexes are expected to be swiftly internalized by the infected macrophages.

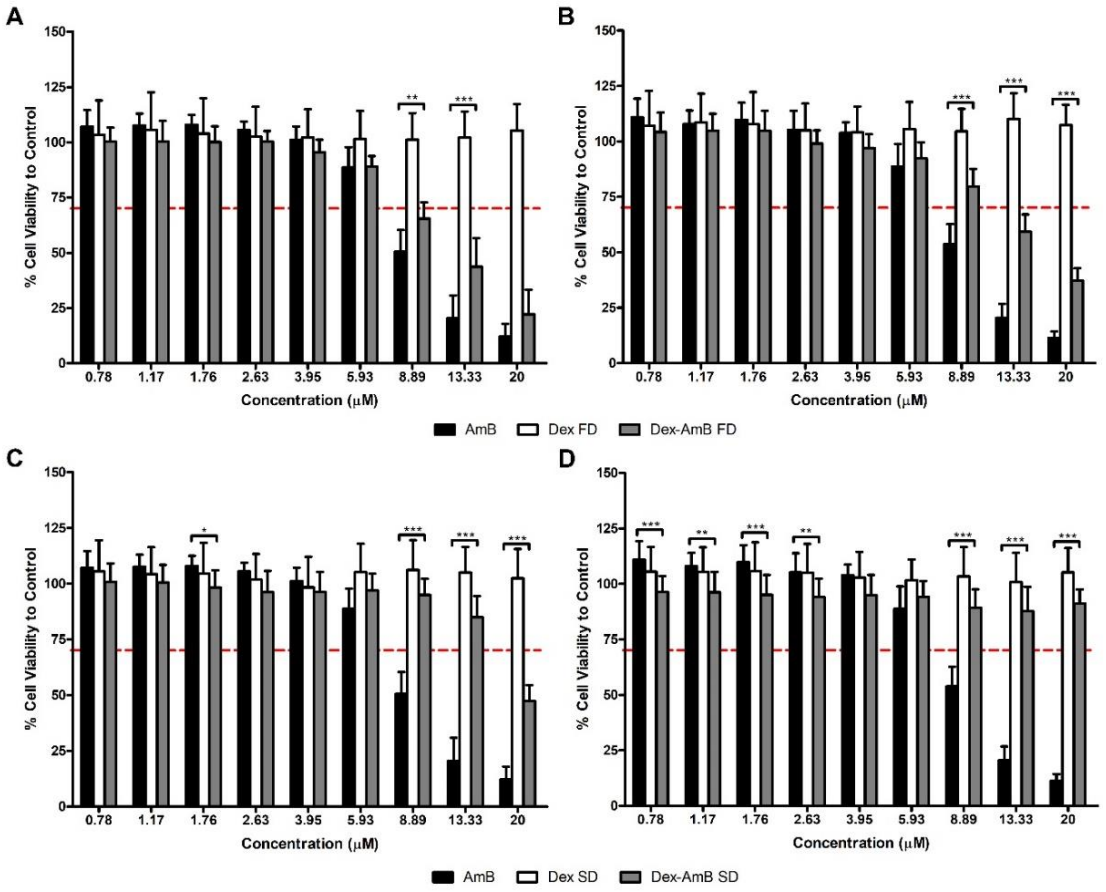

Figure 3.6 - Viability of (**A** and **C**) L929 and (**B** and **D**) HBMEC cells after treatment with Dex-AmB nanocomplexes. Cell viability was evaluated by resazurin assay after treatment with different doses of Dex-AmB FD (**A** and **B**) and Dex-AmB SD (**C** and **D**) for 24 h. Data is expressed as percentage relative to the control and presented as mean ± SD of three independent experiments. Dex-AmB FD and Dex-AmB SD treatment conditions were compared with the AmB treatment condition using Bonferroni's multiple comparison post-test ($^{*}p < 0.05$, $^{**}p < 0.01$ and $^{***}p < 0.001$).

3.3.5. Hemolytic activity

Given that hemolysis is a severe side effect of AmB, we tested the hemolytic potential of Dex-AmB FD and Dex-AmB SD at various concentrations (ranging between 1 and 32 μM). According to ASTM E2524-08, materials resulting in over 5 % hemolysis can be classified as hemolytic [68]. Different works in the literature show that pure AmB can lyse more than 70 % RBCs at a concentration of 10 μg/mL (10.8 μM) [19, 38, 53]. In this work, free-AmB was hemolytic toward dog RBCs at 4, 8, 16 and 32 μM, leading to 97.6 ± 7.8 % of hemolysis at the higher concentration (Figure 3.7).

The inclusion of AmB into dextrin allowed a significant decrease in the hemolytic effect. In fact, Dex-AmB FD and Dex-AmB SD at 32 μM promoted 61.5 ± 10.8 % (nearly 1.58-fold less comparatively to free-drug) and 57.7 ± 9.7 % (nearly 1.69-fold less comparatively to free-drug) of hemolysis, respectively, being the hemolytic activity negligible (< 5 %) at 4 μM.

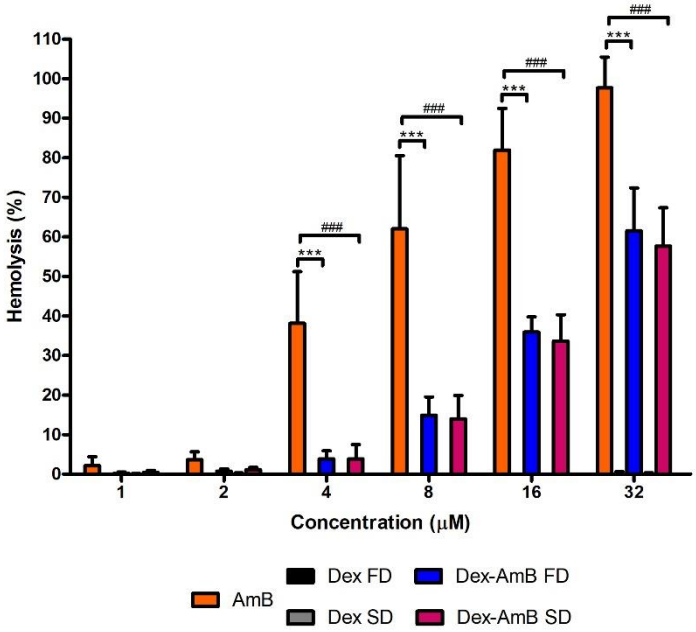

Figure 3.7 - Percentage of hemolysis caused by AmB and Dex-AmB nanocomplexes upon their interaction with dog RBCs with various concentrations (ranging between 1 and 32 μM) for 30 min. Data is expressed as percentage relative to the control and presented as mean ± SD of three independent experiments. Dex-AmB FD (*) and Dex-AmB SD ($^{\#}$) treatment conditions were compared with the AmB treatment condition using Bonferroni's multiple comparison post-test (*** and $^{\#\#\#}$ $p < 0.001$).

This is consistent with findings of Zia et al. [43], who reported that a simple formation of AmB nano-assemblies with Aloe vera leaf extract decreased hemolysis of RBCs, even at 50 μg/mL AmB equivalents. In other studies, significant reduction of hemolysis to negligible levels was shown after AmB encapsulation into PLGA [57, 69], chitosan [70] or polyglutamic acid [53] or conjugation to different polymers such as arabinogalactan [14], sodium alginate [19], gum arabic [18], dextran [17].

This outcome could be attributed to the shielding effect of the polysaccharide on AmB [19]. We also tested the hemolytic activity of the processed polysaccharide and, as expected, negligible hemolysis was observed even at the highest tested concentrations. Overall, our results suggest a wide safety margin of our nanocomplexes in blood-contacting applications comparatively to the free-AmB and their suitability for intravenous administration.

3.3.6. Anti-Leishmanial activity against axenic promastigote and intramacrophagic *L. infantum* amastigotes activity

Amphotericin B is active against both the extracellular promastigote and intracellular amastigote forms promoting the formation of ionic transmembrane channels, by the interaction with membrane ergosterol, leading to parasite death [9, 34]. In this study, the *in vitro* anti-leishmanial activity of AmB and Dex-AmB nanocomplexes was determined 24 h following exposure of *L. infantum* and *L. amazonensis* promastigotes or BMMΦ infected with *L. infantum* amastigotes to different concentrations of the above referred material. Regarding the axenic culture results (Figure 3.8 A and B), free-AmB was highly active against *L. amazonensis* and *L. infantum*, with IC_{50} values of 0.028 ± 0.001 and 0.023 ± 0.010 μM, respectively. Some results reported in the literature, although referring to diverse species of *Leishmania* and presenting some variability, maintain the same tendency.

Petri e Silva et al [71] described an IC_{50} value of 0.22 μM for *L. infantum* promastigotes after a 48 h exposure to AmB. In another study using AmB, IC_{50} values from 0.01 to 0.27 μM were reported, being the promastigote *L. mexicana* the least sensitive strain (0.27 μM) and *L. donovani* the most sensitive strain (0.012 μM) [72] of those tested, effect that was also reported in another study [23]. Chávez-Fumagalli et al. [73] reported IC_{50} values of 0.1 and 0.09 μg/mL for AmB-treated *L. amazonensis* and *L. infantum*, respectively. On the other hand, nanocomplexes also led to decreases in *L. amazonensis* and *L. infantum* viability, although at slightly higher concentrations comparatively to the free-drug. In fact, when comparing the IC_{50} of our nanocomplexes to free-AmB, it is noted that overall the latter has lower IC_{50}. Dex-AmB FD and Dex-AmB SD presented IC_{50} values of 0.056 ± 0.029 and 0.096 ± 0.050 μM, respectively, for *L. amazonensis* (Figure 3.8 A) and of 0.030 ± 0.017 and 0.044 ± 0.025 μM, respectively, for *L. infantum* (Figure 3.8 B). These differences were also observed in the literature for AmB conjugated to dextran [17], gum arabic [18], among others polymers [20, 23].

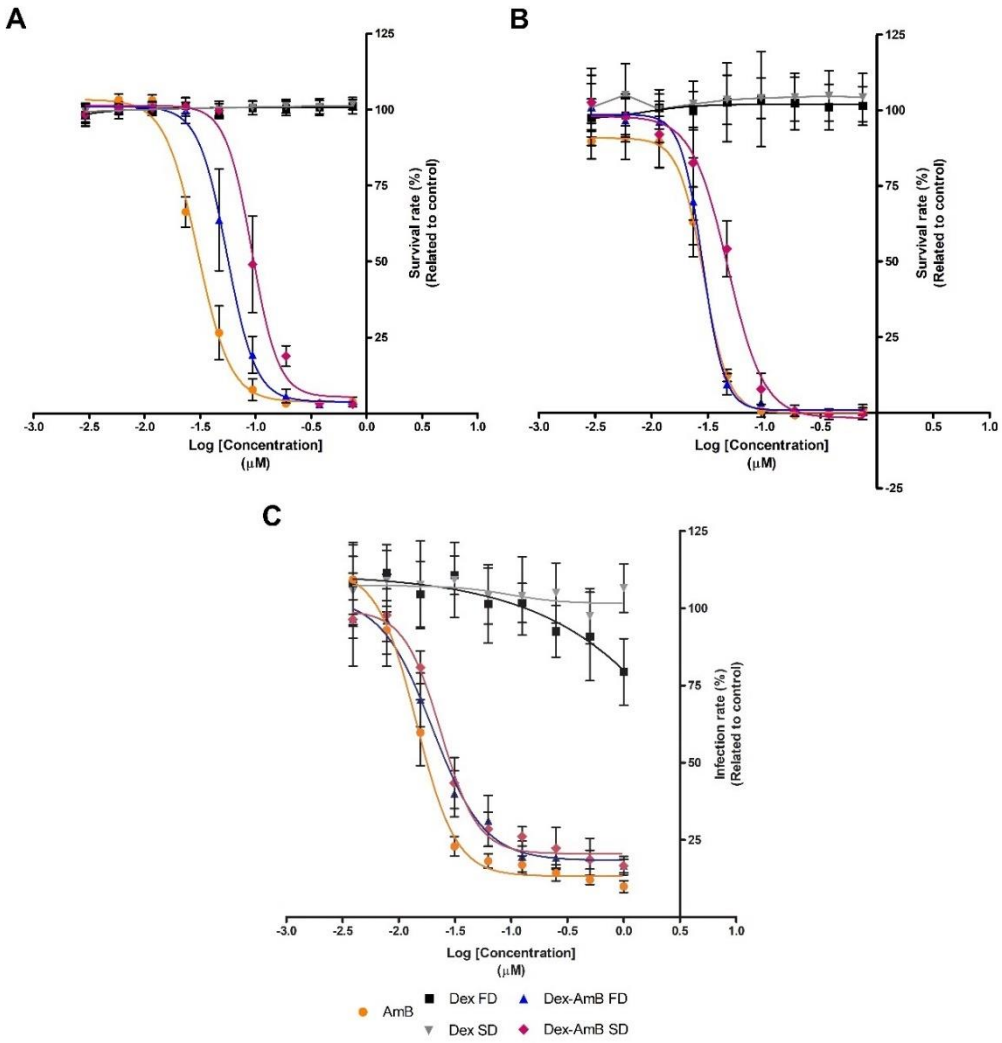

Figure 3.8 - *In vitro* anti-leishmanial activity of free-AmB and Dex-AmB nanocomplexes against axenically grown **(A)** L. amazonensis promastigotes and **(B)** *L. infantum* promastigotes and against **(C)** BMMΦ infected with *L. infantum* amastigotes. Dose-response curves were obtained after 24 h treatment with the different formulations. Results are expressed as mean ± SD of three independent experiments.

The capacity to accurately test *in vitro* anti-leishmanial activity against *Leishmania*-infected BMMΦ is a critical point in the development of new formulations. For that, a protocol [26] for IN Cell Analyzer systems was recently developed and used here to obtain the dose-response curves for the *L. infantum* tested with the formulations, as seen in Figure 3.8 C. Results show that AmB displayed high activity against intramacrophagic *L. infantum* parasites, as already reported in the literature [26, 71, 74]. Dex-AmB nanocomplexes had an activity similar to the free-drug, despite the slightly higher IC_{50} values - 0.017 ± 0.009 and 0.023 ± 0.006 μM for Dex-AmB FD and Dex-AmB SD, respectively - promoting a decrease in the amastigote parasite burden in the used concentration range. These results are consistent with the literature where reduced and unreduced AmB-AG conjugates were able to decrease the percentage of macrophages infected with *L. infantum* (ED_{50} of 0.035 μg/mL and 0.027 μg/mL,

respectively) [75]. Importantly, the finding that Dex-AmB FD and Dex-AmB SD are approximately 2.47- and 1.98-fold more selective than free-drug is very promising (Table 3.3) and proves that the inclusion of AmB into the polysaccharide chain networks applying the simple processing method described in this work was able to improve the leishmanicidal potential of the drug. Dextrin did not show any significant effect, as expected, for all the tested concentrations in both assays.

Table 3.3 - *In vitro* cytotoxicity against intracellular amastigotes and macrophages.

Sample	Amastigotes IC_{50} (μM)	Macrophages CC_{50} (μM)	Selectivity Index (SI) [a]
AmB	0.015 ± 0.003	2.060 ± 0.190	137
Dex-AmB FD	0.017 ± 0.009	5.769 ± 1.273	339
Dex-AmB SD	0.023 ± 0.006	6.263 ± 1.963	272

Means ± SD (n = 3); [a] SI (selectivity index) = CC_{50} /IC_{50}.

3.4. Conclusion

The development of novel delivery systems for AmB to be used in leishmaniasis treatment, that improves the therapeutic index of this 'gold standard' drug, has been pursued over the years. In this work, we report a simple and economic formulation, where, unlike other polysaccharide-AmB formulations reported in the literature, no chemical modifications or solvents are required. Both nanocomplexes are easy to re-disperse in aqueous solutions and display leishmanicidal potential against axenic cultures of promastigotes and against intramacrophagic *L. infantum* amastigotes (selectivity index approximately 2.47- and 1.98-fold superior to the free-AmB). All the presented results strongly suggest the Dex-AmB nanocomplexes have potential as a nanomedicine for leishmaniasis treatment since, in addition to the affordability and simplicity of development, they are less toxic than other AmB based formulations.

3.5. References

1. Vale-Costa, S., et al., *Iron overload favors the elimination of Leishmania infantum from mouse tissues through interaction with reactive oxygen and nitrogen species.* PLoS Negl Trop Dis, 2013. **7**(2): p. e2061.
2. Kedzierski, L., *Leishmaniasis Vaccine: Where are We Today?* J Glob Infect Dis, 2010. **2**(2): p. 177-85.
3. Torres-Guerrero, E., et al., *Leishmaniasis: a review.* F1000Res, 2017. **6**: p. 750.
4. Desjeux, P., *Leishmaniasis: current situation and new perspectives.* Comp Immunol Microbiol Infect Dis, 2004. **27**(5): p. 305-18.
5. Oryan, A. and M. Akbari, *Worldwide risk factors in leishmaniasis.* Asian Pac J Trop Med, 2016. **9**(10): p. 925-932.

6. Kaye, P. and P. Scott, *Leishmaniasis: complexity at the host-pathogen interface.* Nat Rev Microbiol, 2011. **9**(8): p. 604-15.
7. Olivier, M., *Culprit within a culprit.* Nature, 2011. **471**: p. 173.
8. Ehrenfreund-Kleinman, T., et al., *Synthesis and characterization of novel water soluble amphotericin B–arabinogalactan conjugates.* Biomaterials, 2002. **23**(5): p. 1327-1335.
9. Baginski, M., J. Czub, and K. Sternal, *Interaction of amphotericin B and its selected derivatives with membranes: molecular modeling studies.* Chem Rec, 2006. **6**(6): p. 320-32.
10. Baran, M., E. Borowski, and J. Mazerski, *Molecular modeling of amphotericin B–ergosterol primary complex in water II.* Biophysical Chemistry, 2009. **141**(2): p. 162-168.
11. Serafim, C., et al., *Lipoamino acid-based micelles as promising delivery vehicles for monomeric amphotericin B.* Int J Pharm, 2016. **497**(1-2): p. 23-35.
12. Brajtburg, J. and J. Bolard, *Carrier effects on biological activity of amphotericin B.* Clin Microbiol Rev, 1996. **9**(4): p. 512-31.
13. Duncan, R. and M.J. Vicent, *Polymer therapeutics-prospects for 21st century: The end of the beginning.* Advanced Drug Delivery Reviews, 2013. **65**(1): p. 60-70.
14. Ehrenfreund-Kleinman, T., J. Golenser, and A.J. Domb, *Conjugation of amino-containing drugs to polysaccharides by tosylation: amphotericin B-arabinogalactan conjugates.* Biomaterials, 2004. **25**(15): p. 3049-57.
15. Ickowicz, D.E., et al., *Activity, reduced toxicity, and scale-up synthesis of amphotericin B-conjugated polysaccharide.* Biomacromolecules, 2014. **15**(6): p. 2079-89.
16. Hudson, S.P., et al., *Injectable in situ cross-linking hydrogels for local antifungal therapy.* Biomaterials, 2010. **31**(6): p. 1444-1452.
17. Sokolsky-Papkov, M., A.J. Domb, and J. Golenser, *Impact of Aldehyde Content on Amphotericin B–Dextran Imine Conjugate Toxicity.* Biomacromolecules, 2006. **7**(5): p. 1529-1535.
18. Nishi, K.K., et al., *Amphotericin B-Gum Arabic Conjugates: Synthesis, Toxicity, Bioavailability, and Activities Against Leishmania and Fungi.* Pharmaceutical Research, 2007. **24**(5): p. 971-980.
19. Ravichandran, V. and A. Jayakrishnan, *Synthesis and evaluation of anti-fungal activities of sodium alginate-amphotericin B conjugates.* International Journal of Biological Macromolecules, 2018. **108**: p. 1101-1109.
20. Kothandaraman, G.P., et al., *Anti-fungal and anti-leishmanial activities of pectin-amphotericin B conjugates.* Journal of Drug Delivery Science and Technology, 2017. **39**: p. 1-7.
21. Farber, S., et al., *Galactomannan–amphotericin B conjugate: synthesis and biological activity.* Polymers for Advanced Technologies, 2011. **22**(1): p. 119-125.
22. Francis, A.P., S. Gurudevan, and A. Jayakrishnan, *Synthetic polymannose as a drug carrier: synthesis, toxicity and anti-fungal activity of polymannose-amphotericin B conjugates.* J Biomater Sci Polym Ed, 2018. **29**(13): p. 1529-1548.
23. Ravichandran, V., et al., *Synthetic Polysaccharides as Drug Carriers: Synthesis of Polyglucose-Amphotericin B Conjugates and In Vitro Evaluation of Their Anti-Fungal and Anti-Leishmanial Activities.* J Nanosci Nanotechnol, 2018. **18**(4): p. 2405-2414.
24. Silva, D.M., et al., *Structural analysis of dextrins and characterization of dextrin-based biomedical hydrogels.* Carbohydr Polym, 2014. **114**: p. 458-66.
25. Delgado, A.V., et al., *Measurement and interpretation of electrokinetic phenomena.* J Colloid Interface Sci, 2007. **309**(2): p. 194-224.
26. Gomes-Alves, A.G., et al., *Development of an automated image analysis protocol for quantification of intracellular forms of Leishmania spp.* PLOS ONE, 2018. **13**(8): p. e0201747.
27. Sereno, D. and J.L. Lemesre, *Axenically cultured amastigote forms as an in vitro model for investigation of antileishmanial agents.* Antimicrobial Agents and Chemotherapy, 1997. **41**(5): p. 972-976.

28. Gomes, M.S., et al., *Engagement of Toll-like receptor 2 in mouse macrophages infected with Mycobacterium avium induces non-oxidative and TNF-independent anti-mycobacterial activity.* Eur J Immunol, 2008. **38**(8): p. 2180-9.
29. Vinogradov, S.V., T.K. Bronich, and A.V. Kabanov, *Nanosized cationic hydrogels for drug delivery: preparation, properties and interactions with cells.* Adv Drug Deliv Rev, 2002. **54**(1): p. 135-47.
30. Vasir, J.K., M.K. Reddy, and V.D. Labhasetwar, *Nanosystems in Drug Targeting: Opportunities and Challenges.* Current Nanoscience, 2005. **1**(1): p. 47 - 64.
31. Kalluru, R., et al., *Poly(lactide-co-glycolide)-rifampicin nanoparticles efficiently clear Mycobacterium bovis BCG infection in macrophages and remain membrane-bound in phago-lysosomes.* J Cell Sci, 2013. **126**(Pt 14): p. 3043-54.
32. Wang, L., et al., *Safety of nanosuspensions in drug delivery.* Nanomedicine, 2017. **13**(2): p. 455-469.
33. Alvarez, C., D.H. Shin, and G.S. Kwon, *Reformulation of Fungizone by PEG-DSPE Micelles: Deaggregation and Detoxification of Amphotericin B.* Pharmaceutical research, 2016. **33**(9): p. 2098-2106.
34. Abu Ammar, A., et al., *Amphotericin B-loaded nanoparticles for local treatment of cutaneous leishmaniasis.* Drug Deliv Transl Res, 2019. **9**(1): p. 76-84.
35. Mehenni, L., et al., *Preparation and Characterization of Spherical Amorphous Solid Dispersion with Amphotericin B.* Pharmaceutics, 2018. **10**(4).
36. Sun, B., et al., *Linear dextrin as curcumin delivery system: Effect of degree of polymerization on the functional stability of curcumin.* Food Hydrocolloids, 2018. **77**: p. 911-920.
37. Hu, X., et al., *Synthesis and characterization of dextrin monosuccinate.* Carbohydr Polym, 2013. **97**(1): p. 111-5.
38. Gurudevan, S., A.P. Francis, and A. Jayakrishnan, *Amphotericin B-albumin conjugates: Synthesis, toxicity and anti-fungal activity.* Eur J Pharm Sci, 2018. **115**: p. 167-174.
39. Kim, Y.T., et al., *A thermosensitive vaginal gel formulation with HPgammaCD for the pH-dependent release and solubilization of amphotericin B.* Eur J Pharm Sci, 2010. **41**(2): p. 399-406.
40. Gagoś, M. and M. Arczewska, *FTIR spectroscopic study of molecular organization of the antibiotic amphotericin B in aqueous solution and in DPPC lipid monolayers containing the sterols cholesterol and ergosterol.* European Biophysics Journal, 2012. **41**(8): p. 663-673.
41. Schwartzman, G., et al., *Ambiguities in IR and X-ray characterization of amphotericin B.* J Pharm Sci, 1978. **67**(3): p. 398-400.
42. Angra, P.K., et al., *Amphotericin B microspheres: a therapeutic approach to minimize toxicity while maintaining antifungal efficacy.* J Microencapsul, 2009. **26**(7): p. 580-7.
43. Zia, Q., et al., *Biomimetically engineered Amphotericin B nano-aggregates circumvent toxicity constraints and treat systemic fungal infection in experimental animals.* Sci Rep, 2017. **7**(1): p. 11873.
44. Zhou, L., et al., *Preparation, characterization, and evaluation of amphotericin B-loaded MPEG-PCL-g-PEI micelles for local treatment of oral Candida albicans.* International journal of nanomedicine, 2017. **12**: p. 4269-4283.
45. Al-Quadeib, B.T., et al., *Stealth Amphotericin B nanoparticles for oral drug delivery: In vitro optimization.* Saudi Pharmaceutical Journal, 2015. **23**(3): p. 290-302.
46. Zu, Y., et al., *Preparation and characterization of amorphous amphotericin B nanoparticles for oral administration through liquid antisolvent precipitation.* European Journal of Pharmaceutical Sciences, 2014. **53**: p. 109-117.
47. Choi, K.C., et al., *Amphotericin B-incorporated polymeric micelles composed of poly(d,l-lactide-co-glycolide)/dextran graft copolymer.* Int J Pharm, 2008. **355**(1-2): p. 224-30.

48. Sanchez-Brunete, J.A., et al., *Amphotericin B molecular organization as an essential factor to improve activity/toxicity ratio in the treatment of visceral leishmaniasis.* J Drug Target, 2004. **12**(7): p. 453-60.
49. Espada, R., et al., *In vivo distribution and therapeutic efficacy of a novel amphotericin B poly-aggregated formulation.* Journal of Antimicrobial Chemotherapy, 2008. **61**(5): p. 1125-1131.
50. Larabi, M., et al., *New lipid formulation of amphotericin B: spectral and microscopic analysis.* Biochimica et Biophysica Acta (BBA) - Biomembranes, 2004. **1664**(2): p. 172-181.
51. van Etten, E.W., et al., *Mild heating of amphotericin B-desoxycholate: effects on ultrastructure, in vitro activity and toxicity, and therapeutic efficacy in severe candidiasis in leukopenic mice.* Antimicrob Agents Chemother, 2000. **44**(6): p. 1598-603.
52. Petit, C., et al., *Activity of a heat-induced reformulation of amphotericin B deoxycholate (fungizone) against Leishmania donovani.* Antimicrob Agents Chemother, 1999. **43**(2): p. 390-2.
53. Zia, Q., et al., *Self-assembled amphotericin B-loaded polyglutamic acid nanoparticles: preparation, characterization and in vitro potential against Candida albicans.* Int J Nanomedicine, 2015. **10**: p. 1769-90.
54. Tiyaboonchai, W. and N. Limpeanchob, *Formulation and characterization of amphotericin B-chitosan-dextran sulfate nanoparticles.* Int J Pharm, 2007. **329**(1-2): p. 142-9.
55. Mullen, A.B., K.C. Carter, and A.J. Baillie, *Comparison of the efficacies of various formulations of amphotericin B against murine visceral leishmaniasis.* Antimicrobial agents and chemotherapy, 1997. **41**(10): p. 2089-2092.
56. Faheem, A. and Y. Haggag, *Evaluation of nano spray drying as a method for drying and formulation of therapeutic peptides and proteins.* Frontiers in Pharmacology, 2015. **6**(140).
57. Van de Ven, H., et al., *PLGA nanoparticles and nanosuspensions with amphotericin B: Potent in vitro and in vivo alternatives to Fungizone and AmBisome.* Journal of Controlled Release, 2012. **161**(3): p. 795-803.
58. Butani, D., C. Yewale, and A. Misra, *Topical Amphotericin B solid lipid nanoparticles: Design and development.* Colloids Surf B Biointerfaces, 2016. **139**: p. 17-24.
59. Deray, G., *Amphotericin B nephrotoxicity.* J Antimicrob Chemother, 2002. **49 Suppl 1**: p. 37-41.
60. ISO10993-5:2009, *Biological Evaluation of Medical Devices – Part 5: Tests for In Vitro Cytotoxicity.* 2009. 34.
61. Espuelas, M.S., et al., *Polymeric carriers for amphotericin B: in vitro activity, toxicity and therapeutic efficacy against systemic candidiasis in neutropenic mice.* Journal of Antimicrobial Chemotherapy, 2003. **52**(3): p. 419-427.
62. Velásquez, A.M.A., et al., *Efficacy of a Binuclear Cyclopalladated Compound Therapy for Cutaneous Leishmaniasis in the Murine Model of Infection with Leishmania amazonensis and Its Inhibitory Effect on Topoisomerase 1B.* Antimicrobial agents and chemotherapy, 2017. **61**(8): p. e00688-17.
63. Lage, P.S., et al., *Antileishmanial activity and evaluation of the mechanism of action of strychnobiflavone flavonoid isolated from Strychnos pseudoquina against Leishmania infantum.* Parasitol Res, 2015. **114**(12): p. 4625-35.
64. Barros, D., S.A. Costa Lima, and A. Cordeiro-da-Silva, *Surface functionalization of polymeric nanospheres modulates macrophage activation: relevance in leishmaniasis therapy.* Nanomedicine (Lond), 2015. **10**(3): p. 387-403.
65. Alvani, K., X. Qi, and R.F. Tester, *Use of carbohydrates, including dextrins, for oral delivery.* Starch - Stärke, 2011. **63**(7): p. 424-431.

66. Gonçalves, C., et al., *Dextrin nanoparticles: Studies on the interaction with murine macrophages and blood clearance.* Colloids and Surfaces B: Biointerfaces, 2010. **75**(2): p. 483-489.
67. Asai, T., et al., *In vitro biocompatibility of dextrin: the addition of a low concentration of dextrin in the medium promotes the cell activity of L929 mouse fibroblasts.* Cell Biol Int, 2011. **35**(6): p. 645-8.
68. ASTME2524-08(2013), *Standard Test Method for Analysis of Hemolytic Properties of Nanoparticles, ASTM International, West Conshohocken, PA, 2013.*
69. Moraes Moreira Carraro, T.C., et al., *Assessment of in vitro antifungal efficacy and in vivo toxicity of Amphotericin B-loaded PLGA and PLGA-PEG blend nanoparticles.* J Mycol Med, 2017. **27**(4): p. 519-529.
70. Ribeiro, T.G., et al., *Novel targeting using nanoparticles: an approach to the development of an effective anti-leishmanial drug-delivery system.* International journal of nanomedicine, 2014. **9**: p. 877-890.
71. Petri e Silva, S.C., et al., *Effects of nitro-heterocyclic derivatives against Leishmania (Leishmania) infantum promastigotes and intracellular amastigotes.* Exp Parasitol, 2016. **163**: p. 68-75.
72. Escobar, P., et al., *Sensitivities of Leishmania species to hexadecylphosphocholine (miltefosine), ET-18-OCH(3) (edelfosine) and amphotericin B.* Acta Trop, 2002. **81**(2): p. 151-7.
73. Chavez-Fumagalli, M.A., et al., *New delivery systems for amphotericin B applied to the improvement of leishmaniasis treatment.* Rev Soc Bras Med Trop, 2015. **48**(3): p. 235-42.
74. Seifert, K., P. Escobar, and S.L. Croft, *In vitro activity of anti-leishmanial drugs against Leishmania donovani is host cell dependent.* J Antimicrob Chemother, 2010. **65**(3): p. 508-11.
75. Golenser, J., et al., *Efficacious treatment of experimental leishmaniasis with amphotericin B-arabinogalactan water-soluble derivatives.* Antimicrobial agents and chemotherapy, 1999. **43**(9): p. 2209-2214.

CHAPTER 4 - HYALURONIC ACID-AMPHOTERICIN B NANOCOMPLEXES: A PROMISING ANTI-LEISHMANIAL DRUG DELIVERY SYSTEM

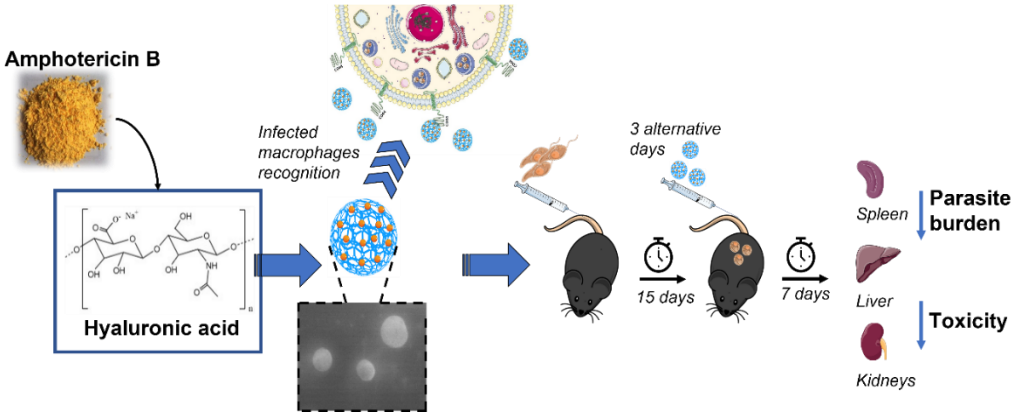

Hyaluronic acid-Amphotericin B self-assembly nanocomplexes (HA-AmB), processed by freeze-drying (FD) or nano spray-drying (SD), were developed using a simple process that favors the non-covalent drug association to the polysaccharide in an amorphous state. The obtained water-soluble formulations presented a nanometric size range (300-600 nm), a high colloidal stability (zeta potential around -39 mV) and a good percentage of associated AmB (15 – 18 %) in aggregated and super-aggregated states. The nanocomplexes showed *in vitro* less cytotoxic and hemolytic effects comparatively to the free-drug. An effective decrease in the intramacrophagic infection with *L. infantum* (IC_{50} of 0.026 and 0.030 μM for HA-AmB FD and HA-AmB SD, respectively) was also observed, being the best balance of safety *vs* efficacy observed for the HA-AmB SD nanocomplex (selectivity index (SI) of 651). Treatment of *L. infantum*-infected C57BL/6 mice with HA-AmB SD nanocomplex for 3 alternative days showed a potent parasite reduction in the spleen and liver, although lower than that achieved with AmBisome® in the liver, but of a similar order of magnitude, bearing no signs of toxicity commonly observed upon free-AmB treatment. Efficacy, stability, safety and low cost features the potential of HA-AmB SD nanocomplex for leishmaniasis therapeutics.

Adapted from Silva-Carvalho, R. et al. (2022). Biomaterials Science, (In Press).

4.1. Introduction

Leishmaniasis is a disease caused by an obligate intra-macrophage protozoa belonging to the *Leishmania* genus that has high rates of morbidity and mortality throughout the world [1, 2]. Depending on the *Leishmania* species involved and the host immune response, this disease displays at least four clinical manifestations ranging in aggressiveness: cutaneous, diffuse cutaneous, mucocutaneous and visceral, which is fatal if untreated [2, 3]. Leishmaniasis is still considered a health concern around the world as the available control or treatment strategies are inadequate. In fact, the low global investment in new anti-parasitic drugs and the lack of human vaccines for leishmaniasis makes chemotherapy the primary method used to control this disease [4, 5]. However, a greater part of these drugs have aggressive side effects, limited effectivity and demand rigorous regimens of treatment [6]. Low patient compliance and treatment failure associated with the excellent biochemical machinery of the parasite can further result in the emergence of parasite resistances and the prevalence of the disease [7, 8]. Among various available drugs, Amphotericin B (AmB) is considered the most important second-line drug for treating leishmaniasis [6, 9]. Unfortunately, the clinical usefulness of AmB is restricted as it is difficult to solubilize, promote side effects and is toxic, mainly to the kidneys, central nervous system and liver [9]. Even the conventional micellar formulation Fungizone® presents serious disadvantages being its use restricted due to nephrotoxicity in the host [10]. To circumvent toxicity issues associated with AmB, several drug delivery systems (Ambisome®, Amphotec® and Abelcet®) have been produced and introduced in the market [11]. Ambisome®, a lipid-based AmB formulation, exhibit high efficiency and permits the use of relatively large doses of the drug, resulting in a better overall treatment. Notwithstanding that, this liposomal formulation is inaccessible to the low-income populations in developing countries, due to the high production costs [12]. Thus, safer, potent and cost-effective strategies have been pursued to improve the therapeutic efficacy of AmB, such as the use of biocompatible and biodegradable polysaccharides as drug carriers [13]. The use of polysaccharides-conjugates allows drug solubilization, toxicity reduction and may enhance cellular uptake by targeting the drug to infected cells [9, 14]. Numerous works have described the conjugation of AmB to different natural polysaccharides, such as arabinogalactan [9, 13, 15], dextran [16, 17], gum arabic [18], sodium alginate [19], pectin [20], galactomannan [21]. Nevertheless, those polysaccharide-based AmB formulations were prepared by a complex reductive amination aiming the covalent conjugation of the drug [13]. In our previous study, Dextrin-AmB nanocomplexes were produced by employing a simple and inexpensive process based on non-covalent interactions. It was shown that the obtained water-soluble formulations possess similar effects to the free-AmB against *Leishmania*-infected macrophages, with reduced cytotoxicity [22].

Hyaluronic acid (HA), a naturally occurring glucosaminoglycan, is a very versatile polysaccharide widely used for various biomedical applications. HA is a highly hydrophilic, biocompatible, biodegradable, mucoadhesive, non-toxic and non-immunogenic [23, 24]. In addition, HA is able to recognize and bind to the Cluster of Differentiation 44 (CD44), a receptor over-expressed by activated/infected macrophages [25], being transported to the phagolysosome after internalization, thus targeting the *Leishmania* parasites which reside in this compartment [26].

4.2. Material and Methods

4.2.1. Reagents

Amphotericin B (AmB) powder from Streptomyces sp., Resazurin Sodium salt, 4',6-diamidino-2-phenylindole (DAPI), Triton X-100, paraformaldehyde, Schneider's Insect medium, sodium tetraborate decahydrate, potassium bromide, phenol red and hemin were purchased from Sigma-Aldrich (Missouri, USA). Glucose anhydrous was purchased from LabChem (Pennsylvania, USA). AmBisome® was gifted from Gilead Sciences (California, USA). Sodium hyaluronate (Primalhyal 20-50 kDa) was gifted from Soliance SA (Pomacle, France). Dimethylsulfoxide (DMSO ATCC® 4-X™) was acquired from American Type Culture Collection (ATCC, Virginia, USA). Dulbecco's Modified Eagle Medium (DMEM), fetal bovine serum (FBS) and penicillin-streptomycin were obtained from Merck Millipore (Massachusetts, USA). Roswell Park Memorial Institute (RPMI) 1640 Glutamax supplemented medium, L-glutamine (GlutaMAX™-I) and minimum essential medium non-essential amino acids solution were purchased from Gibco (Massachusetts, USA). Dialysis tubing with a molecular weight cut-off of 1000 Da was purchased from Orange Scientific (Braine-l'Alleud, Belgium). High-content screening (HCS) CellMask™ Deep Red stain was purchased from Invitrogen (California, USA). Acetonitrile and Formic acid were purchased from Fisher Scientific (New Hampshire, USA).

4.2.2. Hyaluronic acid-Amphotericin B production

Hyaluronic acid-Amphotericin B (HA-AmB) nanocomplexes were obtained as previously reported Dextrin-Amphotericin B formulations [22]. Hyaluronic acid (HA, molecular weight of 20-50 kDa) was mixed with amphotericin B (AmB) (mass ratio of 4:1) and gently dissolved in 0.1 M borate buffer pH 11, protected from light, at 4 °C for 48 h. Subsequently, the solution was dialyzed at 4 °C against dH_2O using a membrane with a molecular weight cut-off 1000 Da, frozen and processed in a freeze-drier (Coolsafe 100-9 Pro, Labogene, Allerød, Denmark) or in a Nano Spray Dryer B-90 HP (Büchi Labortechnik AG, Flawil, Switzerland) at the following conditions: nozzle with a mean pores size of 2-25 µm, vibrational frequency at 120 kHz, feeding rate at 40 %, gas flow at 10 L/min and inlet

temperature at 120 °C. HA without AmB was processed, as control, using the same conditions. All the formulations were sterilized by ethylene oxide for 15 h at 53 ± 1 °C.

4.2.3. HA-AmB characterization

4.2.3.1. Size and zeta potential

Nanocomplexes and AmBisome® mean size and zeta potential were measured by Dynamic Light Scattering (DLS), after dissolution in dH_2O using a Malvern Zetasizer NanoZS, (Malvern Instruments Ltd., Worcestershire, UK). Measurements were performed in triplicate.

4.2.3.2. Morphology analysis

4.2.3.2.1. Scanning electron cryo-microscopy (Cryo-SEM)

HA-AmB nanocomplexes, dispersed in dH_2O at 2 mg/mL, were rapidly cooled in sub-cooled nitrogen and transferred under vacuum to the cryo stage (Gatan, Alto 2500, UK). The specimens were fractured, sublimated for 120 seconds at –90 °C and sputter-coated with Au/Pd for 45 seconds. The samples were then transferred into the observation chamber of an electron microscope (SEM/EDS: JEOL JSM 6301F/Oxford Inca Energy 350 from the Laboratory for Scanning Electron Microscopy and X-Ray Microanalysis at Materials Centre of the University of Porto (CEMUP)). The observation was performed at –150 °C and 15 kV.

4.2.3.2.2. Scanning electron microscopy (SEM)

Spray dried formulation was fixed using a double-sided electrically conductive carbon adhesive tape (PELCO Tabs™, California, USA) on an aluminum pin stub, sputter coated with a 20 Å gold layer and then observed using a scanning electron microscopy (SEM; FEI Quanta 650 FEG Environmental, Field Electron and Ion Company, Oregon, USA). Images were obtained at an excitation voltage of 5 kV.

4.2.3.3. Fourier-transform infrared spectroscopy (FTIR)

FTIR was carried out in an ABB Bomem FTLA2000-104 spectrophotometer (Québec, Canada) using dry KBr to obtain a solid pellet. The analysis was performed at a resolution of 4 cm^{-1} averaging 64 scans.

4.2.3.4. Differential scanning calorimetry (DSC)

DSC of the formulations was achieved with a DSC 600 Perkin-Elmer (Massachusetts, USA). A known amount of samples equivalent to 0.7 mg of AmB were weighed in aluminum DSC pans.

Analysis was performed from 25-235 °C at a heating rate of 10 °C/min under nitrogen atmosphere. An empty pan was used as the reference and all samples were analyzed in triplicate.

4.2.3.5. Powder X-ray diffraction (XRD)

For XRD analysis, samples were placed in a Bragg-Brentano geometry and scanned from 5° to 50° 2θ angular range using a PANalytical X'Pert Pro X-ray diffractometer equipped with X'Celerator detector and secondary monochromator (Malvern Panalytical, United Kingdom), where Cu Kα radiation was used as X-ray source (40 kV operating voltage; 30 mA current).

4.2.3.6. UV-Vis spectral study

Ultraviolet spectroscopic analysis of AmB, AmBisome® and HA-AmB nanocomplexes was performed in the range of 300-450 nm on a UV-visible spectrophotometer (JASCO V-560 series, Jasco Inc., Maryland, USA) operated at a band width of 5 nm, data pitch of 1 nm and scanning speed of 400 nm/min. The aggregation state of AmB was monitored as the ratio of peak I (315-350) to the peak IV (408-410). Free-AmB and AmB in the formulations were both analyzed at the same concentration (10 μM).

4.2.3.7. Determination of drug content and association efficiency

AmB content (% w/w) and association efficiency (AE %) in the nanocomplexes were determined using a High-Performance Liquid Chromatography (HPLC) system Finnigan LXQ from ThermoElectron Corporation (Thermo Fisher Scientific, Massachusetts, USA), equipped with an ion trap Mass Spectrometer (MS) (Thermo Fisher Scientific, Massachusetts, USA) and a 2998 photodiode array (PDA) wavelength detector (Waters Corporation, Massachusetts, USA). Briefly, AmB and nanocomplexes were dissolved in acetonitrile:milli-Q water:formic acid (39.22:58.33:2.45 % (v/v)) under mild stirring and protected from light during 2 h at room temperature, diluted to a specific concentration using acetronitrile:milli-Q water (39.22:60.78 % (v/v)) and then filtered through a 0.22 μm pore size Nylon filter (Tecnocroma, Caldas da Rainha, Portugal). The mobile phase was composed by (A) milli-Q water with 0.1 % (v/v) formic acid and (B) acetonitrile with 0.1 % (v/v) formic acid. The elution method was performed with a solvent gradient of 80 % A and 20 % B, reaching 10 % A and 90 % B at 15 min and 80 % A and 20 % B at 25 min, condition that was maintained until the end of the analysis (30 min). The mass spectrometer was operated in ESI positive ion mode with the ion spray voltage 5000 V and using the Selected Ion Monitoring mode with scan ranges from 923 to 925 m/z and the UV detection wavelengths were defined to 387 and 408 nm.

4.2.4. *In vitro* assays

4.2.4.1. Cells and culture description

Human embryonic kidney (HEK293T) cells were kindly provided by Dr. Tiago dos Santos (i3S - Instituto de Investigação e Inovação em Saúde, Universidade do Porto, Portugal; INEB - Instituto de Engenharia Biomédica, Universidade do Porto, Portugal). Cells were grown at 37 °C in a 5 % CO_2 atmosphere within Dulbecco's modified essential medium (DMEM) supplemented with 10 % (v/v) iFBS and 1 % (v/v) Penicillin (10000 U/mL)-Streptomycin (10000 µg/mL).

Bone marrow-derived macrophages (BMMΦ) were generated by adapting the protocol described by Gomes et al. [27]. Briefly, bone-marrow cells, collected by flushing femurs and tibia of C57BL/6 mice with DMEM, were centrifuged, suspended in DMEM supplemented with 1 % (v/v) Minimum Essential Medium Non-Essential (MEM) amino acids solution, 10 % (v/v) iFBS, 50 U/mL penicillin, 50 µg/mL streptomycin (cDMEM) and 20 % (v/v) L929 cell conditioned medium (LCCM), as a source of macrophage colony-stimulating factor, and incubated in petri dishes at 37 °C in a 5 % CO_2 atmosphere. Twenty-four hours later, non-adherent cells were collected with warm cDMEM + 20 % (v/v) LCCM, plated in a 96-well plate (2 x 10^5 cells/mL) and incubated once again at 37 °C in a 5 % CO_2 atmosphere. On the 4th and 7th days, half of the medium was renewed and on the 10th day cells became fully differentiated into macrophages.

4.2.4.2. Cytotoxicity assay

Cytotoxicity (resazurin) assay was performed to evaluate *in vitro* toxicity of the HA-AmB nanocomplexes. BMMΦ (2 x 10^5 cells/mL) and HEK293T (1 x 10^5 cells/mL) were seeded in 96-well plates and incubated for 24 h at 37 °C, in a 5 % CO_2 atmosphere, with increasing concentrations of free-AmB and HA-AmB nanocomplexes (0.78-67.5 µM). Cytotoxicity was determined after incubating the cells with 10 % (v/v) of a 2.5 mM resazurin solution at 37 °C, in a 5 % CO_2 atmosphere, for another 4 h. Fluorescence was measured (λex 560/λem 590) in a Biotek Cytation 3 microplate reader (Biotek, Vermont, USA). Results were expressed as the mean percentage ± SD of viable cells relatively to control and the assay was performed in triplicate at least three times.

4.2.4.3. Hemolysis

A known number of red blood cells (RBCs) (1 x 10^8 cells/mL), obtained from a healthy dog after owners' agreement, were incubated in a 48-well plate containing 50 µL of HA-AmB nanocomplexes (containing 1 - 32 µM AmB equivalents in final volume of 500 µL) at 37 °C for 30 min under

agitation (120 rpm). Free-AmB was dissolved in 200 µL of DMSO and further diluted in PBS pH 7.4 (final DMSO percentage inferior to 1 %) before treating the RBCs. After stipulated time, treated blood was centrifuged for 10 min at 1200 x g, 4 °C and the supernatant collected in order to determine the extent of hemolysis by measuring the absorbance at 540 nm. Results were expressed as a percentage of hemolysis with respect to the amount of hemoglobin released in the presence of 1 % (v/v) Triton X-100, a positive control for 100 % cell lysis.

4.2.4.4. Parasites

L. amazonensis (MHOM/BR/LTB0016) and *L. infantum* promastigotes (MHOM/MA/67/ITMAP-263) were cultured at 25 °C in Schneider's Insect medium supplemented with 10 % (v/v) heat inactivated fetal bovine serum (iFBS), 100 U/mL penicillin, 100 µg/mL streptomycin, 5 mM HEPES pH 7.4 and 5 µg/mL phenol red and in RPMI 1640 Glutamax supplemented with 10 % (v/v) iFBS, 50 U/mL penicillin, 50 µg/mL streptomycin and 20 mM HEPES pH 7.4, respectively. Axenic amastigotes of *L. infantum* were obtained as described in the literature [28] and maintained at 37 °C, 5 % CO_2 in MAA/20 medium supplemented with 20 % (v/v) iFBS, 2 mM L-Glutamine and 0.023 mM hemin. Different morphological features (round and immobile organisms, about 2-3 µm long and without visible flagella) were assessed by microscopy in order to determine the culture purity (around 95 %).

4.2.4.5. *In vitro* inhibitory effects on *Leishmania* axenic cultures

Promastigotes of *L. infantum* and *L. amazonensis* at a density of 3 x 10^5 cells/well were seeded in 96-well plates using complete RPMI medium or complete Schneider's Insect medium, respectively, containing increasing concentrations of free-AmB and HA-AmB nanocomplexes (0.0029 - 0.75 µM) and the plates were incubated for 24 h at 26 °C. After the incubation period, 20 µL of a 2.5 mM resazurin solution prepared in PBS and filtered was added to each well; then the plates were incubated for additional 24 h at 26 °C. Using a SpectraMAX GeminiXS microplate reader (Molecular Devices LLC, California, USA) the fluorescence intensity was measured (λex 560/λem 590). The results were expressed as the mean percentage ± SD of viable parasites relatively to control and the assay was performed in triplicate at least three times.

4.2.4.6. *In vitro* inhibitory effects on *L. infantum* intramacrophage amastigotes

BMMΦ in 96-well plates were infected with *L. infantum* amastigotes at a multiplicity of infection (MOI) of 10 per macrophage. After 6 h, non-phagocytosed parasites were removed by washing with cDMEM medium and infected cells were incubated for 24 h more prior to treating with free-AmB

and HA-AmB nanocomplexes (0.0039 - 1 μM). Twenty-four hours later, cell monolayers were fixed with paraformaldehyde and stained with DAPI and with HCS CellMask™ Deep Red stain to be analyzed in an IN Cell Analyzer 2000 microscope (GE Healthcare, Illinois, USA) as described by Gomes-Alves, A. G. et al [29]. Anti-leishmanial activity results were expressed as the mean percentage ± SD of infected cells relatively to control. The assay was performed in triplicate, at least three times.

4.2.5. *In vivo* assays

4.2.5.1. Animals

C57BL/6 and National Marine Research Institute (NMRI) mice, purchased from the animal facility of the Instituto de Investigação e Inovação em Saúde (i3S), were housed in individually-ventilated cages under pathogen-free conditions in an Animal Biosafety level 2 (ABSL2) room at i3S animal facility, with a 12 h light/12 h dark cycle and provided with commercial pellet diets and sterile distilled water ad libitum. Animals for each experiment were age (at 8 to 16 weeks) and sex matched. Depending on the assays, mice were euthanized by isoflurane anesthesia followed by cervical dislocation. Animals' welfare, confirmed through observation of physical appearance and register of weight variations for each animal, was guarantee until sacrifice using enrichment material.

4.2.5.2. Systemic toxicity

Female C57BL/6 mice (with 6-8 weeks of age) were randomly distributed into seven groups (n = 3) for treatment with AmBisome® and HA-AmB SD nanocomplex (selected due to better *in vitro* performance). One hundred microliters of the formulations, dispersed in sterile 5 % (w/v) dextrose for 24 h, at 4 °C, and protected from light, were intravenously (i.v.) administered in the lateral vein of the tail at a dose regimen of 1 and 3 mg AmB/Kg body weight, every other day for a total of 5 days (3 administrations). Control groups were treated with 5 % (w/v) dextrose. Twenty-four hours after the last treatment, mice were anesthetized (50–75 mg/kg ketamine and 0.5–1 mg/kg medetomidine) through i.p. and euthanized by cervical dislocation for liver, kidney and spleen collection.

4.2.5.3. Evaluation of *in vivo* anti-leishmanial activity in *L. infantum* mice model

The *in vivo* anti-leishmanial efficacy of HA-AmB SD was studied against *L. infantum*-infected mice. Female C57BL/6 mice (with 8 weeks of age) were first randomly divided into four groups of 6 animals, as follows: group I (non-infected control group treated with 5 % (w/v) dextrose); group II

(infected control group treated with 5 % (w/v) of Dextrose); group III (infected group treated with Ambisome®); group IV (infected group treated with HA-AmB SD nanocomplex). *L. infantum* promastigotes were passaged through NMRI mice to ensure infectivity. After that, 200 µL of PBS pH 7.4 containing 2×10^7 *L. infantum* promastigotes in stationary phase were injected in the lateral vein of the mice tail belonging to the groups II, III and IV. At 15 days after infection, two randomly selected animals of the group II were euthanized and the liver and spleen removed and homogenized in aseptic conditions, to confirm infection. Treatments with 100 µL of AmBisome® and HA-AmB SD nanocomplex dissolved in sterile 5 % (w/v) dextrose were started on the same day, by i.v administration in the lateral vein of the mice tails for 3 alternative days (1 mg/Kg/day). Control groups received sterile 5 % (w/v) dextrose. Animals were sacrificed 3 days after the end of the treatment and liver and spleen were aseptically removed and weighted. A small part of the organs was kept for histology and the rest again weighted and homogenized, respectively, in 2 and 3 mL of complete Schneider's medium supplemented with 20 % iFBS, 100 U/mL penicillin, 100 mg/mL streptomycin, 5 mg/mL phenol red and 5 mM HEPES sodium salt at pH 7.4. To determine formulations activity, parasite burden in each organ was estimated using a limiting dilution approach [30]. Briefly, homogenates were first diluted to a final concentration of 10 mg/mL and then four-fold serial dilutions were performed in quadruplicate, in a 96-well plate. After 14 days at 25 °C, the wells were examined and the last dilution containing viable promastigotes was recorded and used to determine the number of parasites per organ (parasite burden).

4.2.5.4. Tissue samples and histopathological analysis

Liver, spleen and kidneys collected from the sacrificed animals were fixed in 4 % buffered paraformaldehyde and paraffin-embedded. Tissue sections (2 µm-thick) were stained with hematoxylin & eosin (H&E) (performed at the Molecular Pathology and Immunology department from the Instituto de Ciências Biomédicas Abel Salazar (ICBAS) from University of Porto (Porto, Portugal)) and visualized by optical microscopy.

4.2.5.5. Ethics statement

Animals were handled in compliance with the standards for good animal practice as defined by national authorities (DGV, Law nu1005/92 October 23) and European legislation (EEC/86/609). All procedures involving animals, that respected the 3Rs of replacement, reduction and refinement, were performed in a laminar flow hood cabinet and were approved by the local Animal Ethics Committee of i3S and licensed by the Portuguese Directorate-General of Food and Veterinary

Medicine (DGAV, Ministry of Agriculture, Rural Development and Fishing), on July 7th, 2020 (reference: 009887/2020-07-07) (see appendix).

4.2.6. Statistical analysis

Statistical analysis was caried out using GraphPad Prism 5 (GraphPad Software, California, USA). Two-way ANOVA followed by Bonferroni's multiple comparison post-test was performed wherever appropriate. For the *in vivo* study, the non-parametric analysis of variance Mann-Whitney U test was used to evaluate the differences between treatment groups and control. Results were expressed as mean ± SD and significance was considered as $p < 0.05$. The half maximal inhibitory concentration (IC_{50}) and half maximal cytotoxic concentration (CC_{50}) were calculated by nonlinear regression analysis.

4.3. Results and Discussion

4.3.1. Drug and Hyaluronic acid compatibility: Nanocomplexes production

Hyaluronic acid-AmB formulations were simply prepared by mixing HA and AmB in alkaline borate buffer (pH 11). AmB is a molecule that is classified as a zwitterion since it contains equal NH_3^+ and COO^- groups at neutral pH value. At pH 11, AmB presents negative charge (due to ionized group COO^-). The formation of aggregates is limited owing to the electrostatic repulsions; thus the drug is soluble [31, 32]. Also, the boric acid forms complexes with AmB diols, which also helps to increase its solubility and minimize aggregate formation [9]. When the pH drops below 10, following dialysis against water, AmB becomes neutral and aggregates in weakly-coupled structures (via the dipole-dipole interactions between chromophores [33]) causing lower solubility [31]. However, in the presence of HA, we observed no aggregation during the dialysis process, suggesting the formation of some sort of complex between the two molecules. The soluble nanocomplexes obtained were dried and analyzed by FTIR, DSC and XRD. The FTIR spectra of AmB, HA FD, HA-AmB FD, HA SD and HA-AmB SD are shown in Figure 4.1. In the spectra of the nanocomplexes, all the characteristic peaks of HA, described in the literature [34, 35], were identified, suggesting that no chemical alterations in the polysaccharide structure are occurring. More specifically, hydrogen-bonded -OH stretching vibrations and C-H stretching vibrations are observed at about 3413.7 cm^{-1} and 2916.1 cm^{-1}, respectively. The two sharp bands at 1616.2 and 1411.7 cm^{-1} are assigned to the asymmetrical C=O stretching and symmetrical C–O stretching, respectively; the three peaks centered at 1153.3, 1080, and 1041.4 cm^{-1} corresponding to the C-O-C (O-bridge), C-O (exocyclic) and C-OH groups, respectively and the band at 945.05 cm^{-1} to the asymmetrical out-of-phase ring vibration. Characteristic peaks of AmB

(C=C stretching vibration from polyene (1558.3 cm^{-1}); C=O stretching vibration from the carbonyl ester group (1689.5 cm^{-1}); CH_2 and CH_3 symmetric stretching vibrations (2877.5 cm^{-1}); C-C-H bending (chromophore) as well as CH bending (trans-polyene) (1010.6 cm^{-1}); C=O asymmetric stretching vibrations (1068.4 cm^{-1}) and C-H bending and CH_3 rocking vibrations (891.04 cm^{-1})) that have been identified in other polymer-based formulations [19, 20, 36], are not visible in the nanocomplexes spectra (both SD and FD), probably due to the superposition of the HA and AmB peaks. Furthermore, the fact that no new absorbance bands on the HA-AmB nanocomplexes spectra could be observed suggest that no chemical reactions occurred. Kim et al. [37] also showed the disappearance of AmB specific bands after drug association with hydroxypropyl-γ-cyclodextrin, probably due to inclusion complexation of the drug into the polymer cavity.

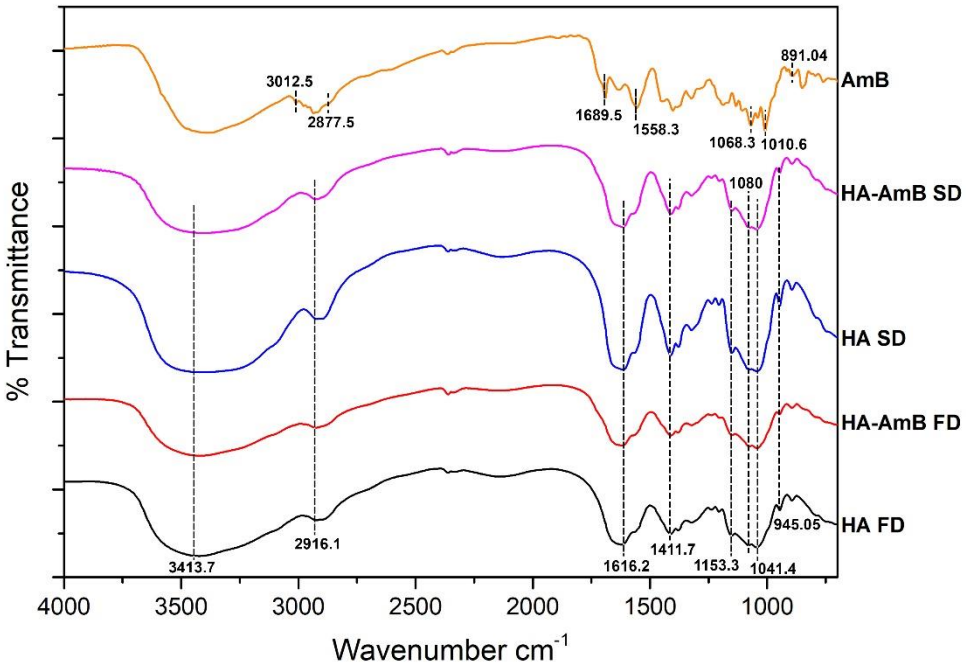

Figure 4.1 - FTIR spectra of HA and HA-AmB nanocomplexes, processed by freeze-dryer and spray-dryer, and free-AmB.

The DSC thermograms in Figure 4.2 show the thermal behavior of AmB and the nanocomplexes spanning the temperature in the range 25-235 °C. AmB present two endothermic peaks, as referred in the literature [38], here determined at 165.9 and 199.5 °C. Similarly to the pure HA described in the literature [39, 40], HA processed by freeze-drying (Figure 4.2 A) or nano spray-drying (Figure 4.2 B) showed also two peaks; an endothermic one around 160.7 (FD) and 171.7 °C (SD), that could be ascribed to the desorption of strongly bound water and an exothermic peak around 228.7 (FD) and 226.6 °C (SD), attributed to the polysaccharide thermal decomposition. Regarding the HA-AmB FD (Figure 4.2 A) and HA-AmB SD (Figure 4.2 B) nanocomplexes, an almost complete disappearance of

the AmB endothermic peaks was observed, being only visible the HA endothermic peak, shifted for lower temperatures.

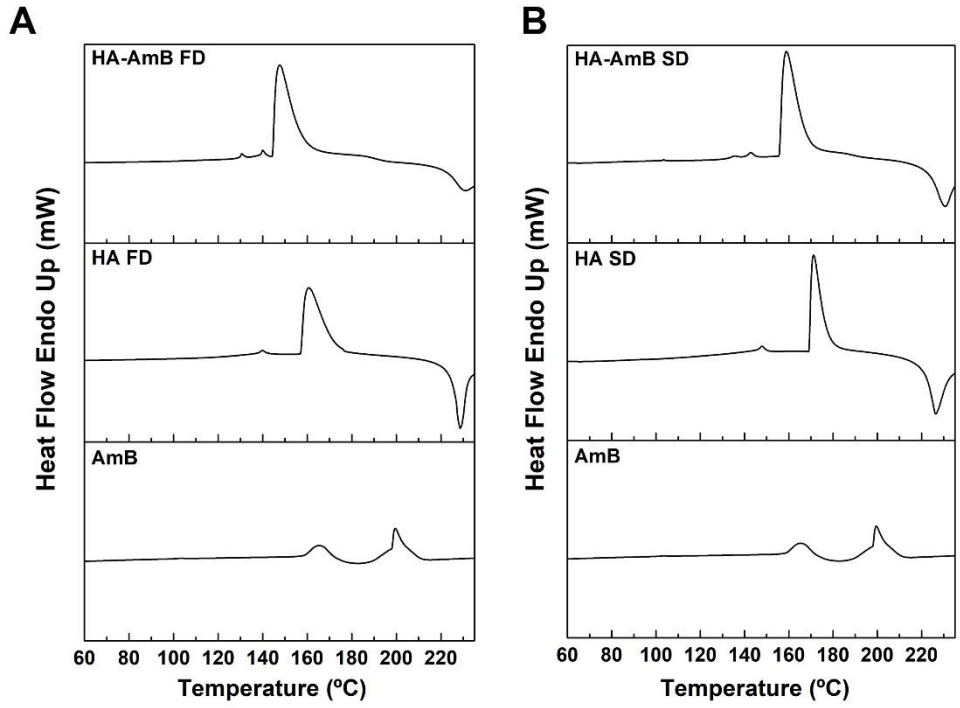

Figure 4.2 - DSC curves of AmB, physical mixture of HA and AmB, **(A)** HA FD and HA-AmB FD nanocomplex and **(B)** HA SD and HA-AmB SD nanocomplex.

This thermal behavior could suggest the formation of an amorphous inclusion complex between the AmB and the HA. A similar phenomenon was found in AmB-cyclodextrin complexes [37], AmB/MPEG-PCL-g-PEI micelles [41] and in AmB encapsulated in pegylated poly(D, L-lactide-co-glycolide) (PLGA) copolymer nanoparticles [42] or in chitosan anchored PLGA nanoparticles [43].

In the powder X-ray diffractogram of free-AmB (Figure 4.3), sharp peaks at 2θ scattered angle of 14.06, 17.26 and 21.7 were observed, confirming the drug crystalline structure [12, 37]. The characteristic peaks of AmB were absent in the nanocomplexes diffractogram (Figure 4.3), only a large diffraction peak being visible, as observed for the processed polysaccharide, suggesting that the amorphous AmB is present in the nanocomplexes. Similar results were reported elsewhere [12, 44, 45]. Therefore, DSC and XRD allowed to confirm the amorphization of AmB in the presence of the polysaccharide. The higher energy state of the amorphous drug formulation is stabilized through the interactions with the polymeric chain networks. Furthermore, amorphization can improve the bioavailability of poorly water soluble drugs by improving its solubility and dissolution rates [46].

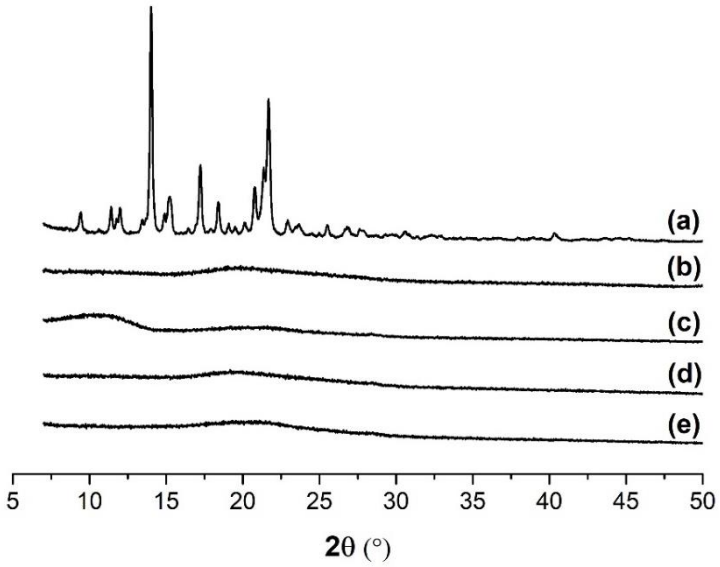

Figure 4.3 - Powder X-ray diffraction patterns of **(a)** AmB, **(b)** HA FD, **(c)** HA-AmB FD nanocomplex, **(d)** HA SD and **(e)** HA-AmB SD nanocomplex.

4.3.2. Nanocomplexes characterization and aggregation state

The simple and straightforward method promoted the AmB association in the polysaccharide matrix, leading the formation of a self-assembly material - the HA-AmB FD and HA-AmB SD nanocomplexes. Despite the simplicity of the used process, the overall yield of HA-AmB FD nanocomplex (79.9 %) was in the range of values described in the literature for other more complex polysaccharide formulations [9, 19], whereas HA-AmB SD presented a lower yield (57.2 %), as expected considering the more complex drying technique used (Table 4.1). Up-scaling the process should result in improved recovery yields, especially in the latter case. The formulations, that easily disperse in aqueous environment, present a mean diameter of 562 ± 20 and 318 ± 35 nm, respectively, with a narrow size distribution (PDI bellow 0.5) (Table 4.1). Particle size has an important role in the biodistribution of the drug, influencing its biological activity [47]. Despite the larger size of our formulations comparatively to the commercial formulation Ambisome® (here determined to have a size of 89 ± 1 nm and a charge of –51.8 ± 3.5 mV), the obtained results prove the suitability of the nanocomplexes to be used as anti-leishmanial nanomedicine since, according to the literature, the obtained size ranges (hundreds of nm) enhance macrophage phagocytic activity [48, 49] and the targeting to infected macrophages [50]. Moreover, intravenously injected nanoparticles within the described size range are mostly taken up by the spleen [48], a *Leishmania*-infected macrophage rich organ. The high zeta potential of the HA-AmB FD and HA-AmB SD nanocomplexes, around –39 mV, ensures long-term colloidal stability in aqueous suspension, since the repulsive forces between similarly charged particles increases stability by preventing aggregation [51].

Table 4.1 - Average size, zeta potential and Overall yield (%) of the produced HA-AmB nanocomplexes dissolved in dH_2O. Results are expressed as mean ± SD of at least three independent assays.

Samples	Overall Yield (%)	Size (nm)	PDI	ζ potential (mV)
HA-AmB FD	79.9	562 ± 20	0.4 ± 0.08	-39.6 ± 2.9
HA-AmB SD	57.2	318 ± 35	0.2 ± 0.02	-39.4 ± 1.1

To evaluate the morphological pattern of the nanocomplexes, cryo-SEM and SEM studies were carried out. Figure 4.4 A and B shows that both nanocomplexes exhibited a spherical shape and were well dispersed without aggregation when in aqueous solution, proving the colloidal stability of the formulations. From the SEM analysis (Figure 4.4 C), HA-AmB SD in its powder form also presents a spherical morphology with smooth non-porous surface.

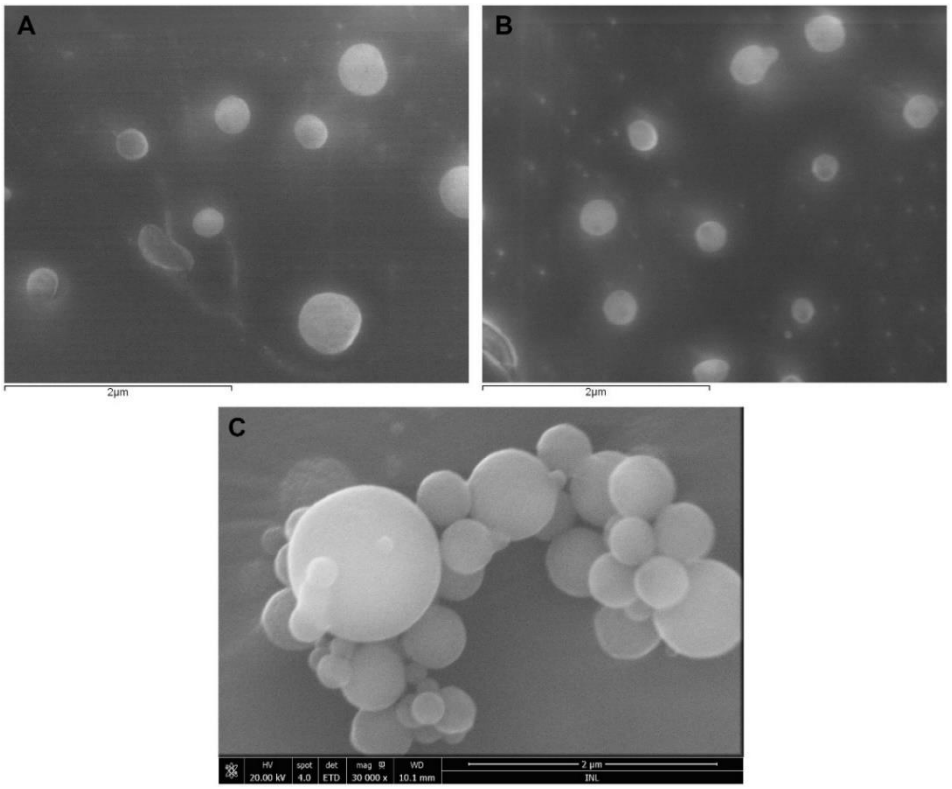

Figure 4.4 - Morphology of **(A)** HA-AmB FD and **(B** and **C)** HA-AmB SD nanocomplexes in dH_2O determined by cryo-SEM **(A** and **B)** (magnification of 30 000x; scale bar = 2 µm) and SEM **(C)**. All the images were obtained at a magnification of 30 000x (scale bar = 2 µm).

HPLC-PDA-MS was applied for AmB quantification. This is a suitable technique to analyze formulations where AmB is not covalently linked to the polysaccharide, thus being detectable with high sensitivity

through the mass spectra. Nevertheless, in this work UV absorption spectra was used as well for quantification purposes. This technique was employed to determine AmB content (% w/w) and association efficiency (AE%) in the produced nanocomplexes (Table 4.2). The detection methods used in the applied protocol, MS and UV (at 387 and 408 nm), allowed to estimate consistently similar AmB content and AE%. More specifically, HA-AmB FD presented an AmB content and an AE% in the range of 17.51-18.73 % and 66-71 %, respectively, whereas HA-AmB SD presented 15.12-15.82 % and 42-44 %, respectively. The differences in the determined AE% between the two formulations are related with the obtained yield which, as referred above, is slightly lower for the spray drying method. Ehrenfreund-Kleinman et al. [9] showed that the drug content in a formulation where AmB was covalently linked to oxidized arabinogalactan ranged from 15-26 % and 14-25 %, depending on whether an imine or amine bond was used, respectively. In another similar study where AmB was conjugated to oxidized sodium alginate, an incorporation efficiency in the range of 80–96 % was estimated [19]. Tiyaboonchai et al. [52] showed a drug association efficacy of up to 65 % in amphotericin B-chitosan-dextran sulfate nanoparticles and Lima et al. [53] showed a drug loading and an encapsulation efficiency of 11.23 % and 73.42 %, respectively, for self-assembled AmB-cashew gum nanoparticles with high acetylation. The formulations in this study were developed using a very simple and straightforward production process without chemical modifications. Notwithstanding, the obtained values referred above are comparable to previously cited polysaccharide-based formulations tested for AmB coupling/incorporation or encapsulation. As mentioned above, up-scaling may significantly improve the association efficiency obtained.

Table 4.2 - AmB association efficiency (%) and drug content (% w/w) of the produced HA-AmB nanocomplexes. Results are expressed as mean ± SD of at least three independent assays.

Samples	Drug content (%)			AmB association efficiency (%)		
	MS (923-925 m/z)	UV (387 nm)	UV (408 nm)	MS (923-925 m/z)	UV (387 nm)	UV (408 nm)
HA-AmB FD	18.73 ± 1.57	17.51 ± 0.61	17.70 ± 0.81	66 ± 4.65	70 ± 2.43	71 ± 3.26
HA-AmB SD	15.82 ± 2.03	15.12 ± 0.61	15.73 ± 0.82	44 ± 5.63	42 ± 1.67	43 ± 2.24

The aggregation and solubility of AmB depends on several factors (e.g., solvents and ionic strength, pH, temperature, final concentration and surfactants [54-57]). It has a huge impact on its cytotoxicity and activity [54, 55]. Spectrophotometric studies are useful for deducing the molecular state of AmB in aqueous environment, and, therefore, the safety of different formulations, since AmB in monomeric form is soluble and safe comparatively to the aggregated one, that is toxic towards mammalian cells [54, 58]. The ratio of absorbance between the first and the fourth peaks of the UV-vis spectra gives the extent of AmB aggregation, being a value < 1 characteristic of the monomeric form and a value > 2 to a super-aggregated form, the later having a lower toxicity [54, 59]. Considering that AmB aggregation state could be affected by the carrier system [60], we evaluated this feature in the nanocomplexes by UV-vis spectroscopy and compare it with free-AmB and AmBisome® (Figure 4.5). AmB presents an absorption spectrum with the four typical bands reported in several works [52, 55], here determined at 410, 387, 368 and 350 nm, and a A350/A410 ratio of 0.32 (after dissolution in 0.1 M borate buffer pH 11 and dilution in dH_2O), meaning its presence in monomeric form. In the nanocomplexes, the first peak of HA-AmB FD and HA-AmB SD underwent a hypsochromic shift and became stabilized at 332 nm and 331 nm, respectively, being the ratio between the bands I/IV of 3.61 and 4.23, respectively. Both spectra are very similar to the one obtained for AmBisome®, commonly referred in the literature as containing AmB in a mixture of different states after dissolution in dH_2O [55].

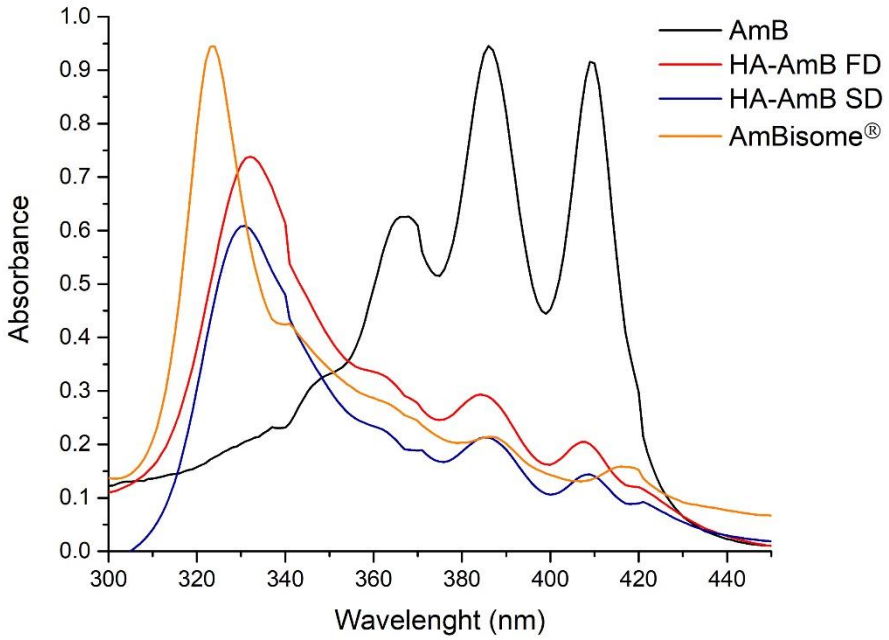

Figure 4.5 - Study of AmB aggregation in its free state or in the AmBisome® and HA-AmB nanocomplexes after dissolution in dH_2O.

The hypsochromic shift observed for the first peak in the AmBisome® spectrum is very accentuated and occurs possibly due to the high association of the drug to the liposome bilayer. This is important since AmB release of the formulation is retarded and, therefore, the toxicity decreases [61]. Considering the spectral high ratios determined for our formulations and in agreement with Espada et al. [55], the AmB present in our nanocomplexes might be in both aggregate and super aggregate states. Also, by the similarities between the spectra of our formulations and AmBisome®, we can assume that AmB in our formulations may also be well associated with the polysaccharide (although the hypsochromic deviation is not so prominent), which may reduce the toxicity of our material.

4.3.3. *In vitro* cytotoxic effects of the nanocomplexes

4.3.3.1. Cell viability

Since nephrotoxicity is highly associated with AmB therapy and macrophages are the host cell of the parasite [62, 63] and therefore, expected to act also as a reservoir of the drug, the toxicity of AmB and HA-AmB nanocomplexes was assessed using a kidney-derived HEK293T cell line and primary culture of BMMΦ. The toxicity induced by the free-AmB and the above referred formulations as a function of drug concentration is shown in Figure 4.6. Regarding the BMMΦ (Figure 4.6 A and C), HA-AmB FD and HA-AmB SD presented cytotoxic concentration (CC_{50}) of 8.37 ± 2.12 and 19.52 ± 1.31 μM, respectively, after 24h exposure. AmB exhibited a more prominent toxicity (CC_{50} of 2.05 ± 0.18 μM). More specifically, AmB concentration as high as 1.76 μM resulted in a cell viability decrease to levels under the 70 % threshold (value that is associated to cytotoxicity [64]) whereas the same was only observed for HA-AmB FD (Figure 4.6 A) and HA-AmB SD (Figure 4.6 C) at concentrations above 5.93 and 13.33 μM, respectively. As hypothesized by Gurudevan et al. [65], the lower toxicity observed for the nanocomplexes could be attributed to the fact that it enters in the cells in a more controlled way, by endocytosis mediated by CD44 receptors, instead of a passive diffusion. Nevertheless, additional studies must be carried out to confirm this assumption. Furthermore, the presence of AmB in its super-aggregated form and not only in aggregated form could be also a good explanation for the observed lower toxicity. Figure 4.6 B and D shows that none of the HA-AmB nanocomplexes promoted a reduction in HEK293T cell viability to levels below the threshold, even at the highest doses tested. In fact, high survival rates were observed in all the tested doses of the nanocomplexes (above 90 %), while free-AmB was cytotoxic to concentrations above 8.89 μM.

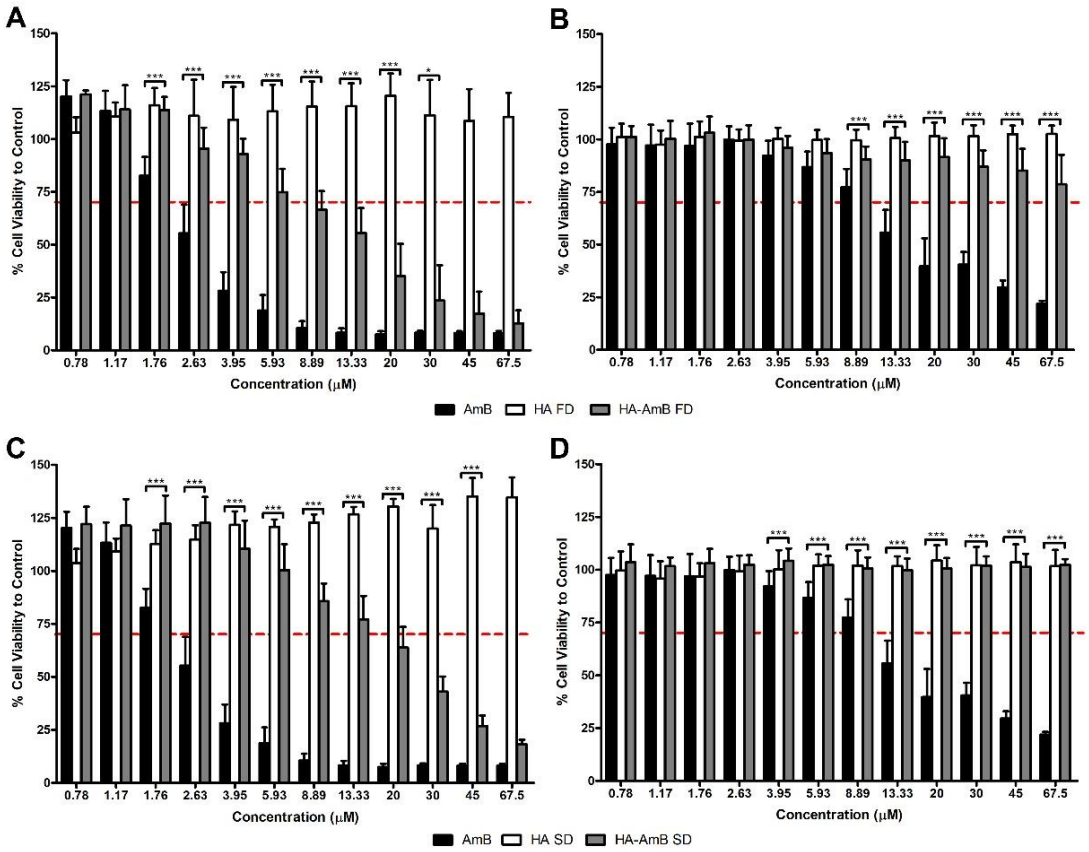

Figure 4.6 - Effect of HA-AmB nanocomplexes on **(A** and **C)** BMMΦ and **(B** and **D)** HEK293T cells viability. Cells were treated for 24 h with different doses (67.5 to 0.78 μM) of HA-AmB FD **(A** and **B)** and HA-AmB SD **(C** and **D)** and the viability was assessed by resazurin assay. All the results are expressed as percentage relative to the control and presented as mean ± SD of at least three independent experiments. HA-AmB FD and HA-AmB SD treatment conditions were compared with the AmB (*) using Bonferroni's multiple comparison post-test (* $p < 0.05$ and *** $p < 0.001$).

Different studies in the literature shows that AmB conjugation to oxidized polymers (e.g. arabinogalactan [66], polymannose [36], sodium alginate [19], dextran [17], galactomannan [21]) or encapsulation in polymeric delivery systems [38, 41, 65, 67-69] significantly reduces the toxic effects of the drug against macrophages and kidney cells. Interestingly and similarly to our process in terms of simplicity, Zia et al. [51] showed that by mixing AmB with Aloe vera leaf extract, super-aggregated AmB nano-assemblies that exhibited less toxicity against the mammalian cell lines HEK-293 and J774A.1 (IC_{50} of 120 or > 200 mg/L, respectively) were obtained. Here we prove that a simple inclusion of the drug to the polysaccharide allowed to obtain a formulation that displays also reduced toxicity. Furthermore, the use of HA improved even more this feature comparatively to our previous work regarding AmB nanocomplexes with dextrin [22].

4.3.3.2. Hemolytic activity

As a measure of *in vitro* toxicity, red blood cells (RBCs) lysis has been also studied. AmB was the most toxic formulation for the dog's RBCs at almost all the tested doses (2, 4, 8, 16 and 32 μM), promoting a hemolysis rate between 13.4 – 83.6 % (Figure 4.7). As referred in the literature, hemolysis is a severe side effect of AmB [70]. Nishi et al. [18] showed that pure AmB was hemolytic at 3.5 μg/mL (± 3.8 μM), causing 50 % of RBCs lysis.

Several works have been reporting strategies to decrease the hemolytic effect of AmB by either conjugation to polysaccharides [18-20, 71] or by encapsulation to delivery systems [72, 73]. The HA-AmB FD and HA-AmB SD nanocomplexes exhibited more than 50 % of hemolysis at the highest concentration tested (32 μM) (Figure 4.7). Nevertheless, even at this concentration a significant decrease of the hemolytic effect (1.410- and 1.497-fold less, respectively), comparatively to the free-AmB, was observed. Negligible percentage of hemolysis (< 5 %) was observed for HA-AmB FD at 2 μM (2.8 ± 1.6 %) and for HA-AmB SD at 4 μM (1.3 ± 1.4 %). To some extent, the polysaccharide is exerting a stabilizing and protective effect on the drug, decreasing its toxicity towards RBCs and increasing the safety margin of our nanocomplexes for intravenous administration.

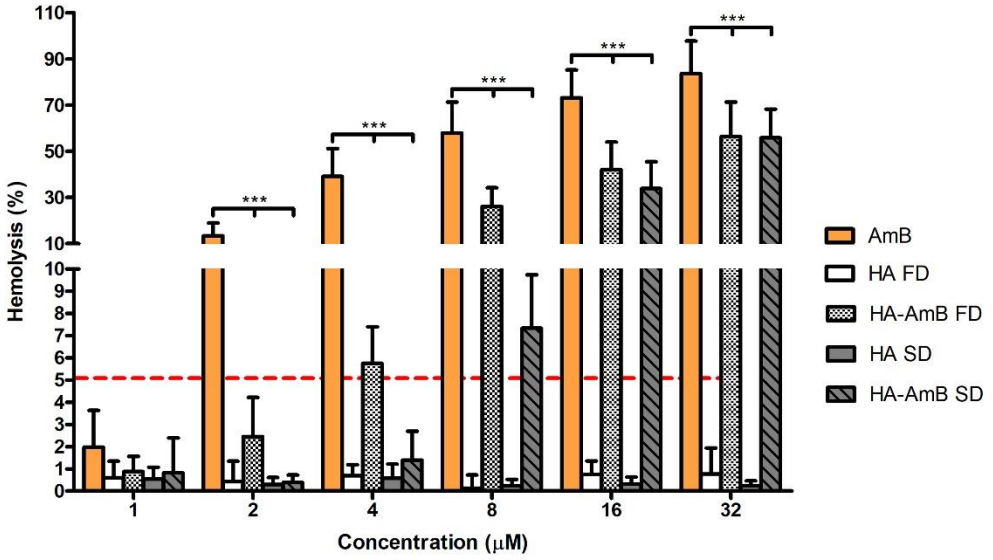

Figure 4.7 - Hemolytic activity of AmB and HA-AmB nanocomplexes. The extent of dog's RBCs damage after incubation for 30 min with different concentrations (1 – 32 μM) of the above referred formulations was measured as percentage of lysis of total erythrocytes. All the results are expressed as percentage relative to the control and presented as mean ± SD of at least three independent experiments. HA-AmB FD and HA-AmB SD treatment conditions were compared with the AmB using Bonferroni's multiple comparison post-test (*** $p < 0.001$).

4.3.3.3. *In vitro* anti-leishmanial effect of the HA-AmB nanocomplexes on axenic promastigotes and on infected macrophages

In the present study, the *in vitro* anti-leishmanial effect of the developed HA-AmB nanocomplexes was examined against different *Leishmania* life cycle (promastigote and amastigote). First, we confirmed the activity of the formulations against *L. amazonensis* and *L. infantum* promastigotes as previously described [22]. The nanocomplexes had a potent anti-leishmanial activity, being this effect in both strains slightly superior for HA-AmB FD than for HA-AmB SD (Figure 4.8). More specifically, the IC_{50} values determined for *L. amazonensis* and *L. infantum* promastigotes were 0.072 ± 0.037 and 0.026 ± 0.014 μM, respectively, for HA-AmB FD and 0.101 ± 0.052 and 0.043 ± 0.023 μM, respectively, for HA-AmB SD. Furthermore, we tested the effect of the freeze- or spray-dried HA and, as can be seen in Figure 4.8, both were inactive against both parasites. The activity of the developed formulations was similar to the reference drug AmB that presented IC_{50} values of 0.032 ± 0.007 and 0.028 ± 0.010 μM (Table 4.3), values that are in the range of the ones reported for *L. donovani* (0.003 to 0.15 μM) [74] or *L. amazonensis* (0.10 μg/mL, equivalent to 0.11 μM) and *L. infantum* (0.09 μg/mL, equivalent to 0.097 μM) [75].

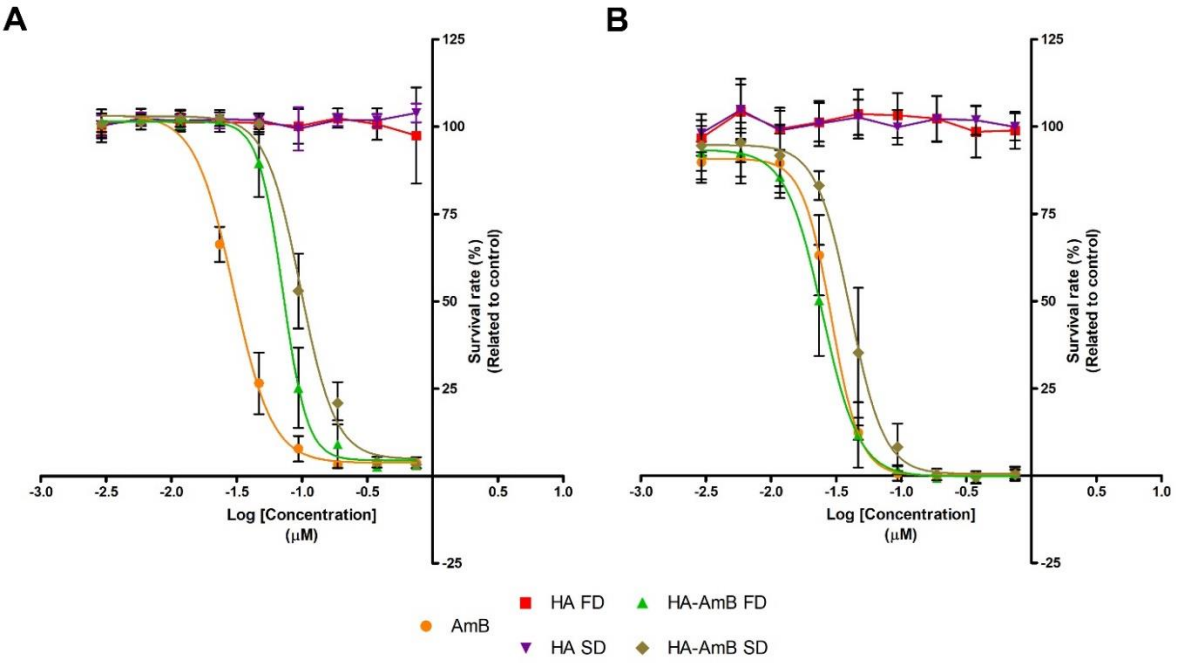

Figure 4.8 - Dose-response curves of the *in vitro* anti-leishmanial activity of free-AmB and HA-AmB nanocomplexes against **(A)** *L. amazonensis* and **(B)** *L. infantum* axenic cultures after 24 h of treatment with different concentrations (0.0029 - 0.75 μM) of the above referred formulations. Data is expressed as mean ± SD of at least three independent experiments.

Table 4.3 - IC_{50} values of the anti-leishmanial reference compound AmB and of HA-AMB nanocomplexes against extracellular promastigotes of *L. amazonensis* and *L. infantum*.

Sample	Promastigotes IC_{50} (µM)	
	L. amazonensis	*L. infantum*
AmB	0.032 ± 0.007	0.028 ± 0.010
HA-AmB FD	0.072 ± 0.037	0.026 ± 0.014
HA-AmB SD	0.101 ± 0.052	0.043 ± 0.023

Means ± SD (n = 3)

The efficacy of the nanocomplexes was also evaluated against the intracellular form of the parasite since this is the infective form for the vertebrate hosts. For that, amastigotes of *L. infantum* were used. Thus, the anti-leishmanial effect of the formulations on *L. infantum* amastigotes was determined in infected BMMΦ cultures. Figure 4.9 shows the obtained dose-response curves for each treatment. As expected, free-AmB displayed the highest activity with an IC_{50} of 0.018 ± 0.005 µM (Table 4.4). Reported IC_{50} values are for example 0.08 µg/mL (± 0.087 µM) for *L. amazonensis*-infected macrophages [76] and 0.037 µM for *L. infantum*-infected macrophages [29]. Regarding the nanocomplexes, both presented an anti-leishmanial activity very similar to that of free-drug (Figure 4.9), with IC_{50} values of 0.026 ± 0.012 µM for HA-AmB FD and 0.030 ± 0.010 µM for HA-AmB SD (Table 4.4). Of note, the observed increased activity of HA-AmB SD against intramacrophagic *L. infantum* amastigotes comparatively to the axenic *L. infantum* promastigotes (approximately 1.44-fold reduction of the IC_{50} value), an effect that was not observed for HA-AmB FD, could be due to a more efficient uptake by macrophages of HA-AmB SD nanocomplexes. Nevertheless, supplementary studies must be carried out to confirm this hypothesis.

Golenser et al. [77] showed the efficacy of unreduced or reduced AmB-arabinogalactan (AG) covalent conjugates in the treatment of macrophages infected with *L. major* (ED_{50} of 0.17 and 0.31 µg/mL, respectively) and *L. infantum* (0.027 and 0.035 µg/mL, respectively). Another work showed that mannosylated gelatin nanoparticles are a promising targeted AmB delivery system since a 5.4-fold reduction in IC_{50} was achieved in the treatment of *L. donovani*-infected macrophages, comparatively to free drug [78].

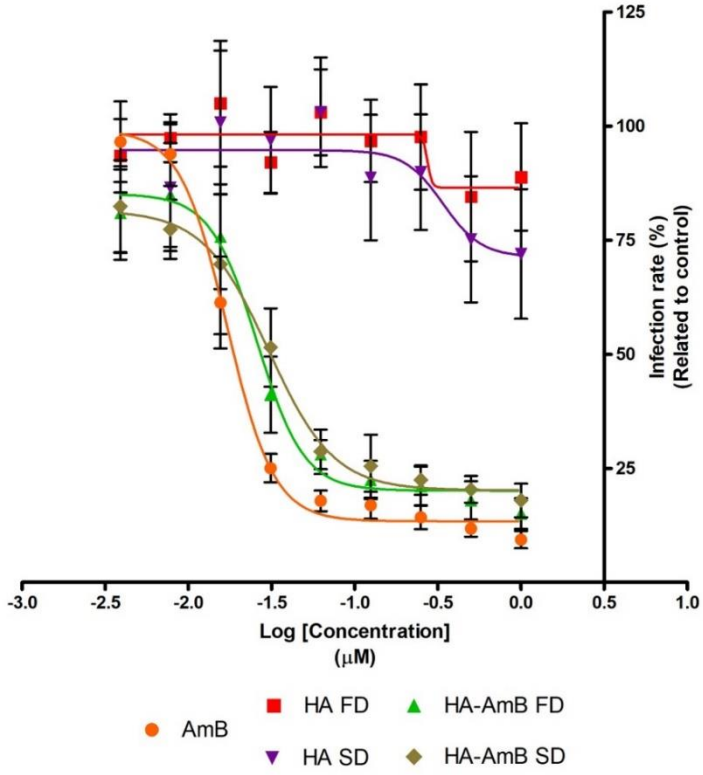

Figure 4.9 - *In vitro* effect of AmB and HA-AmB nanocomplexes on intracellular amastigotes. *L. infantum*-infected BMMΦ were treated for 24 h with different concentrations (0.0039 to 1 μM) of the above referred formulations. Data (mean ± SD of at least three independent experiments) was obtained employing an automated image analysis protocol available for the IN Cell Analyzer system and used for the obtention of the dose-response curves.

Sousa-Batista et al. [76] showed that the activity of PLGA microparticles loaded with deoxycholate AmB against *L. amazonensis*-infected macrophage was similar to that of free deoxycholate AmB (IC_{50} of 0.05 and 0.08 μg/mL, respectively); furthermore, this formulation was 2-fold more selective than free-drug (selectivity index (SI) of 50 and 25, respectively). In this study, we observed also that the therapeutic window between the determined IC_{50} and CC_{50} of both nanocomplexes (Table 4.4) is wider than that of AmB. More specifically, the SI determined for HA-AmB FD and HA-AmB SD were around 322 and 651, respectively, values that are approximately 2.8- and 5.7-fold more selective than the ones obtained for AmB (SI of 114). Furthermore, comparatively to our recent published study regarding Dex-AmB nanocomplexes [22], it was possible to understand, in the case of the spray-dried formulations, that the use of HA improved even more the SI (272 vs 651). This suggests that the use of hyaluronic acid does not interfere with the known mechanism of AmB and acts like a "Trojan Horse", further improving the balance of safety *versus* effectiveness of the drug. Based on demonstrated *in vitro* anti-leishmanial activity and reduced cytotoxicity, *in vivo* studies were conducted in C57BL/6 mice using the HA-AmB SD nanocomplex.

Table 4.4 - *In vitro* evaluation of the anti-leishmanial and cytotoxic effects of AmB and HA-AmB nanocomplexes against *L. infantum*-infected macrophages and non-infected macrophages, respectively.

Sample	Amastigotes IC_{50} (μM)	Macrophages CC_{50} (μM)	Selectivity Index (SI) [a]
AmB	0.018 ± 0.005	2.05 ± 0.18	114
HA-AmB FD	0.026 ± 0.012	8.37 ± 2.12	322
HA-AmB SD	0.030 ± 0.010	19.52 ± 1.31	651

Means ± SD (n = 3).

[a] SI (selectivity index) = CC_{50} /IC_{50}.

4.3.4. *In vivo* assays

4.3.4.1. *In vivo* systemic toxicity assessment

Renal and hepatic functions deterioration is a serious limiting side effect of using AmB, even for commercial formulations [62, 71], being its effects well known and referred in the literature [18, 71, 79-81]. For instance, hemorrhage, coagulative necrotic areas and presence of pale hepatocytes as well as single-cell necrosis of hepatocytes with neutrophil aggregation were observed in the liver of mice treated with Fungizone® [71, 81]. Free-AmB seems to promote mild necrotic hepatocytes with moderate infiltration of portal tract by inflammatory cells in mice liver [80]. In the case of the nephrotoxicity, AmB is capable of promoting renal vasoconstriction (which reduces the renal blood flow and glomerular filtration rate [79]) and decrease the viability of renal tubular epithelial cells through alterations in cell membrane permeability, via pore formation [82, 83], promoting tubular necrosis [18]. Also, degenerative changes of renal glomerular tuft associated with abundant inflammatory cell infiltrates and intercellular edema has been observed [80]. In this study, mice were intravenously treated with 1 and 3 mg AmB/Kg of body weight of HA-AmB SD nanocomplex for 3 alternative days. Afterwards, liver, kidneys and spleen were collected for histological assessment. Table 4.5 summarizes the principal histological findings observed by the analysis of the H&E's slides of the specimens that have been taken from the organs of the treated mice. Results revealed that the control groups showed normal histology in the liver, being only observed a slight focal inflammatory infiltrate of eosinophils in the bile duct (present in 1/3 animals). In terms of kidneys and spleen, no alterations were observed. Likewise, the control group treated with pure HA (at 1 or 3 mg/Kg) did not present significant alterations in the analyzed organs. When mice were treated with 1 mg/Kg of AmBisome®, only a slight mixed focal inflammatory infiltrate around the bile duct (1/3 animals) was detected. In the case of the animals treated with 3 mg/Kg of AmBisome®, the inflammatory infiltrate (mononuclear cells) around the bile duct (1/3 animals)

became slightly multifocal and a focal zone of incipient necrosis (1/3 animals) was also observed. In the kidneys, administration of 3 mg/Kg of AmBisome® only promoted a slight interstitial edema (1/3 animals), mild subacute interstitial nephritis (1/3 animals), slight focal interstitial fibrosis (1/3 animals) and a mild focal vascular ectasia (1/3 animals). A slight follicular hyperplasia and subacute splenitis as well as slight presence of megakaryocytes (extramedullary hematopoiesis) was also observed in the spleen of one animal treated with 1 mg/Kg of AmBisome®. Interestingly, no alterations in the spleen were observed after using the highest dose. Therefore, all of the referred alterations in the collected organs of the mice treated with AmBisome® were, as expected, minimal and without a significant impact in the quality of the animal health. In fact, AmBisome® treatment has been associated with significantly reduced toxicity profile. Indeed, according to the literature, only on a multiple-high dose exposure basis (above 10 mg/Kg administered for various consecutive days) the histopathological alterations observed in the animal's liver and kidneys are more prominent but still minimal in severity. Olsen et al. [84] demonstrated that a multiple-dose testing of 14 daily i.v. injections of 5, 15, or 25 mg/kg AmBisome® were associated to none or minimal renal histological changes. In fact, renal tubular changes in the different treatment groups were in that work predominantly minimal in severity, only a mild tubular change in a mouse treated with 25 mg/kg AmBisome® being observed. Regarding the HA-AmB SD nanocomplex treatment group, hepatic tissues analysis revealed a slight focal mixed inflammatory infiltrate with perivascular distribution in mice treated with 1 mg/Kg (2/4 animals) as well as a slight multifocal mixed inflammatory infiltrate with perivascular distribution and hepatocyte degeneration (1/4 animals), being the last one considered a more aggressive alteration. All the animals treated with 3 mg/Kg of HA-AmB SD presented only a slight multifocal mixed inflammatory infiltrate with perivascular distribution (3/3 animals). In the kidneys, administration of 1 mg/Kg of the nanocomplex only promoted a slight diffuse interstitial fibrosis (1/4 animals), a slight dilation of the tubule lumen (1/4 animals) and a mild diffuse multifocal vascular ectasia (2/4 animals). With the highest dose used, a slight diffuse interstitial fibrosis (1/3 animals), tubular ectasia with presence of some hyaline casts (1/3 animals) and a mild diffuse multifocal vascular ectasia (2/3) were observed. Nevertheless, one of the animals presented hyaline casts diffusely distributed in tubular lumen with some evidence of crystalluria (1/3 animals). There are numerous types of crystals that can be formed in the kidney and accumulate in the tubules, leading to acute renal failure due to toxic effects [85]. Despite being considered a worrying health risk, this alteration was only observed in one animal that was treated with the highest dose in study.

Table 4.5 - Summary of the histological alterations observed after mice treatment with HA-AmB SD nanocomplex and AmBisome®.

Organ	Histological findings	Treatments						
		CTR (5 % w/v dextrose)	HA		AmBisome®		HA-AmB SD	
			1 mg/Kg	3 mg/Kg	1 mg/Kg	3 mg/Kg	1 mg/Kg	3 mg/Kg
Liver	Inflammatory infiltrate around the bile duct	Slight focal (eosinophils) (1/3)	-	-	Slight focal (mixed cells) (1/3)	Slight multifocal (mononuclear) (1/3)	-	-
	Zone of incipient necrosis	-	-	-	-	Focal presence (1/3)	-	-
	Mixed inflammatory infiltrate with a perivascular distribution:	-	-	-	-	-	Slight focal (2/4); Slight multifocal with hepatocyte degeneration (1/4)	Slight multifocal (3/3)
	Vascular ectasia	-	-	Slight (2/3)	-	-	-	-
Kidneys	Edema	-	-	-	-	Slight interstitial (1/3)	-	-
	Nephritis	-	-	-	-	Slight (1/3)	-	-
	Fibrosis	-	-	-	-	Slight focal interstitial (1/3)	Slight diffuse interstitial (1/4)	Slight diffuse interstitial (1/3)

	Vascular ectasia	-	-	-	-	Mild focal (1/3)	Mild diffuse multifocal (2/4)	Mild diffuse multifocal (2/3)
	Hyaline casts diffusely distributed in tubular lumen with some evident crystalluria	-	-	-	-	-	-	Presence (1/3)
	Tubular ectasia	-	-	-	-	-	-	Presence (with some hyaline casts) (1/3)
	Dilation of the tubule lumen	-	-	-	-	-	Slight (1/4)	-
Spleen	Follicular hyperplasia	-	Slight (3/3)	Slight (2/3)	Slight (1/3)	-	-	-
	Follicular lympholysis	-	-	-	-	-	Slight (1/4)	-
	Splenitis	-	-	-	Slight Subacute (1/3)	-	Slight (1/4)	-
	Megakaryocytes (extramedullary hematopoiesis)	-	-	-	Slight presence (1/3)	-	Slight (1/4) to moderate (1/4) presence	-
	Hemosiderosis	-	-	-	-	-	Multifocal (1/4)	-

As observed for the AmBisome® group, treatment with HA-AmB SD nanocomplex did not cause any type of aggressive modification in the spleen, some signs of splenitis, follicular lympholysis, megakaryocytes and extramedullary hematopoiesis being observed only for the 1 mg/Kg dose. Despite some alterations in the liver and kidneys being considered more aggressive, no alterations in the weight of the removed organs were observed (Figure 4.10 A). All animals presented good physical appearance and normal behavior, exhibited no signs of alterations in the weight with exception for the group treated with 3 mg/Kg of HA-AmB SD nanocomplex (Figure 4.10 B). However, only the lower dose will be used to test the anti-leishmanial efficacy of the nanocomplex. All of the described findings indicate that treatment with the developed nanocomplex led to no detectable aggressive events.

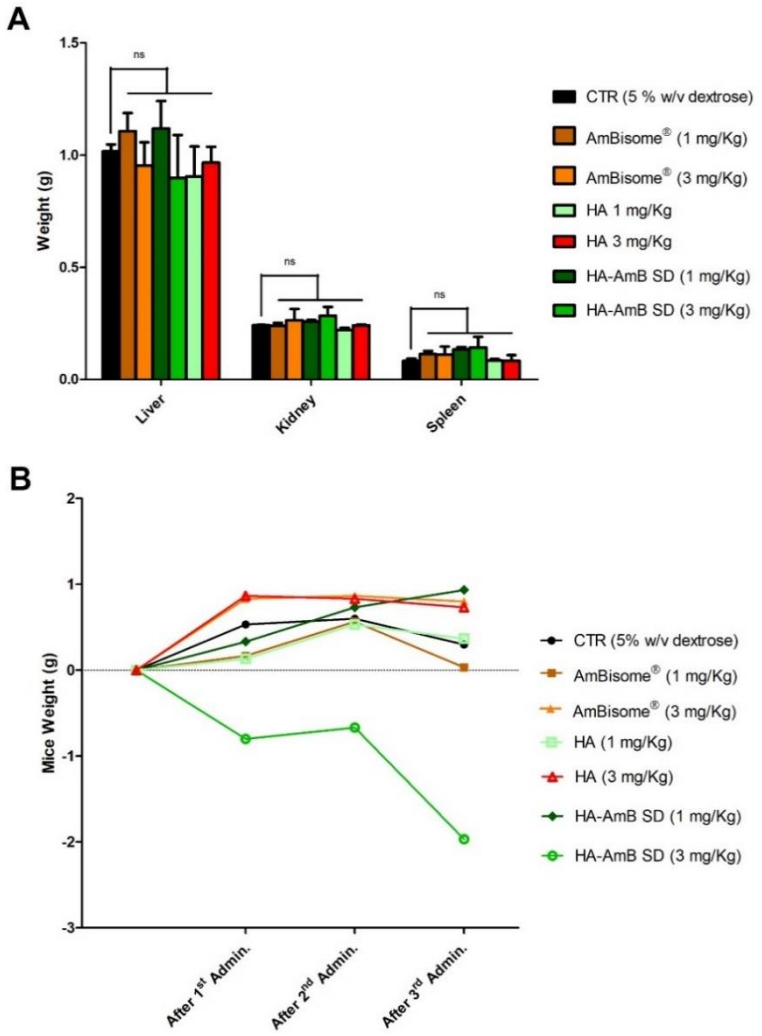

Figure 4.10 - Weight of the **(A)** collected organs and **(B)** mice after intravenous treatment with different formulations at 1 and 3 mg/Kg. Data is expressed as mean ± SD. For the collected organs, bonferroni's multiple comparison post-test was used to evaluate differences between control and the treatment groups and no significant alterations were observed.

4.3.4.2. *In vivo* anti-leishmanial activity in infected mice

The efficacy of the HA-AmB SD nanocomplex at 1 mg/Kg and administered for 3 alternative days was assessed in mice after 15 days of infection with *L. infantum* (VL model). In all treated groups a significant parasite burden reduction on the splenic (Figure 4.11 A) and hepatic (Figure 4.11 B) tissues were observed.

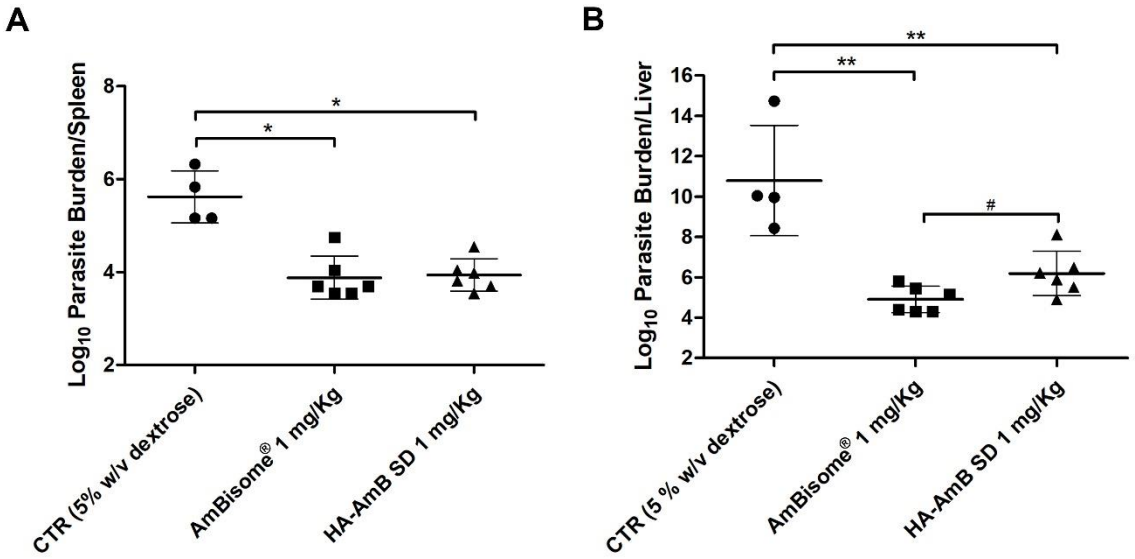

Figure 4.11 - Parasite burden evaluation in infected and treated C57BL/6 mice by dilution assay. C57BL/6 mice were intravenously infected in the lateral vein of the tail with 2×10^7 *L. infantum* promastigotes in stationary phase and 15-days after infection they were treated with 5 % w/v dextrose, AmBisome® and HA-AmB SD nanocomplex. Treatments were performed for 3 alternative days and the parasite load in the **(A)** spleen and **(B)** liver was evaluated. Each symbol represents one animal and the horizontal bars represent the mean $\log_{10}$ of the number of parasites per organ. Nonparametric Mann-Whitney U test was used to evaluate differences between the control group and the AmBisome® and HA-AmB SD treatments (*$p < 0.05$ and **$p < 0.01$) or between both treatments ($^{\#}p < 0.05$).

When given in the above referred regimen, HA-AmB SD nanocomplex promoted a 1.68-$\log_{10}$ reduction in the splenic parasites as compared to the control group and was as effective as AmBisome®, that promoted a 1.74-$\log_{10}$ reduction. Concerning the liver, although less active than AmBisome® but with a similar order of magnitude, the developed nanocomplex promoted a significant reduction in the parasite burden (4.60-$\log_{10}$ reduction *versus* 5.89-$\log_{10}$ reduction in the case of AmBisome®). Several reports in the literature show the *in vivo* efficacy of different AmB polymer-based formulations administered intravenously, using regimens similar to the one adopted in this study [38, 86, 87]. For instance, AmB encapsulated sodium alginate-glycol chitosan stearate nanoparticles promoted a reduction of *L. donovani* parasite burden in hamsters by 70 % with a dose of 1 mg/kg/day for 5 consecutive days [86]. Another study showed that AmB-PLGA

nanospheres promoted a reduction of *L. infantum* parasite burden in the spleen and liver of mice by 2-$\log_{10}$ with a single dose or 3-daily doses at 1 mg/kg [87]. This type of formulations could even be further modified with some targeting moieties in the surface, like mannose, in order to potentiate the targeting effect [38]. Interestingly, as with our formulations, Mohamed-Ahmed et al. [88] developed a non-covalent complex of AmB with poly(α-glutamic acid) (AmB-PGA complex) and showed its *in vivo* anti-leishmanial potential. Administration of 1.25 or 2.50 mg/kg (for 3 alternate days over a 5-day period) of this system to *L. donovani*-infected mice promoted a high amastigote inhibition in the hepatic tissue (84.4 and 94.4 %, respectively), effect that was similar to the one obtained with AmBisome® (95.5%).

Our results clearly demonstrate that using a very simple and straightforward method it is possible to obtain a promising and cheap formulation to be used in VL treatment. Furthermore, weight loss (a sensitive and objective sign of health problems) was monitored in all treatment groups. Table 4.6 shows the changes in body weight of animals for each group; as expected, no significant alterations were observed.

Table 4.6 - Body weight changes (mean ± SD) according to each experimental group.

Treatment groups	**Body weight (g)**		
	Before infection	Before euthanasia	Change (%)
Non-infected	20.0 ± 1.2	21.0 ± 0.7	1.1 g (5.5 %)
CTR (5 % w/v dextrose)	20.6 ± 1.8	21.4 ± 1.1	0.8 g (3.9 %)
AmBisome® (1 mg/Kg)	20.8 ± 1.6	22.0 ± 1.9	1.2 g (5.8 %)
HA-AmB SD (1 mg/Kg)	20.9 ± 1.2	21.9 ± 1.7	1.0 g (5.0 %)

Moreover, none of the treatments induced measurable systemic repercussions over time, since no alterations in the weight of the removed organs was observed (the significant increase in the spleen weight in all the treatment groups comparatively to the non-infected group could be explained by the infection itself) (Figure 4.12) The histological observations in both organs were similar for the different groups (Table 4.7).

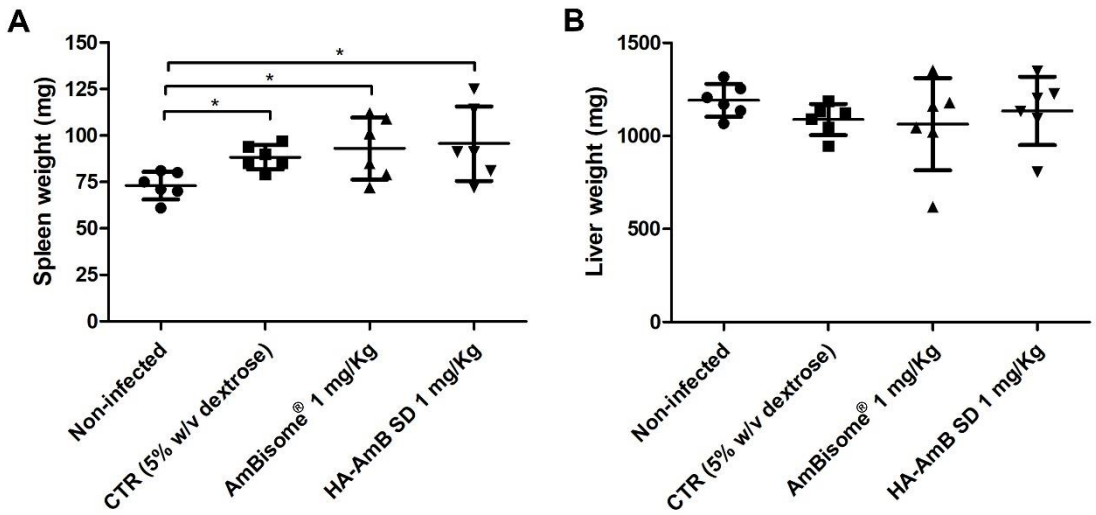

Figure 4.12 - Weight of the **(A)** spleens and **(B)** livers collected from the treated mice. Each symbol represents one animal and the horizontal bars represent the mean weight of the organs. Bonferroni's multiple comparison post-test was used to evaluate differences between each group and only in the spleen was observed significant differences between the non-infected groups and the infected/treated groups (*$p < 0.05$).

Table 4.7 - Histological alterations observed after intravenous treatment of *L. infantum*-infected mice with 1 mg/Kg of HA-AmB SD nanocomplex and AmBisome®.

Organ	Histological findings	Treatments			
		CTR (5 % w/v dextrose)	Infected CTR (5 % w/v dextrose)	AmBisome 1 mg/Kg	HA-AmB SD 1 mg/Kg
Liver	Inflammatory infiltrate	Slight periportal (lymphoid) (1/3)	Slight multifocal (lymphoid) (1/4)	Slight multifocal (lymphoid) (1/3)	Slight multifocal and subacute (3/3)
	Lymphoid agglomerates	-	Multifocal to perivascular and periportal (2/4)	Multifocal to perivascular and periportal (2/3)	-
	Congestion	Generalized (1/3)	Generalized (1/4)	Generalized (1/3)	Generalized (1/3)
	Hydropic degeneration	Generalized (2/3)	Generalized (1/4)	-	-
	Vascular ectasia	Presence (1/3)	Presence (2/4)	Presence (2/3)	Presence (3/3)
Spleen	Follicular hyperplasia	-	Slight (2/4)	-	Slight (2/3)
	Hemosiderosis	Diffuse presence (1/3)	-	-	-

4.4. Conclusions

In this study, changes in the main limitations associated with the use of AmB for leishmaniasis treatment, such as poor aqueous solubility and overall toxicity, were achieved through the inclusion of the drug within the hyaluronic acid chain network. Using a simple and economic approach, two non-covalent self-assembling nanocomplexes (HA-AmB FD and HA-AmB SD) were developed and characterized. The obtained nanocomplexes, containing AmB in both aggregate and super aggregate states, have shown to be stable in aqueous environment. In fact, in the presence of HA, AmB solubility was enhanced due to its amorphization. Moreover, this straightforward strategy allowed also to improve the therapeutic index of the AmB. The cytotoxicity and hemolytic activity of AmB in the nanocomplexes was significantly decreased while the anti-leishmanial effect against axenic cultures of promastigotes and against intramacrophagic *L. infantum* amastigotes was very similar to that of the free drug. This study also highlights the *in vivo* safety and effectiveness of the HA-AmB SD nanocomplex in reducing the parasite burden in the spleen and liver of *L. infantum*-infected C57BL/6 mice after a short treatment regimen.

4.5. References

1. Rochelle do Vale Morais, A., et al., *In-vitro and in-vivo antileishmanial activity of inexpensive Amphotericin B formulations: Heated Amphotericin B and Amphotericin B-loaded microemulsion.* Exp Parasitol, 2018. **192**: p. 85-92.
2. Burza, S., S.L. Croft, and M. Boelaert, *Leishmaniasis.* Lancet, 2018. **392**(10151): p. 951-970.
3. Desjeux, P., *Leishmaniasis: current situation and new perspectives.* Comp Immunol Microbiol Infect Dis, 2004. **27**(5): p. 305-18.
4. Croft, S.L. and V. Yardley, *Chemotherapy of leishmaniasis.* Curr Pharm Des, 2002. **8**(4): p. 319-42.
5. Chatelain, E. and J.R. Ioset, *Drug discovery and development for neglected diseases: the DNDi model.* Drug Des Devel Ther, 2011. **5**: p. 175-81.
6. Ghorbani, M. and R. Farhoudi, *Leishmaniasis in humans: drug or vaccine therapy?* Drug Des Devel Ther, 2018. **12**: p. 25-40.
7. Kapil, S., P.K. Singh, and O. Silakari, *An update on small molecule strategies targeting leishmaniasis.* European Journal of Medicinal Chemistry, 2018. **157**: p. 339-367.
8. Machado-Silva, A., et al., *New perspectives for leishmaniasis chemotherapy over current anti-leishmanial drugs: a patent landscape.* Expert Opinion on Therapeutic Patents, 2015. **25**(3): p. 247-260.
9. Ehrenfreund-Kleinman, T., et al., *Synthesis and characterization of novel water soluble amphotericin B–arabinogalactan conjugates.* Biomaterials, 2002. **23**(5): p. 1327-1335.
10. Laniado-Laborin, R. and M.N. Cabrales-Vargas, *Amphotericin B: side effects and toxicity.* Rev Iberoam Micol, 2009. **26**(4): p. 223-7.
11. Herbrecht, R., et al., *The lipid formulations of amphotericin B.* Expert Opin Pharmacother, 2003. **4**(8): p. 1277-87.
12. Zu, Y., et al., *Preparation and characterization of amorphous amphotericin B nanoparticles for oral administration through liquid antisolvent precipitation.* European Journal of Pharmaceutical Sciences, 2014. **53**: p. 109-117.

13. Ehrenfreund-Kleinman, T., J. Golenser, and A.J. Domb, *Conjugation of amino-containing drugs to polysaccharides by tosylation: amphotericin B-arabinogalactan conjugates.* Biomaterials, 2004. **25**(15): p. 3049-57.
14. Bruni, N., et al., *Nanostructured delivery systems with improved leishmanicidal activity: a critical review.* International journal of nanomedicine, 2017. **12**: p. 5289-5311.
15. Ickowicz, D.E., et al., *Activity, reduced toxicity, and scale-up synthesis of amphotericin B-conjugated polysaccharide.* Biomacromolecules, 2014. **15**(6): p. 2079-89.
16. Hudson, S.P., et al., *Injectable in situ cross-linking hydrogels for local antifungal therapy.* Biomaterials, 2010. **31**(6): p. 1444-1452.
17. Sokolsky-Papkov, M., A.J. Domb, and J. Golenser, *Impact of Aldehyde Content on Amphotericin B–Dextran Imine Conjugate Toxicity.* Biomacromolecules, 2006. **7**(5): p. 1529-1535.
18. Nishi, K.K., et al., *Amphotericin B-Gum Arabic Conjugates: Synthesis, Toxicity, Bioavailability, and Activities Against Leishmania and Fungi.* Pharmaceutical Research, 2007. **24**(5): p. 971-980.
19. Ravichandran, V. and A. Jayakrishnan, *Synthesis and evaluation of anti-fungal activities of sodium alginate-amphotericin B conjugates.* International Journal of Biological Macromolecules, 2018. **108**: p. 1101-1109.
20. Kothandaraman, G.P., et al., *Anti-fungal and anti-leishmanial activities of pectin-amphotericin B conjugates.* Journal of Drug Delivery Science and Technology, 2017. **39**: p. 1-7.
21. Farber, S., et al., *Galactomannan–amphotericin B conjugate: synthesis and biological activity.* Polymers for Advanced Technologies, 2011. **22**(1): p. 119-125.
22. Silva-Carvalho, R., et al., *Development of dextrin-amphotericin B formulations for the treatment of Leishmaniasis.* International Journal of Biological Macromolecules, 2020. **153**: p. 276-288.
23. Choi, K.Y., et al., *Hyaluronic acid-based nanocarriers for intracellular targeting: interfacial interactions with proteins in cancer.* Colloids Surf B Biointerfaces, 2012. **99**: p. 82-94.
24. Oh, E.J., et al., *Target specific and long-acting delivery of protein, peptide, and nucleotide therapeutics using hyaluronic acid derivatives.* J Control Release, 2010. **141**(1): p. 2-12.
25. Sladek, Z. and D. Rysanek, *Expression of macrophage CD44 receptor in the course of experimental inflammatory response of bovine mammary gland induced by lipopolysaccharide and muramyl dipeptide.* Res Vet Sci, 2009. **86**(2): p. 235-40.
26. Montanari, E., et al., *Pursuing Intracellular Pathogens with Hyaluronan. From a 'Pro-Infection' Polymer to a Biomaterial for 'Trojan Horse' Systems.* Molecules, 2018. **23**(4).
27. Gomes, M.S., et al., *Engagement of Toll-like receptor 2 in mouse macrophages infected with Mycobacterium avium induces non-oxidative and TNF-independent anti-mycobacterial activity.* Eur J Immunol, 2008. **38**(8): p. 2180-9.
28. Sereno, D. and J.L. Lemesre, *Axenically cultured amastigote forms as an in vitro model for investigation of antileishmanial agents.* Antimicrobial Agents and Chemotherapy, 1997. **41**(5): p. 972-976.
29. Gomes-Alves, A.G., et al., *Development of an automated image analysis protocol for quantification of intracellular forms of Leishmania spp.* PLOS ONE, 2018. **13**(8): p. e0201747.
30. Vale-Costa, S., et al., *Iron overload favors the elimination of Leishmania infantum from mouse tissues through interaction with reactive oxygen and nitrogen species.* PLoS Negl Trop Dis, 2013. **7**(2): p. e2061.
31. Gagoś, M., et al., *Anomalously high aggregation level of the polyene antibiotic amphotericin B in acidic medium: implications for the biological action.* Biophys Chem, 2008. **136**(1): p. 44-9.
32. Wasko, P., et al., *Toward Understanding of Toxic Side Effects of a Polyene Antibiotic Amphotericin B: Fluorescence Spectroscopy Reveals Widespread Formation of the Specific Supramolecular Structures of the Drug.* Molecular Pharmaceutics, 2012. **9**(5): p. 1511-1520.

33. Wasko, P., et al., *Toward understanding of toxic side effects of a polyene antibiotic amphotericin B: fluorescence spectroscopy reveals widespread formation of the specific supramolecular structures of the drug.* Mol Pharm, 2012. **9**(5): p. 1511-20.
34. Luan, T., et al., *A study on the nature of intermolecular links in the cryotropic weak gels of hyaluronan.* Carbohydrate Polymers, 2012. **87**(3): p. 2076-2085.
35. Wu, Y., *Preparation of low-molecular-weight hyaluronic acid by ozone treatment.* Carbohydrate Polymers, 2012. **89**(2): p. 709-712.
36. Francis, A.P., S. Gurudevan, and A. Jayakrishnan, *Synthetic polymannose as a drug carrier: synthesis, toxicity and anti-fungal activity of polymannose-amphotericin B conjugates.* J Biomater Sci Polym Ed, 2018. **29**(13): p. 1529-1548.
37. Kim, Y.T., et al., *A thermosensitive vaginal gel formulation with HPgammaCD for the pH-dependent release and solubilization of amphotericin B.* Eur J Pharm Sci, 2010. **41**(2): p. 399-406.
38. Ghosh, S., et al., *Amphotericin B-loaded mannose modified poly(d,l-lactide-co-glycolide) polymeric nanoparticles for the treatment of visceral leishmaniasis: in vitro and in vivo approaches.* RSC Advances, 2017. **7**(47): p. 29575-29590.
39. Kafedjiiski, K., et al., *Synthesis and in vitro evaluation of thiolated hyaluronic acid for mucoadhesive drug delivery.* Int J Pharm, 2007. **343**(1-2): p. 48-58.
40. Fallacara, A., et al., *Formulation and Characterization of Native and Crosslinked Hyaluronic Acid Microspheres for Dermal Delivery of Sodium Ascorbyl Phosphate: A Comparative Study.* Pharmaceutics, 2018. **10**(4).
41. Zhou, L., et al., *Preparation, characterization, and evaluation of amphotericin B-loaded MPEG-PCL-g-PEI micelles for local treatment of oral Candida albicans.* International journal of nanomedicine, 2017. **12**: p. 4269-4283.
42. Al-Quadeib, B.T., et al., *Stealth Amphotericin B nanoparticles for oral drug delivery: In vitro optimization.* Saudi Pharmaceutical Journal, 2015. **23**(3): p. 290-302.
43. Singh, P.K., et al., *Macrophage-targeted chitosan anchored PLGA nanoparticles bearing doxorubicin and amphotericin B against visceral leishmaniasis.* RSC Advances, 2016. **6**(75): p. 71705-71718.
44. Choi, K.C., et al., *Amphotericin B-incorporated polymeric micelles composed of poly(d,l-lactide-co-glycolide)/dextran graft copolymer.* Int J Pharm, 2008. **355**(1-2): p. 224-30.
45. Shu, C., et al., *Amphotericin B-conjugated polypeptide hydrogels as a novel innovative strategy for fungal infections.* Royal Society open science, 2018. **5**(3): p. 171814-171814.
46. Einfal, T., O. Planinsek, and K. Hrovat, *Methods of amorphization and investigation of the amorphous state.* Acta Pharm, 2013. **63**(3): p. 305-34.
47. Danaei, M., et al., *Impact of Particle Size and Polydispersity Index on the Clinical Applications of Lipidic Nanocarrier Systems.* Pharmaceutics, 2018. **10**(2).
48. Moghimi, S.M., A.C. Hunter, and J.C. Murray, *Nanomedicine: current status and future prospects.* FASEB J, 2005. **19**(3): p. 311-30.
49. Siefert, A.L., et al., *Immunomodulatory nanoparticles ameliorate disease in the Leishmania (Viannia) panamensis mouse model.* Biomaterials, 2016. **108**: p. 168-176.
50. Kalluru, R., et al., *Poly(lactide-co-glycolide)-rifampicin nanoparticles efficiently clear Mycobacterium bovis BCG infection in macrophages and remain membrane-bound in phago-lysosomes.* J Cell Sci, 2013. **126**(Pt 14): p. 3043-54.
51. Zia, Q., et al., *Biomimetically engineered Amphotericin B nano-aggregates circumvent toxicity constraints and treat systemic fungal infection in experimental animals.* Sci Rep, 2017. **7**(1): p. 11873.

52. Tiyaboonchai, W. and N. Limpeanchob, *Formulation and characterization of amphotericin B-chitosan-dextran sulfate nanoparticles.* Int J Pharm, 2007. **329**(1-2): p. 142-9.
53. Lima, M.R., et al., *Hydrophobization of cashew gum by acetylation mechanism and amphotericin B encapsulation.* Int J Biol Macromol, 2018. **108**: p. 523-530.
54. Barwicz, J., S. Christian, and I. Gruda, *Effects of the aggregation state of amphotericin B on its toxicity to mice.* Antimicrob Agents Chemother, 1992. **36**(10): p. 2310-5.
55. Espada, R., et al., *Effect of aggregation state on the toxicity of different amphotericin B preparations.* International Journal of Pharmaceutics, 2008. **361**(1): p. 64-69.
56. Mazerski, J., J. Grzybowska, and E. Borowski, *Influence of net charge on the aggregation and solubility behaviour of amphotericin B and its derivatives in aqueous media.* Eur Biophys J, 1990. **18**(3): p. 159-64.
57. Legrand, P., et al., *Effects of aggregation and solvent on the toxicity of amphotericin B to human erythrocytes.* Antimicrob Agents Chemother, 1992. **36**(11): p. 2518-22.
58. Huang, W., et al., *Ion channel behavior of amphotericin B in sterol-free and cholesterol- or ergosterol-containing supported phosphatidylcholine bilayer model membranes investigated by electrochemistry and spectroscopy.* Biophys J, 2002. **83**(6): p. 3245-55.
59. Bartlett, K., et al., *Effect of heat-treated amphotericin B on renal and fungal cytotoxicity.* Antimicrob Agents Chemother, 2004. **48**(1): p. 333-6.
60. Adams, M.L. and G.S. Kwon, *Relative aggregation state and hemolytic activity of amphotericin B encapsulated by poly(ethylene oxide)-block–poly(N-hexyl-l-aspartamide)-acyl conjugate micelles: effects of acyl chain length.* Journal of Controlled Release, 2003. **87**(1): p. 23-32.
61. Adler-Moore, J.P. and R.T. Proffitt, *Amphotericin B lipid preparations: what are the differences?* Clin Microbiol Infect, 2008. **14 Suppl 4**: p. 25-36.
62. Deray, G., *Amphotericin B nephrotoxicity.* J Antimicrob Chemother, 2002. **49 Suppl 1**: p. 37-41.
63. Podinovskaia, M. and A. Descoteaux, *Leishmania and the macrophage: a multifaceted interaction.* Future Microbiol, 2015. **10**(1): p. 111-29.
64. ISO10993-5:2009, *Biological Evaluation of Medical Devices – Part 5: Tests for In Vitro Cytotoxicity*. 2009. 34.
65. Gurudevan, S., A.P. Francis, and A. Jayakrishnan, *Amphotericin B-albumin conjugates: Synthesis, toxicity and anti-fungal activity.* Eur J Pharm Sci, 2018. **115**: p. 167-174.
66. Kagan, S., et al., *Toxicity mechanisms of amphotericin B and its neutralization by conjugation with arabinogalactan.* Antimicrob Agents Chemother, 2012. **56**(11): p. 5603-11.
67. Espuelas, M.S., et al., *Polymeric carriers for amphotericin B: in vitro activity, toxicity and therapeutic efficacy against systemic candidiasis in neutropenic mice.* Journal of Antimicrobial Chemotherapy, 2003. **52**(3): p. 419-427.
68. Van de Ven, H., et al., *PLGA nanoparticles and nanosuspensions with amphotericin B: Potent in vitro and in vivo alternatives to Fungizone and AmBisome.* Journal of Controlled Release, 2012. **161**(3): p. 795-803.
69. Abu Ammar, A., et al., *Amphotericin B-loaded nanoparticles for local treatment of cutaneous leishmaniasis.* Drug Deliv Transl Res, 2019. **9**(1): p. 76-84.
70. Monroig-Bosque, P.D.C., et al., *The utility of therapeutic plasma exchange for amphotericin B overdose.* Transfus Apher Sci, 2018. **57**(6): p. 756-758.
71. Falk, R., A.J. Domb, and I. Polacheck, *A novel injectable water-soluble amphotericin B-arabinogalactan conjugate.* Antimicrob Agents Chemother, 1999. **43**(8): p. 1975-81.
72. Kaneo, Y., et al., *Nanoparticles of hydrophobized cluster dextrin as biodegradable drug carriers: solubilization and encapsulation of amphotericin B.* Journal of Drug Delivery Science and Technology, 2014. **24**(4): p. 344-351.

73. Matoso Sombra, F., et al., *Nanocapsules of Sterculia striata acetylated polysaccharide as a potential monomeric amphotericin B delivery matrix.* Int J Biol Macromol, 2019. **130**: p. 655-663.
74. Vermeersch, M., et al., *In vitro susceptibilities of Leishmania donovani promastigote and amastigote stages to antileishmanial reference drugs: practical relevance of stage-specific differences.* Antimicrob Agents Chemother, 2009. **53**(9): p. 3855-9.
75. Chavez-Fumagalli, M.A., et al., *New delivery systems for amphotericin B applied to the improvement of leishmaniasis treatment.* Rev Soc Bras Med Trop, 2015. **48**(3): p. 235-42.
76. Sousa-Batista, A.J., et al., *Novel and safe single-dose treatment of cutaneous leishmaniasis with implantable amphotericin B-loaded microparticles.* International Journal for Parasitology: Drugs and Drug Resistance, 2019. **11**: p. 148-155.
77. Golenser, J., et al., *Efficacious treatment of experimental leishmaniasis with amphotericin B-arabinogalactan water-soluble derivatives.* Antimicrobial agents and chemotherapy, 1999. **43**(9): p. 2209-2214.
78. Nahar, M., et al., *In vitro evaluation of surface functionalized gelatin nanoparticles for macrophage targeting in the therapy of visceral leishmaniasis.* J Drug Target, 2010. **18**(2): p. 93-105.
79. Santos, D.C.M., et al., *Metabolomics as a tool to evaluate the toxicity of formulations containing amphotericin B, an antileishmanial drug.* Toxicology research, 2016. **5**(6): p. 1720-1732.
80. Mohamed, H.A., et al., *Antifungal activity of oral (Tragacanth/acrylic acid) Amphotericin B carrier for systemic candidiasis: in vitro and in vivo study.* Drug Delivery and Translational Research, 2018. **8**(1): p. 191-203.
81. Lincopan, N., et al., *Toxicity of an effective amphotericin B formulation at high cationic lipid to drug molar ratio.* Experimental and Toxicologic Pathology, 2006. **58**(2): p. 175-183.
82. Lemke, A., A.F. Kiderlen, and O. Kayser, *Amphotericin B.* Appl Microbiol Biotechnol, 2005. **68**(2): p. 151-62.
83. Loo, A.S., S.A. Muhsin, and T.J. Walsh, *Toxicokinetic and mechanistic basis for the safety and tolerability of liposomal amphotericin B.* Expert Opinion on Drug Safety, 2013. **12**(6): p. 881-895.
84. Olson, J.A., et al., *Toxicity and efficacy differences between liposomal amphotericin B formulations in uninfected and Aspergillus fumigatus infected mice.* Medical Mycology, 2014. **53**(2): p. 107-118.
85. Cohen, S.M., *Crystalluria and Chronic Kidney Disease.* Toxicol Pathol, 2018. **46**(8): p. 949-955.
86. Gupta, P.K., et al., *Self Assembled Ionically Sodium Alginate Cross-Linked Amphotericin B Encapsulated Glycol Chitosan Stearate Nanoparticles: Applicability in Better Chemotherapy and Non-Toxic Delivery in Visceral Leishmaniasis.* Pharmaceutical Research, 2015. **32**(5): p. 1727-1740.
87. Costa Lima, S.A., et al., *Crucial CD8+ T-lymphocyte cytotoxic role in amphotericin B nanospheres efficacy against experimental visceral leishmaniasis.* Nanomedicine: Nanotechnology, Biology and Medicine, 2014. **10**(5): p. e1021-e1030.
88. Mohamed-Ahmed, A.H.A., et al., *Antileishmanial activity, uptake, and biodistribution of an amphotericin B and poly(α-Glutamic Acid) complex.* Antimicrobial agents and chemotherapy, 2013. **57**(10): p. 4608-4614.

CHAPTER 5 - COVALENT CONJUGATION OF AMPHOTERICIN B TO HYALURONIC ACID: AN INJECTABLE WATER-SOLUBLE CONJUGATE WITH REDUCED TOXICITY AND ANTI-LEISHMANIAL POTENTIAL

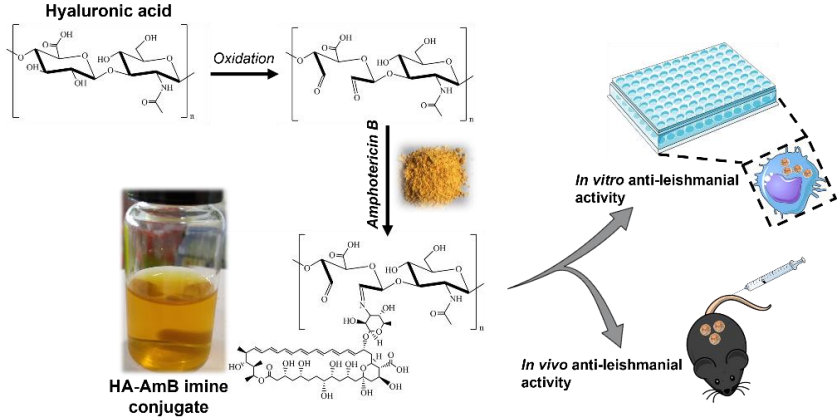

Amphotericin B (AmB) is a highly hydrophobic drug with significant leishmanicidal activity, whose use is limited by its poor water solubility and adverse effects. Polymer-drug conjugates are proposed as a delivery system designed to overcome those limitations while improving drug bioavailability, safety and activity. Here, AmB was covalently linked to periodate-oxidized hyaluronic acid (HA) (oxidation degree of 30.1 ± 5.6 %) via Schiff base (HA-AmB imine). The conjugate presents high water solubility and self-assembles into particles with a mean size of 88.2 ± 17.6 nm, a negative charge (-28.3 ± 0.9 mV) and a drug content of 17.8 ± 1.4 %. Spectroscopic studies revealed the presence of AmB in aggregate and super-aggregated form in the conjugate which could explain the significant reduction of the *in vitro* cytotoxicity and hemolytic activity. The formulation showed not only *in vitro* anti-leishmanial activity against *L. infantum*-infected macrophages (IC_{50} = 0.023 μM) but also against an *in vivo* infected mice model, promoting a 1.32- and a 4.98-$\log_{10}$ suppression of the *L. infantum* amastigote burden in the spleen and liver, respectively, without toxic effects. In summary, this study describes the safe and effective use of water-soluble HA-AmB imine conjugates for leishmaniasis treatment.

Adapted from Silva-Carvalho, R. et al. (2022). Biomacromolecules, 23, 1169-1182.

5.1. Introduction

Approximately 40 % of the pharmaceuticals market and 90 % of the developmental pipeline consist of poorly water-soluble drugs [1]. Drug delivery strategies aim to overcoming solubility issues, avoid low bioavailability and unsuitable pharmacokinetics [1, 2]. Among them, polymer-drug conjugates (PDC) - pharmacologically active nanoscale constructs in which the therapeutic agent is covalently linked to a water-soluble polymeric carrier [3, 4] - are considered promising and of great interest [2]. Since the work developed by Von Horst Jatzkewitz more than 60 years ago (conjugation of mescaline to polyvinylpyrrolidone) [5] the field of PDCs has expanded remarkably. In fact, PDCs present several advantages over conventional therapies as the nano size allows to improve water solubility and stability of the drug and its protection from systemic degradation, increases the drug load, allows its sustained or targeted release, and enhances the pharmacokinetics (drug bioavailability, plasma half-life, biodistribution, accumulation and elimination) [2, 4, 6].

Natural polymers, more specifically polysaccharides, are widely used in PDC-based formulations. Polysaccharides are water-soluble, biocompatible and biodegradable, their metabolic products are non-toxic and normally non-immunogenic, and possess functional groups for chemical modification (such as hydroxyl, amino, carboxylic acid, aldehydes) [3, 7]. A plethora of natural polysaccharides, including dextran, polysialic acid and hyaluronic acid (HA), are being used for this purpose due to their safety as well as to their affinity for certain receptors that promote a targeted drug delivery [2, 7]. Most of the PDCs, either marketed or in clinical trials, are formulated with polyethylene glycol (PEG), the most commonly used polymer although presenting some toxicity [8]. PDCs have been developed for the treatment of cancer [9-12], diabetes [13], pain [14] and arthritis [15]. However, several papers demonstrate the potential of the polysaccharide-drug conjugates, namely for the treatment of infectious diseases, more specifically of a vector-borne disease such as leishmaniasis [16-20].

The genus *Leishmania* are parasitic protozoa responsible for leishmaniasis, a neglected disease that affects mainly economically disadvantaged individuals in many developing countries and various animal populations in all over the world [21]. This disease, that presents a wide spectrum of clinical manifestations with different aggressiveness [22, 23], has high rates of morbidity and mortality being still considered a global health concern (with approximately 2 million cases each year [23, 24]). Its complexity represents a challenge and treatment is still problematic nowadays, being chemotherapy the primary method used due to the lack of human vaccines [25]. The chemotherapeutic agents are very expensive and present high toxicity, contributing to poor patient compliance and ultimately to the spread of the disease and appearance of resistant *Leishmania* strains [26]. The polyene amphotericin B (AmB) is

considered an effective drug due to its broad spectrum of activity and is recommended as a second-line treatment for visceral and mucocutaneous leishmaniasis. Nevertheless, it's clinical use is limited due to its low solubility, toxicity and aggressive side effects to the kidneys and liver [27]. Only AmBisome®, a liposome based AmB formulation, improved the current scenario for the treatment of leishmaniasis since it has an acceptably low toxicity, even at high doses [28, 29]. Notwithstanding, concerns regarding the high production costs of this formulation, shelf-life issues and loss of AmB activity [29] as well as some reported severe allergic reactions [30, 31] make the development of new therapeutic strategies crucial. Several studies reported the improved solubility, therapeutic efficacy and safety (reduced toxicity) of AmB after covalent conjugation through reductive amination to different oxidized polysaccharides – gum arabic [19], dextran [18], sodium alginate [32], arabinogalactan [16, 17, 27, 33, 34], galactomannan [35], pectin [20]. In this paper, HA with a weight average molar mass of 50 kDa was oxidized in order to obtain di-aldehyde derivatives that are reactive with AmB amine group via Schiff base (imine bond) leading to the formation of a water-soluble HA-AmB conjugate. Leishmaniasis treatment efficacy depends on the targeting of the parasites that are mainly localized inside infected macrophages. Thus, a delivery system able to distinguish infected from non-infected macrophages would be ideal. Furthermore, the release of AmB intracellularly, where parasites are mainly localized, enhances the therapeutic activity and reduces possible cytotoxic effects. Cluster of differentiation 44 (CD44), receptor for hyaluronate-mediated motility (RHAMM) has been identified as one of the main HA receptors [36]. In normal physiological conditions, macrophages do not internalize HA. However, Sladek and collaborators [37] have shown that CD44 receptor is highly expressed in macrophages during the initiation of an inflammatory response, being a good marker to distinguish between infected and non-infected macrophages. Therefore, considering the intracellular location of the parasites and the need of an efficient drug delivery and targeting to *Leishmania*-infected macrophages, HA-AmB conjugate could be a used as a drug-delivery system for enhanced efficacy of the treatment.

5.2. Material and Methods

5.2.1. Reagents

Sodium hyaluronate (Primalhyal, molecular weight (Mw) ± 50 kDa) was gifted from Soliance SA (Pomacle, France). Amphotericin B (AmB) powder from Streptomyces sp., potassium periodate, sodium borohydride, diethylene glycol (DEG), potassium hydrogen phthalate (KHP), hydroxylamine hydrochloride, methyl orange, phenolphthalein, dimethyl sulfoxide (DMSO), resazurin sodium salt, 4',6-diamidino-2-phenylindole (DAPI), Triton X-100, paraformaldehyde, Schneider's Insect medium, phenol red, hemin, HEPES sodium salt, sodium tetraborate decahydrate and potassium bromide were

purchased from Sigma-Aldrich (Missouri, USA). Glucose anhydrous was purchased from LabChem (Pennsylvania, USA). AmBisome® was gifted from Gilead Sciences (California, USA). Dulbecco's Modified Eagle Medium (DMEM), fetal bovine serum (FBS) and penicillin-streptomycin were obtained from Merck Millipore (Massachusetts, USA). L-glutamine (GlutaMAX™-I) and minimum essential medium non-essential amino acids solution were purchased from Gibco (Massachusetts, USA). Dialysis tubing with a molecular weight cut-off of 2000 Da were from Orange Scientific (Braine-l'Alleud, Belgium). High-content screening (HCS) CellMask™ Deep Red stain was purchased from Invitrogen (California, USA).

5.2.2. Periodate oxidation of HA

Oxidation of vicinal diols within the monomeric units of HA (Mw of disaccharide units of 401 g/mol) was performed using sodium periodate ($NaIO_4$) as reported in the literature [19], with some modifications. In short, 500 mg of HA were dissolved in 20 mL of distilled water (dH_2O) (1.25 mmol of disaccharide units) and, under continuous stirring, 134 mg of $NaIO_4$ (0.625 mmol) was gradually added (1:0.5 mol ratio HA disaccharide units/IO_4^-). The solution was stirred in the dark for 3 h at room temperature. To stop the reaction, 59.2 µL of DEG (66.3 mmol) was added and the mixture stirred for 2 h more in the above referred conditions. The resultant oxidized HA (OxHA) was separated from excess periodate and reaction by-products through dialysis at 4 °C against dH_2O (dialysis bag of MWCO 2000 Da) for two days, with three changes of water. The purified OxHA was then lyophilized in a freeze-drier (Coolsafe 100-9 Pro, Labogene, Allerød, Denmark) at -100 °C for 96 h, yielding a white solid foam that was stored in the desiccator.

5.2.3. Determination of HA Degree of Oxidation: ^{1}H NMR Spectroscopy and Hydroxylamine Hydrochloride Titration Method

Oxidation of HA was qualitatively confirmed by ^{1}H NMR analysis. In brief, samples were prepared by dissolving 10 mg of freeze-dried OxHA and HA separately in 1 mL of deuterium oxide (D_2O). The ^{1}H NMR spectra were recorded using a 400 MHz Bruker Avance II spectrometer system (Bruker, Massachusetts, USA). The number of scans were above 30.

Hydroxylamine hydrochloride titration was performed to estimate the degree of oxidation (DO %) of OxHA using a modified protocol reported elsewhere [38]. OxHA and HA (100 mg) were dissolved in 25 mL of 0.25 M hydroxylamine hydrochloride solution (pH 4.0) containing 0.05 % v/v of methyl orange. The solutions were maintained under magnetic stirring for 3 h at room temperature and the hydrochloric acid released in the reaction was then titrated with 0.1 M NaOH standard solution. The

titration end point was reached when the solution turned from red to light yellow-orange (the transition interval of methyl orange is 3.0 (red) ≤ pH ≤ 4.4 (yellow) and within the transition interval the mixed color is orange [39]). Estimation of DO % (equation 1) was calculated based on the volumes of sodium hydroxide used in the titration:

$$Degree\ of\ oxidation\ (\%) = \frac{V_{NaOH} \times C_{NaOH}}{m/M} \times 100 \quad (1)$$

were V_{NaOH} is the volume of NaOH consumed at the equivalence point, C_{NaOH} is the molar concentration of the NaOH solution, which in turn was determined with a titration against KHP using 0.5 % w/v phenolphthalein as indicator, m is the dry weight of OxHA used and M is the molecular weight of a single D-glucuronic acid in the disaccharide unit of HA since only this monomer can suffer oxidation [40] (Mw of D-glucuronic acid minus a water molecule that is lost during the condensation reaction to form the glycosidic bond between the D-glucuronic acid and N-acetyl-D-glucosamine monomers: 194.139 g/mol – 18 g/mol = 176.139 g/mol).

5.2.4. HA-AmB imine synthesis

An adapted protocol from Ehrenfreund-Kleinman et al. [27] was used to conjugate AmB to the OxHA (HA-AmB imine conjugate, denominated here as HA-AmBi). In brief, OxHA and AmB were dissolved in 0.1 M borate buffer pH 11 in a mass ratio of 4:1 and continuously stirred in dark for 48 h at 4 °C. In the end, the solution was dialyzed (MWCO 2000 Da) against dH_2O for 48 h at 4 °C and freeze-dried (Coolsafe 100-9 Pro, Labogene, Allerød, Denmark).

5.2.5. Physicochemical characterization of HA-AmB imine conjugates

5.2.5.1. Fourier-transform infrared spectroscopy (FTIR)

FTIR spectroscopic analysis of AmB, HA, OxHA and HA-AmBi were carried out employing a Bruker FTIR Spectrometer ALPHA II (Bruker, Massachusetts, USA) in the transmission mode, operating at a resolution of 4 cm^{-1}. Two milligrams of the samples were mixed with 200 mg of dry potassium bromide to obtain a solid pellet that was scanned three times to check the authenticity of data. The spectra were taken between 4000 cm^{-1} and 700 cm^{-1} by averaging 24 scans for each spectrum.

5.2.5.2. Differential scanning calorimetry (DSC)

The DSC thermal profiles of a known amount of the samples equivalent to 0.7 mg of AmB were obtained using a DSC 600 Perkin-Elmer (Massachusetts, USA). Each sample was heated in hermetically sealed aluminum pans at a rate of 10 °C/min up to 235 °C under a N_2 atmosphere. The apparatus was calibrated using an empty sealed pan as a reference. All samples were analyzed in triplicate.

5.2.5.3. Size and zeta potential

The mean size, polydispersity index (PDI) and zeta potential of the conjugate dissolved in dH_2O (final concentration of 1 mg/mL) were determined by dynamic light scattering (DLS) using a Malvern Zetasizer NanoZS, (Malvern Instruments Ltd., Worcestershire, UK). Three independently produced samples were filtered using 0.22 μm syringe filter (Polyethersulfone (PES), Teknokroma, Barcelona, Spain) and analyzed at least five times.

5.2.5.4. Morphology analysis: scanning electron cryo-microscopy (Cryo-SEM)

Cryo-SEM observations were performed in the Laboratory for Scanning Electron Microscopy and X-Ray Microanalysis, at Materials Centre of the University of Porto (CEMUP), using a High-resolution Scanning Electron Microscope (JEOL JSM 6301 F) with X-Ray Microanalysis (Oxford INCA Energy 350) and a cryo stage (Gatan Alto 2500). HA-AmBi, dispersed in dH_2O at 3 mg/mL and filtered using 0.22 μm syringe filter, were rapidly cooled in sub-cooled nitrogen and transferred under vacuum to the cryo stage. The specimen was fractured, sublimated for 120 s at –90 °C and coated with Au/Pd by sputtering for 45 s and with 12 mA current. The sample was then transferred into the SEM chamber and observed at a temperature of –150 °C.

5.2.5.5. Quantification of AmB content in the conjugate

The AmB content (%) (equation 2) in the conjugate was determined by UV absorption at 387 nm (BioTek Cytation 3 microplate reader, BioTek, Vermont, USA). A calibration curve was obtained dissolving AmB in 0.1 M of borate buffer pH 11, in a concentration range from 0.25 to 0.02 mg/mL. The HA-AmBi was also dissolved and quantified in the same buffer, at a concentration of 1 mg/mL.

$$AmB\ content\ (\%) = \frac{m_{AmB}}{m_{HA-AmBi}} \times 100 \quad (2)$$

where m_{AmB} is the mass determined by UV-vis and $m_{HA\text{-}AmBi}$ is the mass weighted for the assay, per milliliter of solution.

5.2.5.6. Stability of the polysaccharide-drug interaction

To assess the stability of the AmB-HA linkage, a solution of HA-AmBi at a concentration of 2 mg/mL in 0.1 M borate buffer, was placed inside a dialysis bag of MWCO 2000 Da and dialyzed, in the dark and under continuous stirring at 4 °C, against 0.1 M borate buffer pH 11 (for three days with two changes per day) and against dH_2O (for two days with three changes per day). In the end, the solution was frozen and processed in a freeze-drier. The AmB content (%) of this material was determined as reported in the section 5.2.5.5.

5.2.5.7. Spectral measurements

UV-Visible spectra of AmB and HA-AmBi were obtained using a UV-visible spectrophotometer (JASCO V-560 series, Jasco Inc., Maryland, USA). Briefly, HA-AmBi was dispersed and diluted in dH_2O to reach an AmB concentration of 10 μM and then scanned in the range of 300-450 nm at a band width of 5 nm, data pitch of 1 nm and scanning speed of 400 nm/min. The spectrum of AmB dissolved in 0.1 M borate buffer pH 11, and diluted in dH_2O to a final concentration of 10 μM, was also obtained. Measurements of the solutions (200 μL) were performed in a quartz cuvette and the ratio of the absorbance of peak I (315–350) to the peak IV (408–410) was used to monitor the aggregation state of AmB.

5.2.6. Biological activity of HA-AmB imine conjugate

5.2.6.1. Parasites and cells: culture conditions

Axenic amastigotes of *L. infantum* were obtained as described in the literature [41] and maintained at 37 °C, 5 % CO_2 in MAA/20 medium supplemented with 20 % (v/v) iFBS, 2 mM L-Glutamine and 0.023 mM hemin. Different morphological features (round and immobile organisms, about 2-3 μm long and without visible flagella) were assessed by microscopy in order to determine the culture purity (around 95 %).

Human embryonic kidney (HEK293T) cell line (kindly provided by Dr. Tiago dos Santos (i3S - Instituto de Investigação e Inovação em Saúde, Universidade do Porto, Portugal; INEB - Instituto de Engenharia Biomédica, Universidade do Porto, Portugal)) was maintained in Dulbecco's modified essential medium (DMEM) supplemented with 10 % (v/v) iFBS and 1 % (v/v) Penicillin (10.000 U/mL)-Streptomycin (10.000 μg/mL) (complete DMEM medium) at 37 °C with 5 % CO_2. Bone marrow-derived macrophages (BMMΦ) were generated using an adapted protocol described elsewhere [42]. Briefly, bone marrow cells, obtained by flushing femurs and tibia of C57BL/6 mice with incomplete Dulbecco's Modified Eagle's Medium (DMEM), were centrifuged and the pellet resuspended in DMEM medium supplemented with 1 % (v/v) Minimum Essential Medium Non-Essential (MEM) amino acids solution, 10 % (v/v) inactivated FBS, 50 U/mL penicillin, 50 μg/mL streptomycin (cDMEM) and 20 % (v/v) L929 cell conditioned medium (LCCM) as a source of macrophage colony-stimulating factor (M-CSF). Cells were then placed in petri dishes and incubated for 24 h at 37 °C with 5 % CO_2. After that, non-adherent cells were collected, counted and plated in a 96-well plate at a cell density of 2 x 10^5 cells/mL. Cells were incubated for 10 more days, with half of the cDMEM + 20 % LCCM medium being renewed on the 4th and 7th days.

5.2.6.2. *In vitro* cytotoxicity evaluation

Viability of HEK293T cell line and BMMΦ primary cells after incubation with AmB, AmBisome® and HA-AmBi (sterilized through filtration using 0.22 μm syringe filter) was assessed by resazurin assay. HEK293T cells and BMMΦ primary cells were cultured in 96-well flat bottom tissue culture plates at a density of 1×10^5 cells/mL (incubated 24 h in cDMEM) and 2×10^5 cells/mL (incubated 10 days in cDMEM + 20 % LCCM as referred in the section 5.2.6.1), respectively, and incubated for 24 h at 37 °C (5 % CO_2 atmosphere) with the different formulation at various concentrations (0.78 – 67.5 μM AmB equivalents). To assess the cell viability after treatment, 10 % (v/v) of a 2.5 mM resazurin solution was added to each well and cells were incubated at 37 °C with 5 % CO_2 for another 4 h. Fluorescence was measured (λex 560/λem 590) in a BioTek Cytation 3 microplate reader (BioTek, Vermont, USA) and results were expressed as the mean percentage ± SD of viable cells relatively to control. Using the GraphPad Prism software, a nonlinear regression was applied to calculate the concentration of a drug that kills half the BMMΦ cells (CC_{50}). The assay was performed in triplicate at least three times.

5.2.6.3. Hemolytic activity

A known number of red blood cells (RBCs) (1 x 10^8 cells/mL), obtained from a healthy dog was collected after owners' agreement, were incubated in a 48 well plate containing 50 μL of HA-AmBi (containing 1-32 μM AmB equivalents in the final volume of 500 μL) at 37 °C, for 30 min, under agitation (120 rpm). Free-AmB was dissolved in 200 μL of DMSO and further diluted in PBS pH 7.4 (%DMSO < 1) before treating the RBCs. HA and OxHA were also included as control. After 30 min of incubation, treated blood was centrifuged for 10 min at 1200 × g, 4 °C, supernatant was collected and its absorbance was recorded at 540 nm for released hemoglobin. Triton X-100 (1 % (v/v)) was used as a positive control for 100 % cell lysis. Results (mean of three independent experiments) are expressed as a percentage of hemolysis.

5.2.6.4. Treatment of infected macrophages

BMMΦ plated in 96-well plates were infected with 3×10^5 of *L. infantum* amastigotes/well (multiplicity of infection (MOI): 1 macrophage/10 parasites) for 6 h at 37 °C in 5 % CO_2. Afterwards, free parasites were removed by extensive washing with incomplete DMEM medium, and infected cells were incubated for additionally 24 h period prior to treatment with different doses of AmB and HA-AmBi (0.0039 - 1 μM AmB equivalents). Twenty-four hours later, cells were fixed with 4 % (w/v) paraformaldehyde for 15 min, permeabilized with 0.1 % (v/v) Triton X-100 for 15 min and stained

for high content analysis in an IN Cell Analyzer 2000 microscope (GE Healthcare, Illinois, USA) with DAPI and HCS CellMask™ Deep Red stain, as reported in the literature [43]. Results were expressed as the mean percentage ± SD of infected cells relatively to control. The assay was performed in triplicate, at least three times.

5.2.6.5. Animals and ethics statement

C57BL/6 and National Marine Research Institute (NMRI) mice were purchased from the animal facility of the Instituto de Investigação e Inovação em Saúde (i3S). All animals were housed at i3S facilities, under specific pathogen-free conditions, and fed ad libitum. Mice were used at 6 to 8 weeks of age. Depending on the assays, mice were euthanized by isofluorane anesthesia or with an intraperitoneal (i.p.) injection of 50-75 mg/Kg ketamina and 0.5-1 mg/Kg medetomidina followed by cervical dislocation. The experimental animal procedures were approved by the local Animal Ethics Committee of i3S and were licensed by the Portuguese Directorate-General of Food and Veterinary Medicine (DGAV, Ministry of Agriculture, Rural Development and Fishing), on July 7th, 2020 (reference: 009887/2020-07-07) (see appendix). Animals were handled in strict accordance with good animal practice as defined by national authorities (DGV, Law nu1005/92 October 23) and European legislation (EEC/86/609).

5.2.6.6. *In vivo* toxicity assay

Female C57BL/6 mice (with 6-8 weeks of age) were treated with 100 μL of AmBisome® and HA-AmBi dispersed in sterile 5 % w/v dextrose at a dose regimen of 1 and 3 mg AmB/Kg body weight. Control groups received 5 % (w/v) dextrose. Treatments were administered intravenously in the lateral vein of the tail for 3 alternative days and, 24 h after the last administration, mice were anesthetized with isoflurane and euthanized by cervical dislocation for liver, kidney and spleen collection.

5.2.6.7. *In vivo* anti-leishmanial activity of HA-AmB imine conjugate: limiting dilution assay

L. infantum promastigotes were passaged through NMRI mice before the infection. Female C57BL/6 mice (with 6-8 weeks of age) were injected in the lateral vein of the tail with 200 μL of sterile PBS pH 7.4 containing 2×10^7 *L. infantum* stationary-phase promastigotes. Fifteen days post infection, two randomly selected mice from the control group were euthanized and the spleen and liver collected in aseptic conditions, to confirm infection. After that, 100 μL of AmBisome® and HA-AmBi dissolved in sterile 5 % (w/v) dextrose were i.v administered in the lateral vein of the

tail at a dose regimen of 1 mg/kg, every other day, for a total of 5 days (3 administrations). Control groups (infected and non-infected) received 5 % (w/v) dextrose. Three days after the last treatment, animals were euthanized in aseptic conditions and both spleen and liver collected and weighted. A small part of the organs was kept for histology and the rest again weighted and homogenized, respectively, in 2 and 3 mL of complete Schneider's medium supplemented with 20 % iFBS, 100 U/mL penicillin, 100 mg/mL streptomycin, 5 mg/mL phenol red and 5 mM HEPES sodium salt at pH 7.4. Parasite burden in each organ was estimated using a limiting dilution approach, as described previously [44]. For that, homogenates were first diluted to a final concentration of 10 mg/mL. Subsequently, four-fold serial dilutions of the homogenized tissue suspensions were performed in quadruplicate, in a 96-well plate. The wells were examined for viable promastigotes after an incubation of 14 days at 25°C. The last dilution containing promastigotes was recorded and used to determine the number of parasites per organ (parasite burden).

5.2.6.8. Histological analysis

Collected organs from the sacrificed animals were fixed in 4 % buffered paraformaldehyde and paraffin-embedded. Tissue sections with 2 μm thickness were stained with hematoxylin & eosin (H&E) (performed at the Molecular Pathology and Immunology department from the Instituto de Ciências Biomédicas Abel Salazar (ICBAS) from University of Porto (Porto, Portugal)) and visualized by optical microscopy.

5.2.7. Statistical analysis

Statistical analysis was performed using GraphPad Prism 5 software (GraphPad Software, San Diego, CA, USA). Data was expressed as mean ± SD an its normality was checked by performing Kolmogorof-Smirnoff test. Multiple comparisons were performed with Two-way ANOVA followed by post hoc Bonferroni's test. For the *in vivo* study, the non-parametric analysis of variance Mann-Whitney U test was used to evaluate the differences between treatment groups and control. A confidence interval of 95 % ($p < 0.05$) was considered for statistical significance. The half maximal inhibitory concentration (IC_{50}) and half maximal cytotoxic concentration (CC_{50}) were calculated by nonlinear regression analysis.

5.3. Results and Discussion

5.3.1. HA oxidation

With the aim to exploit HA mediated targeting, a covalent conjugate with AmB was designed and formulated. For that, HA was oxidized with sodium periodate, generating two aldehyde groups. The

overall recovery yield was 78.9 ± 2.7 %. The oxidation of HA was confirmed qualitatively by FTIR and ^{1}H NMR analysis. Figure 5.1 A shows the FTIR spectra of native HA and OxHA. The characteristic peaks of HA reported in the literature [45, 46] are observed in both spectra with slight shifts, namely the broad hydroxyl group stretch (-OH) at 3431.0 cm^{-1}; the C-H stretch at 2923.8 cm^{-1}, the asymmetrical –C=O stretch and the symmetrical –C–O stretching at 1618.6 and 1412.4 cm^{-1}, respectively. Also, three signals centered at 1148.4, 1078.3, and 1043.3 cm^{-1}, assigned to the –C–O–C (O-bridge), the –C–O (exocyclic) and the –C–OH groups, respectively, are observed as well as the band at 946.42 cm^{-1}, assigned to asymmetrical out-of-phase ring vibration.

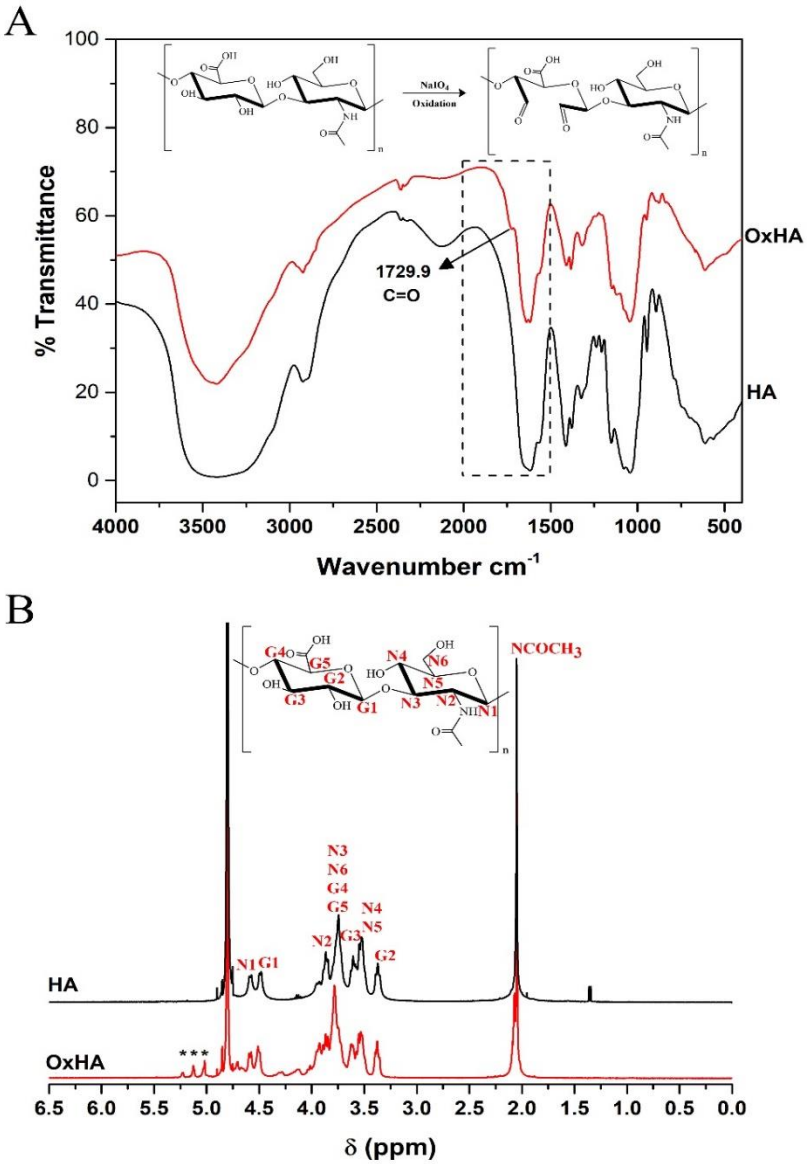

Figure 5.1 - FTIR **(A)** and ^{1}H NMR **(B)** spectra of native HA and periodate oxidized HA.

The generation of aldehyde groups on HA through periodate oxidation was confirmed by the presence of a shoulder at 1729.9 cm^{-1} that, as reported elsewhere [47], corresponds to the –C=O stretching

vibration. This peak was absent on the native HA spectrum. Unlike the broad and strong –C=O bands of carboxyl group (1618.6 cm^{-1}), the –C=O stretching vibration of the aldehyde group is not very strong as they can potentially react with numerous hydroxyl groups of HA leading to the reversible formation of hemiacetals [48]. Through ^{1}H NMR analysis of HA (Figure 5.1 B) it was possible to identify a sharp singlet signal at δ = 2.049 ppm which was assigned to methyl protons of *N*-acetyl ($–COCH_3$) group and a broad multiplet superimposed between approximately 3.371 and 3.952 ppm, assigned to various proton signals in the sugar rings that are difficult to identify individually (δ = 3.371 ppm (G2); δ = 3.606 ppm (G3); δ = 3.845 ppm (N2); δ = 3.526 - 3585 ppm (N4 and N5); δ = 3.744 ppm (N3, N6, G4 and G5) [49]). The double signals at 4.481 and 4.572 ppm (G1 and N1, respectively) correspond to the anomeric protons, attached to the carbons adjacent to oxygen atoms [50]. Similarly to the work of Liu et al. [51], in the OxHA spectrum it is possible to observe new and weak peaks (possibly due to the formation of hemiacetals) at 5.018, 5.124 and 5.231 ppm, which are assigned to aldehyde protons and are absent in the HA spectrum, confirming the successful oxidation of the polysaccharide.

The degree of oxidation was quantitatively determined by the reaction between hydroxylamine hydrochloride and aldehyde groups, at pH 4, leading to the formation of hydrochloric acid (HCl). The amount of HCl generated is equivalent to the number of aldehyde groups present in OxHA, which can be quantified by titration with sodium hydroxide. The degree of oxidation (%DO) using a molar ratio of 1:0.5 (disaccharide units:periodate) was 30.1 ± 5.6 %, approximately half of the maximum theoretical oxidation.

5.3.2. Synthesis and characterization of HA-AmB imine conjugates

After the formation of active HA by oxidation, the primary amine of AmB was conjugated to the aldehyde groups of the polysaccharide through imine bond as shown in Figure 5.2. The HA-AmBi, an orange colored product, was obtained in 85.7 ± 2.6 % yield.

The conjugation of AmB with the polysaccharide was ascertained by FTIR (Figure 5.3). The spectrum of the HA-AmBi shows the characteristic peaks of the polysaccharide that were described above. The characteristic peaks of AmB: 1686.7 cm^{-1} (–C=O, carbonyl ester stretching vibration); 1556.8 cm^{-1} (–C=C stretching vibration from the polyene); 1010.3 cm^{-1} (–C–C–H bending (chromophore) as well as –CH bending (trans-polyene)) and 1068.1 cm^{-1} (–C–O asymmetric stretching vibration) [52, 53]) are not visible in the analysis of the conjugate, as reported in other works where AmB was conjugated

to sodium alginate [32] or where amorphous inclusion complexes between the drug and dextrin were produced [54], possibly due to the superposition with the more abundant OxHA peaks.

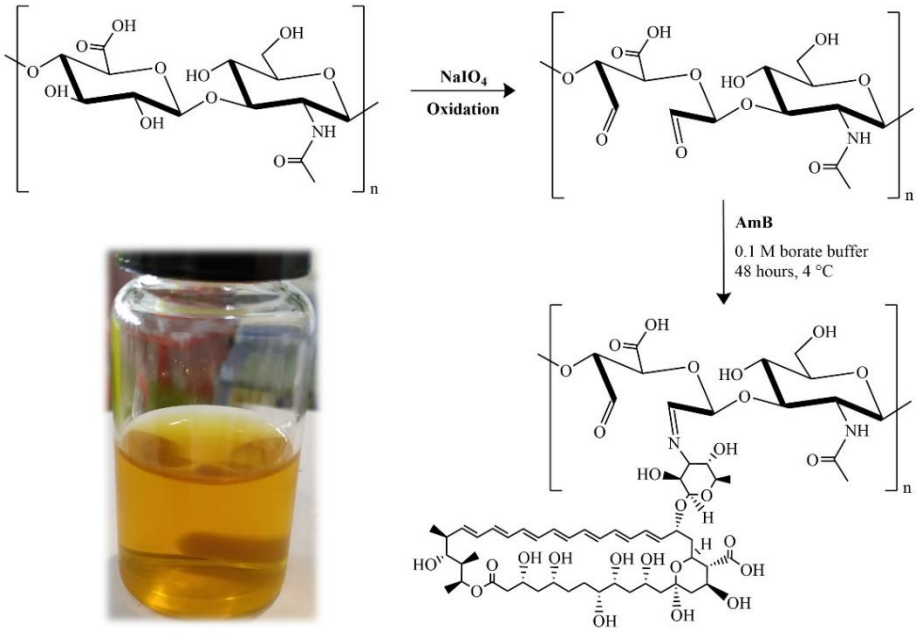

Figure 5.2 - Synthesis of HA-AmBi.

Also, the formation of new bands, like the one that was described by Kothandaraman et al. [20] as being characteristic of the imine bond (1614 cm^{-1}, –C=N) between oxidized pectin and AmB, were not observed. However, the conjugation reaction between OxHA and AmB can be confirmed since the peak at 1729.9 cm^{-1}, typical of the aldehyde group, is absent in the conjugate. Similar results were observed in the conjugation of AmB to oxidized arabinogalactan [27].

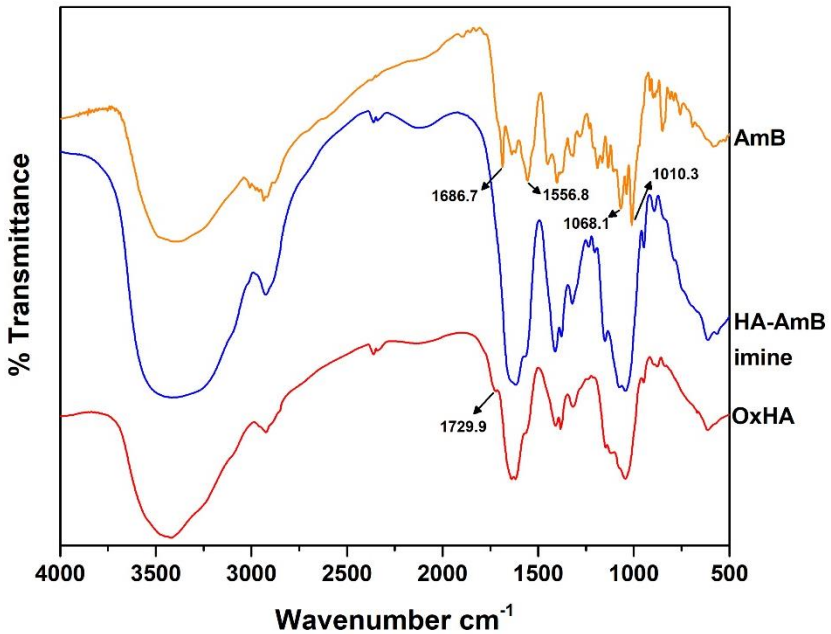

Figure 5.3 - A comparative FTIR analysis of free-AmB, OxHA and HA-AmBi.

DSC analysis was employed to assess physical state of the drug in the conjugate. DSC curves are illustrated in Figure 5.4, showing the thermal behavior of HA, OxHA, HA-AmBi and free-AmB in a range of 50-235 °C. It was observed that AmB present two endothermic peaks at 166.2 °C and 200.9 °C, which is consistent with the literature [55]. Regarding HA spectrum, two peaks were observed, as reported by Kafedjiiski et al. [56]; one endothermic, at 160.7 °C, that could be associated to the desorption of strongly bound water and another exothermic, at 228.7 °C, due to combustion reaction. The same behavior was observed with OxHA (endothermic peak at 144.4 °C and exothermic one at 211.9 °C) and HA-AmBi (endothermic peak at 122.6 °C and exothermic one at 207.6 °C). However, in both OxHA and HA-AmB conjugates the peaks shifted to lower temperatures and present lower intensity, suggesting an alteration of the polymer matrix microstructure [57] after oxidation and drug conjugation. In addition, in the case of HA-AmBi, AmB endothermic peak almost disappeared completely, which suggest the obtention of a material containing AmB in an amorphous state, as also reported for AmB-cyclodextrin complexes [58], AmB-dextrin nanocomplexes [54] and for AmB encapsulated in different nanoparticle systems [59-61].

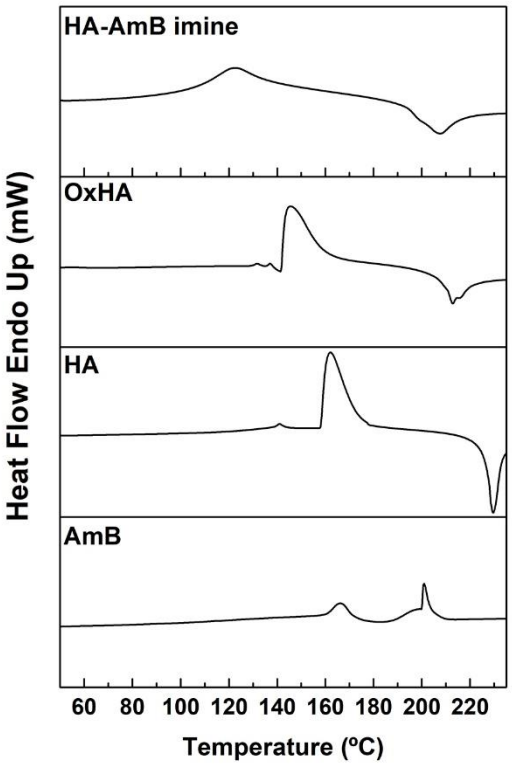

Figure 5.4 - DSC curves of AmB, HA, OxHA and HA-AmBi.

The higher energy state of the amorphous drug formulation is stabilized through the interactions with the polymeric chain networks. Furthermore, amorphization can improve the bioavailability of poorly water-soluble drugs by improving its solubility and dissolution rates [62, 63]. In fact, the conjugates

self-assemble into spherical nanoparticles in aqueous environments (Figure 5.5), being the low water-solubility of the AmB overcome. The particle size analysis is of paramount importance to a drug carrier system, especially when parenteral administration is envisaged [64]. The average size of HA-AmBi dispersed in dH_2O were in the nanosize range (Table 5.1). DLS analysis showed a mean diameter of 101 ± 16 nm, with some polydispersity (PDI bellow 0.5). After filtration a smaller size is obtained 88 ± 18 nm, associated to a more homogeneous size distribution (PDI around 0.3).

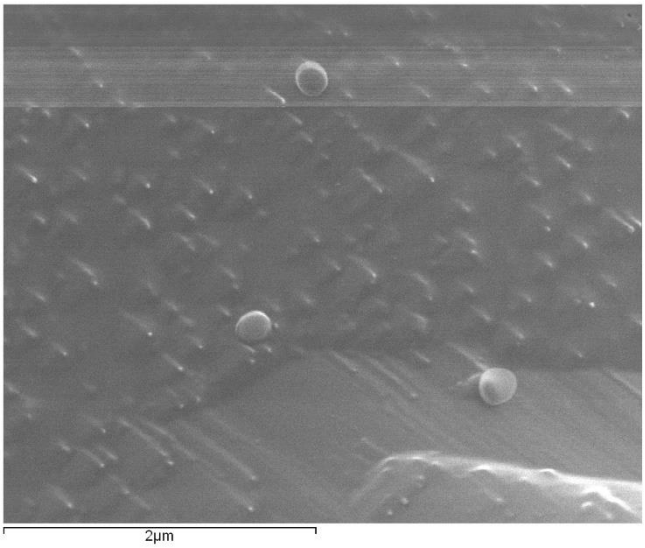

Figure 5.5 - Morphology of HA-AmBi conjugate dispersed in dH_2O observed through Cryo-SEM (magnification of 30 000x; scale bar = 2 µm).

The size of the obtained formulation is very similar to that of the commercial formulation Ambisome® (around 78 nm [65]). The zeta potential was found to be -31.7 ± 1.4 mV which ensures good dispersion and stability after dissolution in dH_2O, due to the high repulsive forces between the particles. After filtration, the potential decreased slightly (-28.3 ± 0.9 mV) but the colloidal stability and the easy redispersion without aggregation was maintained.

Table 5.1 - Physicochemical characteristics of HA-AmBi. Results are expressed as mean ± SD.

	HA-AmB imine	
	Before filtration	**After filtration**
Mean particle size (nm)	101 ± 16	88 ± 18
PDI	0.4 ± 0.1	0.3 ± 0.1
ξ potential (mV)	-31.7 ± 1.4	-28.3 ± 0.9
Drug content (% w/w) *	17.8 ± 1.4	

* Determined by UV-vis at 387 nm and after dissolution in 0.1 M borate buffer pH 11

The AmB content (% w/w) in the conjugates dissolved in 0.1 M borate buffer pH 11 was estimated by UV-vis. An AmB content of 17.8 ± 1.4 % w/w was determined, which indicates a good yield of conjugation, considering that an initial amount of 20 % w/w was used in the reaction (Table 5.1). Furthermore, only a 23.8 % reduction in the total drug content (final content of 13.6 ± 0.9 % w/w of AmB) was observed after submitting the HA-AmBi (at 2 mg/mL) to an extensive dialysis against 0.1 M borate buffer pH 11 (for three days with two changes per day) and against dH_2O (for two days with three changes per day), to force the removal of any free drug. This extraction was necessary since it has been found that AmB can interact non-covalently with HA. The impact of the sterilization by filtration in the drug concentration of a HA-AmBi solution was also assessed. When the conjugate was dissolved in dH_2O (at 1 mg/mL) and then filtered using 0.2 µm sterile filters, a 1.0625-fold reduction in the measured absorbance was observed (e.g., from 0.833 to 0.784 nm). Thus, the loss of material and, therefore, the reduction in the AmB concentration in a solution after sterilization was negligible and will not have a great impact on future assays.

UV-vis spectra were also used to evaluate the molecular organization of AmB with regards to its aggregation state. A close association between AmB state of aggregation and its toxicity towards host cells is reported in the literature [66]. In fact, AmB toxicity is related to its structure and its tendency to aggregate forming dimers (stabilized via the dipole-dipole interactions between chomophores) or tetramers (via hydrogen bond between the hydroxyl group and oxygen of dimers) [67] or to interact with lipids, leading to the formation of transmembrane ion pores in cholesterol-containing membranes, that potentiates cellular destruction [66]. AmB has typical UV-vis absorption in the range of 300-420 nm with four characteristic peaks of an heptaene chromophore [66], determined in this study at 350, 368, 386 and 410 nm (Figure 5.6). The changes in the AmB spectrum according to its monomeric (value inferior to 1), aggregated (value between 1 and 2) or super-aggregated form (value superior to 2) - that presents lower toxicity [68] and increased activity against *Leishmania* parasites, as reported for *L. donovani* [69] - can be monitored by the ratio of the absorbance between the first and the fourth peaks. The AmB solution analyzed in this study presents a ratio of 0.37 (A350/410), thus being in a monomeric form. After covalent conjugation to the HA, the A329/409 ratio was 2.7, indicating the presence of AmB in super-aggregated forms (Figure 5.6). Similar results were observed for a self-assembling biodegradable polyglutamic acid (PGA)-based formulation of AmB (ratio of 2.39) [70] and for AmB nano-assemblies synthesized employing Aloe vera leaf extract (ratio superior to 2) [29].

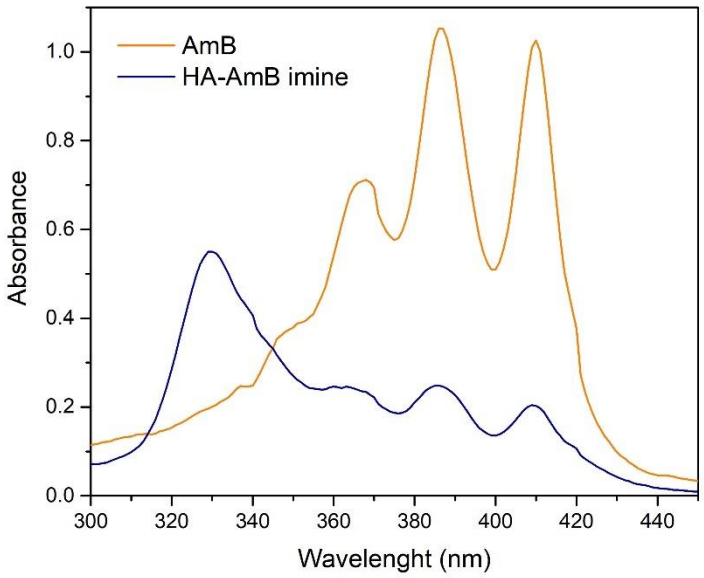

Figure 5.6 - UV-vis spectra corresponding to the aggregation state of free-AmB (dissolved in 0.1 M borate buffer pH 11 and diluted in dH_2O) and HA-AmBi. Both formulations were diluted in dH_2O a final concentration of 10 μM of AmB and analyzed at room temperature.

However, we also envisage AmB in an aggregate form in the HA-AmBi since the first peak of the spectrum blue-shifted only to 329 nm (super-aggregated forms of AmB are normally associated to a shift in the λmax of the first peak to values inferior to 325 nm [71, 72]). Of note, studies similar to ours reported that the drug was almost in the monomeric form (ratio values inferior to 1) after conjugation to a polysaccharide [6, 20, 32]; nevertheless the type of solvents used in those studies for the analysis (water, buffers or organic solvent), which has extreme impact in the outcome [71], were not specified.

5.3.3. Evaluation of the *in vitro* cytotoxicity of the HA-AmB imine conjugate

Conventional treatments based in the use of AmB are associated with noticeable toxicity [27], affecting its applicability. The *in vitro* toxicity of the free-AmB and HA-AmBi were firstly assessed towards primary macrophages (BMMΦ) (host cells of the parasites) (Figure 5.7 A) and kidney cells (HEK293T cell line) (due to its nephrotoxicity) (Figure 5.7 B). AmB showed high toxicity towards BMMΦ (CC_{50} of 3.16 ± 1.08 μM) and HEK293T cells (CC_{50} of 9.43 ± 0.20 μM), promoting a reduction in cell viability at doses above 2.63 and 3.95 μM, respectively. Compared to the free-drug, the HA-AmBi was significantly less toxic against HEK293T cells since no toxic effects were observed for all the tested doses (Figure 5.7B). Concerning the BMMΦ cells, the imine conjugate promoted some toxicity at doses above 5.93 μM (Figure 5.7A). Reduction of this effect against macrophages could possibly be achieved through sodium borohydride reduction of the free aldehyde groups, leading to the development of a HA-AmB

amine conjugate. Nevertheless, as reported by Sokolsky-Papkov et al. [18] for a Dextran-AmB amine conjugate, this procedure reduces not only the toxicity but also the antiparasitic activity. With that in mind, we decided to keep the conjugates in its imine form.

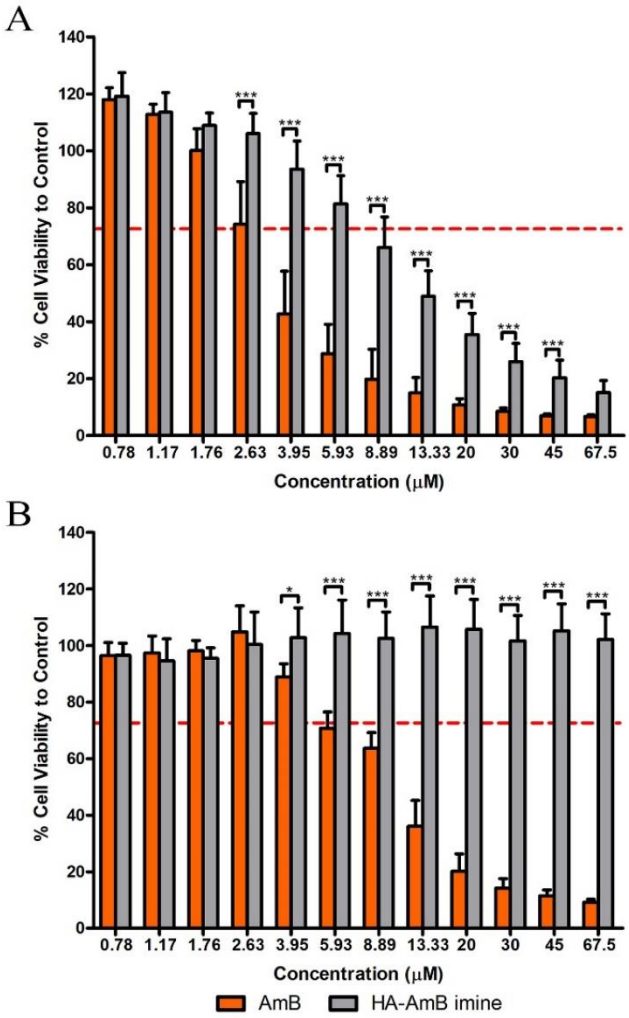

Figure 5.7 - *In vitro* cytotoxicity of AmB and HA-AmBi. BMMΦ cells **(A)** and HEK293T cells **(B)** were treated for 24 h with a specific range of both formulations' doses (0.78 – 67.5 μM) and cell viability was determined by resazurin assay. Results are expressed as percentage relative to the control and presented as mean ± SD of at least three independent experiments. Treatment with the imine conjugate was compared with the AmB using Bonferroni's multiple comparison post-test (* $p < 0.05$ and *** $p < 0.001$).

Overall, the AmB conjugation to the polysaccharide managed to mitigate the levels of toxicity observed for the free-drug since the survival rate was significantly higher in all the HA-AmBi tested doses compared to the control, being observed a 2.94-fold increase in the CC_{50} (9.29 ± 2.90 μM). Our results are in accordance with several reports on the literature which demonstrated that different oxidized polysaccharides conjugated with AmB presented reduced toxicity [18, 32, 35]. This type of conjugation induces changes in the drug mode of action in a way that prevents its toxic effects to

mammalian cells. Kagan et al. [73] showed that the conjugation of AmB with oxidized arabinogalactan neutralizes the toxic activity of the free drug by preventing the formation of channels in the plasma membrane, as well as changes in endosomal compartments, which is important for the maintenance of the endosomal pH gradient required for normal membrane trafficking. The difference in the observed toxic effects between free-AmB and HA-AmBi can be explained by the prevention of AmB molecule self-association in dimers or tetramers (required to form channels in cholesterol-containing membranes (mammalian cells)). As described in section 5.3.2, the obtained formulation contains mostly AmB in its super-aggregated form, which may explain the observed diminished toxicity.

Anemia is a common issue associated with AmB therapy. Thus, the *in vitro* hemolytic activity was assessed estimating the red blood cells (RBCs) membrane damage, since the intravenous administration of the formulation is intended. It has been described in the literature that AmB at concentrations below 2 μM induces a reversible membrane permeabilization in the RBCs, while at higher concentrations it promotes lysis [74]. The conjugation of AmB to the polysaccharide resulted in a significant decrease in the hemolysis activity comparatively to the control, this effect being observed in all the tested doses (Figure 5.8). At lower concentrations (1 μM), no significant hemolysis was observed with any of the formulations (% of hemolysis inferior to 5).

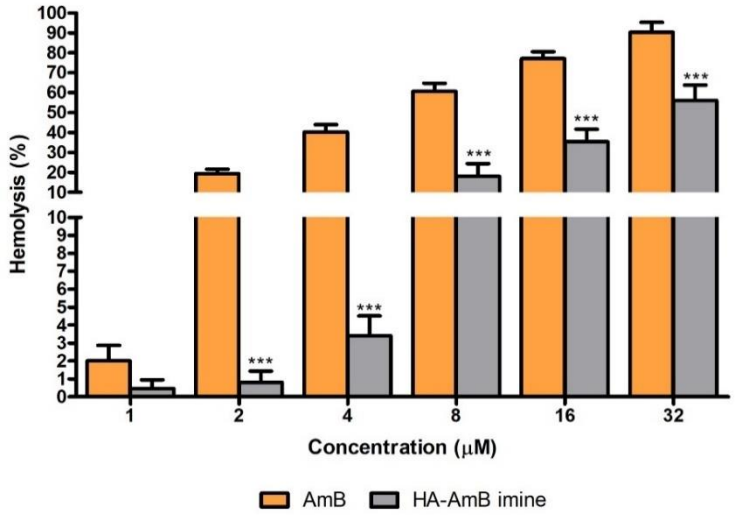

Figure 5.8 - Extent of dog's RBCs damage after incubation with free AmB and HA-AmBi (at equivalent concentrations) for 30 min at 37 °C. Results, presented as mean ± SD of at least three independent experiments, are expressed as percentage relative to the control. Significant differences with AmB were calculated using Bonferroni's multiple comparison post-test and are indicated with *** $p < 0.001$.

In fact, negligible hemolysis was still observed with imine conjugate at the doses of 2 and 4 μM of AmB (maximum % of hemolysis was 0.8 ± 06 and 3.4 ± 1.1, respectively) whereas a stock solution of AmB in DMSO and diluted in PBS pH 7.4 to the same concentrations above referred produced 19.4

± 2.2 and 40.3 ± 3.7 % of hemolysis, respectively. According to the literature [19, 52], HA promotes to some extent a protective and stabilizing effect improving AmB hemocompatibility, effect that was also observed for drug conjugates with gum arabic [19], sodium alginate [32], arabinogalactan [27], among other polysaccharides [20, 35].

5.3.4. *In vitro* anti-leishmanial activity in *L. infantum*-infected macrophages

As *Leishmania* is an intracellular parasite, it is essential to ascertain whether the formulation is able to reach the amastigote inside the host cells, promoting a selective effect. For that, the activity of HA-AmBi against amastigote forms of *L. infantum* was determined in *Leishmania*-infected macrophages. As expected, HA-AmBi was toxic to intracellular parasites, reducing the infection burden, and exhibited dose-dependent efficacy (Figure 5.9), effect that was comparable to that of the AmB (IC_{50} = 0.023 μM vs 0.018 μM, respectively), as shown in Table 5.2.

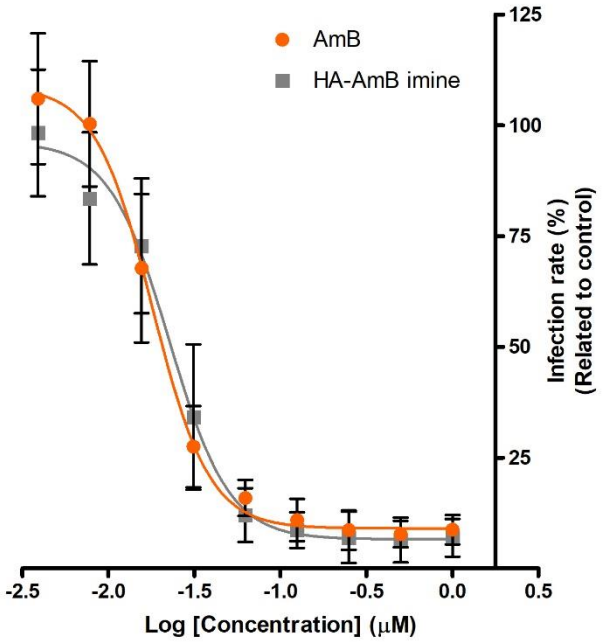

Figure 5.9 - *In vitro* effect of AmB and HA-AmBi on intracellular amastigotes. *L. infantum*-infected BMMΦ were treated for 24 h with different concentrations (0.0039 to 1 μM) of the above referred formulations. Data (mean ± SD of at least three independent experiments) was obtained employing an automated image analysis protocol available for the IN Cell Analyzer system and used for the obtention of the dose-response curves.

Therefore, AmB retained its known effect against *Leishmania*-infected macrophages, even after its covalent conjugation to HA. Similar findings were reported after AmB conjugation to oxidized arabinogalactan. The obtained Arabinogalactan-AmB (AG-AmB) imine conjugate presented a 50 %

effective concentration (EC_{50}) of 0.027 μg/mL (± 0.029 μM) against *L. infantum* in infected macrophages [16]. Another study showed that AmB conjugated to N-(2-hydroxypropyl)methacrylamide (HPMA) copolymer maintained a biological activity against intracellular *L. donovani* amastigotes in BMMΦ, effect that was comparable with that of free AmB (EC_{50} = 0.03 μg/mL (± 0.032 μM) for both) [75]. Furthermore, it was noticed in our study that the HA-AmBi have a safety and efficacy balance greater than the free-AmB, meaning that it has a wider selectivity index (SI) against intracellular amastigotes of *L. infantum* in macrophages (SI of 404) than only AmB (SI of 176).

Table 5.2 - *In vitro* cytotoxicity of HA-AmBi against intracellular amastigotes and macrophages.

Sample	Amastigotes IC_{50} (μM)	Macrophages CC_{50} (μM)	Selectivity Index (SI) [a]
AmB	0.018 ± 0.001	3.16 ± 1.08	176
HA-AmBi	0.023 ± 0.004	9.29 ± 2.90	404

Means ± SD (n = 3).

[a] SI (selectivity index) = CC_{50} /IC_{50}.

5.3.5. *In vivo* assays: systemic toxicity and anti-leishmanial activity in infected mice

Selective reduction of the parasite burden without systemic toxicity is the ideal goal of any new therapeutics against leishmaniasis. AmB is renowned for its nephrotoxicity and hepatotoxicity. Even the current treatments for visceral leishmaniasis, based in the use of commercially available liposomal and colloidal formulations, are administered as slow infusion and doses regimens including 21 days of infusion, to avoid those negative effects. A comparative multiple dose toxicity assessment was performed by evaluating the effect of HA-AmBi and AmBisome® (at 1 and 3 mg AmB/Kg of body weight) on liver, kidneys and spleen histology. Results of weight gain and loss of control groups (5 % dextrose and HA at 1 and 3 mg/Kg) as well as of animals treated with the AmB-based formulations are summarized in Table 5.3. Control and AmBisome®-treated groups showed normal weight gain, while animals treated with HA-AmBi showed a decline in weight, being this effect more prominent at a dosage of 3 mg/Kg. Throughout the experience, behavioral and physical signs, such as weight loss of more than 15 %, were monitored to define the point at which an animal (or group of animals) is removed from the study through euthanasia. Since only a weight loss around 11.7 % was observed and the animals presented normal coat condition or posture and no signs of apathy, withdrawal or increased aggression, this group was maintained until the end of the assay. Regarding the histological analysis (Table 5.4), no particular toxicity or abnormal pathological alteration of liver, kidneys and spleen were observed for mice treated with 5 % dextrose and HA or AmBisome® at 1 and 3 mg/Kg.

Regarding the animals treated with 1 mg/Kg of HA-AmBi, despite no abnormal alterations in the kidneys and spleen being observed, analysis of the hepatic tissues revealed an interstitial and diffuse inflammatory infiltrate and the presence of well-circumscribed multifocal areas of intensely eosinophilic hepatocellular degeneration surrounded by mixed inflammatory infiltrate. Those alterations, that could be considered more aggressive, were only observed in one animal of this group. Interestingly, no abnormal alterations in the liver and spleen were observed using the higher dosage of 3 mg/Kg. However, one animal treated with that dose presented in the kidney's multifocal tubular intraepithelial steatosis, numerous hyaline casts and chronic multifocal interstitial nephritis.

Table 5.3 - Body weight changes (mean ± SD) according to each experimental group.

Treatment groups	**Body weight (g)**		
	Before 1st administration	Before euthanasia	Change (%)
CTR (5 % w/v dextrose)	19.10 ± 0.44	19.40 ± 0.66	0.30 g (+1.57 %)
AmBisome® (1 mg/Kg)	19.47 ± 1.05	19.50 ± 1.21	0.03 g (+0.17 %)
AmBisome® (3 mg/Kg)	18.57 ± 0.81	19.37 ± 0.95	0.80 g (+4.31 %)
HA (1 mg/Kg)	18.57 ± 1.08	18.93 ± 0.55	0.37 g (+1.97 %)
HA (3 mg/Kg)	17.97 ± 0.59	18.70 ± 0.35	0.73 g (+4.08 %)
HA-AmBi (1 mg/Kg)	19.43 ± 0.64	18.93 ± 0.40	0.50 g (–2.57 %)
HA-AmBi (3 mg/Kg)	17.67 ± 1.57	15.60 ± 1.51	2.07 g (–11.70 %)

Some reports of issues detected in Fungizone®-treated mice can be found: **liver -** focal lesions consisting of inflammatory cells surrounding a cluster of necrotic hepatocytes, isolated foci of necrotic hepatocytes, hepatocytes in the centrilobular zone showing degenerative features and bile duct damage [76]; **kidneys -** vascular and cellular degenerative changes characterized by dilatation of blood vessels and focal hemorrhage, luminal tubular epithelial exfoliation, widened glomerular vascular space with focal glomerular tubular necrosis [77]). Thus, it is possible to infer a marked reduction in injury observed in our study with the covalent conjugate, *i.e.* reduced impact in the quality of the animal health, as compared to Fungizone®.

Additionally, no signs of nephromegaly and hepatomegaly were observed (Figure 5.10). Despite no significant histological abnormalities being observed, animals treated with 1 mg/Kg of HA-AmBi presented a significant splenomegaly comparatively to the control groups which could be associated to an increased workload of the spleen.

Table 5.4 - Histological alterations observed after mice treatment with HA-AmBi and AmBisome®.

Treatments		Histological Findings		
		Liver	**Kidneys**	**Spleen**
CTR	**5 % w/v dextrose**	• Mononuclear inflammatory infiltrate; • Bile duct hyperplasia; • Vascular ectasia;	-	• Follicular hyperplasia;
HA	**1 mg/Kg**	-	-	• Slight follicular hyperplasia;
	3 mg/Kg	• Vascular ectasia;	-	• Slight follicular hyperplasia;
AmBisome®	**1 mg/Kg**	• Multifocal inflammatory infiltrate (eosinophils and neutrophils); • Presence of hepatocytes with large nuclei and lumpy chromatin; • Presence of mitotic cells (Regeneration/dysplasia); • Slight cellular tumefaction and hydropic degeneration;	• Slight chronic inflammation with luminal tubular dilation;	• Slight multifocal to coalescent follicular hyperplasia;
	3 mg/Kg	• Multifocal inflammatory infiltrate (eosinophils and neutrophils); • Mild chronic periportal inflammatory infiltrate; • Vascular ectasia;	• Slight multifocal inflammatory infiltrate (mixed cells);	• Slight follicular hyperplasia;
HA-AmBi	**1 mg/Kg**	• Multifocal inflammatory infiltrate (mixed cells); • Multifocal to interstitial subacute inflammatory infiltrate; • Interstitial and diffuse inflammatory infiltrate; • Well-circumscribed multifocal areas of intensely eosinophilic hepatocellular degeneration surrounded by mixed inflammatory infiltrate;	-	• Slight follicular hyperplasia; • Diffuse hemosiderosis;
	3 mg/Kg	• Slight multifocal to interstitial subacute inflammatory infiltrate;	• Numerous hyaline casts and chronic multifocal	• Megakaryocytes (extramedullary hematopoiesis);

	• Moderate multifocal to interstitial subacute inflammatory infiltrate; • Agglomerates of mixed inflammatory infiltrates (perivascular to interstitial); • Vascular ectasia;	interstitial nephritis; • Multifocal tubular intraepithelial steatosis;	• White pulp follicular hyperplasia;

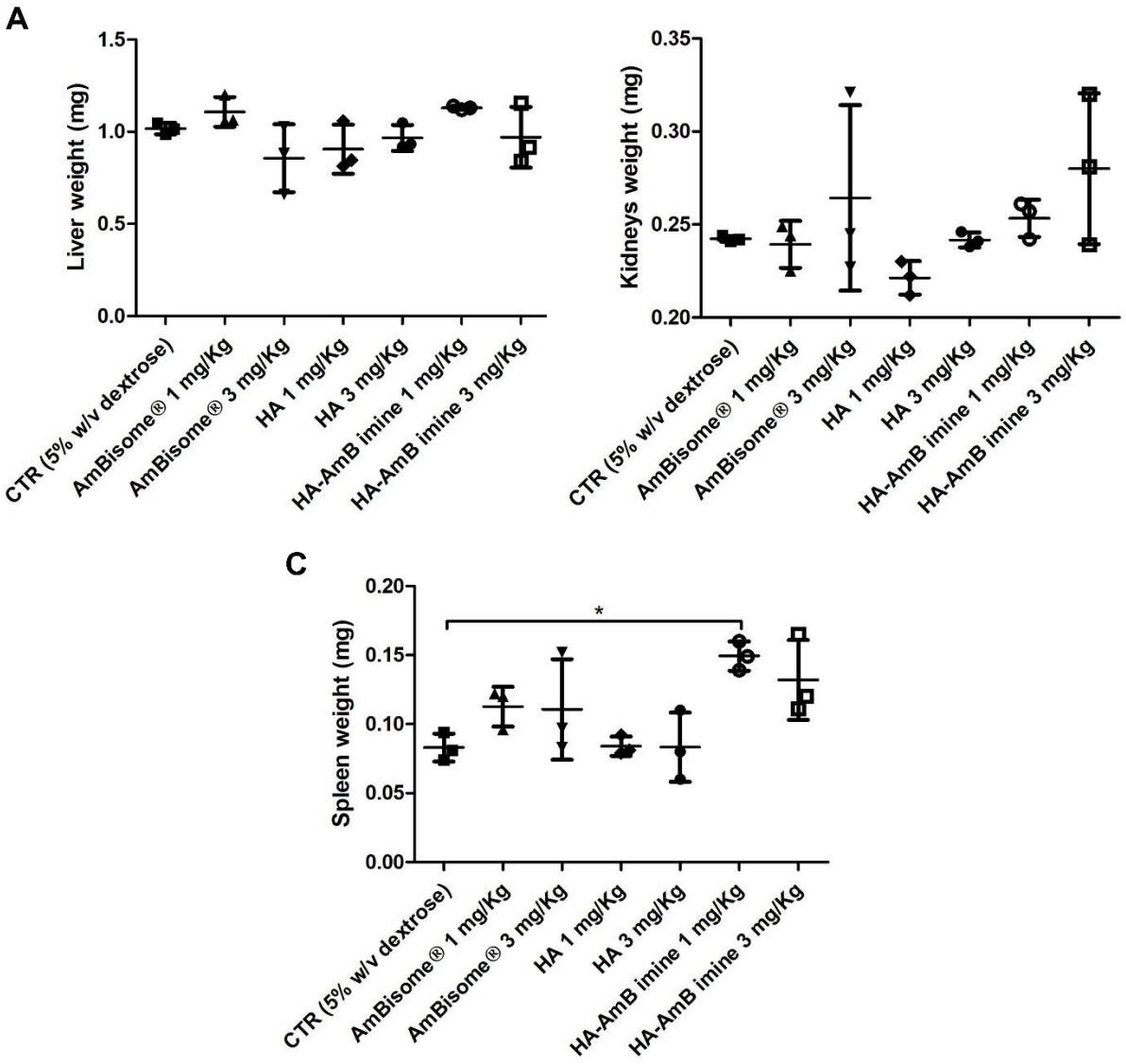

Figure 5.10 - Weight of the **(A)** liver, **(B)** kidneys and **(C)** spleen collected from the treated mice. Each symbol represents one animal and the horizontal bars represent the mean weight of the organs. Bonferroni's multiple comparison post-test was used to evaluate differences between each group and only in the spleen was observed significant differences between the CTR (5 % dextrose) group and the HA-AmBi (1 mg/Kg) group (*$p < 0.05$).

C57BL/6 mice were also infected with *L. infantum* stationary promastigotes and, when a chronic infection was stablished (15 days after challenge), they were treated with HA-AmBi and AmBisome®

at 1 mg AmB/Kg body weight for 3 alternative days in order to assess their efficacy in reducing the parasitic infection. In the literature, some works report the development of PDCs using a plethora of polymers and AmB, for leishmaniasis treatment [6, 16-20]. Nevertheless, only the work developed by Golenser et al. [16] displayed *in vivo* results to prove the anti-leishmanial efficacy of the Arabinogalactan-AmB (AG-AmB) imine conjugate in a lesion suppression model of infection. Authors showed that the subcutaneous injection of the conjugates at 6 mg/kg (treatment started 2 days after infection and was administered six times on alternate days) was significantly more effective than AmBisome® in delaying the appearance of lesions, in BALB/c mice infected with *L. major* promastigotes. When an established infection was treated (1 month after parasite injection and with visible lesions), AG-AmB imine conjugate was somewhat slightly more effective than AmBisome®. Furthermore, it was always referred that subcutaneous administration of the formulations were more effective than intravenous administration [16]. In our study, the *in vivo* potential of a PDC-based formulation developed with HA and AmB for the VL treatment was showed after intravenous administration. Table 5.5 displays the obtained results from the limiting dilution approach. Treatment of the infected mice with HA-AmBi clearly promoted a significant reduction in the parasite burden in the spleen (1.32-$\log_{10}$ reduction), when compared to the control group.

Table 5.5 - *In vivo* anti-leishmanial activity of AmBisome® and HA-AmBi against *L. infantum*-infected mice.

Treatment groups	Spleen weight ± SD (mg)	Log_{10} parasite burden ± SD	Reduction	Liver weight ± SD (mg)	Log_{10} parasite burden ± SD	Reduction
Non-infected	73.0 ± 7.4 ^{a}	-	-	1191.7 ± 88.3 ^{d}	-	-
CTR (5 % w/v dextrose)	88.3 ± 6.6 ^{b}	5.6 ± 0.6	-	1088.0 ± 83.3 ^{d}	10.8 ± 2.7	-
AmBisome® (1 mg/Kg)	93.0 ± 16.6 $^{b, c}$	3.9 ± 0.5 *	1.74 $\log_{10}$	1151.6 ± 131.4 ^{d}	4.9 ± 0.7 $^{\#\#}$	5.89 $\log_{10}$
HA-AmBi (1 mg/Kg)	98.5 ± 4.0 ^{c}	4.3 ± 0.5 *	1.32 $\log_{10}$	1400.7 ± 114.7 ^{e}	5.8 ± 0.9 $^{\#\#}$	4.98 $\log_{10}$

Nonparametric Mann-Whitney U test was used to evaluate statistical differences between the groups:

$^{a\text{-}e}$ Different letters in the same column indicate significant statistical differences ($p < 0.01$).

* $p < 0.05$, AmBisome® and HA-AmBi versus CTR (spleen).

$^{\#\#}$ $p < 0.01$, AmBisome® and HA-AmBi versus CTR (liver).

This effect was even more pronounced in the liver, with a significant reduction of 4.98-$\log_{10}$. In both organs, three administrations of the conjugate every other day were comparable to AmBisome® in reducing the parasite burden in infected mice (1.74-$\log_{10}$ and 5.89-$\log_{10}$ reduction in the spleen and liver, respectively). The safety of the VL treatment is as fundamental as its effectiveness. Despite the significant increase in the spleen and liver weight (Table 5.5) comparatively to the control and non-infected groups, no signs of particular toxicity and abnormal pathological alteration were observed in the histological analysis of both organs (Table 5.6). Of note, in the spleen all groups displayed a significant splenomegaly comparatively to the non-infected group, which could be explained by the infection itself (Table 5.5).

Table 5.6 - Histological alterations observed after intravenous treatment of *L. infantum*-infected mice with 1 mg/Kg of HA-AmBi and AmBisome®.

Treatment	Histological Findings	
	Liver	**Spleen**
CTR (5 % w/v dextrose)	• Slight periportal inflammatory infiltrate of lymphoids; • Generalized congestion and hydropic degeneration; • Discrete vascular ectasia;	• Diffuse hemosiderosis;
Infected CTR (5 % w/v dextrose)	• Slight multifocal inflammatory infiltrate of lymphoids; • Lymphoid agglomerates (multifocal to perivascular and periportal); • Generalized congestion and hydropic degeneration; • Vascular ectasia;	• Slight follicular hyperplasia;
AmBisome (1 mg/Kg)	• Slight multifocal inflammatory infiltrate of lymphoids; • Lymphoid agglomerates (multifocal to perivascular and periportal); • Generalized congestion; • Vascular ectasia;	-
HA-AmBi (1 mg/Kg)	• Slight multifocal and subacute inflammatory infiltrate;	• Diffuse hemosiderosis;

In addition, clinical signals such as ataxia, weakness and weight loss were not observed in any group; *e.g.* HA-AmBi and AmBisome® treated mice presented a positive variation in weight by 5.8 %, for both cases, and non-infected and control group presented a positive variation of 5.5 and 3.9 %, respectively (Figure 5.11).

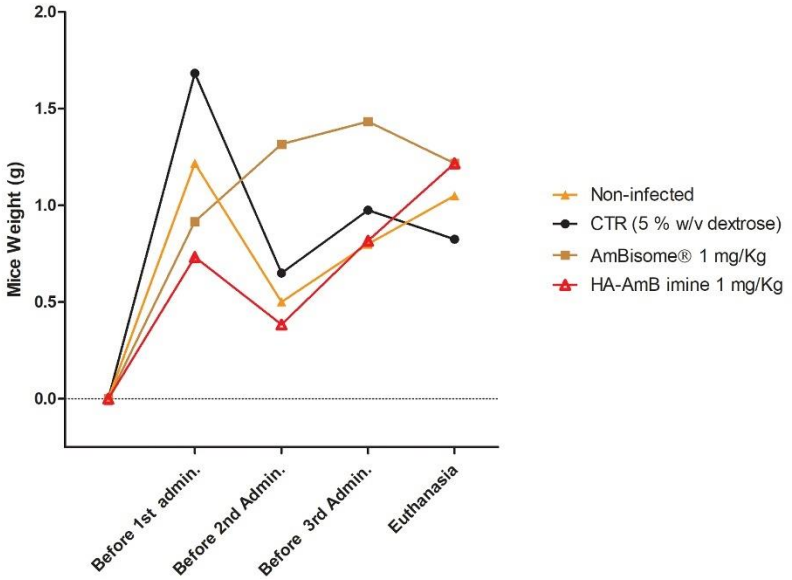

Figure 5.11 - Weight variation of the non-infected and infected mice over the treatments.

5.4. Conclusion

A method for producing a stable water-soluble polysaccharide-AmB conjugate was described in this study. AmB was conjugated via imine bond to oxidized HA, yielding an amorphous nano-sized formulation with a high conjugation yield of active AmB in an aggregate/super-aggregate forms. The HA-AmBi presented improved solubility in aqueous environments and significantly mitigated the *in vitro* toxicity and hemolytic activity of AmB, while preserving the *in vitro* and *in vivo* anti-leishmanial activity, with no signs of particular toxicity and abnormal pathological alteration. This strategy offers a safe and efficacious system for a suitable delivery of AmB and, therefore, present some potential for future use as a nanomedicine in leishmaniasis treatment.

5.5. References

1. Bhakay, A., et al., *Bioavailability Enhancement of Poorly Water-Soluble Drugs via Nanocomposites: Formulation Processing Aspects and Challenges.* Pharmaceutics, 2018. **10**(3).
2. Thakor, P., et al., *Polymer–drug conjugates: recent advances and future perspectives.* Drug Discovery Today, 2020. **25**(9): p. 1718-1726.
3. Girase, M.L., P.G. Patil, and P.P. Ige, *Polymer-drug conjugates as nanomedicine: a review.* InternInt J Polym Mater, 2020. **69**(15): p. 990-1014.
4. Ekladious, I., Y.L. Colson, and M.W. Grinstaff, *Polymer–drug conjugate therapeutics: advances, insights and prospects.* Nature Reviews Drug Discovery, 2019. **18**(4): p. 273-294.
5. Jatzkewitz, H., *Peptamin (glycyl-l-leucyl-mescaline) bound to blood plasma expander (polyvinylpyrrolidone) as a new depot form of a biologically active primary amine (mescaline).* Z. Naturforsch., 1995. **10**: p. 27–31.
6. Ravichandran, V., et al., *Synthetic Polysaccharides as Drug Carriers: Synthesis of Polyglucose-Amphotericin B Conjugates and In Vitro Evaluation of Their Anti-Fungal and Anti-Leishmanial Activities.* J Nanosci Nanotechnol, 2018. **18**(4): p. 2405-2414.
7. Basu, A., et al., *Polysaccharide-Based Conjugates for Biomedical Applications.* Bioconjugate Chemistry, 2015. **26**(8): p. 1396-1412.

8. Duncan, R., *Polymer therapeutics: Top 10 selling pharmaceuticals — What next?* Journal of Controlled Release, 2014. **190**: p. 371-380.
9. Markman, B., et al., *A phase 1 study of CRLX301, a novel nanoparticle-drug conjugate (NDC) containing docetaxel (DOC), in patients with refractory solid tumors.* Journal of Clinical Oncology, 2016. **34**(15_suppl): p. 2526-2526.
10. Rosato, A., et al., *HYTAD1-p20: a new paclitaxel-hyaluronic acid hydrosoluble bioconjugate for treatment of superficial bladder cancer.* Urol Oncol, 2006. **24**(3): p. 207-15.
11. Luo, Y., et al., *Targeted Delivery of Doxorubicin by HPMA Copolymer-Hyaluronan Bioconjugates.* Pharmaceutical Research, 2002. **19**(4): p. 396-402.
12. Monica, C. and R. Davide, *ONCOFID™-P a Hyaluronic Acid Paclitaxel Conjugate for the Treatment of Refractory Bladder Cancer and Peritoneal Carcinosis.* Current Bioactive Compounds, 2011. **7**(1): p. 27-32.
13. Chen, X., et al., *Polyethylene glycol loxenatide injections added to metformin effectively improve glycemic control and exhibit favorable safety in type 2 diabetic patients.* J Diabetes, 2017. **9**(2): p. 158-167.
14. Miyazaki, T., et al., *NKTR-181: A Novel Mu-Opioid Analgesic with Inherently Low Abuse Potential.* J Pharmacol Exp Ther, 2017. **363**(1): p. 104-113.
15. Mease, P.J., et al., *Effect of certolizumab pegol on signs and symptoms in patients with psoriatic arthritis: 24-week results of a Phase 3 double-blind randomised placebo-controlled study (RAPID-PsA).* Ann Rheum Dis, 2014. **73**(1): p. 48-55.
16. Golenser, J., et al., *Efficacious treatment of experimental leishmaniasis with amphotericin B-arabinogalactan water-soluble derivatives.* Antimicrobial agents and chemotherapy, 1999. **43**(9): p. 2209-2214.
17. Ehrenfreund-Kleinman, T., J. Golenser, and A.J. Domb, *Conjugation of amino-containing drugs to polysaccharides by tosylation: amphotericin B-arabinogalactan conjugates.* Biomaterials, 2004. **25**(15): p. 3049-57.
18. Sokolsky-Papkov, M., A.J. Domb, and J. Golenser, *Impact of Aldehyde Content on Amphotericin B–Dextran Imine Conjugate Toxicity.* Biomacromolecules, 2006. **7**(5): p. 1529-1535.
19. Nishi, K.K., et al., *Amphotericin B-Gum Arabic Conjugates: Synthesis, Toxicity, Bioavailability, and Activities Against Leishmania and Fungi.* Pharmaceutical Research, 2007. **24**(5): p. 971-980.
20. Kothandaraman, G.P., et al., *Anti-fungal and anti-leishmanial activities of pectin-amphotericin B conjugates.* Journal of Drug Delivery Science and Technology, 2017. **39**: p. 1-7.
21. Bates, P.A., *Transmission of Leishmania metacyclic promastigotes by phlebotomine sand flies.* Int J Parasitol, 2007. **37**(10): p. 1097-106.
22. Burza, S., S.L. Croft, and M. Boelaert, *Leishmaniasis.* Lancet, 2018. **392**(10151): p. 951-970.
23. Desjeux, P., *Leishmaniasis: current situation and new perspectives.* Comp Immunol Microbiol Infect Dis, 2004. **27**(5): p. 305-18.
24. Boelaert, M. and S. Sundar, *47 - Leishmaniasis*, in *Manson's Tropical Infectious Diseases (Twenty-third Edition)*, J. Farrar, et al., Editors. 2014, W.B. Saunders: London. p. 631-651.e4.
25. Croft, S.L. and V. Yardley, *Chemotherapy of leishmaniasis.* Curr Pharm Des, 2002. **8**(4): p. 319-42.
26. Kedzierski, L., *Leishmaniasis Vaccine: Where are We Today?* J Glob Infect Dis, 2010. **2**(2): p. 177-85.
27. Ehrenfreund-Kleinman, T., et al., *Synthesis and characterization of novel water soluble amphotericin B–arabinogalactan conjugates.* Biomaterials, 2002. **23**(5): p. 1327-1335.
28. Iborra, S., et al., *Vaccine candidates against leishmania under current research.* Expert Rev Vaccines, 2018. **17**(4): p. 323-334.

29. Zia, Q., et al., *Biomimetically engineered Amphotericin B nano-aggregates circumvent toxicity constraints and treat systemic fungal infection in experimental animals.* Sci Rep, 2017. **7**(1): p. 11873.
30. Nath, P., et al., *Immediate hypersensitivity reaction following liposomal amphotericin-B (AmBisome) infusion.* Tropical doctor, 2014. **44**(4): p. 241-242.
31. Mukhtar, M., et al., *First report on Ambisome-associated allergic reaction in two Sudanese leishmaniasis patients.* The American journal of tropical medicine and hygiene, 2011. **85**(4): p. 644-645.
32. Ravichandran, V. and A. Jayakrishnan, *Synthesis and evaluation of anti-fungal activities of sodium alginate-amphotericin B conjugates.* International Journal of Biological Macromolecules, 2018. **108**: p. 1101-1109.
33. Ickowicz, D.E., et al., *Activity, reduced toxicity, and scale-up synthesis of amphotericin B-conjugated polysaccharide.* Biomacromolecules, 2014. **15**(6): p. 2079-89.
34. Falk, R., A.J. Domb, and I. Polacheck, *A novel injectable water-soluble amphotericin B-arabinogalactan conjugate.* Antimicrob Agents Chemother, 1999. **43**(8): p. 1975-81.
35. Farber, S., et al., *Galactomannan–amphotericin B conjugate: synthesis and biological activity.* Polymers for Advanced Technologies, 2011. **22**(1): p. 119-125.
36. Choi, K.Y., et al., *Self-assembled hyaluronic acid nanoparticles as a potential drug carrier for cancer therapy: synthesis, characterization, and in vivo biodistribution.* Journal of Materials Chemistry, 2009. **19**(24): p. 4102-4107.
37. Sladek, Z. and D. Rysanek, *Expression of macrophage CD44 receptor in the course of experimental inflammatory response of bovine mammary gland induced by lipopolysaccharide and muramyl dipeptide.* Res Vet Sci, 2009. **86**(2): p. 235-40.
38. Zhao, H. and N.D. Heindel, *Determination of Degree of Substitution of Formyl Groups in Polyaldehyde Dextran by the Hydroxylamine Hydrochloride Method.* Pharmaceutical Research, 1991. **8**(3): p. 400-402.
39. Kahlert, H., G. Meyer, and A. Albrecht, *Colour maps of acid–base titrations with colour indicators: how to choose the appropriate indicator and how to estimate the systematic titration errors.* ChemTexts, 2016. **2**(2): p. 7.
40. Muhammad, M., et al., *Synthesis and Characterization of Oxidized Polysaccharides for In Situ Forming Hydrogels.* Biomolecules, 2020. **10**(8): p. 1185.
41. Sereno, D. and J.L. Lemesre, *Axenically cultured amastigote forms as an in vitro model for investigation of antileishmanial agents.* Antimicrobial Agents and Chemotherapy, 1997. **41**(5): p. 972-976.
42. Gomes, M.S., et al., *Engagement of Toll-like receptor 2 in mouse macrophages infected with Mycobacterium avium induces non-oxidative and TNF-independent anti-mycobacterial activity.* Eur J Immunol, 2008. **38**(8): p. 2180-9.
43. Gomes-Alves, A.G., et al., *Development of an automated image analysis protocol for quantification of intracellular forms of Leishmania spp.* PLOS ONE, 2018. **13**(8): p. e0201747.
44. Vale-Costa, S., et al., *Iron overload favors the elimination of Leishmania infantum from mouse tissues through interaction with reactive oxygen and nitrogen species.* PLoS Negl Trop Dis, 2013. **7**(2): p. e2061.
45. Abu Elella, M.H., R.R. Mohamed, and M.W. Sabaa, *Synthesis of novel grafted hyaluronic acid with antitumor activity.* Carbohydrate Polymers, 2018. **189**: p. 107-114.
46. Wu, Y., *Preparation of low-molecular-weight hyaluronic acid by ozone treatment.* Carbohydrate Polymers, 2012. **89**(2): p. 709-712.
47. Su, W.-Y., Y.-C. Chen, and F.-H. Lin, *Injectable oxidized hyaluronic acid/adipic acid dihydrazide hydrogel for nucleus pulposus regeneration.* Acta Biomaterialia, 2010. **6**(8): p. 3044-3055.

48. Ossipov, D.A., et al., *Functionalization of Hyaluronic Acid with Chemoselective Groups via a Disulfide-Based Protection Strategy for In Situ Formation of Mechanically Stable Hydrogels.* Biomacromolecules, 2010. **11**(9): p. 2247-2254.
49. Bodnár, M., et al., *Preparation and characterization of cross-linked hyaluronan nanoparticles.* Colloid and Polymer Science, 2009. **287**(8): p. 991-1000.
50. Schanté, C.E., et al., *Chemical modifications of hyaluronic acid for the synthesis of derivatives for a broad range of biomedical applications.* Carbohydrate Polymers, 2011. **85**(3): p. 469-489.
51. Liu, C., et al., *Glycol chitosan/oxidized hyaluronic acid hydrogels functionalized with cartilage extracellular matrix particles and incorporating BMSCs for cartilage repair.* Artificial Cells, Nanomedicine, and Biotechnology, 2018. **46**(sup1): p. 721-732.
52. Gurudevan, S., A.P. Francis, and A. Jayakrishnan, *Amphotericin B-albumin conjugates: Synthesis, toxicity and anti-fungal activity.* Eur J Pharm Sci, 2018. **115**: p. 167-174.
53. Gagoś, M. and M. Arczewska, *FTIR spectroscopic study of molecular organization of the antibiotic amphotericin B in aqueous solution and in DPPC lipid monolayers containing the sterols cholesterol and ergosterol.* European Biophysics Journal, 2012. **41**(8): p. 663-673.
54. Silva-Carvalho, R., et al., *Development of dextrin-amphotericin B formulations for the treatment of Leishmaniasis.* Int J Biol Macromol, 2020. **153**: p. 276-288.
55. Mehenni, L., et al., *Preparation and Characterization of Spherical Amorphous Solid Dispersion with Amphotericin B.* Pharmaceutics, 2018. **10**(4).
56. Kafedjiiski, K., et al., *Synthesis and in vitro evaluation of thiolated hyaluronic acid for mucoadhesive drug delivery.* Int J Pharm, 2007. **343**(1-2): p. 48-58.
57. Fallacara, A., et al., *Formulation and Characterization of Native and Crosslinked Hyaluronic Acid Microspheres for Dermal Delivery of Sodium Ascorbyl Phosphate: A Comparative Study.* Pharmaceutics, 2018. **10**(4).
58. Kim, Y.T., et al., *A thermosensitive vaginal gel formulation with HPgammaCD for the pH-dependent release and solubilization of amphotericin B.* Eur J Pharm Sci, 2010. **41**(2): p. 399-406.
59. Zhou, L., et al., *Preparation, characterization, and evaluation of amphotericin B-loaded MPEG-PCL-g-PEI micelles for local treatment of oral Candida albicans.* International journal of nanomedicine, 2017. **12**: p. 4269-4283.
60. Zu, Y., et al., *Preparation and characterization of amorphous amphotericin B nanoparticles for oral administration through liquid antisolvent precipitation.* European Journal of Pharmaceutical Sciences, 2014. **53**: p. 109-117.
61. Al-Quadeib, B.T., et al., *Stealth Amphotericin B nanoparticles for oral drug delivery: In vitro optimization.* Saudi Pharmaceutical Journal, 2015. **23**(3): p. 290-302.
62. Graeser, K.A., et al., *The Role of Configurational Entropy in Amorphous Systems.* Pharmaceutics, 2010. **2**(2): p. 224-244.
63. Einfal, T., O. Planinsek, and K. Hrovat, *Methods of amorphization and investigation of the amorphous state.* Acta Pharm, 2013. **63**(3): p. 305-34.
64. Vinogradov, S.V., T.K. Bronich, and A.V. Kabanov, *Nanosized cationic hydrogels for drug delivery: preparation, properties and interactions with cells.* Adv Drug Deliv Rev, 2002. **54**(1): p. 135-47.
65. Olson, J.A., et al., *Comparison of the Physicochemical, Antifungal, and Toxic Properties of Two Liposomal Amphotericin B Products.* Antimicrobial Agents and Chemotherapy, 2008. **52**(1): p. 259.
66. Larabi, M., et al., *New lipid formulation of amphotericin B: spectral and microscopic analysis.* Biochimica et Biophysica Acta (BBA) - Biomembranes, 2004. **1664**(2): p. 172-181.

67. Wasko, P., et al., *Toward understanding of toxic side effects of a polyene antibiotic amphotericin B: fluorescence spectroscopy reveals widespread formation of the specific supramolecular structures of the drug.* Mol Pharm, 2012. **9**(5): p. 1511-20.
68. Bartlett, K., et al., *Effect of Heat-Treated Amphotericin B on Renal and Fungal Cytotoxicity.* Antimicrobial Agents and Chemotherapy, 2004. **48**(1): p. 333.
69. Petit, C., et al., *Activity of a heat-induced reformulation of amphotericin B deoxycholate (fungizone) against Leishmania donovani.* Antimicrob Agents Chemother, 1999. **43**(2): p. 390-2.
70. Zia, Q., et al., *Self-assembled amphotericin B-loaded polyglutamic acid nanoparticles: preparation, characterization and in vitro potential against Candida albicans.* Int J Nanomedicine, 2015. **10**: p. 1769-90.
71. Espada, R., et al., *Effect of aggregation state on the toxicity of different amphotericin B preparations.* International Journal of Pharmaceutics, 2008. **361**(1): p. 64-69.
72. Rochelle do Vale Morais, A., et al., *In-vitro and in-vivo antileishmanial activity of inexpensive Amphotericin B formulations: Heated Amphotericin B and Amphotericin B-loaded microemulsion.* Exp Parasitol, 2018. **192**: p. 85-92.
73. Kagan, S., et al., *Toxicity mechanisms of amphotericin B and its neutralization by conjugation with arabinogalactan.* Antimicrob Agents Chemother, 2012. **56**(11): p. 5603-11.
74. Legrand, P., et al., *Effects of aggregation and solvent on the toxicity of amphotericin B to human erythrocytes.* Antimicrob Agents Chemother, 1992. **36**(11): p. 2518-22.
75. Nicoletti, S., K. Seifert, and I.H. Gilbert, *N-(2-hydroxypropyl)methacrylamide–amphotericin B (HPMA–AmB) copolymer conjugates as antileishmanial agents.* International Journal of Antimicrobial Agents, 2009. **33**(5): p. 441-448.
76. Gershkovich, P., et al., *Biodistribution and tissue toxicity of amphotericin B in mice following multiple dose administration of a novel oral lipid-based formulation (iCo-009).* Journal of Antimicrobial Chemotherapy, 2010. **65**(12): p. 2610-2613.
77. Asthana, S., et al., *Targeted chemotherapy of visceral leishmaniasis by lactoferrin-appended amphotericin B-loaded nanoreservoir: in vitro and in vivo studies.* Nanomedicine (Lond), 2015. **10**(7): p. 1093-109.

CHAPTER 6 – FINAL REMARKS

This chapter contains the principal conclusions drawn from the work described in the previous chapters and proposes recommendations/suggestions for further research.

6.1. General Conclusions

In developing and third world countries, leishmaniasis is still endemic since, due to economic reasons, the access to affordable treatment is limited. Furthermore, the lack of industrial investment in the development of new drug treatments contributes to the enormous failure to control this disease that causes disability and, in many cases, death. Toxicity of the drugs, cost and emerging resistance limit the leishmaniasis treatment options. In the last years, there has been an increase in the efforts for the development of new medicines/formulations for this neglected disease by employing nanotechnology. Several AmB delivery systems are in the pipeline in order to secure an effective therapy in endemic areas. Within this scope, we had set ourselves to produce an economic, effective and safe water-soluble polysaccharide-based AmB delivery system. To do so, two polysaccharides were selected – dextrin (Dex) and hyaluronic acid (HA) - and a simple mixing process was employed as well as two drying processes – freeze-drying (FD) and spray drying (SD). In this part of the work (**Chapters 3** and **4**), different self-assembling nanocomplexes (Dex-AmB and HA-AmB) were successful developed, using a simple, straightforward and reproducible method based on the mixture of dextrin or hyaluronic acid with AmB in alkaline borate buffer, followed by dialysis, favoring the non-covalent drug association to the polysaccharide chains. Given the simplicity of the process, we believe a low-cost formulation is obtained. One key aspect when developing a biomaterial for intravenous administration is its size, which has an important role in the biodistribution of the drug, influencing its biological activity. The produced nanocomplexes, dried by either FD or SD, are suitable for anti-*Leishmania* nanomedicines since they present a size range (between 200 and 600 nm) expected to be targeted by the macrophage phagocytic activity. The nanocomplexes obtained with Dex are slightly smaller than the ones obtained with HA. Nevertheless, other attractive physicochemical properties were improved in the latter case, namely with regards to the narrow size distribution profile and high negative surface charge, that ensures colloidal stability in aqueous medium. Freeze- or spray-dried nanocomplexes were fully rehydrated and no agglomerates were observed, regardless of the polysaccharide used. This behavior could be associated to the observed AmB amorphization – effect that improves the bioavailability of this type of poor-water soluble drugs, by increasing their solubility and dissolution rates, as well as stability.

The developed nanocomplexes appears to offer some attractive properties as leishmaniasis therapeutics. In this sense, the safety of the formulations, which is a primary concern due to the intrinsic toxicity of AmB, was also extensively studied. *In vitro* cytotoxicity against primary macrophages and renal cells, as well as the hemolytic activity, were assessed for all the produced nanocomplexes (Dex-AmB FD, Dex-AmB SD, HA-AmB FD and HA-AmB SD). Overall, toxicity was significantly attenuated in all of the formulations

comparatively to the free-drug; nevertheless, according to the experimental results, the best performance in terms of cytotoxicity was achieved using HA-AmB SD nanocomplex, which reduced the viability of macrophages only at doses superior to 13.33 μM. The observed reduction in the *in vitro* toxicity (mostly for the HA-AmB nanocomplexes) could be related with two observations:

- the presence of AmB in the formulation mostly in a super-aggregated state (associated to diminished toxicity);
- the improved association of the drug with the hyaluronic acid (postulated due to similarities between the UV-vis spectra of our formulations and AmBisome®), which mitigates somehow the uncontrolled release of the drug, exerting a stabilizing and protective effect.

In addition to the toxicity reduction, inclusion of the drug into the polysaccharides chain network using the developed method do not interfere with the pharmacological activity of AmB, since all of the formulations presented potential to reduce the *in vitro* parasite viability in axenic cultures, as well as in infected macrophages (to an extent similar to that obtained with the free-drug). Since HA-AmB SD was the formulation that displayed a superior safety margin for intravenous administration, e.g., a better selectivity index, this material was the one selected for *in vivo* systemic toxicity and anti-leishmanial activity studies.

Those assays were performed in parallel with another formulation that was developed using a method described in the literature where AmB is covalently linked to an oxidized polysaccharide via Schiff base (imine bond) (**Chapter 5**). As for the HA-AmB SD nanocomplex, this new formulation was also developed using hyaluronic acid, given its affinity for the macrophage receptors CD44, contributing for a better active targeting and internalization. This polysaccharide was firstly oxidized with sodium periodate (OxHA) and then the AmB was covalently linked, rendering a high-water soluble material (HA-AmBi) that presents a nanometric size, very similar to the one reported for the commercial formulation Ambisome®, a low polydispersion index, colloidal stability due to a high negative surface charge and amorphous AmB, mostly in super-aggregated form. Considering the *in vitro* assays, covalent attachment of AmB to the polysaccharide mitigates the drug toxicity while maintaining its anti-leishmanial activity. Nevertheless, by comparing the *in vitro* results of both formulations (HA-AmB SD vs HA-AmBi), a better outcome in terms of safety and efficacy balance (selectivity index) were observed for the non-covalent nanocomplex, for comparable drug content.

In regard to the *in vivo* systemic toxicity assays, results suggest that in contrast to toxic AmB, HA-AmB SD nanocomplex and HA-AmBi did not adversely affect the host liver, kidney and spleen histology. Alterations in the liver and kidneys, observed only in a very reduced number of animals, were very mild

in comparison with the results reported in the literature for free-AmB. Indeed, the animals in each treatment group always behaved normally without significant alterations in weight. The *in vivo* anti-leishmanial study, where the reduction of the parasite burden in *L. infantum*-infected mice was analyzed, confirmed the potential of the formulations. According to the results, at 1 mg/Kg, both formulations promoted a significant reduction in the spleen and liver parasite burden (HA-AmB SD nanocomplex: 1.68-$\log_{10}$ and 4.60-$\log_{10}$ reduction, respectively; HA-AmBi: 1.32-$\log_{10}$ and 4.98-$\log_{10}$ reduction, respectively), effect that was exerted in the same extent as AmBisome®, exception made for the nanocomplex that underperformed comparatively the commercial gold standard in the reduction of the parasite burden in the liver.

Overall, both *in vitro* and *in vivo* experiments demonstrate an innovative approach to AmB therapy since it is possible to infer that the HA-AmB SD nanocomplex obtained using the method developed in this work, having the same effect to the covalent formulation, is advantageous due to its simplicity, making this formulation with anti-leishmanial potential more affordable and faster to produce.

6.2. Future Work

Needless to say that further work is yet to be done to better understand the potential of this simple formulations of polysaccharide-AmB, especially the ones based on hyaluronic acid. Different *in vitro* and *in vivo* studies are proposed for future work:

- ✓ Further evaluation of the *in vitro* anti-leishmanial activity of the HA-based nanocomplexes against *L. donovani*-infected macrophages. *L. donovani* is a very dangerous parasite strain that is found only in the Old World (India, Bangladesh, Ethiopia, Sudan and South Sudan), where it is notoriously associated with VL (and PKDL), and is mostly transmitted from human to human, being directly fatal.
- ✓ Use the near-infrared fluorescent dye cy5.5 to synthesize cy5.5-conjugated HA (or cy5.5-conjugated AmB) and develop a Cy5.5-HA-AmB nanocomplex. This formulation will be used for:
    - *in vitro* uptake studies by infected and non-infected macrophages and evaluation of the formulation affinity for the CD44 receptor by determining the extent and efficiency of the internalization by flow cytometry analysis and laser scanning confocal microscopy;
    - *in vivo* biodistribution studies in the IVIS Lumina system for the assessment, in a non-invasive imaging way, of the potential of the formulation to deliver this kind of pharmaceutical to the target site;
    - *in vivo* blood half-life using the IVIS Lumina system by measuring fluorescence intensity of the whole blood collected from mice at different time points;

- ✓ Development of pharmacokinetic studies by examining the concentration of AmB in the blood and specific organs, through HPLC, at various time intervals. This will provide important insights to understand the host's clinical response to the formulation, since *Leishmania* is an intracellular residing parasite and the drug concentration in the microenvironment of the parasite rather than that in the host circulation is pivotal.
- ✓ Application of the nanocomplexes in *L. infantum- or L. donovani*-infected BALB/c mice models (with different periods of infection) and evaluation of their effects regarding:
    - the *in vivo* anti-leishmanial activity through the limiting dilution assays after i.v. administration of the formulations at different treatment regimens;
    - the immunomodulatory activity by measuring through ELISA the cytokine profile in the splenocytes of the infected and treated animals, and compare that with that of AmB and AmBisome®.

Appendix – DGAV License

REPÚBLICA PORTUGUESA | AGRICULTURA

dgav Direção Geral de Alimentação e Veterinária

Exma. Sra.
Dra. Catarina Carona
I3S - Instituto de Investigação e Inovação em Saúde Rua Alfredo Allen, 208
4200-135 Porto

2020-07-07 009887

Nossa referência	Vossa referência	Vossa data

Assunto: PROTEÇÃO DOS ANIMAIS UTILIZADOS PARA FINS CIENTÍFICOS E/OU OUTROS FINS CIENTÍFICOS - PEDIDO DE AUTORIZAÇÃO PARA REALIZAÇÃO DE PROJETO DE EXPERIMENTAÇÃO ANIMAL

Na sequência do pedido efetuado por V. Exª no sentido de poder ser autorizada a realização do projeto experimental designado "Desenvolvimento de um nanocomplexo de ácido hialurónico-Anfotericina B para o direcionamento e tratamento de Leishmaniose", tendo como investigadora responsável a Dra. Ana Maria Luís Ramos Tomás, cabe-me informar que o mesmo foi avaliado de acordo com o Artigo 44º do Decreto-Lei n.º 113/2013, de 7 de agosto, relativo à "proteção dos animais utilizados para fins científicos".

Mais se reforça que, deverá existir uma apertada monitorização dos sinais de dor, sofrimento ou angústia dos animais submetidos aos procedimentos, para que a aplicação dos limites críticos estabelecidos para cada um dos procedimentos se faça de forma adequada a cada animal, tendo em conta a necessidade de impedir que os sinais de dor, sofrimento ou angústia severos se prolonguem sem a tomada de medidas mitigantes dos mesmos.

Uma vez que o projeto em apreço envolve a realização de procedimentos cuja classificação de severidade prospetiva se enquadra na categoria **Moderada**, terá que ser submetido a uma avaliação retrospetiva de acordo com o ponto 3, do Artigo 45º do documento legislativo acima referido.

1

ANO INTERNACIONAL DA SANIDADE VEGETAL 2020

CAMPO GRANDE, Nº 50 1700-093 LISBOA TELEF. 21 323 95 00 FAX. 21 346 35 18

Mais se informa V. Exª que o projeto em apreço recebeu uma **avaliação favorável** e foi **autorizado** de acordo com o n.º 1, do Artigo 42º do mesmo diploma legislativo.

A monitorização dos sinais de dor, sofrimento ou angústia dos animais submetidos aos procedimentos, classificados prospectivamente em termos de severidade nas categorias **ligeira** e **moderada** deverá ser feita no sentido de se atualizar a severidade efetiva a que os mesmos ficarão, na realidade, sujeitos.

Finalmente, resta-me especificar, de acordo, com o discriminado no n.º2, do Artigo 46º, do atrás referido Decreto-Lei, o seguinte:

- **O utilizador que realiza o projeto:** Senhor Reitor Professor Doutor António Sousa Pereira;
- **A pessoa responsável pela execução global do projeto e pela sua conformidade com a autorização do mesmo:** Dra. Ana Maria Luís Ramos Tomás
- **O estabelecimento onde o projeto vai ser realizado:** Biotério do I3S - Instituto de Inovação em Saúde.

Com os melhores cumprimentos.

O Diretor Geral

Fernando Bernardo

Graça Mariano
Subdiretora-Geral
Por despacho de delegação de competências nº 8140/2018
publicado no DRE, II série nº 159, de agosto de 2018

DSPA-DBEAI SBX

CAMPO GRANDE, Nº 50 1700-093 LISBOA TELEF. 21 323 95 00 FAX. 21 346 35 18